Yasushi Nagata

Editor

Stereotactic Body Radiation Therapy

Principles
and Practices

∑ Springer

Stereotactic Body Radiation Therapy

Yasushi Nagata
Editor

Stereotactic Body Radiation Therapy

Principles and Practices

Springer

Editor
Yasushi Nagata
Department of Radiation Oncology
Hiroshima University Hospital
Hiroshima, Japan

Foreword

Stereotactic body radiotherapy (SBRT) became possible when advanced diagnostic imaging detected small lesions and radiotherapy was applied to the precise tumor location. Diagnostic imaging advancement is indebted to Professor Shinji Takahashi, who developed computerized tomography (CT) that could detect much smaller lesions in the lung than chest X-ray could. Also adequate metastatic work-up can select out pure stage I non-small-cell lung cancer from other sites of metastasis that can be handled by SBRT with or without systemic treatment.

It is very important to know that SBRT uses a much higher dose per fraction compared to conventional radiotherapy, which means the usual linear-quadratic (LQ) model and biologically effective dose (BED) do not apply for SBRT. We have learned 4 R (re-oxygenation, re-distribution, repopulation, and repair) when conventional fractionated radiotherapy was used, which is not applied for SBRT for small lesions. SBRT has effects against tumor vasculature and enhances host immunity, leading to increased antitumor effects. This is an exciting area to investigate in future.

Advancement of sophisticated radiation treatment equipment and understanding the physics of utilization of the equipment for SBRT rapidly became clinical applications for the primary lung or hepatic lesions as well as for other metastatic lesions. Because of a high dose per fraction, technical aspects and quality assurance to deliver the radiation to the tumor precisely and avoid a high dose of radiation to the critical surrounding normal tissue are critical issues for SBRT.

To understand tumor motion and control tumor motion have been major challenges for mainly lung lesions. To visualize hepatic lesions or other metastatic lesions, e.g., those in the pancreas or soft tissue, can be difficult without contrast enhancement or fiducial markers. The most challenging part of SBRT in addition to controlling tumor motion is lesions to be treated by this technique close to the critical organs, e.g., blood vessels, brachial plexus, esophagus, major airway bile ducts, small bowel, and the stomach. We have not established a consensus of dose fractionation of SBRT especially for centrally located lesions.

Methods of stereotactic body irradiation and fixation have changed with the introduction of SBRT compared to therapy for the brain, head, and neck cancer. Lesions in the lung are particularly difficult to irradiate due to respiratory and cardiac movements. The method used for stereotactic body irradiation is set in each facility to maintain precise determination of tumor position. The four-dimension computed tomography (4D CT) scan method is necessary to simulate and treat the lung lesions with the free-breathing irradiation using a dynamic tumor tracking method.

If the tumor moves more than 1 cm, the breath-hold technique is usually recommended. How to immobilize patients for SBRT is a critical issue to target tumors precisely. As SBRT requires a high degree of positional precision, a fixation device is used to increase precision and repeatability by maintaining the patient in the same position for the duration of the treatment.

Various immobilization devices are available, each of which has advantages and disadvantages. It is necessary to choose the appropriate device for the therapeutic method used in each facility. A real-time tracking radiotherapy system (RTRT system) was developed in 1998. The first RTRT system was able to recognize a 2.0-mm gold marker location in a patient with an accuracy of 1 mm every 0.03 s during delivery of irradiation from a synchronized Linac. When a gold marker inserted in the patient was out of the range of the gating window, Linac stopped irradiation. When a gold marker was inside the range of the gating window from the planned position, irradiation was delivered. With this technique, the clinical results have been reported on SBRT for non-small cell lung cancer (NSCLC), hepatocellular carcinoma (HCC), adrenal tumor, and spinal Schwannoma. Analysis of marker motion was also done and several interesting findings were reported.

SBRT is a promising treatment for early-stage NSCLC and provides a highly effective and safe therapy as long as quality assurance (QA) has been done correctly and tumor motion has been well controlled. As a result, SBRT has become one of the standards of care for delivering definitive treatment in medically inoperable patients. Important features of modern SBRT are the supplementary techniques such as intensity-modulated radiotherapy, volumetric-modulated arc therapy, or flattened filter-free beams with image-guided radiotherapy (IGRT) and dose-calculation algorithms, such as convolution superposition, the Monte Carlo, and the grid-based Boltzmann equation solver (GBBS) method. These techniques and dose-calculation algorithms reduce important errors or inaccuracies in dose distribution. Therefore, the impact of a calculation algorithm on the dose-distribution accuracy is an issue. We do need international collaboration to establish a guideline of QA procedure and adequate dose-fractionation consensus depending on the size and location of the tumor.

Since medically inoperable patients with early-stage lung cancer have been treated by SBRT for more than a decade, and safety and efficacy have been published, medically operable patients with stage I NSCLC have been randomized to be operated on or treated by SBRT. We have to see the results of these randomized studies. Especially long-term side effects of SBRT need to be critically analyzed since these patients with medically operable stage I NSCLC will live long

enough to manifest late effects of radiation. SBRT can be applied for hepatic lesions, primary or metastatic lesions, prostatic cancer, metastatic lesions to the vertebral body, and adrenal gland.

A more recent and very exciting application of SBRT has been to treat metastatic lesions from other primary sites such as melanoma and renal cancer, followed by immunotherapy. This area needs to be investigated for safety and efficacy by phase I/II prospective trials.

Published data of normal tissue toxicity after SBRT have been accumulated and patients' variables have been becoming gradually apparent. How to evaluate the normal tissue toxicity as well as the treatment response after SBRT is also important. The usefulness of 18F-fluorodeoxyglucose-positron emission tomography (FDG-PET) in the evaluation of treatment response and the prediction of tumor progression has been suggested.

How to evaluate the efficacy and toxicity by SBRT is a very complicated issue. A biological model to optimize dose fractionation based on physical dose distribution can be utilized in dose-composition radiotherapy (DCRT). Measurement of circulating tumor DNA might improve the selection of the patients for DCRT and for systemic therapy.

The future of radiotherapy will incorporate advancements in the fields of biology, physics, and imaging. Applying this knowledge to clinical radiotherapy and selecting the most appropriate cancer patients will improve their outcomes.

Department of Radiation Oncology   Ritsuko Komaki,
University of Texas, MD Anderson Cancer Center   M.D., FACR, FASTRO
Houston, TX, USA

Preface

Cancer is one of the major health concerns worldwide, and the proportion of cancer patients requiring radiotherapy (RT) is increasing because of the increase in the number of cancer patients. In Japan, the average life span is 80 years for men and 86 years for women as of 2014. Because of the comorbidities of an aged population, less invasive radiotherapy is more preferred than invasive surgery. In most cases, radiotherapy could be most effective and convenient.

Emerging new technologies have been widely introduced in the field of radiotherapy in recent decades. One of these, stereotactic radiotherapy (SRT), was first used in intracranial tumors in the 1960s. Later, this technique was introduced for extracranial tumors, mainly for lung cancer. One of the leading countries in this field is Japan, where, since the 1990s, various developments, new biological and physics concepts, new imaging modalities, new respiratory gating techniques, and new image-guided radiation therapy (IGRT) machines have become available. Recently, the technique of stereotactic body RT (SBRT) has taken a completely different form from that of the original technique.

This book represents the most updated basic and clinical information on SBRT, and I hope that it will be helpful in facilitating clinical and research activities in the field. Finally, I would like to thank all of the authors for their contributions as well as Springer Japan for their efforts in publishing this book.

Hiroshima, Japan   Yasushi Nagata

Contents

Part I
Introduction

Chapter 1
Introduction and History of Stereotactic Body Radiation Therapy (SBRT)

Yasushi Nagata

1.1 Introduction

Intracranial Stereotactic Radiosurgery (SRS) was a new treatment method for brain tumors introduced in the twentieth century to deliver tight spatial/temporal distribution using a high precision technique. The clinical experience from intracranial SRS, together with the technical developments in conventional RT, initiated the development of Stereotactic Body Radiation Therapy (SBRT) for extracranial tumors characterized by a very high dose per fraction, delivered in a short time. This was started at the Swedish Karolinska University hospital in 1991 with tumors in the liver and lungs by Bromgren and Lax [1–3]. In parallel this method was developed in Japan and clinically introduced in 1994 for lung tumors [4–6]. During the last 5 years of the nineties, SBRT was introduced in several centers in Europe, Japan and USA. Wulf and Herfarth in Germany reported these clinical results on lung cancer in 2001, followed by Timmerman in USA in 2003. In Japan, a Japanese study group of stereotactic body radiation therapy was formed in 1999, and it expands annually. It then transformed into the Japan 3-D conformal external beam radiotherapy group (J-CERG) in 2002. The SBRT procedure was approved by the Japanese government to be covered by the health insurance in 2004. The early reports had already shown very promising results with regard to local control and toxicity for the hypofractionation schedules which were adopted with 10–15 Gy/fraction given in 3–5 fractions during a short time. However, due to the new aspects introduced in SBRT, clinical experience was initially accumulated at a very slow rate and it was only during

Y. Nagata (✉)
Department of Radiation Oncology, Hiroshima University Hospital, Hiroshima, Japan
e-mail: nagat@hiroshima-u.ac.jp

the last decade that outcome data from several centers was available to confirm the initial promising results. In this session, the historical development of SBRT was reviewed.

1.2 Intracranial Radiosurgery

The field of intracranial radiosurgery was mainly developed between 1950 and 1970. The treatment was named as radiosurgery by Leksell as an alternative to neurosurgery. Thereafter, the terminology of stereotactic radiosurgery meant single high dose with accurate spatial precision. The system named as the Gamma Knife is a system with a metal helmet and multiple holes attached to a capsule of 201 multiple gamma sources. The Gamma Knife system developed into from the original system up to a modern new system. The new system has an automatic helmet exchange with multi-leaf collimators. The radiosurgery technique was also possible using a conventional linear accelerator with a 3-dimensional radiosurgery systems. This system included metallic ring to be attached to a patient and fixation system attached to a couch. The 3-dimensional coordinates were essential for SRS. The accuracy of linear accelerator was essential.

1.3 Principles and Methods

To extend the intracranial radiosurgery technology to extracranial tumors, two problems should be solved. First, most extracranial tumors move with or without respiratory motion. With tumor motions, wide ITV margins prevent delivering high dose to the tumor. The other difficulty is the unknown normal tissue toxicity using single high dose. Previous experiences with clinical radiotherapy are based on daily 2 Gy radiotherapy up to 60 or 70 Gy. Therefore, 48–60 Gy in 3–5 fractions are unknown area.

Therefore, initial SBRT was based on stereotactic coordinates using the Stereotactic Body Frame. Patients were stored within a plastic frame with three-dimensional coordinates. After the set-up with these coordinates, single high dose was irradiated with non-coplanar beams.

The other concern is the respiratory tumor movement. To regulate respiratory movement, various methods were used. Initially, abdominal press or breath-hold techniques were most popular methods, thereafter, developed into respiratory gating and chasing methods.

Geometric verification at each treatment is essential for SBRT, it is because single dose set-up error will consequently make local tumor recurrence. Therefore, AP and lateral portal verifications using films were essential before each treatment, which now developed into EPID technology and cone-beam CT technology.

1.4 Dose Fractionation and Normal Tissue Dose Constraints

Even now, the best dose fractionation schedule for lung and liver tumors are unknown. The accurate dose constraints for normal tissue are still unknown. In Japan, Dr. Uematsu used 50 Gy in 10 fractions, followed by Arimoto 60 Gy in 8 fractions, and by Nagata 48 Gy in 4 fractions and. In USA, 60 Gy in 3 fractions was the original, currently 54 Gy in 3 or 48–50 Gy in 4 were popular. In European countries, various fractionations were used at Karolinska Hospital, followed by 45 Gy in 3 fractions and 24 Gy in single fraction. We must be careful that these doses were prescribed at different points either isocenter or margin. The normal tissue dose constraints were set by JCOG (Japan Clinical Oncology Group) mainly proposed by Dr. Shirato.

1.5 Terminology

The name of SBRT was introduced by Timmerman in 2002. He originally used Stereotactic Ablative Radiosurgery for this treatment. However, there were several opposition from radiation oncologists because this treatment is completely different from radiofrequency ablation (RFA). In 2005, Stereotactic body radiation therapy (SBRT) was used as a code of radiation therapy in USA. Extracranial stereotactic radiation therapy (ESRT) was used in Europe late 1990s and pin-pointed radiation therapy was used in Japan late 1990a. In 2010, Stereotactic ablative radiotherapy (SABR) was introduced by Loo et al. It was because the pronunciation of SBRT was difficult. Currently the terminology of SBRT and SABR are both used and are very confusing.

References

1. Lax I, Blomgren H, Näslund I, et al. Stereotactic radiotherapy of malignancies in the abdomen. Methodological aspects. Acta Oncol. 1994;33:677–83.
2. Lax I, Blomgren H, Larson D, et al. Extracranial stereotactic radiosurgery of localized targets. J Radiosurg. 1998;1:135–48.
3. Blomgren H, Lax I, Näslund I, et al. Stereotactic high dose fraction radiation therapy of extracranial tumors using an accelerator. Acta Oncol. 1995;34:861–70.
4. Uematsu M, Shioda A, Tahara K, et al. Focal, high dose, and fractionated modified stereotactic radiation therapy for lung carcinoma patients. Cancer. 1998;82:1062–70.
5. Uematsu M, Shioda M, Suda A, et al. Computed tomography-guided frameless stereotactic radiotherapy for stage I non-small cell lung cancer: a 5-year experience. Int J Radiat Oncol Biol Phys. 2001;51:666–70.

6. Arimoto T, Usubuchi H, Matsuzawa T, et al. Small volume multiple non-coplanar arc radio-therapy for tumors of the lung, head & neck and the abdominopelvic region. Tokyo: Elsevier; 1998.

Bibliography

3rd Acta Oncologica symposium on stereotactic body radiotherapy. Copenhagen: Acta Oncol. 2006;45:771–994.

Bauman P, Nyman J, Hoyer M, et al. Outcome in a prospective phase II trial of medically inoperable stage I non-small cell lung cancer patients treated with stereotactic body radiother-apy. J Clin Oncol. 2009;27:3290–6.

Baumann P, Nyman J, Lax I, et al. Factors important for efficacy of stereotactic body radiotherapy of medically inoperable stage I lung cancer. A retrospective analysis of patients treated in the Nordic countries. Acta Oncol. 2006;45:787–95.

Blomgren H, Lax I, Göranson H, et al. Radiosurgery for tumors in the body: clinical experience using a new method. J Radiosurg. 1998;1:63–74.

Blomgren H, Lax I, Näslund I, et al. Stereotactic high dose fraction radiation therapy of extracra-nial tumors using an accelerator. Acta Oncol. 1995;34:861–70.

Chang JY, Balter PA, Dong L, et al. Stereotactic body radiation therapy in centrally and superiorly located stage I or isolated recurrent non-small-cell lung cancer. Int J Radiat Oncol Biol Phys. 2008;72:967–71.

Dawson L, Eccles C, Craig T. Individualized image guided iso-NTCP based liver cancer SBRT. Acta Oncol. 2006;45:856–64.

Fakiris A, McGarry RC, Yiannoustsons CT, et al. Stereotactic body radiation therapy for early-stage non-small cell lung carcinoma: four-year results of a prospective phase II study. Int J Radiat Oncol Biol Phys. 2009;75:677–82.

Guckenberger M, Meyer J, Wilbert J, et al. Intra-fractional uncertainties in cone-beam CT based image-guided radiotherapy of pulmonary tumors. Radiother Oncol. 2007;83:57–64.

Haedinger U, Wulf J. Quality assurance in stereotactic body radiation therapy. In: Kavanagh BD, Timmerman R, editors. Stereotactic body radiation therapy. Philadelphia: Lippincott, Williams & Wilkins; 2005.

Hara R, Itami J, Kondo T, et al. Clinical outcomes of single-fraction radiation therapy for lung tumors. Cancer. 2006;1006:1347–52.

Herfarth KK, Debus J, Lohr F, et al. Stereotactic single dose radiation therapy of liver tumors: results of a phase I/II trial. J Clin Oncol. 2001;19:164–70.

Herfarth KK, Debus J. Stereotaktische Strahlentherapie von Lebermetastasen. Der Chirurg. 2005;76:564–9.

Hoyer M, Roed H, Sengelov L, et al. Phase-II study on stereotactic radiotherapy of locally advanced pancreatic carcinoma. Radiother Oncol. 2005;76:48–53.

Joyner M, Salter BJ, Papanikolaou N, et al. Stereotactic body radiation therapy for centrally located lung tumors. Acta Oncol. 2006;45:802–7.

Kavanagh B, Schefter T, Cardenes H, et al. Interim analysis of a prospective phase I/II trial of SBRT for liver metastases. Acta Oncol. 2006;45:848–55.

Kavanagh BD, McGarry R, Timmerman RD. Extracranial radiosurgery (stereotactic body radia-tion therapy) for oligometastases. Semin Radiat Oncol. 2006;16:77–84.

Koong AC, Christofferson E, Le Q, et al. Phase II study to assess the efficacy of conventionally fractionated radiotherapy followed by a stereotactic boost in patients with locally advanced pancreatic cancer. Int J Radiat Oncol Biol Phys. 2005;63.

Koong AC, Le Q, Ho A, et al. Phase I study of stereotactic radiosurgery in patients with locally advanced pancreatic cancer. Int J Radiat Oncol Biol Phys. 2004;58:1017–21.

Laagerward F, Van Sornsen de Koste J, Nijssen-Visser M, et al. Multiple "slow" CT scans for incorporating lung tumor mobility in radiotherapy planning. Int J Radiat Oncol Biol Phys. 2001;51:932–7.

Lee S, Choi E, Park H, et al. Stereotactic body frame based fractionated radiosurgery on consecutive days for primary or metastatic tumors in the lung. Lung Cancer. 2003;40:309–15.

Lehnert T, Golling M. Indikationen und Ergebnisse der Lebermetastasenresektion. Radiologe. 2001;41:40–8.

Leksell L. Stereotactic radiosurgery. J Neurol Neurosurg Psychiatry. 1983;46:797–803.

Leksell L. The stereotactic method and radiosurgery of the brain. Acta Chir Scand. 1951;102:316–19.

Loo BW, Chang JY, Dawson LA. Stereotactic ablative radiosurgery: what's in a name. Pract Radiat Oncol. 2011;1:38–9.

McGarry R, Papiez L, Williams M, et al. Stereotactic body radiation therapy for early stage non-small cell lung cancer: phase I study. Int J Radiat Oncol Biol Phys. 2005;63:1010–15.

Mendez-Romero A, Wunderink W, Hussain S, et al. Stereotactic body radiation therapy for primary and metastatic liver tumors: a single-institution phase I–II study. Acta Oncol. 2006;45:831–7.

Nagata Y, Matsuo Y, Takayama K, et al. Survey of SBRT in Japan. Int J Radiat Oncol Biol Phys. 2009;75:343–7.

Nagata Y, Negoro Y, Aoki T, et al. Clinical outcomes of 3D conformal hypofractionated single high dose radiotherapy for one or two lung tumors using a stereotactic body frame. Int J Radiat Oncol Biol Phys. 2002;52:1041–6.

Nagata Y, Takayama K, Matsuo Y, et al. Clinical outcomes of a phase I/II of 48 Gy of stereotactic body radiotherapy in 4 fractions for primary lung cancer using a stereotactic body frame. Int J Radiat Oncol Biol Phys. 2005;63:1427–31.

Norihisa Y, Nagata Y, Takayama K, et al. Stereotactic body radiation therapy for oligometastatic lung tumors. Int J Radiat Oncol Biol Phys. 2008;72:398–403.

Onimaru R, Shirato H, Shimizu S, et al. Tolerance of organs at risk in small-volume, hypofractionated, image-guided radiotherapy for primary and metastatic lung cancers. Int J Radiat Oncol Biol Phys. 2003;56:126–35.

Onishi H, Araki T, Shirato H, et al. Stereotactic hypofractionated high-dose irradiation for stage I non-small cell lung carcinoma. Cancer. 2004;101:1623–31.

Pannetieri V, Wennberg B, Gagliardi G, et al. SBRT of lung tumors: Monte Carlo simulation with PENELOPE of dose distributions including respiratory motion and comparison with different treatment planning systems. Phys Med Biol. 2007;52:4265–81.

Potter L, Steinberg M, Rose C, et al. American Society of Therapeutic Radiology and Oncology and American College of Radiology practice guideline for the performance of stereotactic body radiation therapy. Int J Radiat Oncol Biol Phys. 2004;60:1026–32.

Rusthoven KE, Kavanagh BD, Burri SH, et al. Multi-institutional phase I/II trial of stereotactic radiation therapy for lung metastases. J Clin Oncol. 2009;27:1579–84.

Schefter T, Kavanagh B, Timmerman R, et al. A phase I trial of stereotactic body radiation therapy (SBRT) for liver metastases. Int J Radiat Oncol Biol Phys. 2005;62:1371–8.

Shirato H, Shimizu S, Tadashi S, et al. Real time tumor tracking radiotherapy. Lancet. 1999;353:1331–2.

Takayama K, Nagata Y, Negoro Y, et al. Treatment planning of stereotactic radiotherapy for lung cancer. Int J Radiat Oncol Biol Phys. 2005;61:1565–71.

Timmerman R, Galvin J, Michalski J, et al. Accreditation and quality assurance for Radiation Oncology Group: multicenter clinical trials using stereotactic body radiation therapy in lung cancer. Acta Oncol. 2006;45:779–86.

Timmerman R, McGarry R, Yiannoutsos C, et al. Excessive toxicity when treating central tumors in a phase II study of stereotactic body radiation therapy for medically inoperable early-stage lung cancer. J Clin Oncol. 2006;24:4833–9.

Timmerman R, Papiez L, McGarry R, et al. Extracranial stereotactic radioablation: results of a phase I study in medically inoperable stage I non-small cell lung cancer. Chest. 2003;124:1946–55.

Timmerman RD, Park C, Kavanagh BD. The North American experience with stereotactic body radiation therapy in non-small cell lung cancer. J Thorac Oncol. 2007;27(Suppl.3):S101–12, Appendix.

Timmermann R, et al. Stereotactic body radiation therapy for inoperable early stage lung cancer. JAMA. 2010;303:1070–6.

Wersaell P, Blomgren H, Lax I, et al. Extracranial stereotactic radiotherapy for primary and metastatic renal cell carcinoma. Radiother Oncol. 2005;77:88–95.

Wulf J, Baier K, Mueller G, et al. Dose-response in stereotactic irradiation of lung tumors. Radiother Oncol. 2005;77:83–7.

Wulf J, Guckenberger M, Haedinger U, et al. Stereotactic radiotherapy of primary liver cancer and hepatic metastases. Acta Oncol. 2006;45:838–47.

Wulf J, Haedinger U, Oppitz U, et al. Stereotactic radiotherapy of targets in the lung and liver. Strahlenther Onkol. 2001;177:645–55.

Wulf J, Haedinger U, Oppitz U, et al. Stereotactic radiotherapy of primary lung cancer and pulmonary metastases: a non-invasive treatment approach in medically inoperable patients. Int J Radiat Oncol Biol Phys. 2004;60:186–96.

Xia T, Li H, Sun Q, et al. Promising clinical outcome of stereotactic body radiation therapy for patients with inoperable stage I/II non-small cell lung cancer. Int J Radiat Oncol Biol Phys. 2006;66:117–25.

Yaes RJ, Patel P, Maruyama Y. On using the linear-quadratic model in daily clinical practice. Int J Radiat Oncol Biol Phys. 1991;20:1353–62.

Zimmermann F, Geinitz H, Schill S, et al. Stereotactic hypofractionated radiation therapy for stage I non-small cell lung cancer. Lung Cancer. 2005;48:107–14.

Part II
Basic Principles

Chapter 2
Radiobiology of SBRT

Yuta Shibamoto, Akifumi Miyakawa, Hiromitsu Iwata, and Shinya Otsuka

2.1   Introduction

Stereotactic body radiation therapy (SBRT) has established its role in the definitive treatment of lung and liver cancers. While SBRT has definite advantages in dose distribution, a few radiobiological issues remain unresolved regarding the evaluation of SBRT doses and the effect of high doses per fraction. The first issue is regarding the prolonged beam delivery time. In conventional radiotherapy, daily treatment time is usually within 5 min. In contrast, SBRT takes 15–40 min or even longer for one treatment session with a number of intermissions up to several minutes. Radiobiologically, it is questioned whether the radiation dose delivered with such intermissions is equivalent to that administered without breaks, since it is well known that sublethal damage repair (SLDR) occurs when intervals are set between two radiation doses [1, 2]. To date, several studies have addressed this issue, and we review the results and summarize our previous studies.

The second issue is regarding the evaluation of different fractionation schedules and conversion of radiation doses using mathematical models. Since the optimal fractionation schedule has not yet been established, various fractionation schedules are being tested. To evaluate the treatment outcome, comparison among different fractionation schedules is necessary. For this purpose, many clinicians use the linear-quadratic (LQ) formalism. However, it has been questioned whether the LQ model is really applicable to high-dose-per-fraction treatment [3, 4]. Therefore,

Y. Shibamoto (✉) • A. Miyakawa

Department of Radiology, Nagoya City University Graduate School of Medical Sciences,
1 Kawasumi, Mizuho-cho, Mizuho-ku, Nagoya, Aichi 467-8601, Japan
e-mail: yshiba@med.nagoya-cu.ac.jp

H. Iwata
Nagoya Proton Therapy Center, Nagoya City West Medical Center, Nagoya, Japan

S. Otsuka
Department of Radiology, Okazaki City Hospital, Okazaki, Japan

evaluation of the reliability of LQ formalism in the high-dose range and, if inadequate, proposal of the method to correct the error or alternative models are important issues.

The third issue is the biological effect of high doses per fraction. Several researchers showed that high single doses can be biologically different from low doses used in conventional radiotherapy. These include vascular damages, immunogenic effects, and the influence of hypoxia. In this article, we review recent works on these issues. Some of our studies introduced in this article have been published elsewhere [5], which is reproduced after updating, with permission from the publisher.

2.2 Biological Effects of Intermittent Radiation Delivery

2.2.1 SLDR During Intermittent Radiation In Vitro

We conducted laboratory studies regarding the biological effects of intermittent irradiation. In the first study, the effects of fractionated doses delivered at intervals of a few minutes were evaluated in EMT6 and SCCVII cells [6]. In experiments where 8 Gy was given in 2 fractions, SLDR was observed when the interval was 2 min or longer in EMT6 cells and 3 min or longer in SCCVII cells. In the next experiment where 8 Gy was given in 5 fractions at intervals of 1–5 min, significant SLDR was observed when the interval was 2 min or longer in both cell lines (Fig. 2.1). When the interval was 5 min, 8 Gy in 5 fractions corresponded to 7.38 Gy in a single fraction in EMT6 cells and 7.29 Gy in SCCVII cells.
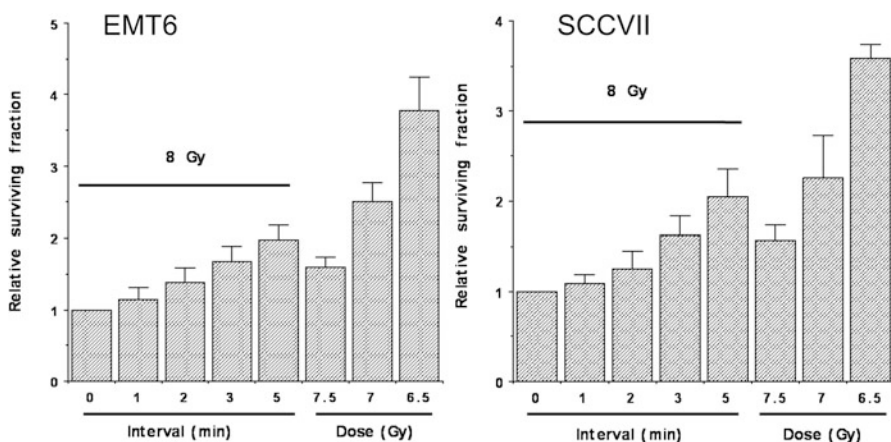

Fig. 2.1 Relative surviving fractions of EMT6 and SCCVII cells after 8 Gy given without a break or in 5 fractions at various intervals. Cell survival after continuous 8-Gy irradiation was regarded as 1. *Bars* represent SD (Reproduced from Ref. [5] with permission from the publisher)
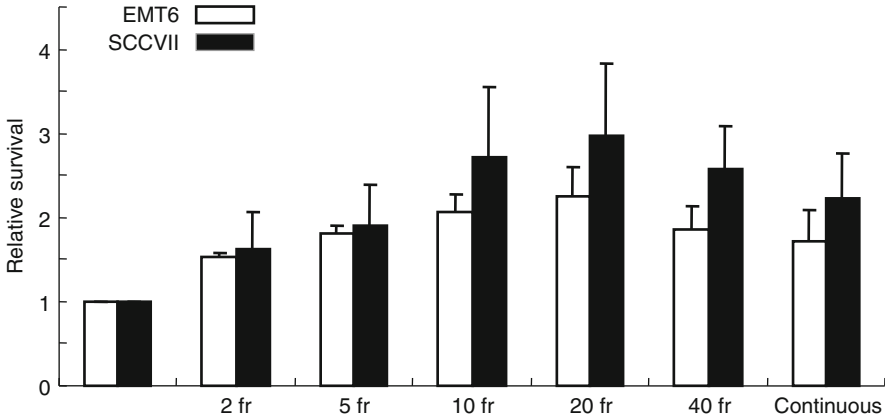
Fig. 2.2 Relative surviving fractions of EMT6 and SCCVII cells after 8 Gy given in 2–40 fractions and prolonged continuous irradiation given over 46 min. The control group received a single dose of 8 Gy over 5.3 min. Cell survival of the control group was regarded as 1. *Bars* represent SD (Reproduced from Ref. [5] with permission from the publisher. Regarding differences between groups, see Ref. [7])

The effects of 2 Gy given in 5 or 10 fractions at intervals of 0.5–5 min were also investigated in EMT6 cells using the cytokinesis-block micronucleus assay [6]. When the interval was 5 min, 5 fractions of 0.4 Gy corresponded to a single dose of 1.72 Gy. With an interval of 3 min each, 10 fractions of 0.2 Gy corresponded to a single dose of 1.76 Gy. It was concluded that dose-modifying factors of 1.08–1.16 need to be considered when the total irradiation time is 20–30 min. However, further *in vivo* study was considered necessary to extrapolate this result to clinical situations.

The next *in vitro* study was conducted to investigate the effects of intermittent irradiation with various fractionation schedules [7]. A total dose of 8 Gy was given to EMT6 and SCCVII cells in 2, 5, 10, 20, and 40 fractions within a fixed period of 15, 30, or 46 min, and the effects were compared with continuous 8-Gy irradiation given at a dose rate of 1.55 Gy/min or at reduced dose rates over 15, 30, or 46 min. When the total radiation time was 15 min, there were no differences in cell survival among the fractionation schedules, but when the period was 30 or 46 min, the radiation effect tended to decrease with an increase in the fraction number up to 20 fractions (Fig. 2.2). Two-fraction irradiation yielded the greatest effect among the fractionated radiation groups. Continuous low-dose-rate irradiation had a greater effect than 20- or 40-fraction irradiation. Implications regarding the clinical application of these results are complicated; nevertheless, this study showed that biological effects could differ with the fractionation schedule even when the total radiation time and dose are identical. To minimize the decrease of biological effects, total irradiation time should be kept as short as possible.
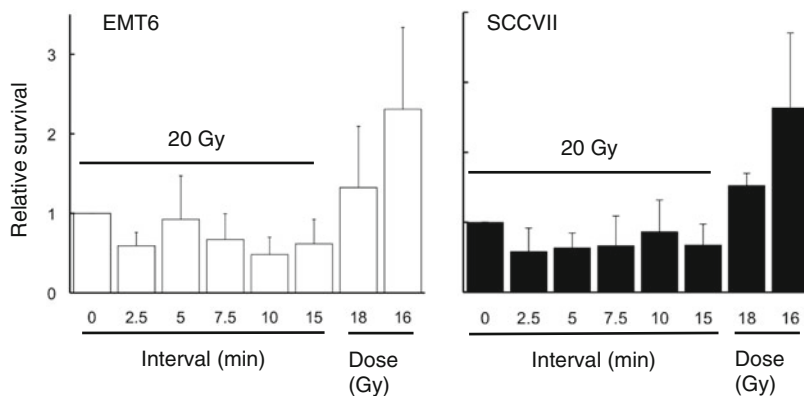
Fig. 2.3 Relative surviving fractions of EMT6 and SCCVII cells irradiated *in vivo* at 16, 18, or 20 Gy without a break or 20 Gy in 5 fractions at various intervals. Cell survival after continuous 20-Gy irradiation was regarded as 1. *Bars* represent SD (Reproduced from Ref. [5] with permission from the publisher)

2.2.2 Effects of Intermittent Irradiation on Murine Tumors and Rapid Reoxygenation In Vivo

Using subcutaneously transplanted EMT6 and SCCVII tumors, the effects of 20 Gy in 2, 5 or 10 fractions delivered at various intervals were investigated [8]. Within 24 h from the first irradiation, the tumors were excised, and tumor cell survival was determined *in vitro*. Figure 2.3 shows the results of a 5-fraction experiment. Contrary to the *in vitro* data, no decrease in radiation effects was observed; instead, by placing 2.5-, 7.5-, 10-, or 15-min intervals for EMT6 tumors and 2.5-, 5-, 7.5-, or 15-min intervals for SCCVII tumors, the effect became stronger. Similar results were obtained in 10-fraction experiments. It was speculated that SLDR *in vivo* might be counterbalanced or overweighed by other phenomena such as reoxygenation.

Therefore, reoxygenation at 0–15 min after 13-Gy irradiation in 1-cm-diameter SCCVII tumors was investigated using a paired survival curve assay [9]. As shown in Fig. 2.4, the hypoxic fraction was 100 % at 0 and 2.5 min after the end of the 13-Gy irradiation, but, at 5 min, it fell to 67 % (95 % confidence interval, 41–93 %). Thus, reoxygenation was observed at 5 min after irradiation. It was suggested that rapid reoxygenation could compensate for SLDR *in vivo*. It should be noted, however, that intermittent radiation decreases the radiation effects *in vivo* due to SLDR when reoxygenation is restricted. This was shown in a growth delay assay of SCCVII tumors [9].

2.2.3 Other Laboratory Studies on the Biological Effects of Intermittent Irradiation

In classic studies by Elkind et al. [1, 2], a significant increase in cell survival due to SLDR was observed when intervals of 30 min or longer were set between two
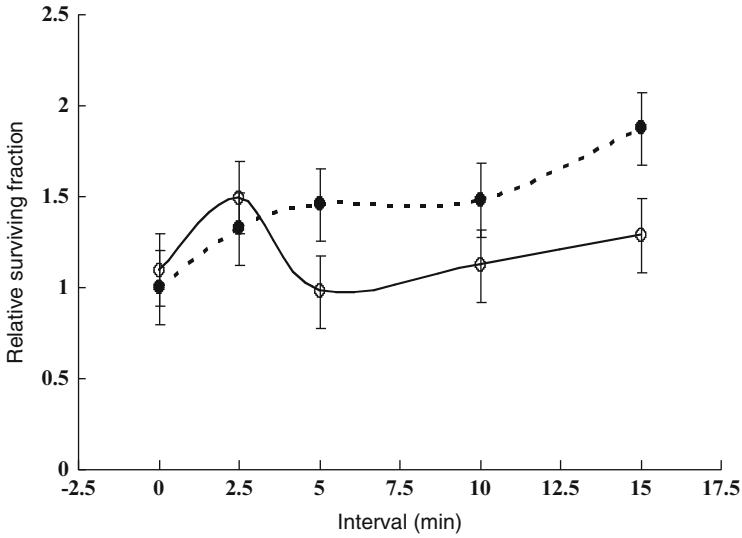
Fig. 2.4 Relative surviving fractions of SCCVII tumor cells after a priming dose of 13 Gy and a second dose of 15 Gy given at 0–15-min intervals to air-breathing (○) or dead (●) mice. The surviving fraction in the dead group that received the second dose immediately after the priming dose was regarded as 1. The hypoxic fraction is given by the surviving fraction of tumor cells in air-breathing mice divided by that in dead mice at respective time points. *Bars* represent SE (Reproduced from Ref. [5] with permission from the publisher)

radiation doses. However, they never investigated shorter intervals. After the 1990s, Benedict et al. [10] attempted to estimate dose-correction factors for stereotactic radiosurgery using U-87MG cells *in vitro*. In their experiments, the effect of radiation decreased with prolongation of the treatment time, and the correction factor of 0.02–0.03 Gy/min was proposed when a total dose of 6–18 Gy was given. This indicates that when the treatment time prolongs by 30 min, 8 Gy would correspond to approximately 7.1–7.4 Gy delivered continuously, giving dose-modifying factors of 1.08–1.13. These results agree with our own.

Moiseenko et al. [11] investigated the correlation between the magnitude of the loss of effect brought about by prolonged radiation delivery and the α/β ratio in three cell lines. When their results were projected to a 30-fraction treatment, the dose deficit to bring cell survival to the same level was 4.1 Gy in one line, but it was as large as 24.9 and 31.1 Gy in the other two lines. The dose deficit did not relate to the α/β ratio of the three cell lines. On the other hand, Zheng et al. [12] also investigated the issue in two hepatocellular carcinoma cell lines, and a significant decrease in cell survival due to prolonged fraction delivery was observed in one line with an α/β ratio of 3.1 Gy but not in another with an α/β ratio of 7.4 Gy. Therefore, the relationship with the α/β ratio remains unclear and requires further investigation.

All these results indicate that SLDR takes place when radiation delivery is prolonged or given intermittently in daily stereotactic irradiation settings. However, it should be noted that these results were obtained using cultured single cells. Until recently, there have been no *in vivo* studies except for our own ones, but other studies have been published. The results of a study by Wang et al. [13] agree with our own; when C57BL mice bearing Lewis lung cancer were irradiated under conditions of limited reoxygenation, intermittent radiation delivery led to a significant reduction in the biological effects. The study by Jiang et al. [14] also showed a similar result. However, more *in vivo* investigations appear to be warranted in the near future. Our study suggests that SLDR *in vivo* can be counterbalanced by reoxygenation. In tumors that reoxygenate rapidly, the adverse effects of prolonging the radiation delivery time may be none or negligible. However, little is known about the reoxygenation in human tumors, so this issue is also an important topic to be investigated in the future to elucidate the effect of intermittent or prolonged radiation delivery in clinical practice.

2.3 Applicability of the LQ Model to High-Dose-per-Fraction Radiotherapy

2.3.1 Current Controversy

To compare different fractionation schedules, the LQ formalism ($n_2d_2/n_1d_1 = (1 + d_1/[\alpha/\beta])/(1 + d_2/[\alpha/\beta])$, where d_1 and d_2 are fractional doses and n_1 and n_2 are fraction numbers) and the biologically effective dose (BED) derived from the LQ model (BED $= D(1 + d/[\alpha/\beta])$, where D is the total dose and d is the fractional dose) are often used because of their convenience and simplicity [4, 15]. While LQ formalism is useful for conversion between relatively low radiation doses as used in conventional radiotherapy, it has been suggested that it is not applicable to higher daily doses or smaller fraction numbers [4, 5]. However, many clinicians have used LQ formalism to convert hypofractionated doses to single doses in their publications [16, 17], and many have used BED to evaluate the doses of stereotactic irradiation [18, 19]. To further complicate the issue, some investigators claim that the LQ model is applicable to stereotactic irradiation [20, 21]. The ground for the latter group is somewhat limited in that the existing clinical data do not significantly deviate from those expected from LQ model calculations, and their data do not necessarily indicate that the LQ model fits best to the high-dose data. Since clinical data usually contain large errors, experimental evaluation of the reliability of the LQ model in single-fraction and hypofractionated radiation schedules appears to be important.

2.3.2 Cell Survival Data for the Reliability of the LQ Model at High Doses per Fraction

The theoretical basis behind the LQ model not being applicable with high doses per fraction is that dose-survival curves for cultured cells cannot be fitted well by the LQ model in high-dose ranges. This has been pointed out for a long time; in the pioneering work of Puck and Markus [22] who established the colony formation assay, the high-dose region of the dose-survival curve was apparently straight in HeLa cells. Therefore, the LQ model, with which the cell survival curve continues to bend downwards at high doses, does not seem to fit the actual curves at high doses. Joiner and Bentzen [4] stated that extrapolation by the LQ model beyond 5–6 Gy per fraction is likely to lack clinically useful precision. More recently, Garcia et al. [23] investigated the compatibility of the LQ model regarding dose-survival curves of 4 cell lines in broad dose ranges. In the 4 lines, the LQ model did not fit the curves at high dose ranges that were >7.5–13 Gy depending on the cell line. Therefore, the inadequacy of the LQ model at high doses was demonstrated.

Our group investigated the reliability of LQ formalism in converting hypofractionated doses (in 2–5 fractions) to single doses in cultured cells and spheroids [24]. The study showed that LQ formalism is inadequate in doing so; the equivalent single doses for the hypofractionated doses calculated by LQ formalism were apparently lower than the equivalent single doses actually measured. LQ formalism underestimated the effect of fractionated irradiation. The magnitudes of errors were 6–19 % for 2- or 3-fraction schedules in V79 and EMT6 single cells, and 18–30 % for 2- to 5-fraction schedules in V79 spheroids. In a more recent study [25], we investigated the applicability of the BED in EMT6 cells. The α/β ratio of the cells determined from single-dose experiments was 3.18 Gy, and a BED3.18 for 20 Gy in 10 fractions was calculated to be 32.6 Gy. Fractional doses yielding the same BED3.18 were calculated for 1-, 2-, 3-, 4-, 5-, 7-, 15- and 20-fraction irradiation using LQ formalism, and then irradiation with these schedules was actually given. The effects of 7-, 15- and 20-fraction irradiation with a BED3.18 of 32.6 Gy were similar to those of the 10-fraction irradiation, while the effects of 1- to 5-fraction irradiation were lower (Fig. 2.5). In this cell line, the LQ model was considered applicable to 7- to 20-fraction irradiation or doses per fraction of 2.57 Gy or smaller.

Since the reoxygenation of hypoxic tumor cells is considered to have a great influence on the compatibility of the LQ model [9, 26], the applicability of LQ formalism for converting hypofractionated doses (in 2–5 fractions) to single doses was evaluated using murine EMT6 tumors [27]. Again, the use of LQ formalism produced large errors; the equivalent single doses for the hypofractionated doses calculated from LQ formalism were much lower than the equivalent single doses actually measured. The magnitudes of errors were larger than those seen in the *in vitro* study; they were 21–31 % for 2- or 3-fraction schedules and 27–42 % for 4- or 5-fraction schedules. The possible larger discrepancy in *in vivo* tumors as compared to *in vitro* single cells and spheroids was considered to be largely due
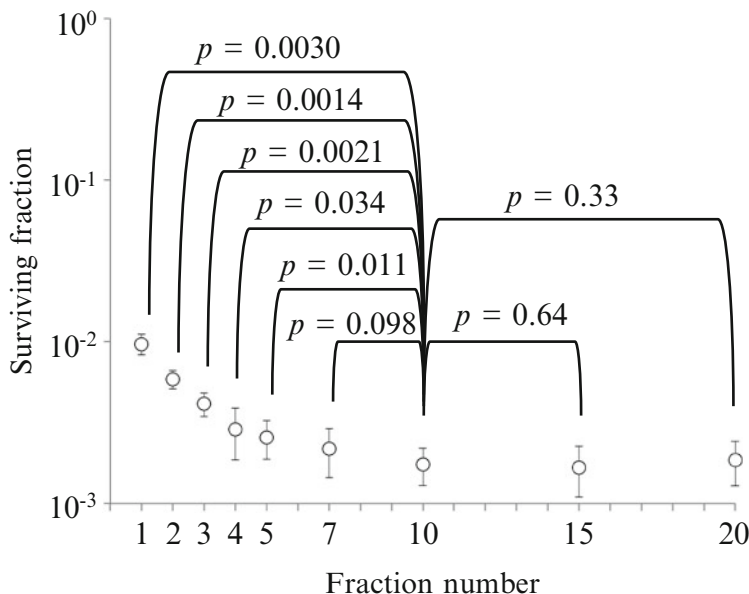
Fig. 2.5 Surviving fractions of EMT6 single cells after single or fractionated irradiation with a BED of 32.6 Gy for an α/β ratio of 3.18 Gy. *Bars* represent standard deviation. If the BED concept is correct, cell survival should be at the same level, irrespective of the fraction number (Reproduced from Ref. [25] with permission from the publisher)

to the reoxygenation during interfraction intervals in the hypofractionated groups. This study clearly showed that LQ formalism is inadequate for high-dose-per-fraction radiotherapy, especially in *in vivo* tumors.

To further evaluate the appropriateness of the BED concept in hypofractionated irradiation, we compared 2- to 5-fraction irradiation schedules simultaneously in the EMT6 tumors in Balb/mice [27]. Total doses of 18–30 Gy were given in 2–5 fractions to the tumor-bearing mice at 4-h intervals, and tumor cell survival was assessed with an *in vivo–in vitro* assay. Cell surviving fractions were plotted against the total dose and BED3.5. In the *in vitro* cell survival determination conducted along with the *in vivo* experiment, the α/β ratio of the cell line was 3.5 Gy, so BED3.5 was adopted as a substitute for "BED10" often used clinically to represent the tumor response. As shown in Fig. 2.6, respective dose-response curves almost overlapped when cell survival was plotted against actual radiation doses. However, the curves tended to shift downwards by increasing the fraction number when cell survival was plotted against BED3.5. If the BED concept is correct, the respective cell survival curves would overlap on this figure. Thus, it seems that BED is inadequate for use in SBRT, especially for tumors. The total dose reflected the actual effect (tumor cell survival) more accurately than BED in this experiment. The calculated BED tended to become larger than expected from the actual effects when the fraction number decreased. Thus, BED tends to overestimate the actual effects with increasing radiation doses.
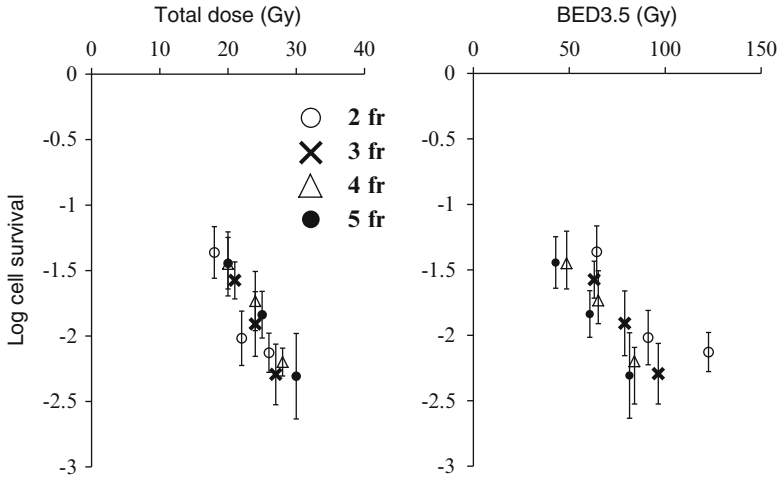
Fig. 2.6 Surviving fractions of EMT6 cells *in vivo* after 2-fraction (○), 3-fraction (X), 4-fraction (△), or 5-fraction (●) irradiation plotted against the total radiation dose and BED3.5. *Bars* represent SE (Reproduced from Ref. [5] with permission from the publisher)

2.3.3 Normal Tissue Response Data for the Reliability of the LQ Model at High Doses per Fraction

The reliability of the LQ model can also be evaluated based on normal tissue data. In classic radiobiology studies, raw data for various normal tissue responses from animal and human studies were presented as a series of dose-response curves [28–31]. Measured responses were plotted against total radiation doses for each schedule. From horizontal cuts, isoeffect doses could be read off, and these isoeffect doses could then be plotted as a log dose against the log number of fractions or log fraction size. Since the isoeffect curves are concave downwards, it is difficult to determine any particular slope for the curves. Instead, the isoeffect curves can be plotted as the reciprocal total dose as a function of the dose per fraction [31]. This reciprocal total dose or F_e plot was elaborated to estimate the α/β ratio of normal tissues [28]. When the normal tissue response data fall in a straight line on this F_e plot, the LQ model is considered to be appropriate. The isoeffect curves for most normal tissues were linear in the dose range of 1–8 Gy [32], suggesting that the LQ model is adequate in this range of dose per fraction. Brenner [21] found that the isoeffect curves for the rat spinal cord response, mouse skin reaction, and murine intestinal damage could be visually fitted with straight lines in the dose range between 0 and 25 Gy, and insisted that the LQ model is applicable throughout this dose range. However, statistical validation of the linearity was not performed. Later, Astrahan [33] analyzed the data for various normal tissues in more detail, and found that the LQ formula closely fitted the curve for the late reaction of the mouse spinal cord for fractions up to about 10 Gy. However, the data

for cervical vascular damage did not fit the LQ model but fitted the linear-quadratic-linear (LQL) model, which is stated later. Fowler et al. [34] suggested that for certain epithelial tissues, the LQ model may be applicable up to 23 Gy per fraction.

These observations are somewhat contradictory and confusing, but the discrepancy may be, in part, explained by the α/β ratio for the normal tissue responses. The applicability of the LQ model may not simply depend on the absolute dose per fraction; for a tissue with a large α/β ratio, its applicability may be extended to a higher dose region. This is the case with epithelial tissues that usually have an α/β ratio of around 10 Gy. Since the α/β ratio represents the dose at which cell killing from linear (α) and quadratic (β) components of the LQ formula is equal, the LQ model holds around the dose level of the α/β ratio. However, with the increase in the dose, the β cell kill component dominates in the LQ model, from which actual cell-survival data have been shown to deviate. This deviation appears to become evident in the dose range over two-fold the α/β ratio [23]. From these considerations, it may be said that the model is applicable up to a radiation dose approximately two-fold the α/β ratio.

Recently, Borst et al. [35] analyzed radiation pneumonitis data in patients undergoing SBRT. Various fractionation schedules were employed ranging from 35 Gy in 4 fractions to 60 Gy in 8 fractions. They tried to correlate the mean lung dose with the occurrence of radiation pneumonitis. They found that the data were best fitted by the LQ model with an α/β ratio of 3 Gy. Although the prescribed dose per fraction was 7.5–12 Gy, the mean lung dose per fraction is usually much lower, so it is not surprising that the LQ model fitted their mean lung dose data.

2.3.4   Other Alternatives to the LQ Model

Since it is becoming clearer that LQ formalism is not adequate for stereotactic irradiation, other models have been proposed. These include the universal survival curve model [36], LQL model [37] (or modified LQ model [38]), and generalized LQ (gLQ) model [39]. The universal survival curve model hybridizes the LQ model for low doses and the classic multi-target model ($S = 1-(1-e^{-D/D0})^n$, where S is the surviving fraction, D is the dose, D_0 is a parameter that determines the final slope of the survival curve, and n is the y-intercept of the asymptote) [40] for high doses beyond a single transition dose (D_T). Hence the concept is relatively simple. The LQL model derived from a mechanism-based lethal-potentially lethal model [41] has a mechanistic basis. Although the equations for the LQL model are more complex, cell survival curves extend nearly linearly in a high-dose range, as compared to the LQ model [37]. Therefore, the applicability of the universal survival curve model and LQL model to a high-dose region may be similar. The most recently proposed gLQ model takes SLDR and the conversion of sublethal damage to lethal damage during irradiation into account; the model is designed to cover any dose delivery patterns. All of these newer models seem to fit better than

the LQ model in the high-dose range. We have also evaluated how the LQ and other models fit experimental data. In an *in vitro* study, the classic multitarget model and the repairable-conditionally repairable model tended to fit better than the LQ model at high doses [42]. In the near future, it is desirable for an optimal model to be established for clinical use in high-dose-per-fraction radiotherapy. However, it should be noted that these models are generally applicable to the normal tissue response, especially late damage, and not to tumors, since none of these models takes the reoxygenation phenomenon, as well as cell cycle effects, host immune effects, and effects on vascular/stromal elements, into account. When the overall treatment time becomes longer than that conventionally used, a factor deriving from repopulation should also be considered [43, 44]. In future studies, models that incorporate these factors as well as reoxygenation should be developed in order to use the models for *in vivo* tumor responses to high-dose-per-fraction irradiation and more conventional radiotherapy.

2.4   Radiobiological Effects of High Doses per Fraction

2.4.1   Vascular Damage at High Doses and Secondary Cell Killing

Several investigators reported that high fractional doses of radiation have biological effects higher than predicted by direct tumor cell killing [45]. Park et al. [46] suggested that radiation doses of 10 Gy or higher induce vascular damage, leading to indirect tumor cell death. In an old study, it is shown that clonogenic fractions of Walker 256 rat tumors fell over the first 4 days after irradiation, and this is claimed to be due to vascular damage [47]. Although this is an interesting hypothesis, the data to support it are still fragmentary. In contrast, other data show no evidence of the increased cell kill as a function of time after 10 or 20 Gy irradiation in a rat rhabdomyosarcoma [48]. Thus, more experimental evidences are necessary to suggest that this potential mechanism plays a role in the sensitivity of tumors after high-dose-per-fraction radiotherapy.

2.4.2   Enhanced Antitumor Immunity After Irradiation to Tumor

In metastatic melanoma patients, SBRT to a tumor was reported to contribute to an immunologic rejection of a metastatic lesion at a distant site [49, 50]. Since the data have been reported only for two patients, it remains unclear whether this phenomenon is produced only at high doses per fraction and whether other tumors besides

melanoma experience this effect. Other preclinical data also suggest that radiation enhances the antigenicity of tumors [51–53]. It has been reported that this is greater for fractionated irradiation than for single doses [54]. Radiation schedules tested were similar to those employed in SBRT: 20 Gy × 1, 8 Gy × 3, and 6 Gy × 5 fractions in consecutive days. Among the schedules, the fractionated 8 Gy was the most effective, with the 6 Gy intermediate and the 20 Gy the least effective. Another preclinical study reported a similar enhancement of antitumor immunity by local tumor irradiation, but in the study single 20 Gy had a greater effect than 5 Gy × 4 over 2 weeks [55]. More information is needed to recommend the best doses per fraction and timing of the radiation regimen to optimize this effect. Of major importance is just how general the phenomena of enhanced antitumor immunity by high-dose-per-fraction radiotherapy will be across the spectrum of tumors undergoing radiation therapy.

2.4.3 Importance of Tumor Hypoxia and Reoxygenation

It is now well recognized that most human tumors except for very small ones have radioresistant hypoxic cells. The negative influence of hypoxic cells against local tumor control is apparently greater in hypofractionated radiotherapy and the greatest in single-fraction treatment. In 1-fraction SBRT, it is not possible to utilize the very favorable phenomenon of reoxygenation of hypoxic tumor cells. In 2-fraction treatment, the reoxygenation utilization rate is 50 %, and with increase in the fraction number, this utilization rate goes up to 75 % for 4-fraction treatment, 83 % for 6-fraction treatment and 88 % for 8-fraction treatment. In 30-fraction treatment, this rate is 97 %, so the authors think that 6- to 8-fraction treatment may be reasonably efficient to utilize the reoxygenation phenomenon. In future SBRT studies, this fact should be taken into account in planning the optimal fractionation schedule.

In view of the greater negative influence of hypoxic tumor cells in SBRT, treatment strategies against hypoxic cells are more important than in conventional radiotherapy. Hypoxic cell radiosensitizers did not prove to be very efficient when combined with conventional radiotherapy [56], but they may have a greater chance of success when combined with SBRT. When 2-nitroimidazole sensitizers were combined with intraoperative radiotherapy where a single dose of 20 Gy or higher is usually employed, they led several patients with unresectable nonmetastatic pancreatic cancer to cure [57, 58]. Therefore, studies of nitroazole radiosensitizers in combination with SBRT are encouraged. The use of other agents that exert specific effects against hypoxic cells are also welcome. With the aid of hypoxia-targeting strategies, SBRT is expected to further develop as an alternative to surgery in many tumors.

References

1. Elkind MM, Sutton H. Radiation response of mammalian cells grown in culture. I. Repair of X-ray damage in surviving Chinese hamster cells. Radiat Res. 1960;13:556–93.
2. Elkind MM, Sutton-Gilbert H, Moses WB, et al. Radiation response of mammalian cells grown in culture. V. Temperature dependence of the repair of X-ray damage in surviving cells (aerobic and hypoxic). Radiat Res. 1965;25:359–76.
3. Kirkpatrick JP, Meyer JJ, Marks LB. The linear-quadratic model is inappropriate to model high dose per fraction effects in radiosurgery. Semin Radiat Oncol. 2008;18:240–3.
4. Joiner MC, Bentzen SM. Fractionation: the linear-quadratic approach. In: Joiner M, van der Kogel A, editors. Basic clinical radiobiology. London: Hodder Arnold; 2009. p. 102–19.
5. Shibamoto Y, Otsuka S, Iwata H, et al. Radiobiological evaluation of the radiation dose as used in high-precision radiotherapy: effect of prolonged delivery time and applicability of the linear-quadratic model. J Radiat Res. 2012;53:1–9.
6. Shibamoto Y, Ito M, Sugie C, et al. Recovery from sublethal damage during intermittent exposures in cultured tumor cells: implications for dose modification in radiosurgery and IMRT. Int J Radiat Oncol Biol Phys. 2004;59:1484–90.
7. Ogino H, Shibamoto Y, Sugie C, et al. Biological effects of intermittent radiation in cultured tumor cells: influence of fraction number and dose per fraction. J Radiat Res. 2005;46:401–6.
8. Sugie C, Shibamoto Y, Ito M, et al. The radiobiological effect of intermittent radiation exposure in murine tumors. Int J Radiat Oncol Biol Phys. 2006;64:619–24.
9. Tomita N, Shibamoto Y, Ito M, et al. Biological effect of intermittent radiation exposure in vivo: recovery from sublethal damage versus reoxygenation. Radiother Oncol. 2008;86:369–74.
10. Benedict SH, Lin PS, Zwicker RD, et al. The biological effectiveness of intermittent irradiation as a function of overall treatment time: development of correction factors for linac-based stereotactic radiotherapy. Int J Radiat Oncol Biol Phys. 1997;37:765–9.
11. Moiseenko V, Duzenli C, Durand RE, et al. In vitro study of cell survival following dynamic MLC intensity-modulated radiation dose delivery. Med Phys. 2007;34:1514–20.
12. Zheng XK, Chen LH, Yan X, et al. Impact of prolonged fraction dose-delivery time modeling intensity-modulated radiation therapy on hepatocellular carcinoma cell killing. World J Gastroenterol. 2005;11:1452–6.
13. Wang X, Xiong XP, Lu J, et al. The in vivo study on the radiobiologic effect of prolonged delivery time to tumor control in C57BL mice implanted with Lewis lung cancer. Radiat Oncol. 2011;6:4.
14. Jiang L, Xiong XP, Hu CS, et al. In vitro and in vivo studies on radiobiological effects of prolonged fraction delivery time in A549 cells. J Radiat Res. 2013;54:230–4.
15. Withers HR, Thames Jr HD, Peters LJ, et al. A new isoeffect curve for change in dose per fraction. Radiother Oncol. 1983;1:187–91.
16. Wulf J, Baier K, Mueller G, et al. Dose-response in stereotactic irradiation of lung tumors. Radiother Oncol. 2005;77:83–7.
17. Milano MT, Katz AW, Schell MC, et al. Descriptive analysis of oligometastatic lesions treated with curative-intent stereotactic body radiotherapy. Int J Radiat Oncol Biol Phys. 2008;72:1516–22.
18. Onishi H, Shirato H, Nagata Y, et al. Stereotactic body radiotherapy (SBRT) for operable stage I non-small-cell lung cancer: can SBRT be comparable to surgery? Int J Radiat Oncol Biol Phys. 2011;81:1352–8.
19. Takeda A, Sanuki N, Kunieda E, et al. Stereotactic body radiotherapy for primary lung cancer at a dose of 50 Gy total in five fractions to the periphery of the planning target volume calculated using a superposition algorithm. Int J Radiat Oncol Biol Phys. 2009;73:442–8.
20. Guckenberger M, Klement RJ, Allgaeuer M, et al. Applicability of the linear-quadratic formalism for modeling local tumor control probability in high dose per fraction stereotactic

body radiotherapy for early stage non-small cell lung cancer. Radiother Oncol. 2013;109:13–20.

21. Brenner DJ. The linear-quadratic model is an appropriate methodology for determining iso-effective doses at large doses per fraction. Semin Radiat Oncol. 2008;18:234–9.

22. Puck TT, Marcus PI. Action of X-rays on mammalian cells. J Exp Med. 1956;103:653–66.

23. Garcia LM, Leblanc J, Wilkins D, et al. Fitting the linear-quadratic model to detailed data sets for different dose ranges. Phys Med Biol. 2006;51:2813–23.

24. Iwata H, Shibamoto Y, Murata R, et al. Estimation of errors associated with use of linear-quadratic formalism for evaluation of biologic equivalence between single and hypofractionated radiation doses: an in vitro study. Int J Radiat Oncol Biol Phys. 2009;75:482–8.

25. Miyakawa A, Shibamoto Y, Otsuka S, Iwata H. Applicability of the linear-quadratic model to single and fractionated radiotherapy schedules: an experimental study. J Radiat Res. 2014;55:451–4.

26. Murata R, Shibamoto Y, Sasai K, et al. Reoxygenation after single irradiation in rodent tumors of different types and sizes. Int J Radiat Oncol Biol Phys. 1996;34:859–65.

27. Otsuka S, Shibamoto Y, Iwata H, et al. Compatibility of the linear-quadratic formalism and biologically effective dose concept to high-dose-per-fraction irradiation in a murine tumor. Int J Radiat Oncol Biol Phys. 2011;81:1538–43.

28. Douglas BG, Fowler JF. The effect of multiple small doses of x rays on skin reactions in the mouse and a basic interpretation. Radiat Res. 1976;66:401–26.

29. van der Kogel AJ. Chronic effects of neutrons and charged particles on spinal cord, lung, and rectum. Radiat Res. 1985;8(Suppl):S208–16.

30. Peck JW, Gibbs FA. Mechanical assay of consequential and primary late radiation effects in murine small intestine: alpha/beta analysis. Radiat Res. 1994;138:272–81.

31. Fowler JF. Total doses in fractionated radiotherapy – implications of new radiobiological data. Int J Radiat Biol. 1984;46:103–20.

32. Fowler JF. The linear-quadratic formula and progress in fractionated radiotherapy. Br J Radiol. 1989;62:679–94.

33. Astrahan M. Some implications of linear-quadratic-linear radiation dose-response with regard to hypofractionation. Med Phys. 2008;35:4161–72.

34. Fowler JF, Tomé WA, Fenwick JD, et al. A challenge to traditional radiation oncology. Int J Radiat Oncol Biol Phys. 2004;60:1241–56.

35. Borst GR, Ishikawa M, Nijkamp J, et al. Radiation pneumonitis after hypofractionated radiotherapy: evaluation of the LQ(L) model and different dose parameters. Int J Radiat Oncol Biol Phys. 2010;77:1596–603.

36. Park C, Papiez L, Zhang S, et al. Universal survival curve and single fraction equivalent dose: useful tools in understanding potency of ablative radiotherapy. Int J Radiat Oncol Biol Phys. 2008;70:847–52.

37. Guerrero M, Carlone M. Mechanistic formulation of a linear-quadratic-linear (LQL) model: split-dose experiments and exponentially decaying sources. Med Phys. 2010;37:4173–81.

38. Guerrero M, Li XA. Extending the linear-quadratic model for large fraction doses pertinent to stereotactic radiotherapy. Phys Med Biol. 2004;49:4825–35.

39. Wang JZ, Huang Z, Lo SS, et al. A generalized linear-quadratic model for radiosurgery, stereotactic body radiation therapy, and high-dose rate brachytherapy. Sci Transl Med. 2010;2:39ra48.

40. Butts JJ, Katz R. Theory of RBE for heavy ion bombardment of dry enzymes and viruses. Radiat Res. 1967;30:855–71.

41. Curtis SB. Lethal and potentially lethal lesions induced by radiation – a unified repair model. Radiat Res. 1986;106:252–70.

42. Iwata H, Matsufuji N, Toshito T, et al. Compatibility of the repairable-conditionally repairable, multi-target and linear-quadratic models in converting hypofractionated radiation doses to single doses. J Radiat Res. 2013;54:367–73.

43. Scott OC. Mathematical models of repopulation and reoxygenation in radiotherapy. Br J Radiol. 1990;63:821–3.
44. Nakamura K, Brahme A. Evaluation of fractionation regimen in stereotactic radiotherapy using a mathematical model of repopulation and reoxygenation. Radiat Med. 1999;17:219–25.
45. Brown JM, Carlson DJ, Brenner DJ. The tumor radiobiology of SRS and SBRT: are more than the 5 Rs involved? Int J Radiat Oncol Biol Phys. 2014;88:254–62.
46. Park HJ, Griffin RJ, Hui S, et al. Radiation-induced vascular damage in tumors: implications of vascular damage in ablative hypofractionated radiotherapy (SBRT and SRS). Radiat Res. 2012;177:311–27.
47. Song CW, Cho LC, Yuan J, et al. Radiobiology of stereotactic body radiation therapy/stereotactic radiosurgery and the linear-quadratic model. Int J Radiat Oncol Biol Phys. 2013;87:18–9.
48. Barendsen GW, Broerse JJ. Experimental radiotherapy of a rat rhabdomyosarcoma with 15 MeV neutrons and 300 kV x-rays. I. Effects of single exposures. Eur J Cancer. 1969;5:373–91.
49. Hiniker SM, Chen DS, Knox SJ. Abscopal effect in a patient with melanoma. N Engl J Med. 2012;366:2035. author reply 2035–2036.
50. Postow MA, Callahan MK, Barker CA, et al. Immunologic correlates of the abscopal effect in a patient with melanoma. N Engl J Med. 2012;366:925–31.
51. Lugade AA, Moran JP, Gerber SA, et al. Local radiation therapy of B16 melanoma tumors increases the generation of tumor antigenspecific effector cells that traffic to the tumor. J Immunol. 2005;174:7516–23.
52. Apetoh L, Ghiringhelli F, Tesniere A, et al. Toll-like receptor 4-dependent contribution of the immune system to anticancer chemotherapy and radiotherapy. Nat Med. 2007;13:1050–9.
53. Matsumura S, Wang B, Kawashima N, et al. Radiation-induced CXCL16 release by breast cancer cells attracts effector T cells. J Immunol. 2008;181:3099–107.
54. Dewan MZ, Galloway AE, Kawashima N, et al. Fractionated but not single-dose radiotherapy induces an immune-mediated abscopal effect when combined with anti-CTLA-4 antibody. Clin Cancer Res. 2009;15:5379–88.
55. Lee Y, Auh SL, Wang Y, et al. Therapeutic effects of ablative radiation on local tumor require CD8. T cells: changing strategies for cancer treatment. Blood. 2009;114:589–95.
56. Shibamoto Y, Sugie C, Ito M, Ogino H. The Japanese experiences with hypoxia-targeting pharmacoradiotherapy: from hypoxic cell sensitizers to radiation-activated prodrugs. Expert Opin Pharmacother. 2004;5:2459–67.
57. Shibamoto Y, Ohshio G, Hosotani R, Nishimura Y, Manabe T, Imamura M, et al. A phase I/II study of a hypoxic cell radiosensitizer KU-2285 in combination with intraoperative radiotherapy. Br J Cancer. 1997;76:1474–9.
58. Karasawa K, Sunamura M, Okamoto A, Nemoto K, Matsuno S, Nishimura Y, et al. Efficacy of novel hypoxic cell sensitiser doranidazole in the treatment of locally advanced pancreatic cancer: long-term results of a placebo-controlled randomised study. Radiother Oncol. 2008;87:326–30.

Chapter 3
Physics

Teiji Nishio

3.1 Electromagnetic Wave: X-Rays, Gamma Rays

Electromagnetic waves exhibit wave-particle duality, which means that they have the properties of both particles and waves. Photons travel at the speed of light, and their frequency ν, wavelength λ, and the speed of light c are related by the following equation:

$$\text{c[m/s]} = \lambda \cdot \nu = 3.0 \times 10^8. \tag{3.1}$$

The radiation used in radiation therapy includes high-energy X-rays and gamma rays, which are types of electromagnetic waves. Their energy in radiation therapy is expressed in the unit of MeV. The energy of an electromagnetic wave E is expressed by the following equation including Planck's constant h:

$$E[\text{MeV}] = h \cdot \nu = \frac{h \cdot c}{\lambda} \approx 4.14 \times 10^{-21} \cdot \nu\left[\text{s}^{-1}\right] \approx 1.24 \times 10^{-12}/\lambda[\text{m}]. \tag{3.2}$$

As shown in Fig. 3.1, when matter is irradiated with an incident charged particle, an electromagnetic wave is released from outside of the nucleus in the form of an X-ray, while one is released by the nucleus in the form of a gamma ray. When the incident charged particle is an electron, bremsstrahlung is produced when the direction of the electron is deflected by the Coulomb force of the nucleus of the matter during its passage through the matter.

T. Nishio (✉)

Particle Therapy Division, Research Center for Innovative Oncology, National Cancer Center, 6-5-1 Kashiwanoha, Kashiwa-shi, Chiba 277-8577, Japan
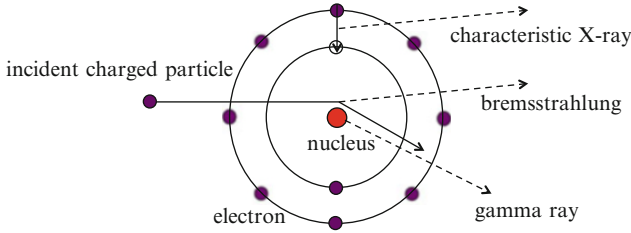e-mail: tnishio@east.ncc.go.jp

Fig. 3.1 The release of X-rays and gamma rays

Characteristic X-rays are electromagnetic radiation with a certain energy whose release corresponds to the filling of an outer-shell electron vacancy produced by the emission of an inner-shell electron of an atom of matter.

3.2 Interactions of Photons with Matter

Interactions of photons with matter depend on the energy of the photons. These interactions include the photoelectric effect, Rayleigh scattering (coherent scattering), Compton scattering (incoherent scattering), pair production, and photonuclear reaction. In radiation therapy, transfer of the energy possessed by photons to matter (i.e. a tumor) is important; it is necessary for this energy to be transferred from photons to electrons, which are charged particles. Therefore, the photoelectric effect, Compton scattering, and pair production are important interactions of photons with matter in radiation therapy (see Fig. 3.2).

3.2.1 Photoelectric Effect

The photoelectric effect is a reaction involving the loss of energy that is caused when photons of relatively low energy are absorbed by matter and bound electrons of atoms or molecules in that matter are released. The maximum kinetic energy E_e that is carried by an electron is given by the following equation. The term W is the work function, which means the minimum energy required to remove an electron from the binding of an atom or a molecule in the matter.

$$E_e \leq E - W, \quad E = h \cdot \nu. \tag{3.3}$$

The energy of a photon absorbed by the matter produces excitation of an atom; this excited atom then returns to its stable ground state by ejecting an Auger electron and an X-ray. Figure 3.3 shows the results of the mass attenuation coefficients $\mu_m = \mu/\rho$ for water, silver, and lead and the cross section as a function of the energy of the incident photon in the photoelectric effect [1]. The term ρ is the

photoelectric effect

$$\sigma_{photo}(E) \propto \frac{Z^5}{E^{3.5}}$$

$E \sim$ keV

pair production

$$\sigma_{pair}(E) \propto Z^2 \cdot E$$

$E \sim$ (mid.-high) MeV

Compton effect

$$\sigma_{comp}(E) \propto \frac{Z}{E} \cdot \log E$$

$E \sim$ (low-mid.) MeV
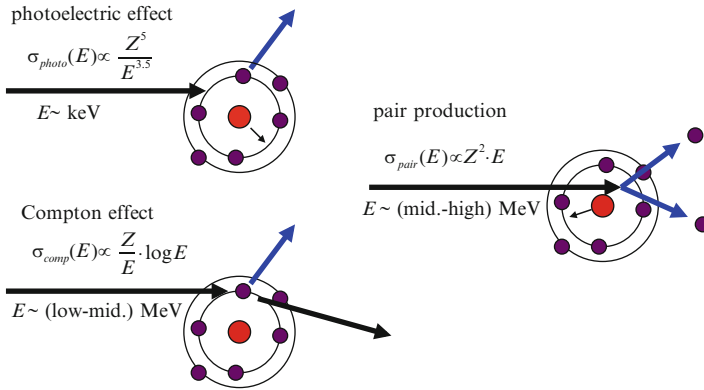
Fig. 3.2 The interactions of incident photons with matter
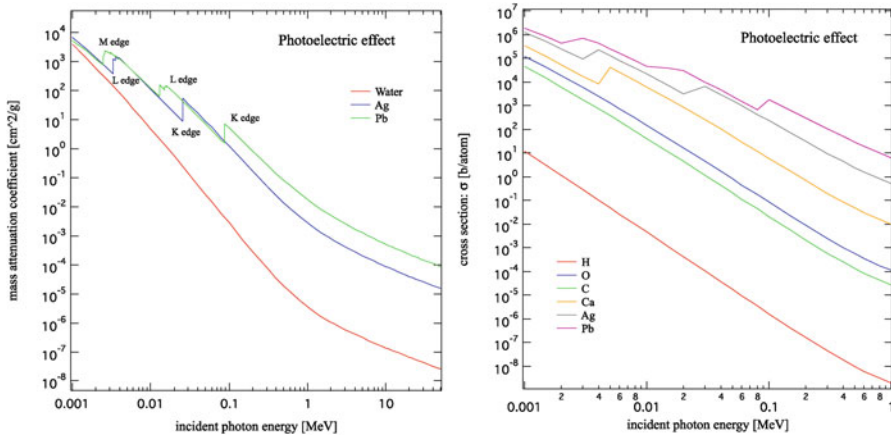
Fig. 3.3 The mass attenuation coefficient and the cross section as functions of the energy of the incident photon in the photoelectric effect [1]

density and μ is the attenuation coefficient. The photoelectric effect tends to emit inner-shell electrons (K-shell, L-shell, and M-shell), which are bound at a higher level of energy; in this regard, the effect causes a physical phenomenon in which an atom made unstable by absorption of the energy of a photon releases a high level of energy each time, but with a smaller number of reactions. As a result, the plot for the cross section of the photoelectric effect shows changes in a stepwise manner according to the bound energies of electrons (see Fig. 3.3).

The cross section of the photoelectric effect is approximately inversely proportional to the 3.5th power of energy of the incident photon and proportional to the 5th power of the atomic number of the matter. In addition, it is proportional to the 3.5th power of the effective atomic number of the matter.
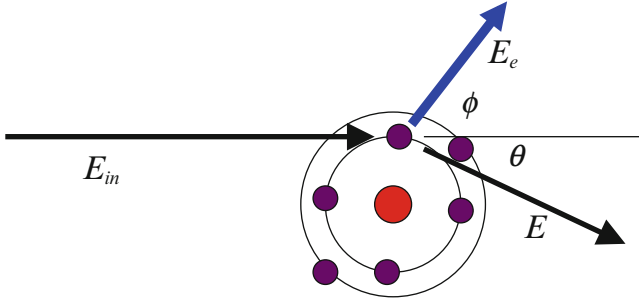
Fig. 3.4 The Compton effect

3.2.2 Compton Scattering

Compton scattering is a scattering phenomenon between a photon and an electron that is caused when the energy of the incident photon is much higher than the bound energy of the electron. The electron is given some of the energy of the incident photon and travels with that given energy as its kinetic energy, while the scattered photon loses energy. When the energy of the incident photon is far lower than the mass energy of the electron, the incident photon hardly loses energy by scattering with an electron. This phenomenon is called Thomson scattering. It is not necessary to consider this scattering phenomenon for photons with energy on the order of MeV, as used in radiation therapy.

As represented in Fig. 3.4, the following equation is given by the law of conservation of momentum and energy in Compton scattering:

$$E = \frac{E_{in}}{1 + \gamma \cdot (1 - \cos\theta)}, \quad E_e = \frac{2 \cdot \gamma \cdot \cos^2\phi}{(1 + \gamma)^2 - \gamma^2 \cdot \cos^2\phi},$$
$$\cot\left(\frac{\theta}{2}\right) = (1 + \gamma) \cdot \tan\phi, \quad \gamma = \frac{E_{in}}{m_e \cdot c^2}. \tag{3.4}$$

where E_{in} is the energy of the incident photon, E is the energy of the scattered photon, θ is the scattering angle of the scattered photon, E_e is the energy of the recoil electron, and ϕ is the scattering angle of the recoil electron. The quantity of $m_e \cdot c^2 \approx 0.511[\text{MeV}]$ is the rest mass energy of an electron. A recoil electron receives the maximum energy by Compton scattering when the scattering angle of the recoil electron $\phi = 0(\theta = \pi)$; and the following equation can then be derived from Eq. (3.4):

$$E_e \leq E_e(\phi = 0) = E_{in} \cdot \frac{2 \cdot \gamma}{1 + 2 \cdot \gamma}. \tag{3.5}$$

The edge of the energy spectrum of a recoil electron with the maximum recoil energy is called the Compton edge. The difference between the wavelength of an

Fig. 3.5 The differential cross section of Compton scattering for every angle of a scattered photon as a function of the energy of the incident photon
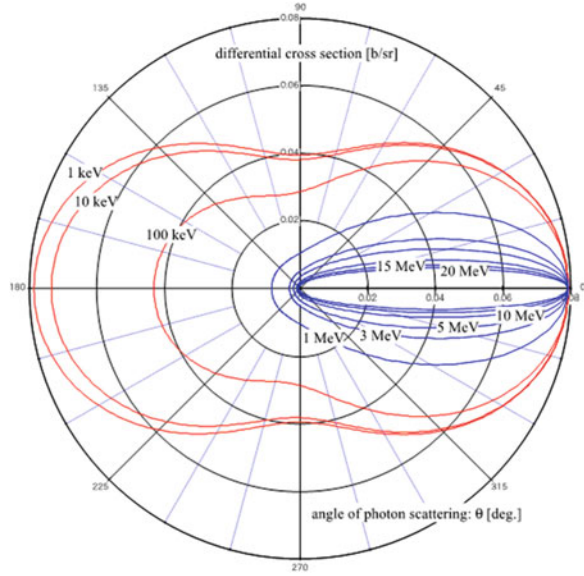
incident photon and that of a scattered photon depends on the scattering angle θ, not on the energy of the incident photon or the scattered photon.

The differential cross section of Compton scattering per unit of solid angle is given by the Klein-Nishina formula:

$$\frac{d\sigma_{comp}(E_{in})}{d\Omega} = r_e^2 \cdot \frac{(1 + \cos^2\theta)}{2\{1 + \gamma \cdot (1 - \cos\theta)\}^2}$$

$$\times \left[1 + \gamma^2 \cdot \frac{(1 - \cos\theta)^2}{(1 + \cos\theta)^2 \cdot \{1 + \gamma \cdot (1 - \cos\theta)\}}\right]. \qquad (3.6)$$

$$r_e = \frac{e^2}{m_e \cdot c^2} \approx 2.818 \times 10^{-13}[cm]. \qquad (3.7)$$

The term r_e is the classical electron radius. Figure 3.5 shows the results of calculation for the differential cross section of Compton scattering for every angle of a scattered photon as a function of the energy of the incident photon using Eqs. (3.6) and (3.7). The red lines in the figure represent the cases of incident photons with energy in the range of 1–100 keV, while the blue lines show those in the range of 1–10 MeV. As shown in the figure, the possibility of causing forward scattering increases when the energy of the incident photon becomes higher. This possibility is extremely high and Compton scattering tends to deposit energy of the incident photon forward for energy on the order of MeV (blue line in the figure), as used in radiation therapy.

The total cross section of Compton scattering σ_{comp} is given by integrating the differential cross section of Compton scattering (Eq. (3.6)) with the total solid angle. The result of the integral calculation is shown in Eq. (3.8).

$$\sigma_{comp}(E_{in}) = \int_0^{4\cdot\pi} (d\sigma_{comp}(E_{in})/d\Omega)d\Omega$$

$$= 2\cdot\pi\cdot r_e^2 \cdot \left[\frac{1+\gamma}{\gamma^2}\cdot\left\{\frac{2\cdot(1+\gamma)}{1+2\cdot\gamma}-\frac{1}{\gamma}\cdot\ln(1+2\cdot\gamma)\right\}+\frac{1}{2\cdot\gamma}\cdot\ln(1+2\cdot\gamma)-\frac{1+3\cdot\gamma}{(1+2\cdot\gamma)^2}\right].$$

$$(3.8)$$

When the total cross section of Compton scattering is divided into the cross section of the Compton scattered photon σ_s and the cross section of the recoil electron σ_a, the following equation is given:

$$\sigma_{comp}(E_{in}) = \sigma_s(E_{in}) + \sigma_a(E_{in}).\qquad(3.9)$$

$$\sigma_s(E_{in}) = \int_0^{4\cdot\pi} \left[\{1+\gamma\cdot(1-\cos\theta)\}^{-1}\cdot(d\sigma_{comp}(E_{in})/d\Omega)\right]d\Omega$$

$$(3.10)$$

$$= \pi\cdot r_e^2 \cdot \left[\frac{1}{\gamma^3}\cdot\ln(1+2\cdot\gamma)+\frac{2\cdot(1+\gamma)\cdot(2\cdot\gamma^2-2\cdot\gamma-1)}{\gamma^2\cdot(1+2\cdot\gamma)^2}+\frac{8\cdot\gamma^2}{3\cdot(1+2\cdot\gamma)^3}\right].$$

Figure 3.6 shows the results of calculation for the total cross section of the Compton scattering, the cross section of the Compton scattered photon and the cross section of the recoil electron as a function of the energy of the incident photon using Eqs. (3.8), (3.9), and (3.10). The figure shows that Compton scattering decreases as the energy of the incident photon increases.

3.2.3   Pair Production

Pair production is the phenomenon of the creation of a pair of an electron and a positron when an incident photon passes through a nearby atomic nucleus. Therefore, pair production does not occur in a vacuum. The generation of this phenomenon requires the energy of an incident photon to be greater than the total mass energy of an electron and a positron. In addition, the mass energy of an electron is the same as that of a positron. The total kinetic energy of an electron and that of a positron after pair production are expressed by the following equation because the recoil energy of an atom can be ignored in pair production.

$$E_+ + E_- = E_{in} - 2\cdot m_e\cdot c^2 = E_{in} - 1.022[\text{MeV}].\qquad(3.11)$$

The term E_- is the kinetic energy of an electron and E_+ is the kinetic energy of a positron. The kinetic energy of an incident photon is divided into an electron and a
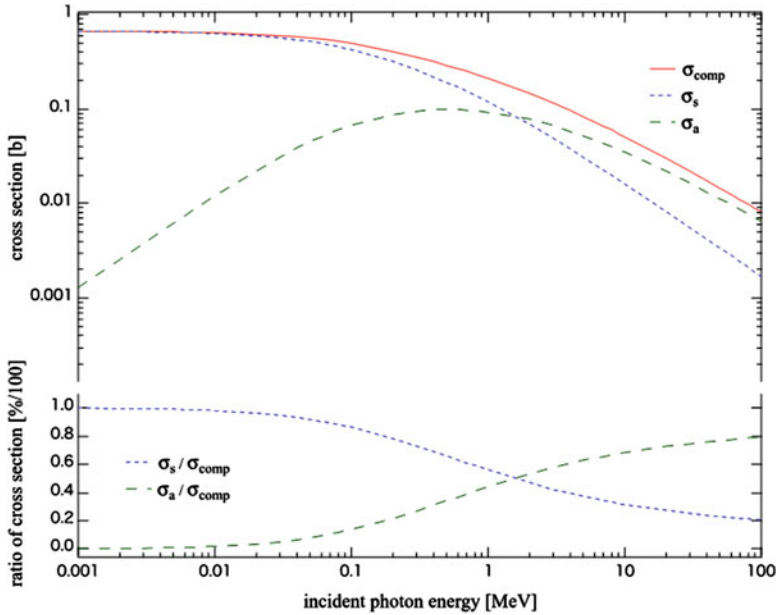
Fig. 3.6 The cross section of Compton scattering as a function of the energy of the incident photon

positron equally when the energy of the incident photon is low, while the division of the energy occurs unequally when the energy of the incident photon is high.

The cross section of pair production is zero in the case of the energy of an incident photon under the threshold energy 1.022 MeV, but it is proportional to the energy of an incident photon that is over this threshold. When the energy of an incident photon is high, the cross section increases slowly and is proportional to $\ln E_{in}$. It is also proportional to the second power of the atomic number of the matter.

3.3   Photon Flux in Matter

When a photon enters matter, the photon flux decreases by five interactions in matter: the photoelectric effect, Rayleigh scattering, Compton scattering, pair production, and photonuclear reaction. Figure 3.7 shows a schematic diagram of photon flux passing through matter. The relational equation is as follows:

$$I_{out} = I_{in} \cdot \exp(-\mu \cdot d), \tag{3.12}$$

where, d is the thickness of matter, I_{in} is the incident photon flux, I_{out} is the photon flux after passing through matter, and μ is the linear attenuation coefficient.
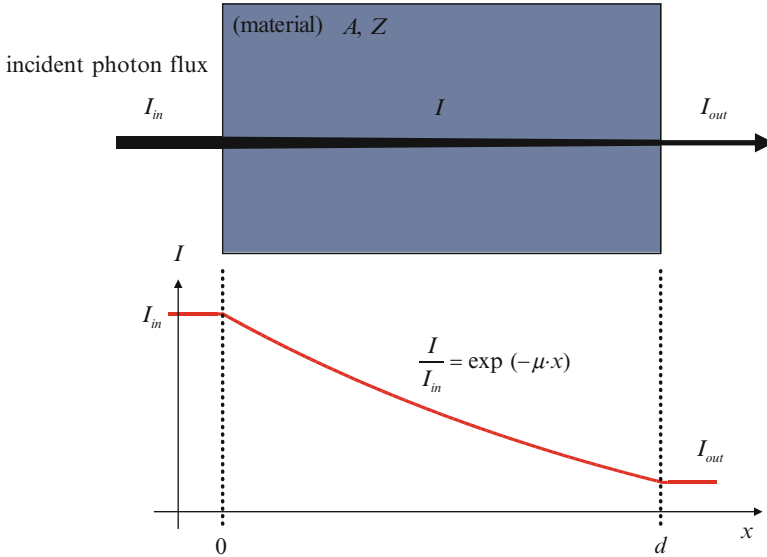
Fig. 3.7 Schematic diagram of photon flux upon passing through matter

The linear attenuation coefficient μ represents the amount of decrease per unit length in matter. It can approximate the total of the linear attenuation coefficient of the photoelectric effect μ_{phot}, Compton scattering μ_{comp}, and pair production μ_{pair} in the case of an incident photon with energy on the order of MeV, as used in radiotherapy.

$$\mu(E) = \sum_i \mu_i(E) \approx \mu_{phot}(E) + \mu_{comp}(E) + \mu_{pair}(E). \qquad (3.13)$$

The relationship between the linear attenuation coefficient μ and the cross section σ for interactions of photons in matter is expressed by $\mu = n \cdot \rho$, using the density ρ and the number density of matter n. In addition, the number density can be expressed by $n = \rho \cdot N_A/A$ using the mass number A and Avogadro's constant N_A. Consequently, the linear attenuation coefficient is given by the following Eq. (3.14):

$$\mu(E) \approx \rho \cdot \frac{N_A}{A} \cdot \left(\sigma_{photo}(E) + Z \cdot \sigma_{comp}(E) + \sigma_{pair}(E) \right). \qquad (3.14)$$

where, σ_{photo}, σ_{comp}, and σ_{pair} are the reaction cross section of the photoelectric effect, Compton scattering, and pair production, respectively.

Figure 3.8 shows the mass attenuation coefficient μ_m, which is calculated by dividing the linear attenuation coefficient μ by the density ρ, for each interaction as a function of the energy of the incident photon in water [1]. It can be observed from the figure that Compton scattering is a dominant interaction in the energy of X-rays

therapeutic X-ray energy
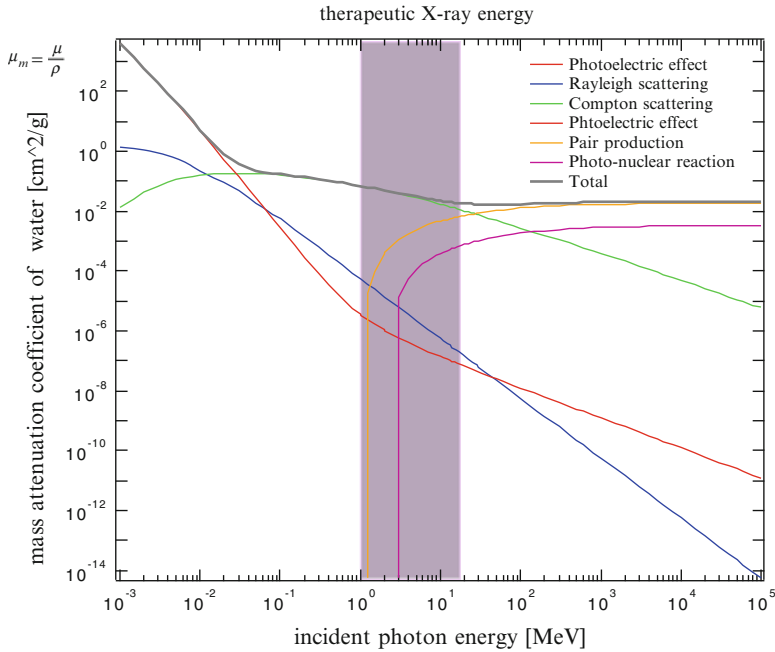
Fig. 3.8 The mass attenuation coefficient of water for each interaction as a function of the energy of the incident photon [1]

used in radiation therapy. The photoelectric effect and Compton scattering can occur almost equally in the energy range of X-rays of about 10–200 keV, as used in diagnostic radiation. Pair production is dominant in the case of very high energy.

Interactions of incident photons with matter cannot be described only by a simple model of attenuation of those photons because the energy distribution and the spatial distribution of the photons actually change in matter. For example, some incident photons become scattered photons, which are scattered forward after Compton scattering, and incident photons including those scattered photons undergo new interactions, especially in the range of energy used in radiation therapy. Therefore, the photon flux upon entering matter does not follow a simple exponential attenuation. Interactions of photons with real matter are very complicated, so it is necessary to consider the energy of the photon and its direction, as well as the mass attenuation coefficient of all energy and the photon flux at a point in the matter, as parameters of those interactions.

3.4 Energy Deposition by Incident Photons to Matter

An incident photon deposits kinetic energy E_e on an electron by interactions such as the photoelectric effect, Compton scattering, and pair production, and the electron deposits the energy on matter while passing through it (see Fig. 3.9). Stopping
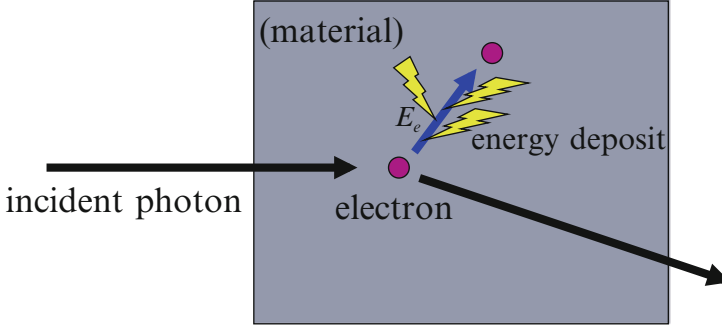
Fig. 3.9 Schematic diagram of energy deposition by an incident photon to matter

power is defined as the energy loss per length along the electron's track and is expressed as $-dE/dx[\text{MeV/cm}]$. Mass stopping power $-dE/\rho \cdot dx[\text{MeV} \cdot \text{cm}^2/\text{g}]$ is obtained by dividing the stopping power by the density of the matter.

Electron velocity while passing through matter is expressed by the following equation using an energy relational equation with special relativity:

$$\frac{m_e \cdot c^2}{\sqrt{1-\beta^2}} = E_e + m_e \cdot c^2. \quad \Rightarrow \quad \beta = \sqrt{1 - \frac{1}{(1+E_e/m_e \cdot c^2)^2}}, \tag{3.15}$$

where, c is the speed of light, $\beta = v/c$, and e and m_e the electron charge and rest mass, respectively. $m_e \cdot c^2$ is the electron rest mass energy and its value is 0.511 MeV. The speed of an electron is above 50 % of the speed of light when the kinetic energy of the electron is only 0.08 MeV.

In terms of the mass-stopping power in the electron energy range that should be taken into consideration in radiation therapy, it can be divided into terms of ionization loss and radiation loss.

$$-\frac{dE_e}{\rho \cdot dx} = \left(-\frac{dE_e}{\rho \cdot dx}\right)_{col} + \left(-\frac{dE_e}{\rho \cdot dx}\right)_{rad}. \tag{3.16}$$

In Eq. (3.16), the first term represents ionization loss and the second represents radiation loss.

The term of an ionization loss is calculated using the Bethe-Bloch formula which describes the stopping power as follows:

$$\left(-\frac{dE_e}{\rho \cdot dx}\right)_{col} = \frac{2 \cdot \pi \cdot m_e \cdot c^2}{\beta^2} \cdot r_e^2 \cdot N_A \cdot \frac{Z}{A}$$
$$\times \left\{ \ln\left(\frac{2 \cdot m_e \cdot c^2 \cdot E_e \cdot \beta^2}{(1-\beta^2) \cdot I^2}\right) + (1-\beta^2) - \left(2 \cdot \sqrt{1-\beta^2} - 1 + \beta^2\right) \cdot \ln 2 + \frac{1}{8} \cdot \left(1 - \sqrt{1-\beta^2}\right)^2 \right\},$$
$$\tag{3.17}$$

where, N_A is the Avogadro's constant and I is the mean excitation potential energy. I for water is 75.0 eV. The term of an ionization loss is in proportional to the atomic number of the matter and inversely proportional to the electron energy.

Similarly, the term of a radiation loss is expressed as follows:

$$\left(-\frac{dE_e}{\rho \cdot dx}\right)_{rad} = \frac{E_e + m_e \cdot c^2}{\beta^2} \cdot \alpha \cdot r_e{}^2 \cdot N_A \cdot \frac{Z^2}{A}$$
$$\cdot \left\{4 \cdot \ln\left(\frac{2 \cdot (E_e + m_e \cdot c^2)}{m_e \cdot c^2}\right) - \frac{4}{3}\right\}. \tag{3.18}$$

where, α is the fine-structure constant and has a constant value.

$$\alpha = \frac{e^2}{\hbar \cdot c} \approx \frac{1}{137}. \tag{3.19}$$

The term of a radiation loss is in proportional to the second power of the atomic number of the matter and to the electron energy.

The electron energy at which ionization loss is equal to radiation loss is called the critical energy E_c and is approximated by the following equation:

$$\left(-\frac{dE_e}{\rho \cdot dx}\right)_{col} = \left(-\frac{dE_e}{\rho \cdot dx}\right)_{rad} . \Rightarrow E_e = E_c \approx \frac{800}{Z + 1.2}[\text{MeV}]. \tag{3.20}$$

The critical energy for water is about 92 MeV using Eq. (3.20).

The results of calculation of the electron-stopping power in water by Eqs. (3.15), (3.16), (3.17), (3.18), and (3.19) are shown in Fig. 3.10. Radiation loses electron-stopping power predominantly in the energy range used in radiation therapy. The distance over which electron energy is $1/e$ due to the loss of almost all of its energy is called the radiation length L_{rad} and that of water is about 36 cm.

The mass of an electron is very small, at only about 1/1,800 that of a proton. Because an electron has a negative elementary electric charge, it is scattered markedly by Coulomb scattering in matter. In addition, an electron is scattered numerous times: this effect is called multiple Coulomb scattering. The term $\langle \theta_e{}^2 \rangle$ denotes the mean square angle of an electron for multiple Coulomb scattering and is given by the following equation:

$$\sqrt{\langle \theta_e{}^2 \rangle} \propto \frac{Z^2}{\beta^2} \cdot \frac{d}{L_{rad}}. \tag{3.21}$$

This equation shows that electron scattering in matter is proportional to the second power of the atomic number of the matter and to the thickness of the matter, while it is inversely proportional to the second power of the speed of an electron and to the radiation length of the matter. Because the speed of the recoil electron that is produced by Compton scattering with X-rays used in radiation therapy is almost
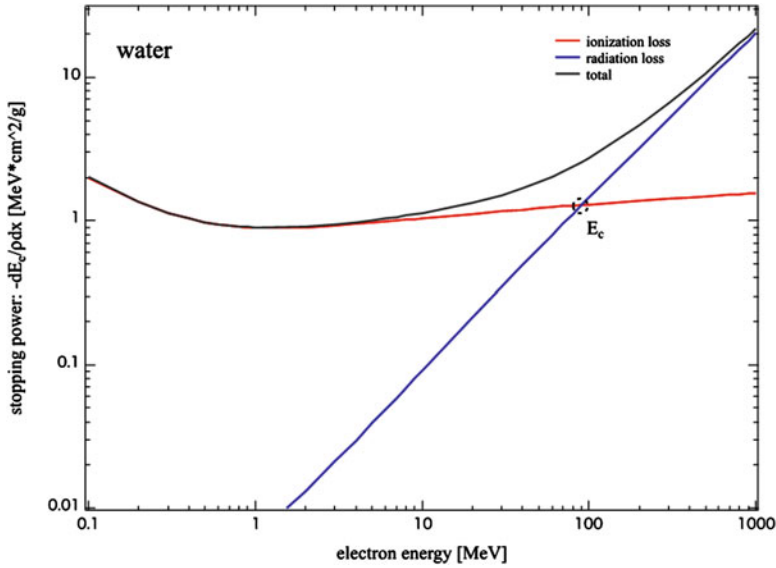
Fig. 3.10 The mass-stopping power for water as a function of electron energy

that of light in the range of kinetic energy of the recoil electron, the ratio of change of the scattering angle is small, at about 10 %.

The range of an electron in matter $R_e \cdot \rho$ can be calculated by integrating the reciprocal of mass-stopping power with electron energy from E_0 to zero, and can be expressed by the following equation:

$$R_e \cdot \rho = \int_{E_0}^{0} \left(-\frac{dE_e}{\rho \cdot dx} \right)_{col}^{-1} dE_e \left[g/cm^2 \right]. \tag{3.22}$$

However, the actual stopping positions of electrons diverge markedly because the electrons pass through matter while changing their directions in complicated ways by multiple Coulomb scattering. Therefore, the calculation results of Eq. (3.22) give electron path lengths in matter.

The energy deposition by electrons to matter that occurs when the X-rays used in radiation therapy irradiate matter is almost entirely due to energy losses of recoil electrons by Compton scattering. In addition, dose kernel K_X is formed by the energy losses of recoil electrons by Compton scattering at a point in matter.
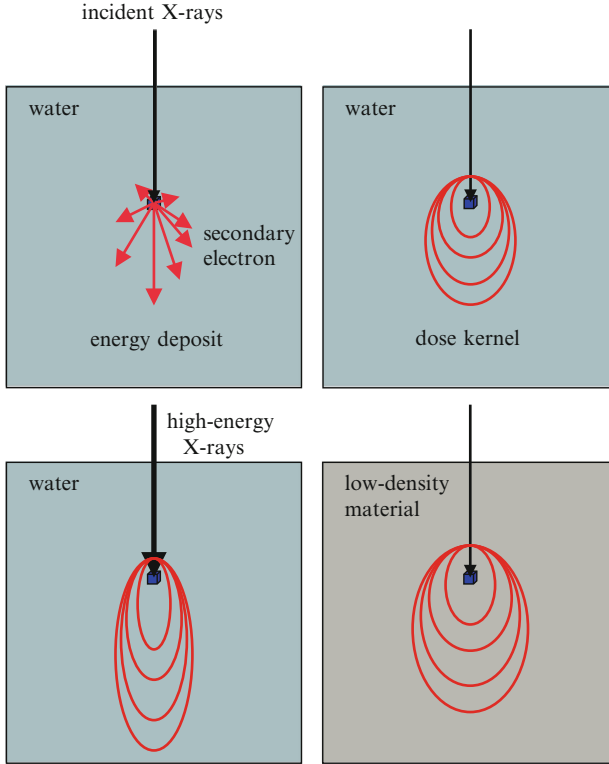
Fig. 3.11 Schematic diagram of shapes of dose kernels in various situations

$$K_X = K_X\left(\frac{d\sigma_{photo}}{d\Omega}, \frac{d\sigma_{comp}}{d\Omega}, \frac{d\sigma_{pair}}{d\Omega}\right) \approx K_X\left(\frac{d\sigma_{comp}}{d\Omega}\right) \approx K_X\left(\frac{d\sigma_a}{d\Omega}\right). \qquad (3.23)$$

The shape of dose kernel K_X depends on the differential cross sections of recoil electrons following the Klein-Nishina formula (3.6). As shown in Fig. 3.11, the shape of dose kernel K_X is elongated forward in the case of incident photons or X-rays with high energy. In low-density matter, the shape of dose kernel K_X expands on the basis of its similarity. The shape of dose kernel K_X expands in a manner depending on the lung density in radiation therapy, whereas the shape in inhomogeneous matter is formed in a boundary region between the high-density area and the low-density area corresponding to the area between the mediastinum and the lungs because of a change in the shape under various conditions, such as incident energy and matter density. Dose distribution is given by convoluting dose kernel K_X within the spatial region inside matter that is irradiated by X-rays used in radiation therapy (see Fig. 3.12).
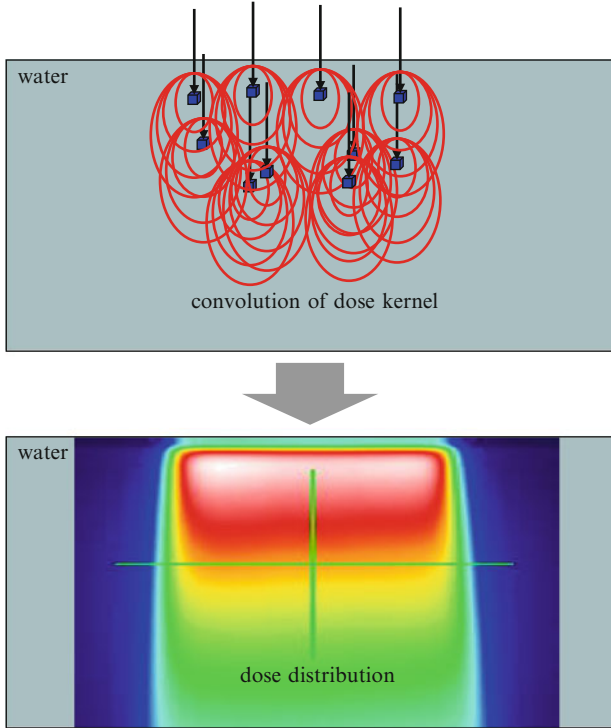
Fig. 3.12 An example of the dose distribution of X-rays used in radiation therapy

3.5 Energy Spectrum and Dose Distribution of Therapeutic X-Rays from a Linear Accelerator (Linac)

A linear accelerator (Linac) is used for X-ray therapy including stereotactic body radiation therapy (SBRT) for the lungs and the liver. Bremsstrahlung X-rays are produced by the phenomenon of bremsstrahlung, which occurs when MeV-energy electrons accelerated by a Linac irradiate a metallic target. Figure 3.13 shows the calculation results of the mass-stopping power for a tungsten (chemical symbol W) target as a function of electron energy. Compared with water (Fig. 3.10), the ratio of bremsstrahlung, which means the radiation loss in mass-stopping power, is larger for electrons with MeV-order energy, as used in radiation therapy. The critical energy for water is about 92 MeV; on the other hand, that for tungsten is small, at about 10 MeV.

Energy spectra of X-rays via bremsstrahlung by a Linac are formed by not only the incident energy of electrons to the target but also the material of the target or a flattening filter and their optical arrangement. Therefore, shapes of the energy spectra differ among Linac manufacturers. Typical energy spectra of X-rays of a Linac are shown in Fig. 3.14 [2].
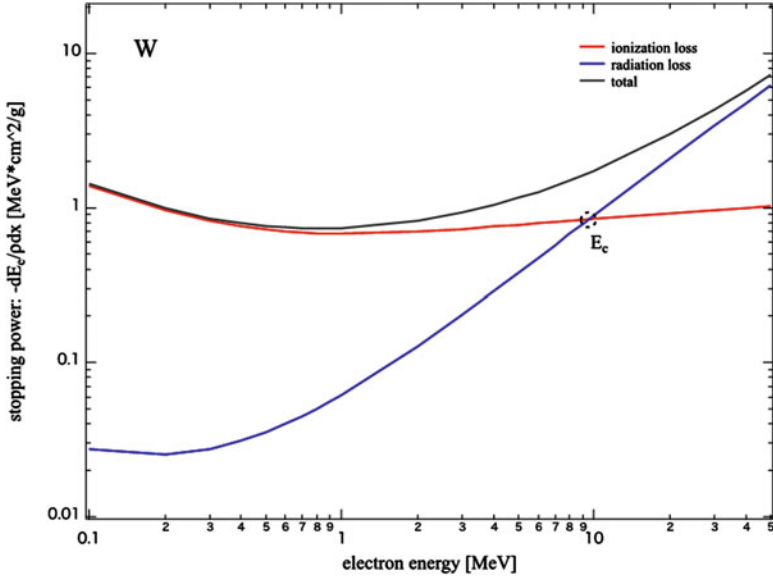
Fig. 3.13 The mass-stopping power for tungsten as a function of electron energy
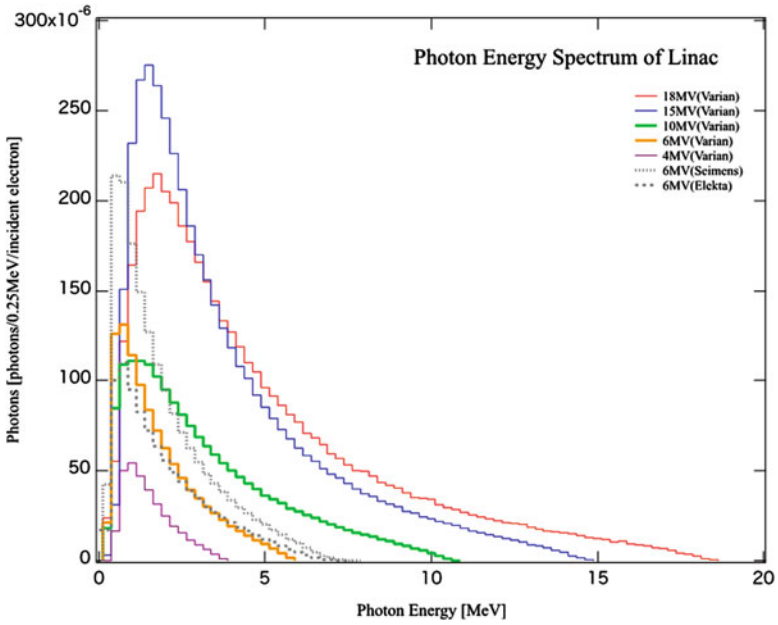
Fig. 3.14 The X-ray energy spectra of Linac [2]
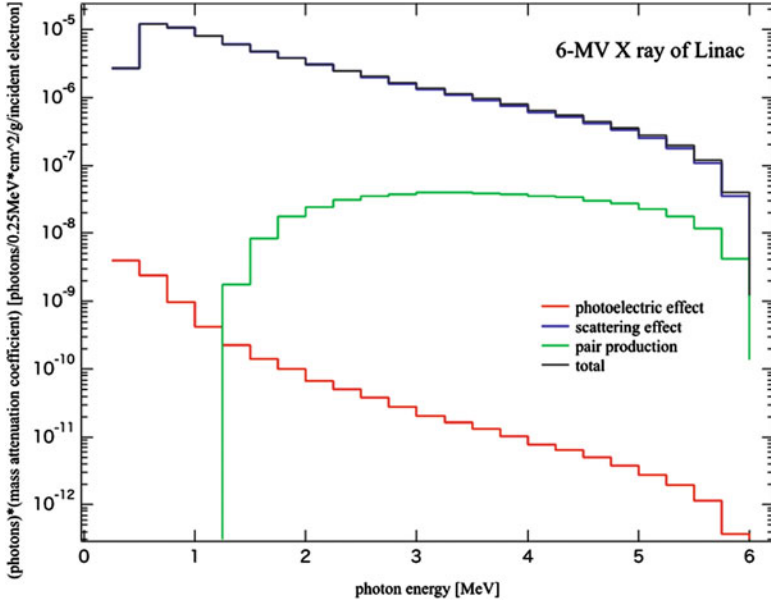
Fig. 3.15 The occupancies for each interaction in the 6-MV X-ray energy spectrum of Linac

Fig. 3.16 The dose kernel
with the 6-MV X-ray
energy spectrum of Linac
calculated by EGS5 (*left*: in
water, *right*: in water/low
density substance)
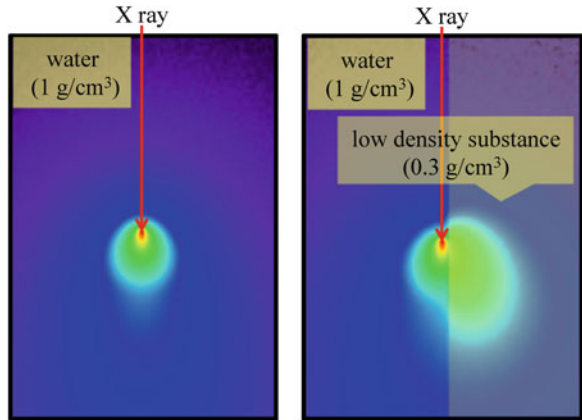
Figure 3.15 shows the product of the energy spectrum of X-rays with 6 MV produced by a Varian Linac and the mass attenuation coefficient for each energy. The value expresses the occupancies for each interaction in the energy spectrum of 6-MV X-rays of the Linac. Figure 3.16 is dose kernel with the 6-MV X-ray energy spectrum of Varian Linac. Dose kernels in homogeneity (water) and inhomogeneity (water / low density substance (30 % of water density)) were calculated by Monte Carlo simulation code: Electron Gamma Shower version 5.0 (EGS5) [3]. And the dose distribution of seven irradiation fields with gantry
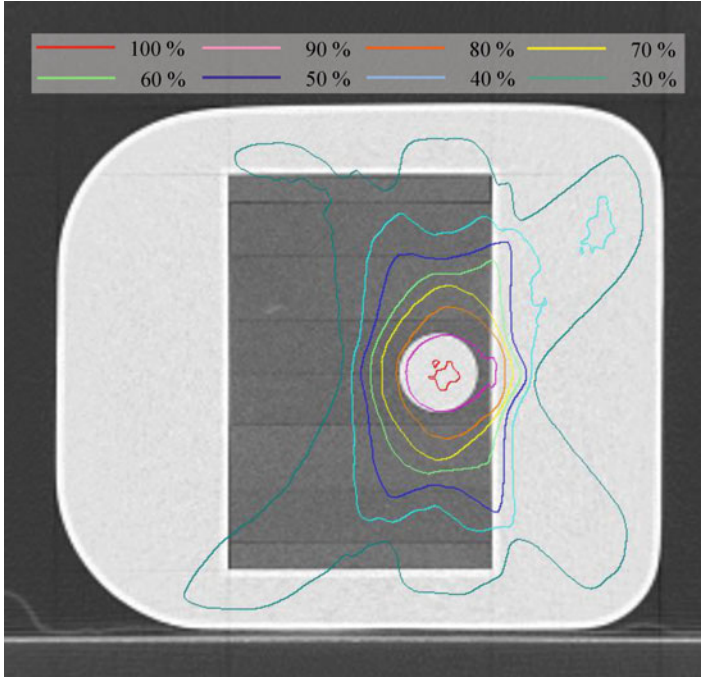
Fig. 3.17 The dose distribution of seven irradiation fields for lung SBRT calculated by EGS5

angles of 5, 50, 135, 175, 220, 280 and 325° in water-tank type lung phantom for lung SBRT [4] calculated by EGS5 is shown in Fig. 3.17. The simulation using the EGS5 was performed with condition of photons of 1.3×10^9, calculation grid size of 1 mm, photon cut-off energy of 10 keV and electron cut-off energy of 200 keV. These simulation data was provided by Medical Physicist S. Kito at Radiation Physics Section, Tokyo Metropolitan Cancer and Infectious Diseases Center Komagome Hospital.

References

1. NIST/XCOM. http://physics.nist.gov/PhysRefData/Xcom/html/xcom1.html
2. Sheikh-Bagheri D, Rogers DWO. Monte Carlo calculation of nine megavoltage photon beam spectra using the BEAM code. Med Phys. 2002;29(3):391–402.
3. Hirayama H, Namito Y, Beilajew AF, Wilderman SJ, Nelson WR The EGS5 Code System. Report SLAC-R-730 and KEK report 2005–8; 2005. http://rcwww.kek.jp/research/egs/egs5_manual/slac730-150228.pdf
4. Nishio T, Shirato H, Ishikawa M, Miyabe Y, Kito S, Narita Y, et al. Design, development of water tank-type lung phantom and dosimetric verification in institutions participating in a phase I study of stereotactic body radiation therapy in patients with T2N0M0 non-small cell lung cancer: Japan Clinical Oncology Group trial (JCOG0702). J Radiat Res. 2014;55(3):600–7.

Chapter 4
Techniques

Masahiko Okumura

4.1 Introduction

The major feature of Stereotactic Body Radiation Therapy (SBRT) is the delivery of a large dose in hypo fractions; therefore, SBRT delivery is expected to deliver a more potent biological effect to the target volume [1]. The reduced treatment time of SBRT with hypo fractions provides many benefits for both patients and hospitals and is a more cost effective treatment modality than traditional radiation therapy. The characteristics of SBRT are dose concentration and uniformity of target, and dramatic dose fall-off away from a target. Therefore, the technical quality assurance (QA) for SBRT requires high confidence in all phases of the treatment process. In SBRT, immobilization, localization, pretreatment dose verification, and image guidance for patient repositioning are required before starting the treatment. Finally, the design of a comprehensive QA program for SBRT is critical to obtain a good clinical outcome.

In this chapter, we would like to review the reported techniques with better QA for SBRT.

4.2 Treatment Delivery Systems for SBRT

Stereotactic radiosurgery (SRS) has been developed for small volumes in the intracranial tumors [2]. In 1968, the Gamma Knife, a commercially available radiation device was developed and it has been widely used everywhere in the

M. Okumura (✉)

Department of Radiology, Faculty of Medicine, Kinki University Hospital, 377-2
Ohno-higashi, Osakasayama, Osaka 589-8511, Japan
e-mail: m_okumura@w2.dion.ne.jp

world. Several irradiation techniques for intracranial tumors have been developed using linear accelerators based on their small physiological movement and the surrounding nerve tissues having a high dose tolerance. Since the 1990s, the technologies of Stereotactic irradiation have been applied to mainly lung tumors and liver tumors.

SBRT differs from the intracranial tumor treatment, and the major problems with lung or liver-SBRT are the degree of tumor movement and surrounding normal tissues caused by respiration, circulation and peristalsis. Therefore, SBRT using a conventional linear accelerator demanded the control techniques for image guidance with breathing and immobilization. The first SBRT using the first stereotactic body frame with a vacuum pillow was started at the Karolinska Hospital in Stockholm [3]. The first report on SBRT using the stereotactic body frame was published in 1995 [4]. In Japan, Uematstu et al. developed a frameless system (FOCAL unit) that can be attached to a linear accelerator, an x-ray simulator, Computed Tomography (CT) and a couch [5].

The moving tumors and surrounding normal tissues are a disadvantage for accurate radiation delivery. As a solution, several approaches for respiration, circulation and peristalsis have been clinically attempted. At the same time, the development of some innovative image-guided radiotherapy systems was promoted. The descriptions below provide the typical radiotherapy devices designed with features well suited for SBRT applications.

The original CyberKnife (Accuray, Sunnyvale, CA) was developed by a neurosurgery and radiation oncology team in Stanford University in the 1990s. The CyberKnife is equipped with a lightweight linear accelerator mounted on a 6D robotic arm. This System can deliver beams from hundreds of non-coplanar, isocentric or non-isocentric angles. At first, the Cyber Knife was developed for radiotherapy of intracranial tumors, and since then the capabilities of the systems have been applied to radiotherapy for extracranial tumors. The CyberKnife is diagnostic radiograph-based image guidance technology for tracking the patients body and target position during treatment. SBRT using the CyberKnife is performed without a rigid immobilization system for the body (e.g. stereotactic body frame).

The Varian and ELEKTA linear accelerators are constructed with the similar system configurations for image-guided strategies. These linear accelerators incorporate image-guided treatment capabilities. On the Varian linear accelerator, an electronic portal imaging device and a kV x-ray imaging system are mounted on the same gantry as the treatment unit. On the other hand, the ELEKTA linear accelerator combines the electronic portal imaging device and a kV x-ray imaging system into one integrated gantry-mounted system. The kV x-ray imaging system can also obtain three-dimensional cone-beam reconstructed images. Both the planar images and cone-beam CT images are used in these image-guidance systems for position verification in SBRT.

The Tomotherapy® (Accuray, Sunnyvale, CA) was developed by Thomas Rockwell Mackie, and he produced a stand-alone tomotherapy linear accelerator in 2003 [6]. The radiation Tomotherapy system is a 6 MV linear accelerator and a

MV CT imaging system mounted in the gantry head of a spiral CT. During treatment delivery, the linear accelerator completes multiple 360° rotations around the patient while the couch passes through the central bore of the system. The MV CT imaging system enables accurate position verification before each radiation delivery and implementation of intensity-modulated radiation therapy (IMRT) and 3D conformal radiation therapy (3DCRT).

The Novalis treatment system was a cooperative development project between Varian Medical Systems, Inc. and BrainLAB, AG. The Novalis TX, which is one of the latest devices, includes ExacTrac, an on-board imager localization system. The ExacTrac system is an image-guided system consisting of two infrared (IR) cameras, two planar x-ray imagers, and a robotic couch. The IR cameras guide the initial patient setup by external IR markers attached to the patient's surface. Two kV planar X-ray images are acquired and coregistered with the 3D CT images using a 3D/2D image registration algorithm. However, the ExacTrac system is generally limited to bony alignment because soft tissue is often not visible on planar images. The Novalis TX is equipped with not only the ExacTrac system for position verification, but also the kV x-ray imaging system for 3D-reconstructed CT images and an electronic portal imaging device for MV planar images on the gantry. The combination strategy with the ExactTrac and these planar imaging systems can be effective for position verification in SBRT.

In Japan, a four-dimensional image-guided radiotherapy system with a gimbaled x-ray head was jointly developed by Mitsubishi Heavy Industries and Kyoto University [7]. This radiotherapy system is called Vero4DRT. The Vero4DRT system allows high-precision radiotherapy with dynamic tracking irradiation. One of the major features of the system is the special circular gantry called an O-ring. The Vero4DRT is a 6 MV C-Band linear accelerator mounted on an O-ring and is equipped with two pairs of kV x-ray imaging systems and an electronic portal imaging device for position verification during treatment. It is capable of pursuing irradiation and delivering irradiation precisely with the help of an agile moving x-ray head on the gimbals. This system offers a dynamic tracking irradiation capability for moving tumors during treatment and adjusting the beam direction according to changes in tumor location. Recently, some studies have been conducted into a real-time tumor tracking method using the Vero4DRT [8].

4.3 Significance of an Integrated Technical Program for SBRT

4.3.1 Definition of Margins on SBRT

The intended cases for SBRT are primary and metastatic lung tumors, liver tumors, the spine and oligometastatic tumors at other locations [9–14]. In particular, the characteristics of lung tumors, liver tumors and mobile tumors are excessive

Table 4.1 Factors to be considered when defining a planning target volume

Category	Intrafractional variations		Interfractional variations	
	Systematic	Random	Systematic	Random
Variation of CTV size	Physiological processes	Physiological processes	Tumor reduction or swelling	Physiological processes
Variation of CTV position	Change in treatment position	Physiological processes	Weight loss	Physiological processes
Variation in the patient position relative to the treatment beams	–	Patient movements	Technical errors	Daily set-up

irregular motion due to respiration, circulation and peristalsis. SBRT treatment should be simulated and planned with the goal of providing the smallest possible margins, while considering the motion of the tumor and normal tissue. The motions depend on variations and uncertainties in the position, size, and shape of tumors and the surrounding normal tissues of the patient. These variations and uncertainties affect the orientations of the tissues, patient, and the beams in relation to the common coordinate system. These errors also occur between the imaging procedure and the treatment planning, and between the treatment planning and first treatment session.

The ICRU50 [15] and ICRU62 [16] as references for Gross Tumor Volume (GTV), Clinical Target Volume (CTV), Planning Target Volume (PTV), and Organs at Risk (OAR) are used as the target definitions in SBRT, as well as conventional radiation therapy. The margins for CTV size and position due to respiratory motion and organ filling can be added as the internal margin. Table 4.1 shows the factors that should be considered, defining the PTV of the ICRU62 definitions [16].

4.3.2   Imaging for SBRT Planning

Imaging for treatment planning in SBRT is based on CT imaging data. Recently, for superposing on CT images, magnetic resonance imaging and positron emission tomography data have also been effectively used for SBRT planning [17]. The variation in CTV size and position depends on respiration motion and organ filling. The magnitude of variation in CTV depends on whether compensation for respiratory motion is adopted during radiotherapy delivery. Particularly, in respiratory motion, the SBRT delivery technique has an impact on the magnitude of motion in tumors and nearby normal tissues. According to an AAPM report on TG101 [18], typical SBRT margins for defining the minimal distance expanding from the CTV to PTV surfaces are 0.5 cm in the axial planes and 1.0 cm in the inferior/superior directions under respiratory depressing conditions.

Table 4.2 Summary of the relationship between the internal margin decision and X-ray CT methods for each respiratory condition

Respiratory motion management	Irradiation method	CT method	Internal margin	Magnitude of internal margin	Delivery time
Free breathing	Common	Slow scan CT or 4D-CT	Add to range of all respiratory phases in the fluoroscopic image or 4D-CT image	Large	Long
Shallow breathing or respiratory depression				Medium	Shirt
Free breathing or shallow breathing	Gating	Fast scan CT or 4D-CT under conditions of the irradiation method	Add to deviation of target position repeatability in each corresponding irradiation technique	Medium	Long
	Intercepting			Small	Long
	pursuing			Small	Shirt
Breath-hold	Static with breath-hold	Fast scan CT under breath-hold	Add to deviation of breath hold repeatability (several CT scans are recommended)	Small	Medium

The magnitude of motion should be analyzed to determine the appropriate internal margin. In general, CTV including the internal margin can be determined by the following CT imaging techniques, (1) four dimensional CT, (2) slow scan CT (e.g. 4 s for a slice), and (3) fast scan CT (multi-slices CT or dynamic scan) under conditions of inspiration and expiration breath-hold [19]. Each CT for considering respiratory motion should be evaluated from the target position between maximum inspiration and expiration, and the repeatability of the target position in the breath hold condition is critical for several CT scans. Note that attention must be paid to the characteristics of each CT acquisition method. For example, the utilization of slow scan CT images may result in under-dosing of the target volume and increased toxicity to surrounding normal tissues in 3D planning calculations [20].

Table 4.2 shows the relationship between the decision on the internal margin and X-ray CT methods for each respiratory condition.

4.4 Relationship Between Energy Selection and Beam Arrangement

When higher photon energy is used, the range of the scattered secondary electron beams becomes wider, and the convergence of the absorbed dose becomes narrower. Secondary electron equilibration is not a measurable condition with high-energy photons and deep depths in small fields. However, the mean energy

of photon and electron beams increases in small fields compared with common fields. In particular, this physical phenomenon has an impact on low density regions (e.g. lung). For this reason, photon energies of 6 MV (or close to that) for tumors in the lungs should be used in SBRT [21, 22]. For tumors below the diaphragm (not passing through lung tissue or other low density tissue), photon energies of 6–20 MV are selected for SBRT delivery [23].

The current conventional linear accelerators for SBRT can deliver radiation beams shaped tightly to the target volume and all around the relevant critical structures. The beam arrangements are performed by 5–10 mm MLCs, a wedge filter (including motorized wedges), and customized blocks. Recently, the appearance of 2.5–3 mm MLCs linear accelerators has made a substantial contribution to creating conformal dose distributions in SBRT.

In general, the irradiation method for SBRT applies five to eight coplanar or non-coplanar static conformal beams. Recently, SBRT delivery has been a combination of intensity- modulated radiation techniques and volumetric-modulated arc techniques.   The determination of beam orientation in SBRT is important to avoid sensitive organs, mechanical constraints, and a short beam path. In general, a large number of beams yields better target dose conformity and dose fall-off away from the target. When the number of beams is sufficiently high, however, the choice of beam direction becomes less significant [18].

In general, commercially available treatment planning systems are used to plan SBRT delivery. The radiation treatment planning system does not usually have parameters of geometric data for linear accelerators. Therefore, after completing a treatment plan for SBRT, a patient-specific QA should be conducted under the same conditions as the actual treatment conditions. The verification of non-interference between the patient and linear accelerator (e.g. gantry head) is critical, and is required for safe and effective treatment.

It should be noted that the delivery time should be shortened as much as possible. A short delivery time avoids geometric errors from intra-fractional movements. (The reason is mainly to avoid geometric errors from intra-fractional movements over longer treatment times.) Shortened delivery times can be achieved with a comprehensive delivery system including an immobilization system, localization system, on-board imaging system, and consideration of the dose rate configuration.

4.5   Radiation Delivery Equipment

In Japan, medical service fee regulations introduced reimbursement for respiratory motion management (RMM) from April 2012 [24]. The topic of RMMs is addressed in more detail in other chapters. The strategies for respiratory motion are based on the following six methods in the 2008 Guidelines for Radiotherapy Planning [24].

 (i) inhalation of oxygen
 (ii) abdominal compression
(iii) learning regular respiratory patterns
(iv) breath hold technique
 (v) gating with respiration
(vi) real-time tumor-tracking

A variety of techniques to account for respiratory motion of moving targets in the thorax and abdomen is described and summarized in the AAPM report on TG 76 [19]. The six methods for respiratory motion are mentioned below based on the examples of TG 76.

(i) Inhalation of oxygen

The inhalation of oxygen method is a shallow breathing technique and it exhibits some improvement in reduction of the respiratory rate and magnitude of breathing [25].

(ii) Abdominal compression

The abdominal compression method is useful for respiratory motion reduction in moving tumors and nearby normal tissues and generally employs abdominal compression, an abdominal band, body shell [12, 26] and stereotactic body frames. The stereotactic body frames typically make use of vacuum cushions and an attached plate that is pressed against the abdomen. The accuracy and reproducibility of both the body frame and pressure plate have been evaluated with a comprehensive assessment report [27]. However, the usage of the body frame has some problems in term of uncertainty of patient setup, increasing respiratory displacement in the anterior-posterior direction, and physical pain.

(iii) Learning regular respiratory patterns

This method relies heavily on the ability of the patients to perform constant respiration independently. Therefore, this mode requires attention in the stability and repeatability for the range and position of moving tumors during treatment delivery.

All methods above are motion-encompassing methods, and it is important to estimate the magnitude of motion in tumors and nearby normal tissues during CT imaging.

(iv) Breath hold technique

Breath-hold techniques are methods of active breath-hold or passive breath-hold during a specific phase of the respiratory cycle. In general, the breath-hold technique is often used with respiratory monitoring. The reproducibility of tumor positions under self breath-hold by the patient's own estimation after sufficient practice and in the absence of a respiratory monitoring device is satisfactorily accurate, and displacements of tumor positions are small [28]. However the reproducibility of tumor positions under self breath-hold does not show high reliability, so the monitoring of tumor position reproducibility is important when operating.

The breath hold technique with respiratory monitoring devices has been performed using active breathing control (ABC) [29], maximum breath-hold (deep-inspiration and breath hold, DIBH) [30], and patient self-judged breath hold techniques. The ABC apparatus comprises two respiratory flow monitors paired with scissor valves to control inspiratory and expiratory paths in the patient. The DIBH consists of an instruction to perform voluntary breath-hold at the end of deep inspiration to immobilize organ motion. A benefit of breath-holding during deep inspiration is the reduced density of the normal lung and minimized proportion of lung volume receiving high-dose radiation compared to total lung volume [28]. In Japan, as one patient self- breath hold method, a respiratory monitoring device that can determine the respiratory level in a patient by measuring the movement of two contacts on the abdomen and chest wall has been developed [31]. This respiratory monitoring system adopts patient self-breath-holding under constant conditions for expiration or inspiration. This device has been commercialized as Abches (APEX Medical, Inc., Japan).

The reproducibility of breath-hold at the expiration phase is more stable than the inspiration phase, but the reproducibility of breath hold position varies between individuals, so the verification of breath hold reproducibility is recommended when using fluoroscopy.

(v) Gating with respiration

There are several respiratory gating techniques, and the typical method is gating using an external respiration signal and gating with internal fiducial markers. The Varian real-Time Position Management^{TM} (RPM) system is a typical respiratory gating technique using external markers and is also used for the breath-hold method. The RPM system is a respiration-gated intermittent irradiation system, by which the movement of the external fiducial marker is placed on the patient's anterior abdominal surface. During treatment, once a stable respiration trace has been established and gating thresholds are verified, gated radiation delivery is initiated. The control for gating respiration is that a beam-hold condition automatically occurs if the patient's breathing level deviates form the intended level.

In Japan, The AZ-733 V Respiratory Gating System (Anzai Medical Co. LTD., Tokyo, Japan) was developed with a Load Cell and Laser Sensor to detect the movement of the patient's body surface. The Load Cell is held on the chest by an elastic belt. The Laser Sensor is placed above the chest. The acquired respiratory waveform is converted to a digital signal and transmitted to a separate laptop PC. The PC monitors the respiratory signal constantly, and when the respiratory signal reaches the preset phase and level of respiration, the PC commands the Wave Deck to output the gating signal to an external radiation modality [19].

(vi) Real-time tumor-tracking

Real-time tumor-tracking irradiation techniques are defined as follows [24]. (i) A technique to perform irradiation by analyzing the relationship between respiratory movements and tumors, and changing the irradiated field in accordance with the respiratory movements (pursuing irradiation). (ii) A technique to perform

irradiation onto a target while it passes through a specified position by observing a tumor using fluoroscopy during the radiation delivery (intercepting irradiation).

Success with pursuing irradiation techniques greatly depends on accurate analysis of the relation between the respiratory phase and position in moving tumors; however, currently pursuing irradiation with some prediction model is widely discussed in papers [32–34].

Real-time tumor-tracking radiotherapy (RTRT), a technique of gating using internal fiducial markers to gate the radiation delivery, is a representative method of intercepting irradiation. An RTRT system was developed jointly by Hokkaido University and Mitsubishi Electric Co. [35]. A fiducial marker (2-mm diameter gold spheres) implanted in or near the tumor is tracked in all three dimensions several times a second using a pair of stereotactic kV x-ray imaging systems in combination with automatic detection software. When each fiducial marker is within an acceptable range of the simulation position for both stereotactic x-ray cameras, the linear accelerator delivers radiation. Onimaru et al. reported that the median tumor movements in the left-right, anterio-posterio, and craniocaudal directions were 1.1 mm, 2.3 mm, and 5.4 mm, respectively [36].

The active breathing control technique has not been approved in the Japanese medical service fee regulations. Typically, it is difficult for (i) inhalation of oxygen or (iii) learning regular respiratory patterns to be used alone. Combined methods of (i) inhalation of oxygen and (ii) abdominal compression or (iii) learning regular respiratory patterns and (v) gating with respiration are recommended.

The level of immobilization for SBRT needs to consider the treatment delivery technique for both detection and correction regarding inter-fraction and intra-fraction variation of tumors and around normal tissues. Immobilization for treatment delivery has an effect on the physical and psychological condition of patients. Therefore, immobilization methods that consider the patient's state and/or delivery system should be carefully chosen in each delivery facility. Table 4.3 shows respiratory monitoring methods and immobilization strategies that have been utilized to reduce PTV margins due to respiratory motion. If the strategy for respiratory motion is considered carefully, the patient fixation for SBRT will be simple.

4.6 Pre-treatment Dosimetric Verification

Highly accurate radiation treatment planning, such as IMRT or SBRT, requires patient-specific quality assurance procedures to ensure the dose distribution and absorbed dose are within the appropriate dose-volume constraints.

At least, a representative point dose, field by field or composite dose distribution should be measured for accuracy assurance in pre-treatment dosimetric verification for SBRT. Figure 4.1 shows some examples of equipment for patient-specific pre-treatment dosimetric verification.

Figure 4.1a shows a two dimensional detector array (MapCHECK, SUN NUCLEAR CORP.) and a water-equivalent plastic phantom for each field

Table 4.3 Summary of the respiratory monitoring methods and immobilization strategies for each respiratory management approach

Respiratory motion management (RMM)	Respiratory monitoring method	Immobilization device	Respiratory reproducibility
Inhalation of oxygen (recommended use with another RMM method)	Following other RMM methods	Following other RMM methods	Depend on methods used
Abdominal compression	X-ray fluoroscopy	Body frame system includes equipment for abdominal compression	Not always accurate [27]
Learning regular respiratory pattern	Metronome, possibly with a gating system	Free, moderately set up system, stereotactic body frame system	Not always accurate
Breath hold	Infrared marker system (RPM, ExacTrac), Breath control assist system (Abches system)	Moderately set up system, stereotactic body frame system	Reportedly good [28, 30]
Gating with respiration	Infrared marker system (RPM, ExacTrac), Three dimensional video camera system, [a]X-ray fluoroscopy using implanted fiducial markers	Moderately set up system, stereotactic body frame system	Not always accurate [37, 38]
Real-time tumor-tracking	X-ray fluoroscopy using implanted fiducial markers, Non-radiographic tumor tracking using an implantable RF seed[a]	Moderately set up system, stereotactic body frame system	Reportedly good [39]

[a]These methods were mentioned in TG reports, however, they are not officially authorized in Japan

measurement. Figure 4.1b shows the RANDO® phantom for film dosimetry and RT3000® phantom (R-Tech, Tokyo Japan) for film dosimetry and a point dose measurement. The measurement with the RT3000 phantom is can be used as an equivalent-water or heterogeneity phantom. The absolute doses at some points (usually the isocenter and point of focus) are measured using a micro ionization chamber, and compared with the calculated doses at the same points. A film is used to compare the measured dose distribution with the planned dose distribution which is determined by the planning system. Figure 4.2 shows the dose distribution matching between the film and planning system data at the isocenter in the axial plane. The QA program for SBRT needs to be performed for specific QA techniques; therefore, the implementation of the QA program requires the team that well understands the planning and delivery of radiotherapy.
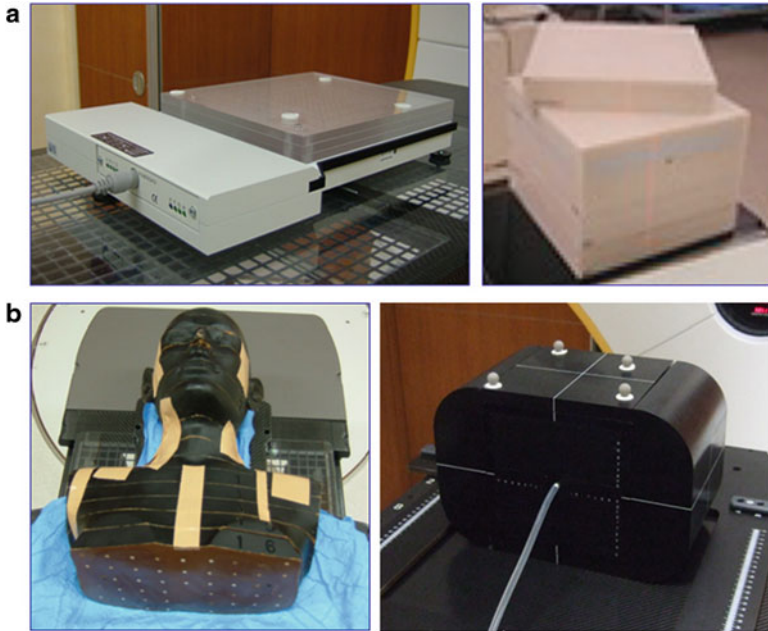
Fig. 4.1 A two dimensional detector array (MapCHECK, SUN NUCLEAR CORP.) and a water equivalent plastic phantom for each field measurement (**a**). The RANDO® phantom for film dosimetry and RT3000® phantom (R-Tech, Tokyo Japan) for film dosimetry and a point dose measurement (**b**) (Courtesy of Dr. Hayashi, Fijita Health University)
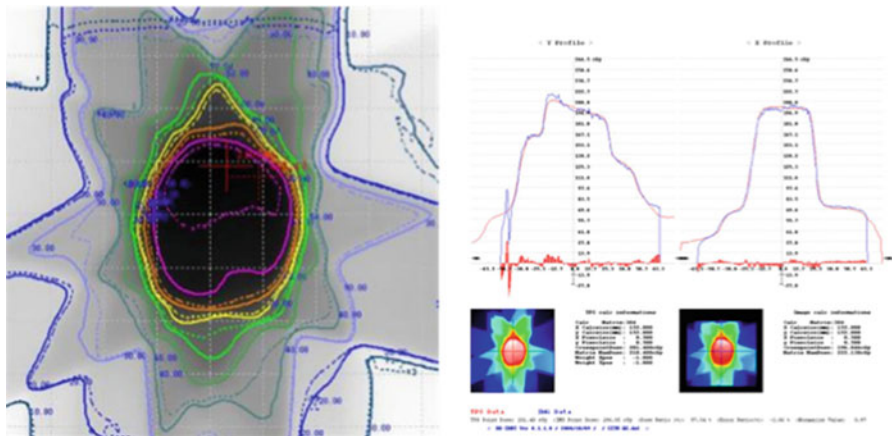
Fig. 4.2 The dose distribution matching for the axial plane of the isocenter between film and planning system data, and a beam profile that is compared with the planning dose distribution with measured planar dose distribution (Courtesy of Dr. Hayashi, Fijita Health University)

References

1. Timmerman RD. An overview of hypofraction and introduction to this issue seminars in radiation oncology. Semin Radiat Oncol. 2008;18:215–22.
2. Leksell L. Stereotactic radiosurgery. J Neurol Neurosurg Psychiatry. 1983;42:797–803.
3. Lax I, Blomgren H, Naslund I, et al. Stereotactic radiotherapy of malignancies in the abdomen. Methodological aspects. Acta Oncol. 1994;33:677–83.
4. Blomgren H, Lax I, Nalund I, et al. Stereotactic high dose fraction radiation therapy of extracranial tumors using an accelerator. Clinical experience of the first thirty-one patients. Acta Oncol. 1995;34:861–70.
5. Uematsu M, Shioda A, Tahara K, et al. Focal, high dose, and fractionated modified stereotactic radiation therapy foe lung carcinoma patients: a preliminary experience. Cancer. 1998;82:1062–70.
6. Mackie TR. History of tomotherapy. Phys Med Biol. 2006;51:427–53.
7. Kamino Y, Miura S, Kokubo M, et al. Development of an ultrasmall C-band linear accelerator guide for a four-dimensional image-guided radiotherapy system with a gimbaled x-ray head. Med Phys. 2007;34:1797–808.
8. Matsuo Y, Ueki N, Takayama K, et al. Evaluation of dynamic tumor tracking radiotherapy with real-time monitoring for lung tumors using a gimbal mounted linac. Radiother Oncol. 2014;112(3):360–4.
9. Herfarth KK, Debus J, Lohr F, et al. Extracranial stereotactic radiation therapy: set-up accuracy of patients treated for liver metastases. Int J Radiat Oncol Biol Phys. 2000;46:329–35.
10. Timmerman R, Papiea L, MacGarry R, Likes L, DesRosiers C, Frost S, et al. Extracranial stereotactic radioablation: result of a phase I study in medically inoperable stage I non-small cell lung cancer. Chest. 2003;124:1946–55.
11. Fukumoto S, Shirato H, Shimzu S, Ogura S, Onimaru R, Kitamura K, et al. Small- volume image-guided radiotherapy using hypofractionated, coplanar, and noncoplanar multiple fields for patients with inoperable stage I nonsmall cell lung carcinomas. Cancer. 2002;95:1546–53.
12. Nagata Y, Negoro Y, Aoki T, Mizowaki T, Takayama K, Kokubo M, et al. Clinical outcomes of 3D conformal hypofractionated single high-dose radiotherapy for one or two lung tumors using a stereotactic body frame. Int J Radiat Oncol Biol Phys. 2002;52:1041–6.
13. Onishi H, Araki T, Shirato H, Hiraoka M, Gomi K, Ymashita T, et al. Stereotactic hypofractionated high-dose irradiation for stage I nonsmall cell lung carcinoma: clinical outcomes in 245 subjects in a Japanese multi institutional study. Cancer. 2004;101:1623–31.
14. Benzil DL, Saboori M, Mogilner AY, Rocchio R, Moorthy CR. Safety and efficacy of stereotactic radiosurgery for tumors of the spine. J Neurosurg. 2004;101:413–18.
15. ICRU. Prescribing, recording, and reporting photon beam therapy, ICRU report 50. Bethesda: International Commission on Radiation Units and Measurements; 1993.
16. ICRU. Prescribing, recording, and reporting photon beam therapy (Supplement to ICRU report 50), ICRU report 62. Bethesda: International Commission on Radiation Units and Measurements; 1999.
17. Okubo M, Nishimura Y, Nakamatsu K, Okumura M, Shibata T, Kanamori S, et al. Radiation treatment planning using positron emission and computed tomography for lung and pharyngeal cancer: a multiple-threshold method for [18F]fluoro-2- deoxyglucose activity. Int J Radiat Oncol Biol Phys. 2010;77:350–6.
18. Benedict AH, Yenice KM, Followill D, Galvin JM, Hinson W, Kavanagh B, et al. Stereotactic body radiation therapy: the report of AAPM Task Group 101. Med Phys. 2010;21:4078–101.

19. Allen A, Stepaniak C, Gore E. Technical and dosimetric aspects of respiratory gating using a pressure-sensor motion monitoring system. Med Phys. 2006;33:145–54.
20. Mori S, Kanematsu N, Mizuno H, Sunaoka M, Endo M. Physical evaluation of CT scan methods for radiation therapy planning: comparison of fast, slow and gating scan using the 256-detector row CT scanner. Phys Med Biol. 2006;51:587–600.
21. DesRoisers PM, Moskvin VP, DesRoisers CM, et al. Lung cancer radiation therapy: Monte Carlo investigation of "under dose" by high energy photons. Technol Cancer Res Treat. 2004;3:289–94.
22. Wang L, Yorke E, Desobry G, et al. Dosimetric advantage of using 6 MV over 15 MV photons in conformal therapy of lung cancer: Monte Carlo studies in patient geometries. J Appl Clin Med Phys. 2002;3:51–9.
23. Nagata Y, Wulf J, Lax I, Timmerman R, Zimmermann F, Stojkovski I, et al. Stereotactic radiotherapy of primary lung cancer and other targets: results of consultant meeting of the International Atomic Energy Agency. Int J Radiat Oncol Biol Phys. 2011;79:660–9.
24. Matsuo Y, Onishi H, Nakagawa K, Nakamura M, Ariji T, Kumazaki Y, et al. Guidelines for respiratory motion management in radiation therapy. J Radiat Res. 2013;54:561–8.
25. Uematsu M, Fukui T, Shioda A, et al. A dual computed tomography and linear accelerator unit for stereotactic radiation therapy: a new approach without cranially fixated stereotactic frame. Int J Radiat Oncol Biol Phys. 1996;35:587–92.
26. Lee S, Yang DS, Choi MS, et al. Development of respiratory motion reduction device (RMRDs) for radiotherapy in moving tumors. Jpn J Clin Oncol. 2004;34:686–91.
27. Negoro Y, Nagata Y, Aoki T, et al. The effectiveness of an immobilization device in conformal radiotherapy for lung tumor: reduction of respiratory movement and evaluation of the daily setup accuracy. Int J Radiat Oncol Biol Phys. 2001;50:889–98.
28. Ohnishi H, Kuriyama K, Komiyama T, et al. CT evaluation of patient deep inspiration self-breath-holding: how precisely can patients reproduce the tumor position in the absence of respiratory monitoring device ? Med Phys. 2003;30:1183–7.
29. Wong JW, Sharpe MB, Jaffray DA, et al. The use of active breathing control(ABC) to reduce margin for breathing motion. Int J Radiat Oncol Biol Phys. 1999;44:911–19.
30. Henly J, Debois MM, Mah D, et al. Deep inspiration breath-hold technique for lung tumors: the potential value of target immobilization and reduced lung density in dose escalation. Int J Radiat Oncol Biol Phys. 1999;45:603–11.
31. Onishi H, Kawakami H, Marino K, Komiyama T, Kuriyama K, Araya M, et al. A simple respiratory indicator for irradiation during voluntary breath holding: a one-touch device without electronic materials. Radiology. 2010;225:917–23.
32. Roland T, Mavroidis P, Shi C, Papanikolaou N. Incorporating system latency associated with real-time target tracking radiotherapy in the dose prediction step. Phys Med Biol. 2010;55:2651–68.
33. Ren Q, Nishioka S, Shirato H, Berbeco RI. Adaptive prediction of respiratory motion for motion compensation radiotherapy. Phys Med Biol. 2007;52:6651–61.
34. Murphy MJ, Pokhrel D. Optimization of an adaptive neural network to predict breathing. Med Phys. 2009;36:40–7.
35. Shimizu S, Shirato H, Ogura S, et al. Detection of lung tumor movement in real-time tumor-tracking radiotherapy. Int J Radiat Oncol Biol Phys. 2001;51:304–10.
36. Onimaru R, Shirato H, Fujino M, et al. The effect of tumor location and respiratory function on tumor movement estimated by real-time tracking radiotherapy (RTRT) system. Int J Radiat Oncol Biol Phys. 2005;63:164–9.
37. Mah D, Hanley J, Rosenzweig KE, et al. Technical aspects of the deep inspiration breath-hold technique in the treatment of thoracic cancer. Int J Radiat Oncol Biol Phys. 2000;48:1175–85.
38. Bert RI, Nishioka S, Shirato H. Residual motion of lung tumors in gated radiotherapy with external respiratory surrogates. Phys Med Biol. 2005;50:3655–67.
39. Shirato H, Shimizu S, Kunieda T, et al. Physical aspects of a real-time tumor-tracking system for gated radiotherapy. Int J Radiat Oncol Biol Phys. 2000;48:1187–95.

Chapter 5
Quality Assurance (QA)

Fujio Araki

5.1 QA Concepts

In its Radiotherapy Risk Profile, the World Health Organization (WHO) states that proper QA measures are imperative to reduce the likelihood of accidents and errors and increase the probability that the errors will be recognized and rectified if they do occur [1]. ASTRO and ACR practice guidelines for the performance of SBRT describe clearly that: "Strict protocols for quality assurance must be followed [2]." For radiotherapy, the WHO defines quality assurance (QA) as: "QA is concerned with all those procedures that ensure consistency of the medical prescription, and safe fulfillment of that prescription, as regards to the dose to the target volume, together with minimal dose to normal tissue, minimal exposure of personnel, and adequate patient monitoring aimed at determining the end result of the treatment."

This is based on the general definition adopted by the International Organization for Standardization (ISO 1995) and also by the British Standards Institute (BSI) that: "QA is defined as all those planned and systematic actions necessary to provide adequate confidence that a structure, system or component will perform satisfactorily in service", or will satisfy given requirements for quality. Quality control (QC) is the regulatory process through which the actual quality performance is measured, compared with existing standards and finally the actions necessary to keep or regain conformance with the standards (ISO).

QC describes the operational techniques and activities that are used to fulfil the requirements for quality. It forms part of the wider quality assurance programmer or system. Quality Standards are the set of accepted criteria against which the quality of the activity in question can be assessed. Quality Audit is an independent review

F. Araki (✉)
Department of Medical Imaging, Faculty of Life Sciences, Kumamoto University, 4-24-1
Kuhonji, Chuoku, Kumamoto 862-0976, Japan
e-mail: f_araki@kumamoto-u.ac.jp

of the quality assurance and quality control programs, which is ideally external to the process or part of the process under review, i.e. performed using independent procedures and by independent persons who are not responsible for the performance of the product or process under review.

5.2 Qualifications and Responsibilities of Personnel

SBRT requires levels of precision and accuracy that surpass the requirements of conventionally fractionated radiation therapy or intensity-modulated delivery. The SBRT process requires a coordinated team effort between the radiation oncologist, the medical physicist, the medical dosimetrist, and the radiation therapist.

The following are minimal recommendations specified by ASTRO/ACR practice guidelines, for staffing levels and staff responsibilities while participating in an SBRT procedure. Specific duties may be reassigned where appropriate. The responsibilities of the radiation oncologist shall be clearly defined and should include the following:

5.2.1 Qualified Radiation Oncologist

1. The radiation oncologist will manage the overall disease-specific treatment regimen, including careful evaluation of disease stage, assessment of comorbidity and previous treatments, thorough exploration of various treatment options (including multidisciplinary conferences and consultation where appropriate), ample and understandable discussion of treatment impact, including its benefits and potential harm, knowledgeable design and conduct of treatment as outlined below, and prudent follow-up after treatment.
2. The radiation oncologist will determine and recommend a proper patient positioning method with attention to site-specific targeting concerns, patient-specific positioning, patient comfort for typically long treatment sessions, stability of setup, and accommodation of devices accounting for organ motion.
3. The radiation oncologist will determine and recommend a procedure to account for inherent organ motion for targets that are significantly influenced by such motion. This activity may include execution of a variety of methods, including respiratory gating, tumor tracking, organ motion dampening, or patient-directed methods.
4. It is the radiation oncologist's responsibility to supervise patient simulation using appropriate imaging methods. The radiation oncologist needs to be aware of the spatial accuracy and precision of the imaging modality. Steps must be taken to ensure that all aspects of simulation, including positioning, immobilization, and methods to account for inherent organ motions, are properly carried out. The radiation oncologist must furthermore ensure that the targeting

accuracy and precision used for the simulation will be reproduced with high certainty when the patient is treated.

5. After the planning images have been acquired, they will be transferred to the treatment-planning computer, and the radiation oncologist will contour the outline of the gross tumor/target volume (GTV). Generally only visible tumor will be targeted, but in certain circumstances the radiation oncologist will use knowledge of the pattern of microscopic spread and knowledge of normal tissue tolerance to enlarge the GTV to constitute the clinical target volume (CTV). In some instances the concept of a "motion-corrected" GTV may be used prior to expanding margins to create a CTV. Subsequently, with knowledge of the mechanical uncertainty of the treatment apparatus, the extent of setup uncertainty, inherent and residual organ motion, and other patient or system-specific uncertainties, the radiation oncologist will coordinate the design for the proper planning target volume (PTV) beyond the clinical tumor target(s). In addition to these tumor targets, the radiation oncologist will see that relevant normal tissues are contoured such that dose volume limits are considered. Locating and specifying the target volumes and relevant critical normal tissues will be carried out after consideration of all relevant imaging studies.

6. The radiation oncologist will convey case-specific expectations for prescribing the radiation dose to the target volume and for setting limits on dose to normal tissue. Participating in the iterative process of plan development, the radiation oncologist will approve the final treatment plan in collaboration with a medical physicist.

7. After obtaining informed consent, the radiation oncologist will attend and direct the actual treatment process. Pre-medications, sedation, pain medicines, or anesthesia will be prescribed as appropriate. Patients will be positioned according to the simulation and treatment plan. Treatment devices used for stereotactic targeting and methods that account for inherent organ motion will be enabled. The conduct of all members of the treatment team will be under the direct supervision of the radiation oncologist.

5.2.2 Qualified Medical Physicist

The medical physicist is responsible for the technical aspects of radiosurgery and must be available for consultation throughout the entire procedure: imaging, treatment planning, and dose delivery. Those responsibilities shall be clearly defined and should include the following:

1. Acceptance testing and commissioning of the SBRT system, thereby assuring its geometric and dosimetric precision and accuracy. This includes:

   (a) Localization devices used for accurate determination of target coordinates.
   (b) The image-based 3D and/or intensity-modulated treatment planning system.
   (c) The SBRT external beam delivery unit.

2. Implementing and managing a quality control (QC) program for the SBRT system to monitor and assure proper functioning of:

   (a) The SBRT external beam delivery unit.
   (b) The image guidance system as well as all other imaging devices used for SBRT.
   (c) The image-based 3D and/or intensity-modulated treatment planning system.

3. Establishing a comprehensive QC checklist that acts as a detailed guide to the entire treatment process.
4. Directly supervising or checking the 3D and/or intensity-modulated treatment planning process.
5. Communicating with the radiation oncologist to discuss the optimal patient plan.
6. Using the plan approved by the radiation oncologist to determine and check the appropriate beam-delivery parameters. This includes the calculation of the radiation beam parameters consistent with the beam geometry.
7. Ensuring that the beam delivery process on the treatment unit accurately fulfills the prescription of the radiation oncologist.

5.2.3 Qualified Radiation Therapist

The responsibilities of the radiation therapist shall be clearly defined and may include the following:

1. Preparing the treatment room for the SBRT procedure.
2. Assisting the treatment team with patient positioning/immobilization.
3. Operating the treatment unit after the radiation oncologist and medical physicist have approved the clinical and technical aspects for beam delivery.

5.2.4 Other Participants

The radiation oncologist, as the primary physician involved in the assessment of patient suitability and supervision of the delivery of SBRT, may choose to obtain consultation from other specialists as necessary.

5.2.5 Equipment QA

Specific quality assurance processes and procedures for SBRT can be grouped in two broad categories: equipment-related and patient-related. As with other delivery

modalities, it is recommended for stereotactic programs to create daily, monthly and annual equipment quality assurance procedures.

Daily QA activities should be designed to verify the basic functionality and safe operation of the delivery and imaging equipment, especially the integrity of individual delivery and imaging devices, localization capabilities, and verification of the coincidence of imaging and therapeutic radiation isocenters of the treatment unit. Monthly QA procedures should be designed to detect trends in performance away from baseline and are focused on the imaging and delivery devices most likely to affect patient treatment. Annual QA procedures should be a thorough test of all aspects of the individual and integrated stereotactic system, including imaging, treatment planning, localization, R/V (record/verification), and delivery devices and processes.

These QA procedures should be designed to detect any deviation from the baseline performance of the system determined at commissioning. AAPM Task Group 142 (TG-142) provides a comprehensive list of test, frequencies and tolerances for linear accelerator-based radiotherapy [3]. While all of the tests are relevant to linac-based SRS/SBRT programs and must be performed accordingly, TG-142 provides more rigorous tolerances for those tests specific to SRS and SBRT treatments. These are summarized in Tables 5.1 and 5.2.

Table 5.1 presents SRS/SBRT-specific linac-related quality assurance requirements, which include the standard linear accelerator tests described in TG-142 and additional tests listed in "Quality and safety considerations in SRS and SBRT" in ASTRO [4]. Daily, monthly, and annual tests in Table 5.1 have specific recommendations based on the nature of the treatments delivered on the individual machine and are supplemented and modified as needed. Several tests deserve additional discussion. First, in addition to mechanical and safety tests in TG-142, a "Winston-Lutz" type of test provides the fundamental assessment of radiation isocenter and should be performed daily. The Winston-Lutz test can be performed by use of a film or an amorphous silicon electronic portal imaging device (EPID). Second, if image guidance is used for either cranial or extracranial localization, a test that verifies proper calibration and operation of those systems should also be performed daily. The Winston-Lutz test for both cones and MLC, covering complete range of gantry, couch, and collimator positions should be performed monthly. A hidden target test using SRS frame and/or IGRT system is performed monthly. Finally, end-to-end tests of both localization and dosimetric capabilities should be performed annually to assess the accuracy and integrity of the SRS/SBRT processes in an integrated manner.

Table 5.2 presents SRS/SBRT-specific imaging-related quality assurance requirements, which include the standard linear accelerator tests described in both the AAPM Task Group 142 report and ASTRO. The tests that verify geometrical arraignment, imaging quality, and imaging dose for planner kV and MV (EPID) imaging and cone-beam CT (kV and MV) should be performed appropriate frequency.

These SRS/SBRT-specific quality assurance requirements recommend annual evaluation of these characteristics. In addition, the report of AAPM task group 101 (TG-101) provides a number of excellent references for medical physicists,

Table 5.1 SRS/SBRT-specific linac-related quality assurance requirements

Procedure	Tolerance
Daily Tests	
Mechanical	
Laser localization	1 mm
Distance indicator (at isocenter)	2 mm
Collimator size indicator : both jaws and MLC	1 mm
Safety	
Stereotactic interlocks (lockout): cone size, backup jaws	Functional
In addition to tests listed above (ASTRO)	
Winston-Lutz test	$\leq$0.75 mm average
IGRT positioning/repositioning	$\leq$1 mm
Imaging subsystem interlocks	Functional
Monthly Tests	
Dosimetry	
Typical dose rate[a] output constancy	2 % (at SRS/SBRT dose rate, MU)
Mechanical	
Treatment couch position indicators[b]	1 mm/0.5°
Localizing lasers	$\leq$1 mm
In addition to tests listed above (ASTRO)	
Winston-Lutz test: both cones and MLC, covering complete range of gantry, couch, collimator positions	$\leq$0.75 mm average, $\leq$1 mm maximum
Hidden target test using SRS frame and/or IGRT system	$\leq$1 mm
Annual Tests	
Dosimetry	
SRS arc rotation mode (range: 0.5–10 MU/deg)	Monitor units set vs delivered:
	1 MU or 2 % (whichever is greater)
	Gantry arc set vs delivered:
	1° or 2 % (whichever is greater)
X-ray monitor unit linearity (output constancy)	$\pm$5 % (2–4 MU),
	$\pm$2 % $\geq$ 5 MU
Mechanical	
Coincidence of radiation and mechanical isocenter	$\pm$1 mm from baseline
Stereotactic accessories, lockouts, etc.	Functional
In addition to tests listed above (ASTRO)	
Verification of small field beam data: output factors, depth dose, and off axis profiles for cones and MLC	$\pm$1 % from baseline
End-to-end localization assessment "hidden target test" using SRS frame and/or IGRT system	$\leq$1 mm
End-to-end dosimetric evaluation using SRS frame and/or IGRT system	$\leq$2 %

The standard linear accelerator tests described in the AAPM Task Group 142 report and additional tests in ASTRO

[a]Dose monitoring as a function of dose rate

[b]Lateral, longitudinal, and rotational

Table 5.2 SRS/SBRT-specific imaging-related quality assurance requirements

Procedure	Tolerance
Daily Tests[a]	
Planar kV and MV (EPID) imaging	
Collision interlocks	Functional
Positioning/repositioning	≤1 mm
Imaging and treatment coordinate coincidence (single gantry angle)	≤1 mm
Cone-beam CT (kV and MV)	
Collision interlocks	Functional
Positioning/repositioning	≤1 mm
Imaging and treatment coordinate coincidence	≤1 mm
Monthly Tests	
Planar kV[b] and MV (EPID) imaging	
Scaling[c]	≤1 mm (kV), ≤2 mm (MV)
Imaging and treatment coordinate coincidence (four cardinal angles)	≤1 mm
Spatial resolution, contrast, uniformity and noise	Baseline
Cone-beam CT (kV and MV)	
Geometric distortion	≤1 mm
Spatial resolution, contrast, HU constancy, uniformity and noise	Baseline
Annual Tests	
Planar kV imaging	
Beam quality/energy	Baseline
Imaging dose	Baseline
Planar MV imaging (EPID)	
Full range of travel SDD	±5 mm
Imaging dose[d]	Baseline
Cone-beam CT (kV and MV)	
Imaging dose	Baseline

The standard linear accelerator tests described in both the AAPM Task Group 142 report and ASTRO
[a]Or at a minimum when devices are to be used during treatment day
[b]kV imaging refers to both 2D fluoroscopic and radiographic imaging
[c]Scaling measured at SSD typically used for imaging
[d]Imaging dose to be reported as effective dose for measured doses per TG 75

clinicians, and therapists in order to outline the best practice guidelines for SBRT [5]. The report of AAPM task group 135 will provide specific guidance for QA of robotic radiosurgery devices [6]. Similarly, the report of AAPM TG-148 describes QA for helical tomotherapy devices [7].

The TG-101 report includes a review of the literature to identify reported clinical findings and expected outcomes for the treatment modality. Information is provided for establishing a SBRT program, including protocols, equipment, resources, and QA procedures. Additionally, suggestions for developing consistent documentation for prescribing, reporting, and recording SBRT treatment delivery is provided. The

Table 5.3 Comparison of typical characteristics of 3D/IMRT radiotherapy and SBRT

Characteristic	3D/IMRT	SBRT
Dose/fraction	1.8–3 Gy	6–30 Gy
No. of fractions	10–30	1–5
Target definition	CTV/PTV (gross disease + clinical extension): Tumor may not have a sharp boundary	GTV/CTV/ITV/PTV (well-defined tumors: GTV = CTV)
Margin	Centimeters	Millimeters
Physics/dosimetry monitoring	Indirect	Direct
Required setup accuracy	TG40, TG142	TG40, TG142
Primary imaging modalities used for treatment planning	CT	Multimodality: CT/MR/PET-CT
Redundancy in geometric verification	No	Yes
Maintenance of high spatial targeting accuracy for the entire treatment	Moderately enforced (moderate patient position control and monitoring)	Strictly enforced (sufficient immobilization and high frequency position monitoring through integrated image guidance)
Need for respiratory motion management	Moderate – Must be at least considered	Highest
Staff training	Highest	Highest + special SBRT training
Technology implementation	Highest	Highest
Radiobiological understanding	Moderately well understood	Poorly understood
Interaction with systemic therapies	Yes	Yes

major feature that separates SBRT from conventional radiation treatment is the delivery of large doses in a few fractions, which results in a high biological effective dose (BED). In order to minimize the normal tissue toxicity, conformation of high doses to the target and rapid fall-off doses away from the target is critical. The practice of SBRT therefore requires a high level of confidence in the accuracy of the entire treatment delivery process. *In SBRT, confidence in this accuracy is accomplished by the integration of modern imaging, simulation, treatment planning, and delivery technologies into all phases of the treatment process; from treatment simulation and planning, and continuing throughout beam delivery.*

In addition to these major features, there are other characteristics that distinguish SBRT from conventional radiation therapy (Table 5.3). These include a general increase in the number of beams used for treatment, the frequent use of noncoplanar beam arrangements, small or no beam margins for penumbra, and the use of inhomogeneous dose distributions and dose-painting techniques (including IMRT). All of these technology improvements result in the highly conformal dose distribution that characterizes the SBRT technique.

Table 5.4 summarizes historical immobilization strategies and their associated localization errors. Stereotactic body frames (e.g., Elekta, Medical Intelligence Body Fix, Leibinger, Yenice, Lech Papiez, etc.) serve both to immobilize the patient physically and provide an initial approximate target localization, which is subsequently refined by in-room image-guided techniques. Body frames typically make use of vacuum cushions for immobilization. Stereotactic localization and targeting can be facilitated by a localizer arch which can be affixed to the body frame or to the linac couch top, and define the reference coordinate system of body frame fiducials. Some body frame systems also include equipment for abdominal compression which can be used to minimize respiratory motion [16, 23, 24]. In addition, a recent QA supplement published in the International Journal of Radiation Oncology Biology Physics [25] suggests a set of annual, monthly, and daily QA activities and tolerances which allow verification of the overall accuracy of various aspects of the IGRT/SBRT treatment process (summarized in Table 5.5).

Table 5.4 Achievable accuracies reported in the literature categorized by body site and immobilization/repositioning device

Author, year	Site	Immobilization/repositioning	Reported accuracy
Lax, 1994[a]	Abdomen	Wood frame/stereotactic coordinates on box to skin marks	3.7 mm Lat, 5.7 mm Long
Hamilton, 1995[b]	Spine	Screw fixation of spinous processes to box	2 mm
Murphy, 1997[c]	Spine	Frameless/implanted fiducial markers with real-time imaging and tracking	1.6 mm radial
Lohr, 1999[d]	Spine	Body cast with stereotactic coordinates	≤3.6 mm mean vector
Yenice, 2003[e]	Spine	Custom stereotactic frame and in-room CT guidance	1.5 mm system accuracy, 2–3 mm positioning accuracy
Chang, 2004[f]	Spine	MI™ BodyFix with stereotactic frame/linac/CT on rails with 6D robotic couch	1 mm system accuracy
Tokuuye, 1997	Liver	Prone position jaw and arm straps	5 mm
Nakagawa, 2000[g]	Thoracic	MVCT on linac	Not reported
Wulf, 2000[h]	Lung, liver	Elekta™ body frame	3.3 mm lat, 4.4 mm long
Fuss, 2004[i]	Lung, liver	MI™ BodyFix	Bony anatomy translation 0.4, 0.1, 1,6 mm (mean X, Y, Z); tumor translation before image guidance 2.9, 2.5, 3.2 mm (mean X, Y, Z)
Herfarth, 2001[j]	Liver	Leibinger body frame	1.8–4.4 mm
Nagata, 2002[k]	Lung	Elekta™ body frame	2 mm

(continued)

Table 5.4 (continued)

Author, year	Site	Immobilization/repositioning	Reported accuracy
Fukumoto, 2002[l]	Lung	Elekta™ body frame	Not reported
Hara, 2002[m]	Lung	Custom bed transferred to treatment unit after confirmatory scan	2 mm
Hof, 2003[n]	Lung	Leibinger body frame	1.8–4 mm
Timmerman, 2003[o]	Lung	Elekta™ body frame	Approx. 5 mm
Wang, 2006[p]	Lung	Medical Intelligence body frame stereotactic coordinates/CT on rails	0.3 ± 1.8 mm AP, -1.8 ± 3.2 mm Lat, 1.5 ± 3.7 mm SI

[a]Reference [8]
[b]Reference [9]
[c]Reference [10]
[d]Reference [11]
[e]Reference [12]
[f]Reference [13]
[g]Reference [14]
[h]Reference [15]
[i]Reference [16]
[j]Reference [17]
[k]Reference [18]
[l]Reference [19]
[m]Reference [20]
[n]Reference [21]
[o]Reference [22]
[p]Reference [23]

Table 5.5 Summary of published QA recommendations for SBRT and SBRT-related techniques

Source	Purpose	Proposed test	Reported achievable tolerance	Proposed frequency
Ryu et al. (2001)[a]	End-to-end localization accuracy	Stereo x ray/DRR fusion	1.0–1.2 mm root mean square	Initial commissioning and annually thereafter
Ryu et al. (2001)[a]	Intrafraction targeting variability	Stereo x ray/DRR fusion	0.2 mm average, 1.5 mm maximum	Daily (during treatment)
Verellen et al. (2003)[b]	End-to-end localization accuracy	Hidden target (using stereo x ray/DRR fusion)	0.41 ± 0.92 mm	Initial commissioning and annually thereafter
Verellen et al. (2003)[b]	End-to-end localization accuracy	Hidden target (using implanted fiducials)	0.28 ± 0.36 mm	Initial commissioning and annually thereafter

Table 5.5 (continued)

Source	Purpose	Proposed test	Reported achievable tolerance	Proposed frequency
Yu et al. (2004)[c]	End-to-end localization accuracy	Dosimetric assessment of hidden target (using implanted fiducials)	0.68 ± 0.29 mm	Initial commissioning and annually thereafter
Sharpe et al. (2006)[d]	CBCT mechanical stability	Constancy comparison to MV imaging isocenter (using implanted fiducials)	0.50 ± 0.5 mm	Baseline at commissioning and monthly thereafter
Galvin et al. (2008)[e]	Overall positioning accuracy, including image registration (frame-based systems)	Winston–Lutz test modified to make use of the in-room imaging systems	≤2 mm for multiple couch angles	Initial commissioning and annually thereafter
Palta et al. (2008)[f]	MLC accuracy	Light field, radiographic film, or EPID	<0.5 mm (especially for IMRT delivery)	Annually
Solberg et al. (2008)[g]	End-to-end localization accuracy	Hidden target in anthropomorphic phantom	1.10 ± 0.42 mm	Initial commissioning and annually thereafter
Jiang et al. (2008)[h]	Respiratory motion tracking and gating in 4D CT	Phantoms with cyclical motion	N/A	N/A
Bissonnette et al. (2008)[i]	CBCT geometric accuracy	Portal image vs CBCT image isocenter coincidence	±2 mm	daily

[a]Reference [26]
[b]Reference [27]
[c]Reference [28]
[d]Reference [29]
[e]Reference [30]
[f]Reference [31]
[g]Reference [32]
[h]Reference [33]
[i]Reference [34]

References

1. World Health Organization (WHO). Radiotherapy risk profile technical manual; 2006, Geneva.
2. Potters L, Kavanagh B, Galvin JM, et al. American Society for Therapeutic Radiology and Oncology (ASTRO) and American College of Radiology (ACR) practice guideline for the performance of stereotactic body radiation therapy. Int J Radiat Oncol Biol Phys. 2010;76:326–32.

3. Klein EE, Hanley J, Bayouth J, et al. Task Group 142 report: quality assurance of medical accelerators. Med Phys. 2009;36:4197–212.
4. Solberg TD, Balter JM, Benedict SH, et al. Quality and safety considerations in stereotactic radiosurgery and stereotactic body radiation therapy. Pract Radiat Oncol 2011;1–49.
5. Benedict SH, Yenice KM, Followill D, et al. Stereotactic body radiation therapy: the report of AAPM Task Group 101. Med Phys. 2010;37(8):4078–101.
6. Dieterich S, Cavedon C, Chuang CF, et al. Report of AAPM TG 135: quality assurance for robotic radiosurgery. Med Phys. 2011;38:2914–36.
7. Langen KM, Papanikolaou N, Balog J, et al. QA for helical tomotherapy: report of the AAPM Task Group 148. Med Phys. 2010;37:4817–53.
8. Lax I, Blomgren H, Naslund I, Svanstrom R. Stereotactic radiotherapy of malignancies in the abdomen. Methodological aspects. Acta Oncol. 1994;33:677–83.
9. Hamilton AJ, Lulu BA, Fosmire H, Stea B, Cassady JR. Preliminary clinical experience with linear accelerator-based spinal stereotactic radiosurgery. Neurosurgery. 1995;36:311–19.
10. Murphy MJ. An automatic six-degree-of-freedom image registration algorithm for image-guided frameless stereotaxic radiosurgery. Med Phys. 1997;24:857–66.
11. Lohr F, Debus J, Frank C, Herfarth K, Pastyr O, Rhein B, et al. Noninvasive patient fixation for extracranial stereotactic radiotherapy. Int J Radiat Oncol Biol Phys. 1999;45:521–7.
12. Yenice KM, Lovelock DM, Hunt MA, Lutz WR, Fournier-Bidoz N, Hua CH, et al. CT image-guided intensity-modulated therapy for paraspinal tumors using stereotactic immobilization. Int J Radiat Oncol Biol Phys. 2003;55:583–93.
13. Chang EL, Shiu AS, Lii MF, Rhines LD, Mendel E, Mahajan A, et al. Phase I clinical evaluation of near-simultaneous computed tomographic image-guided stereotactic body radio-therapy for spinal metastases. Int J Radiat Oncol Biol Phys. 2004;59:1288–94.
14. Nakagawa K, Aoki Y, Tago M, Terahara A, Ohtomo K. Megavoltage CT-assisted stereotactic radiosurgery for thoracic tumors: original research in the treatment of thoracic neoplasms. Int J Radiat Oncol Biol Phys. 2000;48:449–57.
15. Wulf J, Hadinger U, Oppitz U, Olshausen B, Flentje M. Stereotactic radiotherapy of extracra-nial targets: CT-simulation and accuracy of treatment in the stereotactic body frame. Radiother Oncol. 2000;57:225–36.
16. Fuss M, Salter BJ, Rassiah P, Cheek D, Cavanaugh SX, Herman TS. Repositioning accuracy of a commercially available double-vacuum whole body immobilization system for stereotactic body radiation therapy. Technol Cancer Res Treat. 2004;3:59–67.
17. Herfarth KK, Debus J, Lohr F, Bahner ML, Rhein B, Fritz P, et al. Stereotactic single-dose radiation therapy of liver tumors: results of a phase I/II trial. J Clin Oncol. 2001;19:164–70.
18. Nagata Y, Negoro Y, Aoki T, Mizowaki T, Takayama K, Kokubo M, et al. Clinical outcomes of 3D conformal hypofractionated single high-dose radiotherapy for one or two lung tumors using a stereotactic body frame. Int J Radiat Oncol Biol Phys. 2002;52:1041–6.
19. Fukumoto S, Shirato H, Shimzu S, Ogura S, Onimaru R, Kitamura K, et al. Small-volume image-guided radiotherapy using hypofractionated, coplanar, and noncoplanar multiple fields for patients with inoperable stage I nonsmall cell lung carcinomas. Cancer. 2002;95:1546–53.
20. Hara R, Itami J, Kondo T, Aruga T, Abe Y, Ito M, et al. Stereotactic single high dose irradiation of lung tumors under respiratory gating. Radiother Oncol. 2002;63:159–63.
21. Hof H, Herfarth KK, Munter M, Hoess A, Motsch J, Wannenmacher M, et al. Stereotactic single-dose radiotherapy of stage I non-small-cell lung cancer (NSCLC). Int J Radiat Oncol Biol Phys. 2003;56:335–41.
22. Timmerman R, Papiez L, McGarry R, Likes L, DesRosiers C, Frost S, et al. Extracranial stereotactic radioablation: results of a phase I study in medically inoperable stage I non-small cell lung cancer. Chest. 2003;124:1946–55.
23. Wang L, Feigenberg S, Chen L, Pasklev K, Ma CC. Benefit of three-dimensional image-guided stereotactic localization in the hypofractionated treatment of lung cancer. Int J Radiat Oncol Biol Phys. 2006;66:738–47.

24. Wang L, Jacob R, Chen L, Ma C, Movsas B, Feigenberg S, et al. Stereotactic IMRT for prostate cancer: setup accuracy of a new stereotactic body localization system. J Appl Clin Med Phys. 2004;5:18–28.
25. Williamson JF, Thomadsen BR. Quality assurance for radiation therapy, quality assurance of radiation therapy: the challenges of advanced technologies symposium. Int J Radiat Oncol Biol Phys. 2008;71:S1–S214.
26. Ryu I, Chang SD, Kim DH, Murphy MJ, Le QT, Martin DP, et al. Image-guided hypo-fractionated stereotactic radiosurgery to spinal lesions. Neurosurgery. 2001;49:838–46.
27. Verellen D, Soete G, Linthout N, Van Acker S, De Roover P, Vinh-Hung V, et al. Quality assurance of a system for improved target localization and patient set-up that combines real-time infrared tracking and stereoscopic X-ray imaging. Radiother Oncol. 2003;67:129–41.
28. Yu C, Main W, Taylor D, Kuduvalli G, Apuzzo ML, Adler Jr JR. An anthropomorphic phantom study of the accuracy of Cyberknife spinal radiosurgery. Neurosurgery. 2004;55:1138–49.
29. Sharpe MB, Moseley DJ, Purdie TG, Islam M, Siewerdsen JH, Jaffray DA. The stability of mechanical calibration for a kV cone beam computed tomography system integrated with linear accelerator. Med Phys. 2006;33:136–44.
30. Galvin JM, Bednarz G. Quality assurance procedures for stereotactic body radiation therapy. Int J Radiat Oncol Biol Phys. 2008;71:S122–5.
31. Palta JR, Liu C, Li JG. Quality assurance of intensity-modulated radiation therapy. Int J Radiat Oncol Biol Phys. 2008;71:S108–12.
32. Solberg TD, Medin PM, Mullins J, Li S. Quality assurance of immobilization and target localization systems for frameless stereotactic cranial and extracranial hypofractionated radio-therapy. Int J Radiat Oncol Biol Phys. 2008;71:S131–5.
33. Jiang SB, Wolfgang J, Mageras GS. Quality assurance challenges for motion-adaptive radiation therapy: gating, breath holding, and four-dimensional computed tomography. Int J Radiat Oncol Biol Phys. 2008;71:S103–7.
34. Bissonnette JP, Moseley D, White E, Sharpe M, Purdie T, Jaffray DA. Quality assurance for the geometric accuracy of cone-beam CT guidance in radiation therapy. Int J Radiat Oncol Biol Phys. 2008;71:S57–61.

Part III
Clinical Applications

Chapter 6
Fixation

Shinsuke Yano

6.1 Fixation

Methods of stereotactic body irradiation and fixation have changed with the introduction of stereotactic body radiation therapy (SBRT). Compared to the brain, head, and neck cancer, it is difficult to target lesions with the body by stereotactic irradiation due to difficulty in achieving a stationary target. Lesions in the lung are particularly difficult to irradiate due to respiratory and other physiological movements. The method used for stereotactic body irradiation is set in each facility to maintain precise determination of tumor position [1–14]. The four-dimension computed tomography (CT) scan method was introduced in our facility, making use of the improved performance of CT compared to the free-breathing irradiation using dynamic tumor tracking method [9, 14–23].

This chapter discusses our clinical experience with this method focusing on (1) the requirements for the fixation device, (2) the characteristics of representative immobilization, (3) points that require attention for appropriate immobilization and setup, (4) fixation and setup error, (5) points that require attention regarding the dose at the time of immobilization, and (6) the interference of the fixation device with the gantry.

S. Yano (✉)

Division of Clinical Radiology Service, Kyoto University Hospital, 54 Shogoin-Kawaharacho, Sakyo-ku, Kyoto 606-8507, Japan
e-mail: yan@kuhp.kyoto-u.ac.jp

6.2 Requirements of Immobilization for Patient Positioning

As stereotactic body irradiation requires a high degree of positional precision, a fixation device is used to increase precision and repeatability by maintaining the patient in the same position for the duration of the treatment. However, there may be a long delay between position verification and the start of irradiation, and this may increase patient discomfort, which in turn reduces positional precision. Therefore, it is necessary to keep the treatment time as short as possible.

In addition, the monitor units (MUs) needed in one irradiation port can become large, so a number of irradiation ports may be needed. This can result in a long treatment time of around 30 min, including verification with a large dose per fraction in stereotactic body irradiation. The requirements for patient positioning and fixation are as follows:

- Some degree of flexibility to allow the patient to maintain the position for a long time
- Ability to control the patient's movement during treatment
- Ability for the patient to repeatedly maintain the same position naturally
- Repeatability of placement on the bed for each treatment
- Hygienic and maximizes patient comfort

6.3 Types of Immobilization Device for Stereotactic Body Radiation Therapy

Various immobilization devices are available, each of which has advantages and disadvantages. It is necessary to choose the appropriate device for the therapeutic method used in each facility.

Various devices are available to control frame movement and precisely reproduce the patient's position, including a shell for body fixation, vacuum pillow-type fixation [24, 25] (Fig. 6.1), and a body frame [1–6, 16] (Fig. 6.2). Different systems make use of various methods to maximize accuracy, e.g., irradiation can be performed using a board [15, 16] to apply pressure to the abdomen for respiratory depression, with synchronized breathing control, dynamic tumor tracking irradiation [18–23] (Fig. 6.3), respiratory gating irradiation [8, 10, 11], or using an internal marker [23].

To confirm breathing position, we placed an infrared marker [21, 22] on the diaphragm region with an abdominal pressure belt and observed the breathing pattern using a spirometer [13]. Accurate and reproducible fixation could be achieved using this device.

Breathing-related movement can be controlled by suppressing diaphragmatic movement as with an abdominal pressure board. Whether movement is restrained can be determined by observing tumor movement by fluoroscopy, and the strength of pressure applied by the board can be regulated accordingly.
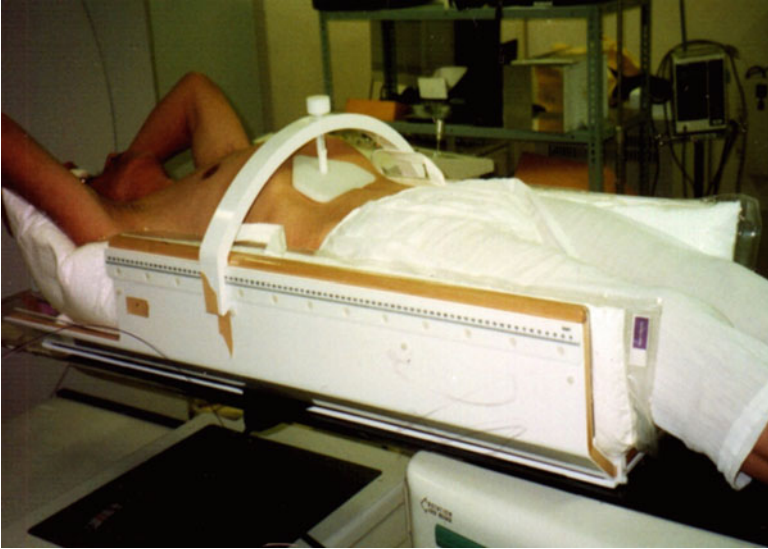
Fig. 6.1 Stereotactic body frame (Elekta): Patient setup using diaphragm control in SBRT. Breathing-related movement of tumor can be controlled
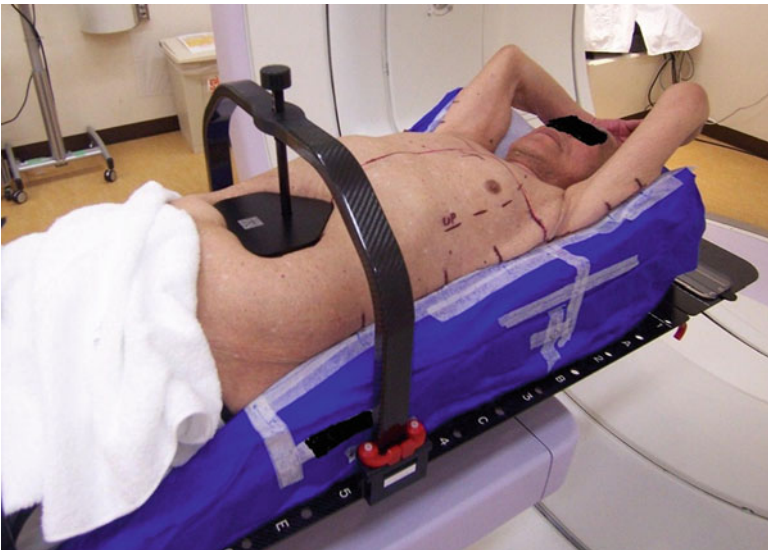

Fig. 6.2 Body FIX (Elekta): Patient setup using diaphragm control in SBRT

Fig. 6.3 Body FIX (Elekta): Patient setup in dynamic tracking irradiation. Positioning for dynamic tracking is setting in immobilization with free breathing condition, and the infrared marker is putting on upper abdomen for acquisition of breathing signal

In cases with a lesion in the lower lung field, diaphragm movement can be restrained by an average of more than 5 mm, and therefore the irradiation range can be minimized by reducing the movement of the tumor [15].

Depending on the case, breathing-related movement may be large when pressure is applied to the diaphragm region. Such movement may be controlled by applying abdominal pressure, but it may be necessary to apply oxygen inhalation as breathing tends to become relatively shallow with such treatment [7].

Then, I explain the function of the fixture with the change of the fixture of our facilities.

When we first began performing stereotactic body irradiation at our facilities during until 2007, we adopted the Stereotactic Body Frame (SBF) [1–6, 16] (Fig. 6.1) developed by the Swedish company Elekta with the cooperation of Karolinska Hospital in Stockholm.

We subsequently introduced the high-flexibility Body Fix [24, 25] (Fig. 6.3) for immobilization, which interfered little with the gantry and showed little dose absorption at our facilities.

Irradiation was carried out in patents under free-breathing conditions by dynamic tumor tracking irradiation [18–23]. It became clear that immobilization techniques with which it was easy to observe movement from each direction in fluoroscopy images were required.

This method is available for liver and pancreatic cancer, and clinical results have been reported for a therapeutic method using SBF adapted for body irradiation [1–6].

Figure 6.4 shows immobilization SBF for use in SBRT of the trunk region. The size and shape of SBF with a minimum opening of 550 mm are designed for
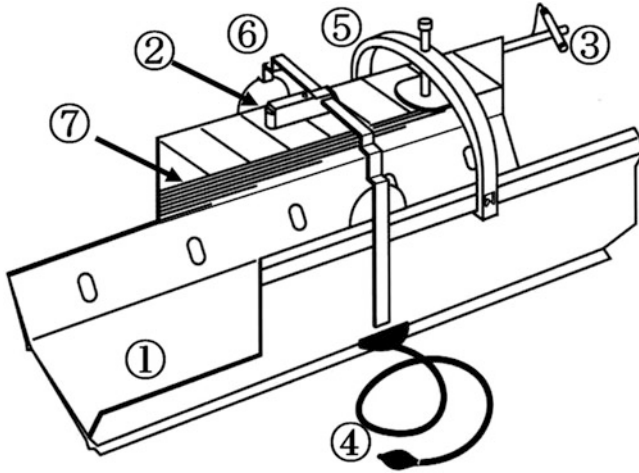
Fig. 6.4 Structure of SBF immobilization: (*1*) Body frame, (*2*) Chest marker, (*3*) Leg maker, (*4*) Level control, (*5*) Diaphragm control, (*6*) XY-axis scale, (*7*) localizer scale for CT image

CT, magnetic resonance (MR), and positron emission tomography (PET). The frame wall is composed of glass fiber and white birch plywood, low-density materials that keep attenuation of the beam to a minimum [16]. There is an atmospheric layer and a vacuum pillow inside the frame. CT level of pillow part is almost equivalent to atmosphere. This part can be molded along the body of the patient. Furthermore, a CT indicator made of polymethyl methacrylate (PMMA), which can read the three-dimensional coordinates on CT, is embedded within the inner wall of the frame, and a Z-axis scale made of plastic is attached to the outer wall. A XY- axis scale for positioning is shaped arch on a frame, and made of aluminum, which can remove during irradiation. There is a level control that made of rubber bag in unilateral of the frame base. This function can control to coordinate the position of horizontal direction with adjusting of air pressure. In addition, as other appliances, laser pointer can be set for skin marker on chest wall (Fig. 6.5a), and the pressure board can be set to control breathing movement on upper abdomen.

The stereotactic body frame (SBF) has many functions that were developed for stereotactic body radiation therapy (SBRT) with a high degree of reproducibility. We introduced Body Fix in place of SBF in our facilities in 2007 as it has a number of advantages in that it is composed of material with little dose absorption, its structure interferes little with the gantry, and it has high spatial flexibility. For dynamic tumor tracking irradiation, the patient is irradiated under free-breathing conditions. Therefore, a fixation device that facilitates observation of the movement of a marker and the lesion in fluoroscopy images during irradiation or verification was required. The fixation device requires precision, and a function to reproduce the setup position of bone exactly is required. Alignment requires use of a skin mark and an adjustment appliance prior to use. Bone position can be reproduced with greater precision and within a shorter time using image-guided radiation therapy

(IGRT) compared to previous methodologies. The position revision in verification enabled automatic reproduction of a position and a tilt with accurate six-axial (X, Y, Z, Roll, Pitch, and Yaw) revision of couch position. However, during setup, it is necessary to reproduce torsion and flexure of the body in a minimum requirement. Accordingly introduction of IGRT, the purpose of the fixture and the necessary matter changed. Use of a fixation device such as Body Fix, which is simple and shows little absorption, is effective for positioning verification using fluoroscopy, such as dynamic tracking irradiation or irradiation synchronized with respiration.

6.4   Points That Require Attention in Immobilization

Long-term patient fixation may be accompanied by patient discomfort, with reduced blood circulation resulting in numbness. In addition, low back pain due to remaining in the same posture for a long time may occur. To prevent these issues, it is necessary to fix the patient in as relaxed a state as possible. It is comfortable for patient that neck and both elbows are lifted up naturally in making immobilization. It is easier for patients to remain in the same position for a long time when they are relatively comfortable, and this improves precision.

For immobilization, we do not begin alignment immediately as it is important to confirm the patient's breathing and to perform the procedure with the patient in a relaxed state. This step must be performed manually in each case, and we explain the positioning procedure to the patient to secure his/her cooperation.

In the case of vacuum-type fixation, we should not be write mark and scan CT soon after making fixation. The patient is awakened after immobilization, and then the point of contact on the skin surface is marked to ensure application to the same position in each treatment (Fig. 6.5b). This can prevent extreme clamping and ensure that there are no differences in the conditions at the time of irradiation.
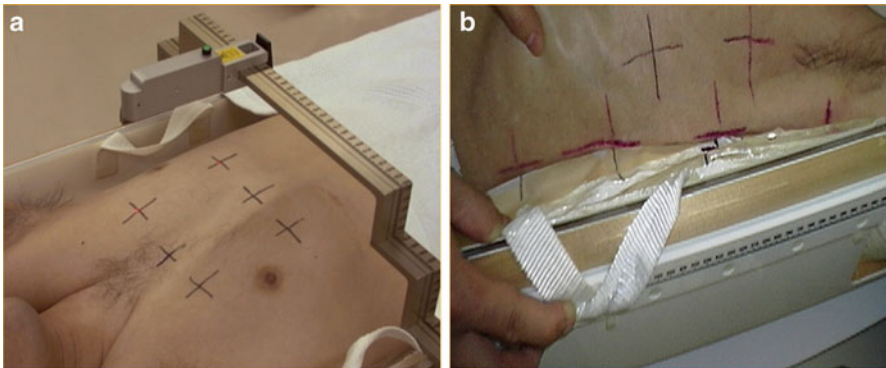

Fig. 6.5 (**a**): Skin marking line on contact point with immobilization is useful for setup in every positioning. (**b**): Chest laser marker on SBF. In positioning, this marker is used for setting to prevent of leaning and twisting body

With regard to the time to irradiate, it is desirable to set as possible the same time in consideration of time after a meal.

In the case of using diaphragm control and shell on chest, there is some possible of deteriorating in precision of setup position, and cause to pain of the patient.

6.5 Immobilization and Setup Error

Due to the high dose of radiation given at each time, repositioning accuracy may influence the radiation dose applied to the lesion.

Patient fixation is closely related to intra- and interfractional setup error. The positional precision depends on accurate repositioning and maintenance of the patient's position during irradiation. Positional precision is confirmed just before irradiation and any error is revised. It is necessary to maintain the position during treatment [26].

The introduction of IGRT technology has enabled bone position to be corrected just before irradiation, along with the position or tilt on X-ray images in six-axial directions, which can reduce the internal fractional setup error. However, we cannot revise the torsion of the body, curve, expansion, or contraction by IGRT revision. It leads to reducing internal fractional setup error to decrease these states by the setup using the fixture as much as possible. It is important that patient movement during irradiation remains within the bounds considered in intrafractional setup error, as outlined in the ICRU-62 report [27] regarding factors related to planning target volume (PTV).

It is important that the fixation device is capable of ensuring that the patient does not move during irradiation. Simultaneously, the fixation device must not be tight and uncomfortable to facilitate relaxation of the patient. If these conditions are satisfied, inter- and intra-fractional setup errors would be reduced, thus lowering the margin setting added to internal target volume (ITV).

Once immobilization has been achieved, adjoining regions of the skin are marked with lines (Fig. 6.5b). Lining up these marks on the right and left sides of the body can prevent rolling of the body axis.

When calvarial position accords in immobilization at the decided position, in the craniocaudal direction, the same position is reproduced every time. Therefore it is important to form the calvarial part of the fixture definitely.

The evaluation of repositioning is usually verified by bone position. For other methods, a tumor position is verified with higher precision by the observation of the internal marker using fluoroscopy or the verification of the organ using CBCT.

Agreement of tumor position according to the internal marker and CBCT increases the degree of positional precision, but changes in the trajectory of the irradiation beam and lesion depth affect the absorbed dose when there are changes in the body axis. Therefore, it is necessary to prevent changes in the body axis as much as possible because the fractional radiation dose is high.

Table 6.1 Setup accuracy using immobilization device for lung stereotactic body radiation therapy

Immobilization device	LAT (mm)	AP (mm)	SI (mm)	Reference
Body fix with dual vacuum	3.1 ± 2.6	3.4 ± 2.9	2.2 ± 1.9	Luo [28]
	2.9 ± 3.3	2.3 ± 2.5	3.2 ± 2.7	Fuss [29]
Body fix	-1.8 ± 3.2	0.3 ± 1.8	1.5 ± 3.7	Wang [30]
Stereotactic body frame	6	4	7	Negoro [15]
	3.3	3.4	4.4	Wulf [6]
	5	5	8	Lax [2]
	2.7 ± 2.3	2.5 ± 1.7	3.4 ± 2.7	Inga [31]
	0.11 ± 3.76	-2.44 ± 3.85	1.31 ± 5.84	Foster [32]
T-bar	3.7	5.1	5.1	Halperin [33]
Expanded form	5.3	3.6	5.4	Halperin [33]
Alpha cradle	2.0 ± 3.1	5.8 ± 1.4	2.9 ± 3.8	Inga [31]

For immobilization, it is necessary to achieve precise repositioning of the bone without leaning or twisting, and to ensure that the position can be maintained throughout treatment. The most suitable fixture choice is expected in consideration of an irradiation method, a collation method, irradiation time in each facility. I introduce the report about the setup error using various immobilization devices (Table. 6.1). An irradiation method and the collation methods are different in each report. For details, I suggest that you take each report into account.

6.6 Absorption Revision

In immobilization, it is necessary to achieve a structure in which there is little absorption or in which revision of absorption is possible, in addition to fixation of the body position. For revision of absorption in the treatment plan, it is necessary to use a device with the same geometry as that used in the planning stages at the time of irradiation. Therefore, for immobilization, it is desirable to fix the device to the same position of the couch at the time of irradiation as during the planning stage. We can reproduce the incident angle of the beam, couch passage distance, and couch absorption as in the treatment plan by appropriate geometric placement at the time of each irradiation dose.

Absorption revision varies according to the type of immobilization, material, and beam placement, and consists of the following:

1. Method to revise monitor unit (MU) value with the absorption factor of immobilization measured beforehand.
2. Method to calculate dose including immobilization to outer contour in the treatment plan.

Although it varies according to the type of immobilization, radiation dose may be reduced by more than 10 % due to absorption depending on the beam direction.

The clinical influence of the decrease in radiation dose associated with immobilization in each irradiation portal cannot be ignored, as it affects the total dose applied in treatment.

It is necessary to consider the precision of a radiation dose, such as changes in the surface dose produced by the size, thickness, and material of the immobilization device or attenuation of the radiation dose with immobilization in SBRT [34].

The following section presents data obtained with SBF, which was initially used at our facility.

6.6.1 Attenuation Rate of Radiation Dose Using an Immobilization Fixation Device

It is important to determine the dose attenuation of the fixation device in preparation for stereotactic body irradiation. The method for evaluation of dose attenuation involves use of a cylindrical phantom with a dose chamber in its center, set up inside the fixation device. We measured the dose attenuation at every gantry angle, and the attenuation rate was normalized relative to the dose in the direction without attenuation.

For example, Fig. 6.6a, b shows a graph of dose attenuation rate using SBF [16]. The rates increased from a gantry angle of 65° at which the beam began to overlap on SBF. Irradiation field completely overlap on SBF from a gantry angle of around 70° that showed more than 6 % of value.

At a gantry angle above 160°, the beam began to overlap to the prop of the couch. Then the radiation dose suddenly decreased on this gantry angle with dose attenuation of SBF and prop of the couch. In a real treatment plan, it is necessary to exclude the setting of beam placement for this part.
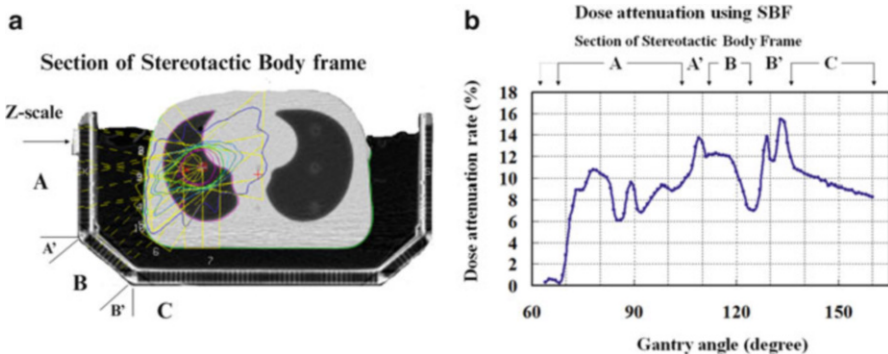

Fig. 6.6 (**a**): Section of SBF for correction of dose attenuation. Attenuation rate varies according to material and structure in immobilization. Section A: lateral panel, Section B: oblique panel, Section C: bottom panel. (**b**): Dose attenuation rate using SBF. As an example, this graph show measurement data of dose attenuation from a gantry angle of 65°–160° using phantom in SBF

Even if the attenuation rate of the radiation dose lies in the domain where the thickness of the frame is flat (A, B, C) (Fig. 6.6a), a change in dose is caused by influence of the internal structure at the incident angle to SBF. The relative decrease in radiation dose attenuation in Z-scale, which there is placed on corner rail of immobilization, was up to 15.4 % at a gantry angle of 133°.

The degree of dose attenuation varied between the sides, base, and angled part of the SBF, and the mean rate of the whole SBF was 9.3 %.

When a non-coplanar beam is used in stereotactic body irradiation, the incident direction of the beam for the fixation device is altered; the attenuation rate is also thought to change.

The dose attenuation rate with a couch angle of 20° increased of approximately 2.5 % compared with an angle of 0°, but the tendency was identical.

As the influence of dose attenuation in one fraction was considerable, it is necessary to revise the dose based on these data.

In preparation for stereotactic body irradiation, when the number of monitor units (MUs) is revised by manual calculations or automatically by the treatment planning device, it is important that corrected dose attenuation is confirmed the dose precision by dosimetry. It should be noted that dose attenuation can change markedly with slight changes in angle on dosimetry.

6.6.2   Influence on Clinical Target Dose in SBRT

Here, we present an example of the influence of dose attenuation on total fraction dose when attenuation of the fixation device occurs at the number portal among all of the irradiation portals in stereotactic body irradiation.

We evaluated the influence of the attenuation rate using SBF on a target dose of radioactivity in 21 clinical cases (Fig. 6.7) [16]. There was little influence on target dose when the SBF was set to a small number of incident irradiation portals relative to the total number of irradiation portals or when the attenuation dose of SBF was small. Without revision in each case, the target dose was decreased by an average of 5 %. In contrast, with a uniform revision value of 9.3 % of the radiation dose at each portal, the influence on target dose was reduced to approximately 1 %. As SBRT applies a large dose, the revision of absorption due to immobilization is an important factor affecting the precision of the radiation dose.

Stereotactic body irradiation is often carried out with multiple fixed portals and has dose attenuation of around 10 % of the fraction dose using fixation devices depending on the direction; this is a major problem in dose precision.

It is necessary to avoid the direction with large attenuation of the fixation device in setting the beam direction, or to revise dose attenuation of the fixation device. It is important to use appropriate materials for the fixation device to reduce the influence of absorption on dose attenuation.
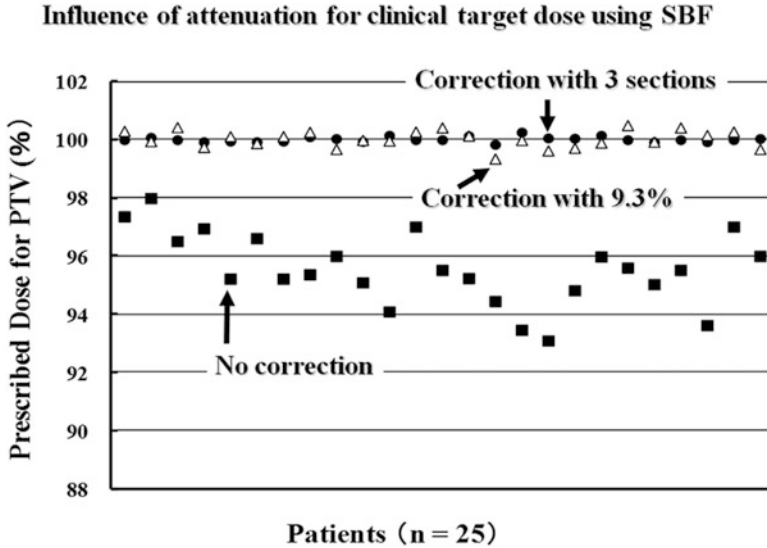
Influence of attenuation for clinical target dose using SBF

Fig. 6.7 Influence of attenuation for clinical target dose using SBF in SBRT. Correction with 3 sections (A, B, C section in Fig. 6.6a, b): perfectly revision for dose attenuation. Correction with 9.3 % (average of attenuation rate): revision almost possible for attenuation. No correction: target dose was decreased by an average 5 %

6.6.3 Changes in Surface Dose Associated with Immobilization

The influence of the administered dose varies according to the selected energy when using immobilization techniques. With immobilization, direct contact is made with the skin; therefore, the skin has a reduced protective effect compared to during procedures performed without a fixation device. When using absorption-type immobilization, it is necessary to establish a sufficient atmospheric layer around the body. We can expect re-build up phenomenal that target region is nearby.

The influence on skin absorption dose depends on field size, and a treatment plan to reduce the overlap of the beam on the skin side as much as possible is necessary.

It is important to measure the dose attenuation associated with immobilization, the change in skin dose by the structure used for immobilization, and its influence on target dose prior to the procedure. As an example of measurement data, the surface dose was 15.5 % without immobilization, but increased to 75.8 % using SBF, representing an increase in surface dose of 60.3 % for the peak dose [16].

This example shows that the increase in surface dose occurs suddenly with changes in material thickness. Therefore, it is necessary to pay close attention when choosing materials. The materials for a fixation device should be as firm as possible to avoid the outer wall part.

Materials of fixation device with atmospheric layers are desirable to utilize a skin protection effect with the re-build up of dose for a contact part to skin. As the

effect when using an absorption-type fixation device fades if the atmospheric layer from the beam incidence direction is thin, it is necessary to maintain an atmospheric layer of ~5-cm thickness.

6.7 Evaluation of Interference by Immobilization

The planner can arrange the beam placement from various directions without limit in the treatment plan. In the treatment room, there are really many cases that cannot realize beam placement decided on treatment planning by a geometric limit.

   When tumor position is shifted to right and left or ventral and dorsal side from midline of body, the couch shift from the center, and the height change. When the migration length is large from center, it is assumed that setting of gantry angle and couch angle is limited. When immobilization is used in a treatment plan, the ranges of gantry and couch angle are limited by the setting position against the couch changes. As a non-coplanar beam is often used in stereotactic body irradiation, it may be limited by the position of the immobilization device, particularly the position of the elbow. It is important to determine the movable range of the gantry and couch that can be used in the planning stage prior to commencing treatment. As an example, Fig. 6.8 shows the movable range of the couch and gantry with changes in the isocenter [16]. In this graph, the gantry angle and couch angle are plotted on
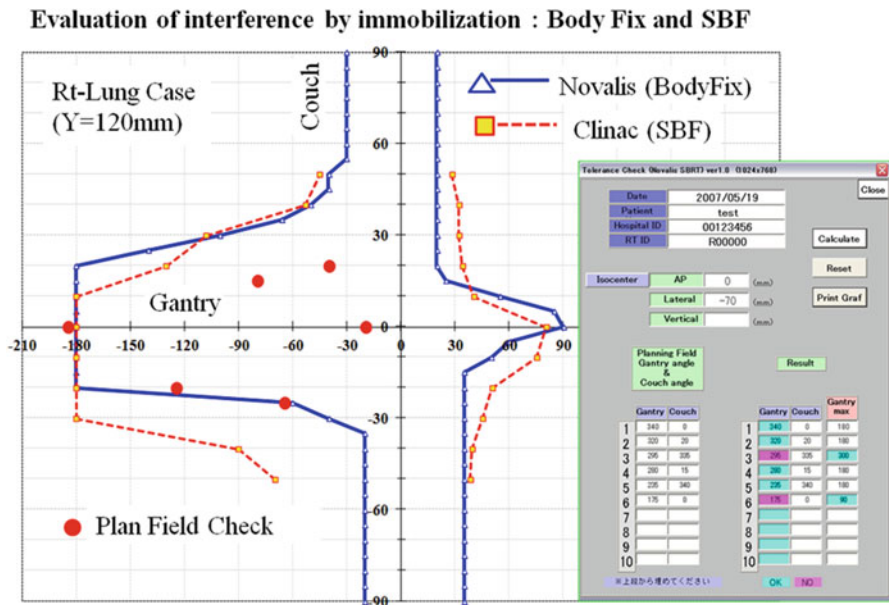

Fig. 6.8 Evaluation of interference by immobilization. Movable range of gantry and couch angle compare with Body Fix and SBF

the vertical axis and the horizontal axis, respectively. With regard to gantry rotation, right side of graph shows clockwise rotation of gantry and left side of graph shows counterclockwise rotation. For the couch angle, upper side of graph shows clockwise rotation from 0°, lower side of graph shows counterclockwise rotation from 0°. With regard to the angle of the gantry and couch, the range of surrounded area indicate the possible range of the setting. This range change condition by isocenter position per patient.

The interference range changes for each device, combination of immobilization, and lesion position. We can set the beam placement without re-planning by plotting the interference range beforehand. Effective and safe treatment can be achieved through irradiation based on a careful treatment plan.

This chapter presents the requirements for fixation, characteristics, and points that require attention for use. As the irradiation methods are different, the most suitable fixation device at each facility is selected in accordance with its purpose.

In addition, fixation devices will in future evolve to support new techniques, such as IGRT, dynamic tracking irradiation, and synchronized breathing control irradiation.

References

1. Lax I. Target dose versus extratarget dose in stereotactic radiosurgery. Acta Oncol. 1993;32 (4):453–7.
2. Lax I, Blomgren H, et al. Stereotactic radiotherapy of malignancies in the abdomen: methodological aspects. Acta Oncol. 1994;33(6):677–83.
3. Blomgren H, Lax I, et al. Stereotactic high dose fraction radiation therapy of extracranial tumors using an accelerator: clinical experience of the first thirty-one patients. Acta Oncol. 1995;4(6):861–70.
4. Blomgren H, Lax I, Goeranson H, et al. Radiosurgery for tumors in the body: clinical experience using a new method. J Radiosurg. 1998;1:63–74.
5. Lax I, Blomgren H, Larson D, et al. Extracranial stereotactic radiosurgery of localized targets. J Radiosurg. 1998;1(2):135–48.
6. Wulf J, Hadinger U, et al. Stereotactic radiotherapy of extracranial targets: CT-simulation and accuracy of treatment in the stereotactic body frame. Radiother Oncol. 2000;57:225–36.
7. Uematsu M, Fukui T, Shioda A, et al. A dual computed tomography and linear accelerator unit for stereotactic radiation therapy: a new approach without cranially fixated stereotactic frame. Int J Radiat Oncol Biol Phys. 1996;35:587–92.
8. Shirato H, Shimizu S, Kitamura K, et al. Four-dimensional treatment planning and fluoroscopic real-time tumor tracking radiotherapy for moving tumor. Int J Radiat Oncol Biol Phys. 2000;48(2):435–42.
9. Nagata Y, Negoro Y, Aoki T, et al. Clinical outcomes of 3D conformal hypofractionated single high-dose radiotherapy for one or two lung tumors using a stereotactic body frame. Int J Radiat Oncol Biol Phys. 2002;52:1041–6.
10. Seppenwoolde Y, Shirato H, Kitamura K, et al. Precise and real-time measurement of 3D tumor motion in lung due to breathing and heartbeat, measured during radiotherapy. Int J Radiat Oncol Biol Phys. 2002;53:822–34.
11. Harada T, Shirato H, Ogura S, et al. Real-time tumor-tracking radiation therapy for lung carcinoma by the aid of insertion of a gold marker using bronchofiberscopy. Cancer. 2002;95:1720–7.

12. Onishi H, Kuriyama K, Komiyama T, et al. Clinical outcomes of stereotactic radiotherapy for stage Inon-small cell lung cancer using a novel irradiation technique: patient self-controlled breath-hold and beam switching using a combination of linear accelerator and CT scanner. Lung Cancer. 2004;45(1):45–55.

13. Kimura T, Hirokawa Y, Murakami Y, et al. Reproducibility of organ position using voluntary breath-hold method with spirometer for extracranial stereotactic radiotherapy. Int J Radiat Oncol Biol Phys. 2004;60(4):1307–13.

14. Nagata Y, Takayama K, Matsuo Y, et al. Clinical outcomes of a phaseI/II study of 48 Gy of stereotactic body radiotherapy in 4 fractions for primary lung cancer using a stereotactic body frame. Int J Radiat Oncol Biol Phys. 2005;63:1427–31.

15. Negoro Y, Nagata Y, Aoki T, et al. The effectiveness of an immobilization device in conformal radiotherapy for lung tumor: reduction of respiratory tumor movement and evaluation of daily set-up accuracy. Int J Radiat Oncol Biol Phys. 2001;50:889–98.

16. Koga S, Yano S, Okada T, et al. Stereotactic radiotherapy using a stereotactic body frame: research on effective irradiation angle and correcting dose. Jpn J Radiol Technol. 2001;57 (11):1395–405.

17. Nakamura M, Narita Y, Matsuo Y, et al. Geometrical differences in target volumes between slow CT and 4D CT imaging in stereotactic body radiotherapy for lung tumors in the upper and middle lobe. Med Phys. 2008;35(9):4142–8.

18. Takayama K, Mizowaki T, Kokubo M, et al. Initial validations for pursuing irradiation using a gimbals tracking system. Radiother Oncol. 2009;93:45–9.

19. Matsuo Y, Sawada A, Ueki N, et al. An initial experience of dynamic tumor tracking irradiation with real-time monitoring using Vero4DRT (MHITM2000). Radiother Oncol. 2012;103:S64.

20. Nakamura M, Mukumoto N, Ueki N, et al. Estimation of a tracking margin in surrogate signal-based dynamic tumor tracking irradiation with Vero4DRT. Int J Radiat Oncol Biol Phys. 2012;84:S851–2.

21. Mukumoto N, Nakamura M, Sawada A, et al. Accuracy verification of infrared marker-based dynamic tumor-tracking irradiation using the gimbaled x-ray head of the Vero4DRT (MHI-TM2000). Med Phys. 2013;40:041706-1-9.

22. Akimoto M, Nakamura M, Mukumoto N, et al. Predictive uncertainty in infrared marker-based dynamic tumor tracking with Vero4DRT. Med Phys. 2013;40:091705-1-8.

23. Ueki N, Matsuo Y, Nakamura M, et al. Intra- and interfractional variations in geometric arrangement between lung tumours and implanted markers. Radiother Oncol. 2014;110:523–8.

24. Shiu AS, Chang EL, et al. Near simultaneous computed tomography image-guided stereotactic spinal radiotherapy: an emerging paradigm for achieving true stereotaxy. Int J Radiat Oncol Biol Phys. 2003;57(3):605–13.

25. Nevinny-Sticked M, Sweeney RA, et al. Reproducibility of patient positioning for fractionated extracranial stereotactic radiotherapy using a double-vacuum technique. Strahlenther Onkol. 2004;180(2):117–22.

26. Geoffrey G, Hsiang-Hsuan M, Craig W, et al. Motion management in stereotactic body radiotherapy. J Nucl Med Radiat Ther. 2012;S6:012.

27. International Commission on radiation units and measurements (ICRU): Report 62, ICRU Publications; 1999.

28. Luo G, Gopalakrishnan M, Zhang Y, et al. Patient setup accuracy and immobilization errors during lung, spine, and liver stereotactic body radiation therapy delivery: preliminary experience using a body fix with dual vacuum immobilization and a robotic couch. Int J Radiat Oncol Biol Phys. 2011;81(2):S61–2.

29. Fuss M, Salter BJ, Rassiah P. Repositioning accuracy of a commercially available double-vacuum whole body immobilization system for stereotactic body radiation therapy. Technol Cancer Res Treat. 2004;3(1):59–67.

30. Wang L, et al. Benefit of three-dimensional image-guided stereotactic localization in the hypofractionated treatment of lung cancer. Int J Radiat Oncol Biol Phys. 2006;66:738–47.

31. Inga S, Geoffrey H, Larry L, et al. Image-guided radiotherapy via daily online cone-beam CT substantially reduces margin requirements for stereotactic lung radiotherapy. Int J Radiat Oncol Biol Phys. 2008;70(4):1045–56.
32. Foster R, Meyer J, Iyengar P, et al. Localization accuracy and immobilization effectiveness of a stereotactic body frame for a variety of treatment sites. Int J Radiat Oncol Biol Phys. 2013;87 (5):911–6.
33. Halperin R, Roa W, Field M, et al. Setup reproducibility in radiation therapy for lung cancer: a comparison between T-bar and expanded form immobilization devices. Int J Radiat Oncol Biol Phys. 1999;43(1):211–6.
34. Arthur J, Lee G, Heng L, et al. Dosimetric effects caused by couch tops and immobilization devices: report of AAPM Task Group 176. Med Phys. 2014;41(6):061501-1-30.

Chapter 7
Respiratory Motion Management

Hiroshi Onishi

7.1 Background

In radiotherapy cancer treatment, the key challenge is how to enable exact delivery of radiation beams to the tumor and to minimize adverse effects on normal tissues in the surrounding region, in particular for stereotactic body radiation therapy (SBRT) or intensity modulated radiation therapy (IMRT). While recent radiotherapy advanced techniques has enabled to reduce setup margin as small as possible, they were late in making measures for organ motion. Internal margin (IM), that is prescribed in international commission of radiation unit and measurements (ICRU) report 62 [1], includes various elements such as respiratory motion, throating motion, bowel volume change and peristaltic movement, urinary bladder volume, inflammatory change, pleural effusion or ascites, muscle contraction, and etc. Though respiratory motion is one of the biggest factors of IM among them, it has a almost regular and voluntary character. Therefore it is important and possible to manage respiratory motion in particular for organs in the chest and upper abdomen. According to the report of American Association of Physicists in Medicine (AAPM) Task Group 76, respiratory motion reduction is necessary in the following conditions: respiratory motion of the tumor is more than 5 mm; clinical goal of treatment can't be acquired without the respiratory motion reduction and it is possible to manage that in each patient and institution. Respiratory motion management should deal with inter- and intra-fractional respiratory motion. While methods for the purpose varied according to irradiation equipment or institution, some representative technique and devices used for respiratory motion management are shown in this chapter.

H. Onishi (✉)

Department of Radiology, University of Yamanashi, Medical campus
(Faculty of Medicine) 1110, shimokato, Chuo, Yamanashi 409-3898, Japan
e-mail: honishi@yamanashi.ac.jp

7.2 Definition of Respiratory Motion Management

The word of respiratory motion management in broad sense generally includes how to make a treatment plan for respiratory moving target regardless of the reduction of its motion range and how to control the patient or the treatment system in order to reduce the intra-fractional tumor motion range. In the current chapter, we call the latter "respiratory motion control (RMC)" and give the particular of it. Japanese medical service fee regulations introduced reimbursement for RMC from April 2012 and a guideline of the application of RMC for the medical service have been developed [2]. RMC must meet the following requirements:

 (i) When the length of respiratory tumor motion exceeds 10 mm without RMC being implemented. The length of the respiratory-induced tumor motion must be measured under free, unforced breathing, and irregularities in the respiration due to hiccups, coughs, sneezes and deep respiration are to be excluded.
 (ii) In the treatment plans, it must be ascertained and recorded that the expansion of area of irradiation required to compensate for respiratory motion can be reduced to ≤5 mm in any direction, three dimensionally.
(iii) At every instance of irradiation treatment, it is necessary to ascertain and record that the tumor is included in the irradiated area determined in (ii), immediately prior to and during the irradiation.

7.3 Factors Affecting RMC

(A) Timing: Respiratory motion includes inter- and intra- fractional elements. In general, the latter is bigger than the former.
(B) Size: Size of respiratory motion depends on the organ site and the tumor location. In general, the tumor located in lower lung has bigger respiratory motion than that in upper lung. The main direction of respiratory motion is cranio-caudal for tumors in lower lung but antero-posterior in upper lung [3]. It was reported that lung tumor moves 5–20 mm, 8–15 mm, and 5–10 mm in cranio-caudal, antero-posterior, and left-right directions, respectively [4, 5]. Other upper abdominal organs such as liver, gall bladder, pancreas, adrenal gland, and kidney have also respiratory motion of 5–20 mm [6, 7].
(C) Trace: In the lung, a intrapulmonary position does not always show univalent correspondence with lung volume because of the trace of the lung position shows irregular loop curves so-called "hysteresis" [8]. The similar hysteresis may be produced in other organs,
(D) Baseline: Shifts of the respiratory cycle are sometimes shown during a long treatment period. Most of the shifts are deeper change due to patient's relaxation [7].

7.4 Methods of RMC

There are 6 ways of management in order to control the respiratory motion.

1. Inhalation of oxygen
   Patients can keep shallow breathing or breath-holding comfortably and long.
2. Compulsory suppress of breathing volume
   It is mainly performed by a method to secure a part of the abdomen by a band or shell (Fig. 7.1), a method that uses an abdominal compression board, and others [9, 10].
3. Learning of regular respiratory patterns
   Respiration with regular rhythm within fixed breathing range is important to achieve good result of RMC. Some kind of audio-feedback method such as utilization of metronome.
4. Breath hold technique
   Patient's breath-hold is performed using some techniques. They include active breathing control [11], self-respiratory cessation with [12] or without [13] using respiratory indicator. Reproducibility of the breath-holding position is generally the best at the end of expiration [14], but has some differences among individuals.
5. Gating with respiration
   In conventional respiratory-gated radiotherapy, the gating window is usually set between the exhale baseline and a 20–30 % amplitude line and the irradiation beam will be triggered when part of the respiratory wave falls into this window. It was reported that respiratory internal margin could be reduced to 1.4 ± 0.7 mm by the gated technique [15].
6. Tumor-tracking with respiration
   It consists of two major aspects: real-time localization of, and real-time beam adaptation to, a constantly moving tumor. Compared to the breath-holding or gated method, tumor-tracking techniques potentially offer additional benefits such as higher delivery efficiency. The tumor-tracking is achieved with [16] or without [17] insertion of fiducial markers.

Fig. 7.1 An example of simple way of abdominal compression using bolus and body-shell

Method of RMC	Respiratory status	Timing of beam-on	Time-efficiency	Internal margin
Suppress			good	large
Breath-hold			bad	small
Gating			bad	medium
Tracking			good	small

Fig. 7.2 Respiratory status, timing of beam-on, time-efficiency, and general size of the internal margin according to methods of respiratory motion control

Respiratory status, timing of beam-on, time-efficiency, and general size of the internal margin according to the representative methods of RMC are shown in Fig. 7.2.

7.5   Planning for the Treatment Under RMC

When performing RMC, a treatment plan must be established assuming the following uncertainties [2]: changes in the tumor form and organs at risk due to respiration; errors between the predicted and actual tumor positions, the length of time from sensing the respiratory phase to the actual initiation of irradiation. The CT examination for treatment planning session should be performed under the individual way according to the RMC method as shown Table 7.1. While fast scan CT or four-dimensional (4D) CT is recommended for the planning of the treatment under breath-hold, respiratory gated, or tracking technique, but fast scan CT is not tolerable for the planning of the treatment under shallow breathing. Slow-scan CT, generally taken with 4.0 or more seconds for a scanning of one-slice, is used for the planning of the treatment under shallow breathing in some facilities, however a particular attention should be paid for the use of slow-scan CT that may have deformity or blurring effect on the internal target volume [18].

Table 7.1 Recommended manners of CT examination for treatment planning session according to the each of RMC method

RMC methods	Planning CT
Shallow breathing (Abdominal compression)	Four-dimensional (4D) or expiration and inspiration or (slow scan)
Breath-holding	Fast scan
Respiratory gating	Fast scan or 4D
Tracking	Fast scan or 4D

7.6 Cautionary Note in RMC

- The most important preparation for a good RMC is a good understanding of the RMC technique and systems in each facility and instruction and exercise for the patient to understand well and perform regular and stabilized breathing through the treatment fraction.
- Tumors often follow complex 3D trajectories and sometimes exhibit hysteresis [8]. Berbeco et al. have shown that, even if one models the tumor trajectory before the treatment, one projection image still may not localize tumor position with sufficient accuracy [19].
- A baseline shift of respiratory status might be produced during a long period of SBRT or IMRT due to relaxation of the patient's mental strain and the body-muscle.
- Abdominal compression might cause the patient's distress that can disturb the respiratory and body-wall condition.
- As the tumor position under the same respiratory waveform pattern in a day does not always correspond to that in other days, confirmation of the tumor position using image-guidance is necessary in every treatment fraction.
- When using fiducial markers, it should be noticed that comparative differences of the location between them and the tumor are changeable during whole treatment term because of migration of the markers or deformation of the lung.
- The quality assurance and control (QA/QC) had better be done in every patient, radiotherapy fractions, and treatment methods or devices.
- A guideline and manual of the RMC method in each facility must be made in combination with a good comprehension of all of radiotherapy staffs.

7.7 Devices for RMC

7.7.1 Measuring Instruments for Respiratory Motion

Common devices to verify the range of tumor motion before treatment are as follows.

- X-ray fluoroscopy
- CT at ends of inspiration and expiration

CT device is integrated with the therapeutic apparatus (cone-beam CT, megavolt CT, and CT-on-rails)

- Four dimensional CT (4DCT)
- Cine magnetic resonance imaging (MRI)
- Cine electronic portal imaging device (EPID)

Common devices to verify the length of tumor motion during the irradiation are as follows.

- Cine electronic portal imaging device (EPID)
- X-ray fluoroscopy
- Model which predicts the 3D position of a tumor from external breathing signals and others
- Beacon transponder (Calypso, Varian Medical System Inc.)

7.7.2   Indicator for Respiratory Monitoring

Respiration status is essential to be monitored for all of RMC techniques. Most of the methods of respiratory monitoring are not according to lung volume itself but the change of body wall as a surrogate for respiratory status. The commonly-used on the market in Japan are as follows shown in Fig. 7.3.

- Abches (Apex Medical Inc. Fig. 7.3a) [12]
- AZ-733 V(Anzai Medical Inc. Fig. 7.3b) [20]
- Breath-track (Engineering System Inc. Fig. 7.3c) [21]
- Air-bag system (Max Medical Inc. Fig. 7.3d)
- Real-time Position Management (RPM) system (Varian Medical Systems, Inc. Fig. 7.3e) [22]
- Active breathing control (ABC) system (Elekta Ltd., Fig. 7.3f) [23]

7.7.3   Special Equipment for RMC

Real time tumor tracking (RTRT) system (Sync TraX, Shimadzu Inc. Fig. 7.4a) [24]

The fluoroscopic real-time tumor-tracking system consists of four sets of diagnostic X-ray television systems, a moving object recognition system, and a patient couch composed of carbon fiber placed in the linear accelerator room. The diagnostic X-ray television system is composed of an X-ray tube embedded under the floor, an image intensifier mounted on the ceiling, and a high-voltage X-ray generator. All four sets of the system are adjusted such that the central axis of the diagnostic X-rays will cross at the isocenter of the linear accelerator. Coordinates of the tumor
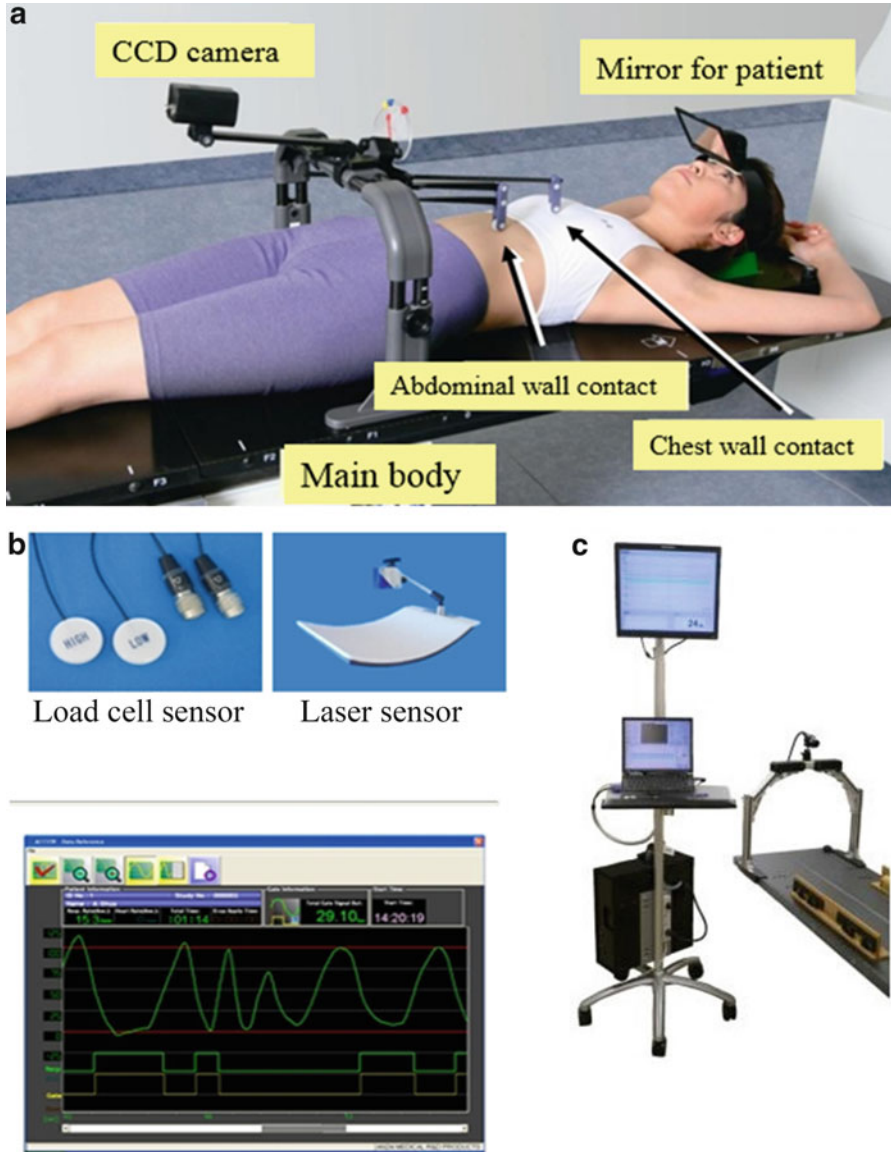
Fig. 7.3 (**a**) (Abches). (**b**) AZ-733 V(Anzai Medical Inc.). (**c**) Breath-track (Engineering System Inc.). (**d**) Air-bag system (Max Medical Inc.). (**e**) Real-time Position Management (RPM) system (Varian Medical Systems, Inc.). (**f**) Active breathing coordinator (ABC) system (Elekta Ltd.)
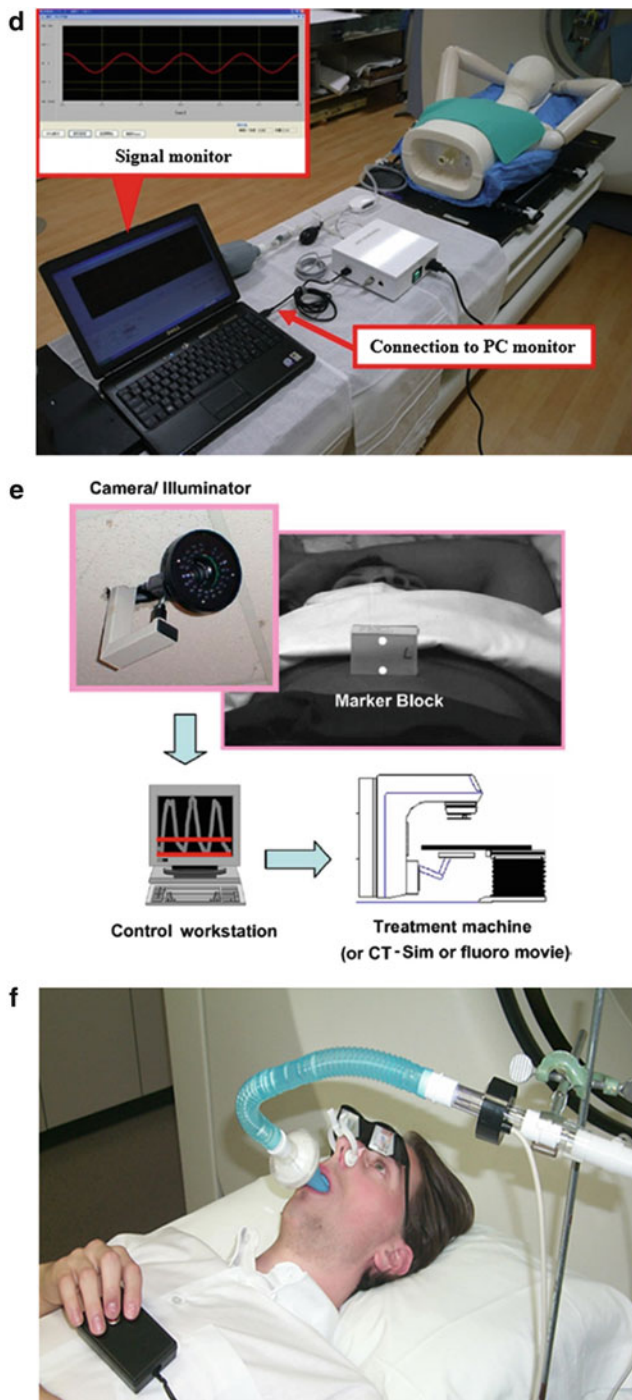
Fig. 7.3 (continued)

center and the gold marker are transferred from the three-dimensional radiotherapy planning system to the RTRT system through the network. The information is transformed using projective geometry and overlapped on the two X-ray television images displayed on the cathode ray tube monitor. The three-dimensional position of the marker is automatically determined during irradiation. Image processors compare the digitized image and the template image of a metallic marker to detect the location of the marker, which is considered representative of the position of the tumor. If the
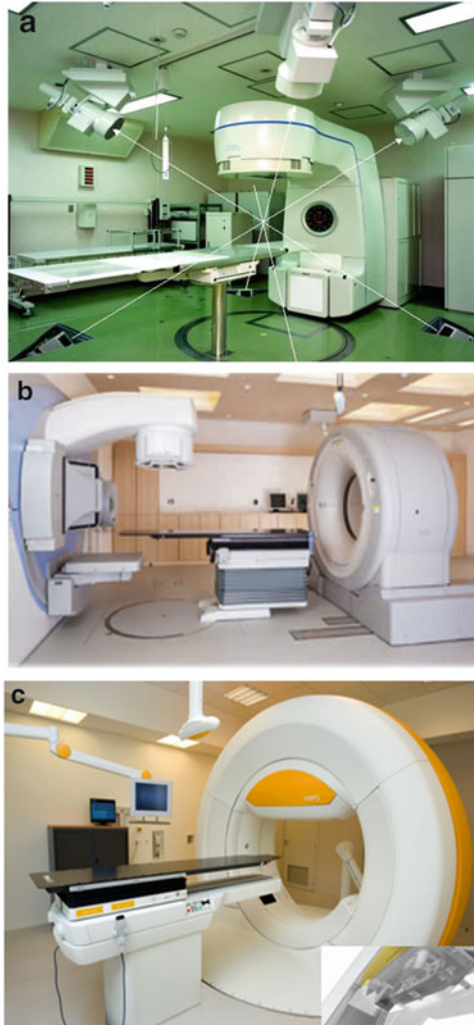

Fig. 7.4 (**a**) Real-time tumor-tracking (RTRT) system (Shimadzu Inc.). (**b**) CT-on-rails system (ELEKTA Inc, Toshiba Medical Inc.). (**c**) Vero 4DRT (Mitsubishi Heavy Industry Inc.). Tumor tracking system using fiducial marker and a linear accelerator equipped with gimbal function. (**d**) CyberKnife G4 (Accuray Inc.) Method of fiducial-less tracking
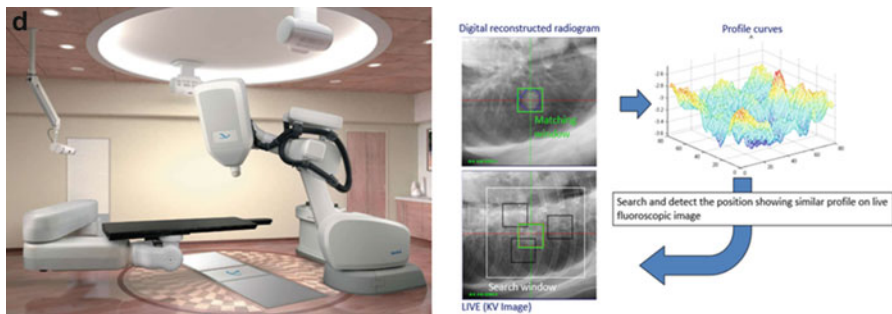
Fig. 7.4 (continued)

coordinates of the marker are within the limits of the predetermined permitted dislocation, the system allows the linear accelerator to irradiate the patient.

CT on rails system (ELECTA Inc. Toshiba Medical Inc. Fig. 7.4b) [25]

A system combining a Toshiba large-bore CT scanner and a ELECTA Synergy linear accelerator is the only CT-on-rails system. The CT-on-rails system enables highly precise SBRT or other high-precision therapy like IMRT for any organs accompanying respiratory motion without fiducial marker under breath-hold technique. After rotating the couch 180°, a patient can receive a CT scan while in the immobilized treatment position just prior to the start of radiation treatment. The table has two rotation axes; one is for isocentric couch rotation and the other is for rotation between the CT and the linear accelerator. The gantry is coaxial to both the CT and the linear accelerator. The advantage of the system over other linear accelerator system that equips on-board kilo- or megavoltage cone-beam CT unit is that it can take more clear CT images in a shorter time. It is highly useful for radiotherapy for lung cancer because lung tumor needs clear CT image taken under breath-hold in order to be setup at a precise image-guided position [26].

Vero4DRT (Mitsubishi Heavy Industries Inc. Fig. 7.4c) [16]

The Vero 4DRT developed by Mitsubishi Heavy Industries enabled real-time dynamic tracking irradiation system. The tracking method is composed of a small-sized linear accelerator unit that can be waved like a gimbals and a modeled formula calculated from real-time fluoroscopy to fiducial markers in or around the tumor and chest wall indicators monitored with infrared rays. The machine identifies the position of a moving tumor in real time based on the information obtained using two X-ray radiography devices and enables concentrated irradiation only to cancer lesion by moving X-ray irradiation head at the same time monitoring entire tumors.

CyberKnife G4 (Accuray Inc. Fig. 7.4d) [17]

CyberKnife System is the world's first and only robotic stereotactic radiotherapy system. Also, it is the only radiotherapy system that can achieve real-time tracking for lung tumors without fiducial marker. It is composed of a precise robotic arm that

manipulates small sized linear accelerator, two directional fluoroscope, six-directional moving couch, and monitoring system for chest wall indicators with infrared rays. Depending on the type of tumor being treated, the CyberKnife System will use different targeting and tracking methods with or without fiducial markers.

References

1. Keall PJ, Mageras GS, Balter JM, et al. The management of respiratory motion in radiation oncology report of AAPM Task Group 76. Med Phys. 2006;33:3874–900.
2. Matsuo Y, Onishi H, Nakagawa K, Nakamura M, Ariji T, Kumazaki Y, Shimbo M, Tohyama N, Nishio T, Okumura M, Shirato H, Hiraoka M, Japan Conformal External Beam Radiotherapy Group, Japan Society of Medical Physics, Japan Society of Medical Physics, Japanese Society of Radiological Technology. Guidelines for respiratory motion management in radiation therapy. J Radiat Res. 2013;54(3):561–8.
3. Shimizu S, Shirato H, Ogura S, et al. Detection of lung tumor movement in real-time tumor-tracking radiotherapy. Int J Radiat Oncol Biol Phys. 2001;51:304–10.
4. Mageras GS, Pevsner A, Yorke ED, et al. Measurement of lung tumor motion using respiratory-correlated CZT. Int J Radiat Oncol Biol Phys. 2004;60:933–41.
5. Shirato H, Seppenwoolde Y, Kitamura K, et al. Intrafractional tumor motion: lung and liver. Semin Radiat Oncol. 2004;14:10–8.
6. Gierga DP, Chen GT, Kung JH, et al. Quantification of respiration-induced abdominal tumor motion and its impact on IMRT dose distributions. Int J Radiat Oncol Biol Phys. 2004;58:1584–95.
7. Nishioka S, Nishioka S, Kawahara M, et al. Exhale fluctuation in respiratory-gated radiotherapy of the lung: a pitfall of respiratory gating shown in a synchronized internal/external marker recording study. Radiother Oncol. 2008;86:69–76.
8. Seppenwoolde Y, Shirato H, Kitamura K, et al. Precise and real-time measurement of 3D tumor motion in lung due to breathing and heartbeat, measured during radiotherapy. Int J Radiat Oncol Biol Phys. 2002;53:822–34.
9. Negoro Y, Nagata Y, Aoki T. The effectiveness of an immobilization device in conformal radiotherapy for lung tumor: reduction of respiratory tumor movement and evaluation of the daily setup accuracy. Int J Radiat Oncol Biol Phys. 2001;50:889–98.
10. Lee S, Yang DS, Choi MS, et al. Development of respiratory motion reduction device system (RMRDs) for radiotherapy in moving tumors. Jpn J Clin Oncol. 2004;34:686–91.
11. Ramouchamps VM, Letts N, Yan D, et al. Three-dimensional evaluation of intra- and interfraction immobilization of lung and chest wall using active breathing control: a reproducibility study with breast cancer patients. Int J Radiat Oncol Biol Phys. 2003;57:968–78.
12. Onishi H, Kawakami H, Marino K, Komiyama T, Kuriyama K, Araya M, Saito R, Aoki S, Araki T. A simple respiratory indicator for irradiation during voluntary breath holding: a one-touch device without electronic materials. Radiology. 2010;255(3):917–23.
13. Onishi H, Kuriyama K, Komiyama T, et al. CT evaluation of patient deep inspiration self-breath-holding: how precisely can patients reproduce the tumor position in the absence of respiratory monitoring devices? Med Phys. 2003;30:1183–7.
14. Kimura T, Hirokawa Y, Murakami Y, et al. Reproducibility of organ position using voluntary breath-hold method with spirometer for extracranial stereotactic radiotherapy. Int J Radiat Oncol Biol Phys. 2004;60:1307–13.
15. Underberg RW, Lagerwaard FJ, Slotman BJ, et al. Benefit of respiration-gated stereotactic radiotherapy for stage I lung cancer: an analysis of 4DCT datasets. Int J Radiat Oncol Biol Phys. 2005;62:554–60.

16. Kamino Y, Takayama K, Kokubo M, et al. Development of a four-dimensional image-guided radiotherapy system with a gimbaled X-ray head. Int J Radiat Oncol Biol Phys. 2006;66:271–8.
17. Bibault JE, Prevost B, Dansin E, Mirabel X, Lacornerie T, Lartigau E. Image-guided robotic stereotactic radiation therapy with fiducial-free tumor tracking for lung cancer. Radiat Oncol. 2012;7:102.
18. Nakamura M, Narita Y, Matsuo Y, Narabayashi M, Nakata M, Yano S, Miyabe Y, Matsugi K, Sawada A, Norihisa Y, Mizowaki T, Nagata Y, Hiraoka M. Geometrical differences in target volumes between slow CT and 4D CT imaging in stereotactic body radiotherapy for lung tumors in the upper and middle lobe. Med Phys. 2008;35:4142–8.
19. Berbeco RI, Jiang SB, Sharp GC, Chen GT, Mostafavi H, Shirato H. Integrated radiotherapy imaging system (IRIS): design considerations of tumour tracking with linac gantry-mounted diagnostic X-rays systems with flat-panel detectors. Phys Med Biol. 2004;49:243–55.
20. Kleshneva T, Muzik J, Alber M. An algorithm for automatic determination of the respiratory phases in four-dimensional computed tomography. Phys Med Biol. 2006;51:N269–76.
21. Nakamura K, Shioyama Y, Nomoto S, Ohga S, Toba T, Yoshitake T, Anai S, Terashima H, Honda H. Reproducibility of the abdominal and chest wall position by voluntary breath-hold technique using a laser-based monitoring and visual feedback system. Int J Radiat Oncol Biol Phys. 2007;68(1):267–72.
22. Kini VR, Vedam SS, Keall PJ, Patil S, Chen C, Mohan R. Patient training in respiratory-gated radiotherapy. Med Dosim. 2003;28:7–11.
23. Wong JW, Sharpe MB, Jaffray DA, Kini VR, Robertson JM, Stromberg JS, Martinez AA. The use of active breathing control (ABC) to reduce margin for breathing motion. Int J Radiat Oncol Biol Phys. 1999;44:911–9.
24. Shirato H, Shimizu S, Shimizu T, Nishioka T, Miyasaka K. Real-time tumour-tracking radiotherapy. Lancet. 1999;353:1331–2.
25. Kuriyama K, Onishi H, Sano N, Komiyama T, Aikawa Y, Tateda Y, Araki T, Uematsu M. A new irradiation unit constructed of self-moving gantry-CT and linac. Int J Radiat Oncol Biol Phys. 2003;55(2):428–35.
26. Onishi H, Kuriyama K, Komiyama T, Tanaka S, Sano N, Aikawa Y, Tateda Y, Araki T, Ikenaga S, Uematsu M. A new irradiation system for lung cancer combining linear accelerator, computed tomography, patient self-breath-holding, and patient-directed beam-control without respiratory monitoring devices. Int J Radiat Oncol Biol Phys. 2003;56:14–20.

Chapter 8
Dose Prescription and Calculation

Kunihiko Tateoka, Junji Suzuki, Yuji Yaegashi, Kazunori Fujimoto, Yuichi Saito, Tadanori Abe, Takuya Nakazawa, Kensei Nakata, Masato Hareyama, and Koichi Sakata

8.1 Introduction

Stereotactic body radiation therapy (SBRT) is a promising treatment method for inoperable early stage non-small cell lung cancer (NSCLC) patients. SBRT delivers very high doses of radiation to the tumor in a small number of fractions using multiple shaped beams that converge on the tumor. High doses are best eliminated in normal tissues using shaped collimation of the primary beam with the fluence attenuating outside of the tumor. Recently, the local control rates of medically inoperable patients with early stage NSCLC are dramatically improved with SBRT compared to treatments with conventional fractions. An important feature of

K. Tateoka (✉)
Department of Radiology, Sapporo Medical University, S1 W16 Chuo-ku,
Sapporo, Hokkaido 060-8543, Japan

Radiation Therapy Research Institute, Social Medical Corporation Teishinkai,
Sapporo, Japan
e-mail: tateoka@sapmed.ac.jp

J. Suzuki
Radiotherapy Center, Suzukake Central Hospital, Hamamatsu, Japan

Y. Yaegashi
Department of Radiology, Kushiro City General Hospital, Kushiro, Japan

K. Fujimoto • M. Hareyama
Radiation Therapy Research Institute, Social Medical Corporation Teishinkai,
Sapporo, Japan

Y. Saito
Department of Radiology, Sapporo Medical University, S1 W16 Chuo-ku,
Sapporo, Hokkaido 060-8543, Japan

National Hospital Organization Hokkaido Cancer Center, Sapporo, Japan

modern SBRT are the supplementary techniques such as intensity modulated radiotherapy (IMRT), volumetric modulated arc therapy, or flattening filter-free beams that have higher dose rate performance than flattened beams of equivalent energy. The flattened filter-free beams can increase the efficiency of treatment delivery with image-guided radiotherapy (IGRT) and dose calculation algorithms such as convolution superposition, Monte Carlo calculation and the grid-based Boltzmann equation solver (GBBS) method, which fine-tune the dose distribution to millimeter accuracy. With these effective techniques, the ablative doses of radiation steeply attenuate beyond the tumor, sparing normal tissues from adverse toxic effects. Therefore, SBRT with modern supplementary techniques is a particularly useful clinical tool in the treatment of early NSCLC.

8.2 Dose Prescription

The typical radiation treatment option for NSCLC was conventionally fractionated radiation, but the reported outcomes were generally grim with disappointing local control rates of 30–50 % and long-term survival rates of only 10–30 % for both medically inoperable NSCLC and stage I NSCLC [1, 2]. These results are likely impacted by the delivery of a truly tumoricidal dose to prevent toxicity caused by the limited dose escalation. The biological effectiveness can be approximated using a widely accepted formula of biologically equivalent dose (BED), where the alpha beta ratio (α/β) is a radiosensitivity parameter unique to each tumor tissue and outcome, and is commonly set to 10 (BED 10) for lung tumor control and acute toxicity. The highest attainable biologically equivalent dose (BED 10) that is deliverable with conventionally fractionated regimens is typically around 80 Gy before toxicities become unacceptable, which is insufficient for consistently eradicating the gross disease in NSCLC. With SBRT and hypo-fractionation innovations, a BED of 100 Gy or larger is safely achievable without excessive toxicity. Multiple SBRT studies have consistently demonstrated high control of the primary

T. Abe
Department of Radiology, Sapporo Medical University, S1 W16 Chuo-ku,
Sapporo, Hokkaido 060-8543, Japan

Department of Radiology, KKR Sapporo Medical Center, Sapporo, Japan

T. Nakazawa
Department of Radiology, Sapporo Medical University, S1 W16 Chuo-ku,
Sapporo, Hokkaido 060-8543, Japan

Department of Radiology, Kushiro City General Hospital, Kushiro, Japan

K. Nakata • K. Sakata
Department of Radiology, Sapporo Medical University, S1 W16 Chuo-ku,
Sapporo, Hokkaido 060-8543, Japan

Table 8.1 Selected studies of SBRT for early-stage non-small cell lung cancer

Author (year)	N	Total dose (Gy)	Daily dose (Gy)	Reference point	Local control	Median follow-up
Arimoto et al. (1998) [3]	24	60	7.5	Isocenter	92 % (not described)	24 months
Uematsu et al. (2001) [4]	50	50–60	10	80 % Margin	94 % (follow-up period)	36 months
Wulf et al. (2004) [5]	20	45–56.2	15–15.4	80 % Margin	95 % (1 year)	10 months
Nagata et al. (2005) [6]	45	48	12	Isocenter	97 % (follow-up period)	30 months
Xia et al. (2006) [7]	43	70(50)	7(5)	Isocenter	95 % (3 years)	27 months
Baumann et al. (2009) [8]	57	45	15	67 % Margin	92 % (3 years)	35 months
Timmerman et al. (2010) [9]	55	54	18	80 % Margin	98 % (3 years)	34 months
Nagata et al. (2010) [10]	64	48	12	Isocenter	69 % (6 years)	45 months

lesion (Table 8.1) [3–10]. For these studies, the local control was 69–92 %. SBRT was found to be highly effective for inoperable stage I NSCLC with mild toxicity. SBRT treatment should be considered the new standard of treatment, replacing conventional radiation therapy.

Examples of organ dose constraints used in major trials in Japan, North America, RTOG (Radiation Therapy Oncology Group) trial, and the international STARS (Study of Anastrozole and Radiotherapy Sequencing) trial are presented in Table 8.2 [11–13]. Note that these dose constraints will likely change as clinical experience with SBRT increases. Moreover, the toxicity depends on the total dose and fraction size of the SBRT treatment. By modulating these parameters, the rates of adverse effects can be lowered and greater flexibility can be achieved in regions amenable to SBRT.

Since SBRT was included in the Japanese national health insurance system in 2004, the number of institutions performing SBRT increased rapidly. The clinical trials for SBRT have been performed for the safety radiation treatment in Japan. According to the Japan Clinical Oncology Group (JCOG) 0403 protocol, the dose prescription is defined as the point dose at the isocenter of the planning target volume (PTV) with inhomogeneity correction, such as the pencil beam convolution with Batho power law or the Clarkson with effective path length correction. Unfortunately, this prescription is not accurate for dose calculations in lung cancer [14]. In the isocenter prescription, a total dose of 48 Gy at the isocenter is delivered with a daily dose of 12 Gy in four fractions within a 2-week period. The PTV prescription was adopted in the JCOG 0702 phase I trial instead of the isocenter prescription, which was adopted in the previous JCOG 0403 phase II trial. In the JCOG 0702 protocol, a inhomogeneity correction algorithm, which is equivalent to superposition algorithms, is required for dose calculation. Additionally, in the

Table 8.2 Dose constraints used in Japan, major North American, and international trials

Organ at risk	JCOG 0403 (4 fractions)	RTOG 0618 (3 fractions)	International STARS trial (4 fractions)
Lung	40 Gy ≤ 100 cc	V20 ≤ 10 %	V20 ≤ 20 %
	Mean dose ≤18 Gy		V10 ≤ 30 %
	V20 ≤ 20 %		V5 ≤ 50 %
	V15 ≤ 25 %		
Spinal cord	≤25 Gy	≤18 Gy	20 Gy ≤ 1 cc
			15 Gy ≤ 10 cc
Esophagus	40 Gy ≤ 1 cc	≤27 Gy	40 Gy ≤ 1 cc
	35 Gy ≤ 10 cc		35 Gy ≤ 10 cc
Trachea	40 Gy ≤ 10 cc	≤30 Gy	35 Gy ≤ 1 cc
			30 Gy ≤ 10 cc
Bronchi	40 Gy ≤ 10 cc	≤30 Gy	40 Gy ≤ 1 cc
			35 Gy ≤ 10 cc
Skin	≤40 Gy	≤24 Gy	40 Gy ≤ 1 cc
			35 Gy ≤ 10 cc

Unless otherwise specified, the limits represent point doses

prescription method, the International Commission on Radiation Units and Measurements (ICRU) recommended methods of dose prescription have been changed from prescription at the isocenter point of the treatment plan to prescription at the periphery of the PTV [15]. Therefore, the dose prescription protocol of SBRT should be prepared by sufficiently considering the irradiation technology, IGRT, and dose calculation algorithm for each facility.

8.3 Dose Calculation

The American Association of Physicists in Medicine (AAPM) Task Group #65 (TG-65) recommended that computed dose distributions should be accurate to 1 % or 2 % [16]. Dose calculation algorithms for radiation therapy have improved to achieve this accuracy level. In SBRT, the presence of heterogeneous tissue (e.g., lung tissue surrounding thoracic tumors) and the use of a smaller field size confound radiation dose computation. Moreover, small-field conditions often occur as a result of transient electronic disequilibrium. In low-density tissues such as the lungs, the re-buildup effect produces underdosage near the tumor interface due to the increasing electron range with increasing energy. The effects of transient electronic disequilibrium and increased electron range in low-density tissues will reduce the central-axis dose beyond an air cavity and potentially result in an underdosage of the tumor [17].
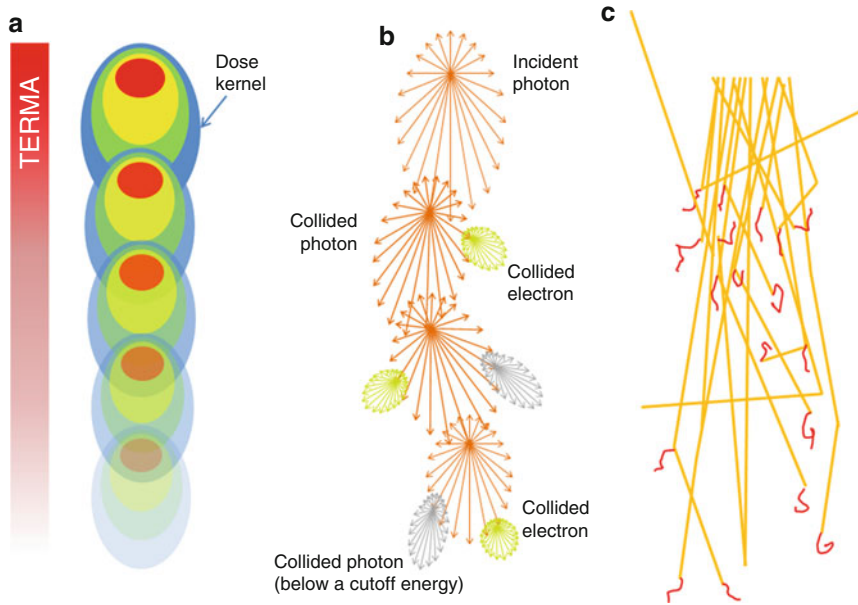
Fig. 8.1 Dose calculation algorithm comparison (**a**) Convolution/superposition method (**b**) GBBS method (**c**) Monte Carlo method

The development of model-based convolution methods has significantly improved the accuracy of dose calculations for such heterogeneous tissues when compared to correction-based methods [18, 19]. Model-based convolution method use physical principles, which describe the actual physical transport in the tissue, to calculate the dose (Fig. 8.1). Monte Carlo-based methods and the grid-based Boltzmann equation solver (GBBS) method provide more accurate dose distributions. In this section, we describe the most widely used algorithms for radiation treatment planning such as the convolution method, convolution/superposition method, Monte Carlo method, and GBBS method.

8.3.1   Convolution Method

The convolution method was proposed by Mackie et al. [20] in 1985. In essence, the energy fluence distribution is convolved with the scatter-spread kernel to obtain the dose. One of the commonly used convolution method in commercial treatment planning systems (TPSs) is pencil beam convolution (PBC) [18]. In the convolution method, the absolute dose at point $\left(\vec{r} \right)$ is given by:

$$D\left(\vec{r}\right) = \int \frac{\mu}{\rho} \Phi_p\left(\vec{r}'\right) A\left(\vec{r} - \vec{r}'\right) d^3\vec{r}' = \int T_p\left(\vec{r}'\right) A\left(\vec{r} - \vec{r}'\right) d^3\vec{r}' \qquad (8.1)$$

where μ/ρ is the mass attenuation coefficient, $\Phi_p\left(\vec{r}'\right)$ is the primary photon fluence, $T_p\left(\vec{r}'\right)$ is the primary energy fluence, known as Terma, and $A\left(\vec{r} - \vec{r}'\right)$ is the pencil beam kernel. The pencil beam kernels represent the absorbed dose distribution in water for a very small beam obtained by the deconvolution of basic measurement data or by Monte Carlo method calculations. Although the PBC methods are generally fast, the accuracy is compromised in the presence of heterogeneous tissue.

8.3.2   Convolution/Superposition Method

When the convolution method is modified to incorporate the density-base scaling of both the primary fluence and electron scatter in heterogeneous tissue, it is called the convolution/superposition method [21]. The absolute dose at point $\left(\vec{r}\right)$ is given by:

$$D\left(\vec{r}\right) = \int T_p\left(\rho_{\vec{r}} \cdot \vec{r}'\right) A\left(\rho_{\vec{r}-\vec{r}'} \cdot \left(\vec{r} - \vec{r}'\right)\right) d^3\vec{r}' \qquad (8.2)$$

where $\rho_{\vec{r}} \cdot \vec{r}'$ is the radiologic path length from the source to primary photon interaction site, and $\rho_{\vec{r}-\vec{r}'} \cdot \left(\vec{r} - \vec{r}'\right)$ is the radiologic path length from the primary photon interaction site to the dose deposition site. In general, the effective density calculated along the scattered ray path is used to change secondary particle contributions or to assign the appropriate value in the scatter kernel using density scaling [16]. Both the convolution/superposition and Clarkson/pencil beam algorithms are well matched at the PTV center embedded in the tissue; however, significant differences exist in the target periphery [22]. Consequently, the analytical anisotropic algorithm (AAA) implemented in the Eclipse Varian Medical Systems TPS is a convolution/superposition method [18, 23, 24]. AAA should provide a better modeling of the dose deposition in the lung and at the interfaces of lung-tumor or lung-tissue [24].

8.3.3   Monte Carlo Method

The Monte Carlo method, which simulates the transport of a large number of photons and particles through tissue, is considered the gold standard in accuracy

given sufficient particle histories [25, 26]. Many Monte Carlo codes have been used in radiation therapy treatment planning: ETRAN (Electron TRANsport) [27], electron gamma Shower (EGS) [28], and BEAM code system [29]. Although the Monte Carlo methods allow consideration of a wide range of complex patient treatment conditions, the calculation time becomes prohibitive as the number of simulated particles is increased [21].

8.3.4 GBBS Method

Methods that deterministically solve the linear Boltzmann transport equation (LBTE) can be referred to as GBBS methods. which solve the LBTE through space, angle, and energy discretizations [30]. The LBTE governs the macroscopic behavior of particle (e.g., gamma ray and electron) interactions with matter. A GBBS-based photon dose calculation algorithm has been implemented in the Eclipse TPS as Acuros XB (AXB). To determine the radiation transport and ultimately the energy deposition, AXB solves the time-independent three-dimensional coupled LBTE system:

$$
\begin{aligned}
&\widehat{\Omega} \cdot \vec{\nabla}\, \Phi^{\gamma} + \sigma_t^{\gamma} \Phi^{\gamma} = q^{\gamma\gamma} + q^{\gamma} \\
&\widehat{\Omega} \cdot \vec{\nabla}\, \Phi^{e} + \sigma_t^{e} \Phi^{e} - \frac{\partial}{\partial E}(S_R \Phi^e) = q^{ee} + q^{\gamma e} + q^{e}
\end{aligned}
\tag{8.3}
$$

where Φ^{γ} and Φ^{e} are the photon and electron angular fluence, respectively, $q^{\gamma\gamma}$, q^{ee}, and $q^{\gamma e}$ are the photon-to-photon, electron-to-electron, and photon-to-electron scattering sources, respectively, q^{γ} and q^{e} are the external photon and electron sources, respectively, and σ_t^{γ} and σ_t^{e} are the total macroscopic photon and electron cross-sections, respectively. Furthermore, E is energy, $\hat{\Omega}$ is the unit vector direction, and S_R is the restricted collisional plus radiative stopping power. Once the electron angular fluence is calculated, the dose $D(i)$ in any output grid voxel i is obtained by

$$
D(i) = \int_0^{\infty} dE \int_{4\pi} d\widehat{\Omega}\, \frac{\sigma_{ED}^e\left(\vec{r}, E\right)}{\rho} \Phi^e\left(\vec{r}, E, \widehat{\Omega}\right)
\tag{8.4}
$$

where σ_{ED}^e is the macroscopic electron energy deposition cross-section, $\vec{r}$ is the spatial position vector, and ρ is the material density. The achievable accuracy of the GBBS and Monte Carlo methods is equivalent and is limited only by uncertainties in the particle interaction data and by the uncertainties in the problem being analyzed [31]. For a more detailed literature review, please see Vassiliev et al. [31, 32].
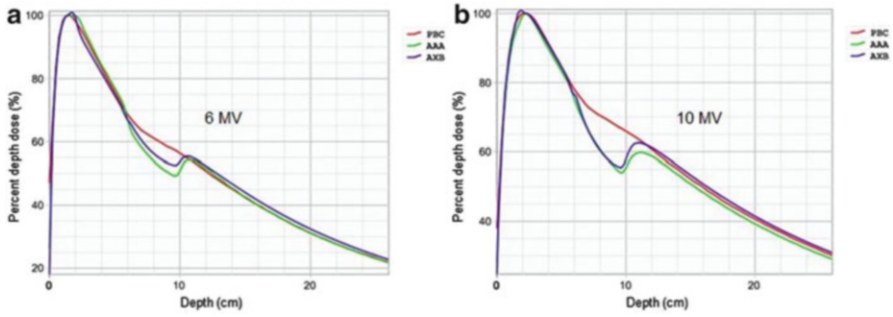
Fig. 8.2 Percent depth dose for 6 (**a**) and 10 MV (**b**) photon beams for a small field (3×3 cm^2) in a virtual heterogonous phantom
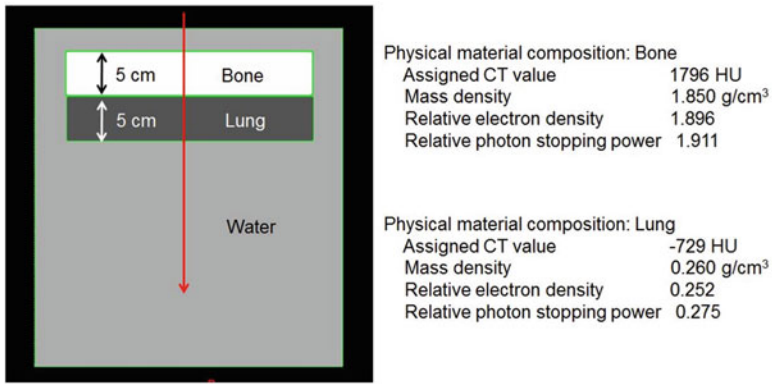

Fig. 8.3 Geometry and composition of the virtual heterogeneous phantom for the percent depth dose on the beam central axis

8.3.5 Comparison Between Dose Calculation Algorithms for Lung SBRT

Several recent studies have shown that AXB can provide a valid and accurate alternative to Monte Carlo calculations in heterogeneous materials [33–35]. Figure 8.2 shows the percent depth dose (PDD) calculated from the AXB, AAA, and PBC dose calculation algorithms for a small field using a virtual heterogeneous phantom (Fig. 8.3). The PBC algorithm is less accurate than the AXB algorithm for low-density materials such as the lung for both the 6 and 10 MV photon beams. The PDD obtained with the AAA algorithm shows under- or over-estimation within low- and high-density materials, respectively, compared to the AXB algorithm. The PDD under-estimation is more prominent at low energies. Figure 8.4 shows different dose distributions between the three dose calculation algorithms for SBRT of the lung. In clinical practice, the electron densities are not as simple as those in a phantom study; the electron densities are more complicated in the body. Therefore,
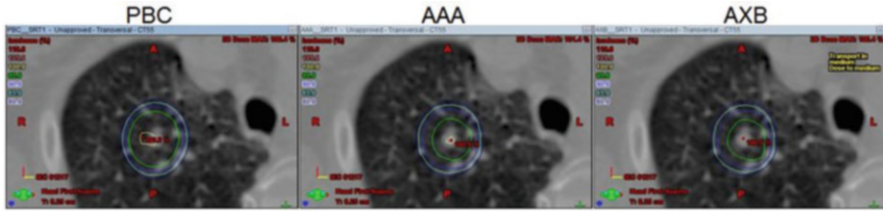
Fig. 8.4 Comparison of dose distributions using different dose calculation algorithms

it is necessary to investigate the calculation accuracy between dose calculation algorithms at each institution.

8.3.6 Grid

As we discussed earlier, the accuracy of the radiation dose calculation in a radiation treatment planning system is affected by the algorithm used for radiation dose calculation. Furthermore, the accuracy of the radiation dose calculation is affected by the number of beams, the electron density of the irradiated region, and the dose grid size [36].

In the lung, head, and neck where the electron density is complicated, the electron density was changed. Therefore, the dose grid size has an influence on the accuracy of the radiation dose calculation [37]. Additionally, the dose grid size becomes an important evaluation factor for the radiation dose calculation in the heterogeneous lung tissue. The dose grid size is selected by considering the electron density of the periphery of the tumor; therefore, the tumor shape is important issue for evaluating the accuracy of the radiation dose calculation for SBRT, IMRT, and 3D conformal radiation therapy (3DCRT).

Dempsey et al. [38] reported that the accuracy of the radiation dose calculation is approximately 1 % in the high-dose region of an IMRT plan using the dose grid size of 2.5 mm. Chang et al. [39] showed the calculated dose error using 2 mm, 3 mm, and 4 mm dose grid sizes were 2.3 %, 4.6 % and 5.6 %, respectively, as compared to the calculated dose from a 1.5 mm dose grid size in an IMRT field.

In SBRT of lung tumors, the high-dose gradient region of the lung tumor periphery shows large electron density differences between the inside and the outside of the tumor. In this region, the high-dose gradient might be similar to the IMRT dose gradient. Therefore, to evaluate the accuracy of radiation dose calculation in the lung tumor periphery where the dose gradient is steep, a small dose grid size should be used. If large dose grid sizes are used in regions with steep dose gradients such as the penumbra, the build-up region, and the periphery of tumor, the accuracy of radiation dose calculation will decrease. However, the time required for
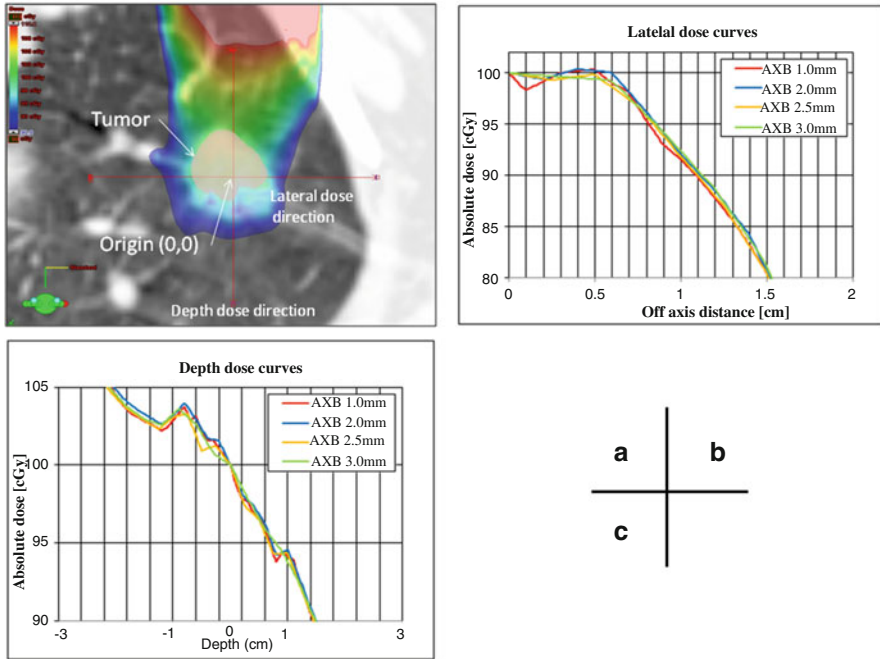
Fig. 8.5 The results of the radiation dose calculation of a lung tumor for AXB using a variation in the dose grid size; (**a**) the dose distribution, (**b**) the profile in the lateral direction, (**c**) the profile in the depth direction

performing the radiation dose calculation increases when the dose grid size decreases. Moreover, there is a lower limit for the selectable dose grid size.

Radiation dose calculation algorithms that take into account the 3D heterogeneity corrections for the scatter component including the secondary electron, such as the superposition or Monte Carlo methods, show differences in the accuracy of radiation dose calculation with respect to changing dose grid sizes. Moreover, these algorithms often under-estimate or over-estimate the actual irradiated dose to the patient depending on the changing electron density in irradiated regions. The dose grid size should be selected by considering the characteristics of the algorithm used for radiation dose calculation. Figure 8.5 shows the results of the radiation dose calculation for PBC, AAA, and AXB using a variation in the dose grid size in the rebuild-up and build-down regions at different density boundaries in the profile in the depth direction and the lateral direction.

For SBRT of lung tumors, the profile of the tumor periphery is influenced by the difference of the electron density between the inside and outside of the tumor and by the dose grid size. Therefore, the selection of the dose grid size should consider the influence of radiation dose calculation algorithms. However, in the SBRT of other tumors (e.g., liver), the electron density change at the periphery of tumor is

small. Therefore, the effects of dose grid size on the radiation dose calculation accuracy might be small.

Therefore, radiation dose calculations for a particular radiation treatment planning system require selecting both the dose grid size and the radiation dose calculation algorithm. Moreover, the dose grid size must be determined to achieve both accurate radiation dose calculations and efficient times of radiation dose calculation.

References

1. Dosoretz DE, Galmarini D, Rubenstein JH, Katin MJ, Blitzer PH, Salenius SA, et al. Local control in medically inoperable lung cancer: an analysis of its importance in outcome and factors determining the probability of tumor eradication. Int J Radiat Oncol Biol Phys. 1993;27:507–16.
2. Kaskowitz L, Graham MV, Emami B, Halverson KJ, Rush C. Radiation therapy alone for stage I non-small cell lung cancer. Int J Radiat Oncol Biol Phys. 1993;27:517–23.
3. Arimoto T, Usubuchi H, Matsuzawa T. Small volume multiple non-coplanar arc radiotherapy for tumors of the lung, head and neck and the abdominopelvic region. In: Lemke HU, editor. CAR'98 computer assisted radiology and surgery. Tokyo: Elsevier; 1998. p. 257–61.
4. Uematsu M, Shioda A, Suda A, Fukui T, Ozeki Y, Hama Y, et al. Computed tomography-guided frameless stereotactic radiotherapy for stage I non-small cell lung cancer: a 5-year experience. Int J Radiat Oncol Biol Phys. 2001;51:666–70.
5. Wulf J, Haedinger U, Oppitz U, Thiele W, Mueller G, Flentje M. Stereotactic radiotherapy for primary lung cancer and pulmonary metastases: a noninvasive treatment approach in medically inoperable patients. Int J Radiat Oncol Biol Phys. 2004;60:186–96.
6. Nagata Y, Takayama K, Matsuo Y, Norihisa Y, Mizowaki T, Sakamoto T, et al. Clinical outcomes of a phase I/II study of 48 Gy of stereotactic body radiotherapy in 4 fractions for primary lung cancer using a stereotactic body frame. Int J Radiat Oncol Biol Phys. 2005;63:1427–31.
7. Xia T, Li H, Sun Q, Wang Y, Fan N, Yu Y, et al. Promising clinical outcome of stereotactic body radiation therapy for patients with inoperable Stage I/II non-small-cell lung cancer. Int J Radiat Oncol Biol Phys. 2006;66:117–25.
8. Baumann P, Nyman J, Hoyer M, Wennberg B, Gagliardi G, Lax I, et al. Outcome in a prospective phase II trial of medically inoperable stage I non-small-cell lung cancer patients treated with stereotactic body radiotherapy. J Clin Oncol. 2009;27:3290–6.
9. Timmerman R, Paulus R, Galvin J, Michalski J, Straube W, Bradley J, et al. Stereotactic body radiation therapy for inoperable early stage lung cancer. JAMA. 2010;303:1070–6.
10. Nagata Y, Hiraoka M, Shibata T, Onishi H. A phase II trial of stereotactic body radiation therapy for operable T1N0M0 non-small cell lung cancer: Japan Clinical Oncology Group (JCOG0403). Int J Radiat Oncol Biol Phys. 2010;78:S27.
11. A phase II trial of stereotactic body radiation therapy for operable T1N0M0 non-small cell lung cancer: Japan Clinical Oncology Group (JCOG0403)
12. Stereotactic body radiation therapy in treating patients with stage I or stage II non-small cell lung cancer that can be removed by surgery (RTOG 0618). http://clinicaltrials.Gov/ct2/show/nct00551369. Accessed 1 June 2011.
13. International randomized study to compare Cyberknife stereotactic radiotherapy with surgical resection in stage I non-small cell lung cancer (STARS). http://clinicaltrials.Gov/ct2/show/nct00840749 (2011). Accessed 1 June 2011.

14. Kappas C, Rosenwald JC. Quality control of inhomogeneity correction algorithms used in treatment planning systems. Int J Radiat Oncol Biol Phys. 1995;32(3):847–58.

15. ICRU. Prescribing, recording, and reporting photon beam therapy. ICRU Report volume 50. Bethesda: International Commission on Radiation Units and Measurements; 1993.

16. Papanikolaou N, Battista J, Boyer A, Kappas C, Klein E, Mackie TR, et al. AAPM Report No. 85: tissue inhomogeneity corrections for megavoltage photon beams: report of Task Group No. 65 of the Radiation Therapy Committee of the American Association of Physicists in Medicine; 2004.

17. Li XA, Yu C, Holmes T. A systematic evaluation of air cavity dose perturbation in megavoltage x-ray beams. Med Phys. 2000;27(5):1011–7.

18. Mohan R, Chui C, Lidofsky L. Differential pencil beam dose computation model for photons. Med Phys. 1986;13(1):64–73.

19. Ulmer W, Harder D. A triple Gaussian pencil beam model for photon beam treatment planning. Z Med Phys. 1995;5:25–30.

20. Mackie TR, Scrimger JW, Battista JJ. A convolution method of calculating dose for 15-MV x rays. Med Phys. 1985;12(2):188–96.

21. Khan FM. Three-dimensional conformal radiation therapy. In: Khan FM, editor. The physics of radiation therapy. 3rd ed. Philadelphia: Lippincott Williams & Wilkins; 2003. p. 467–80.

22. Lee EK, Fox T, Crocker I. Simultaneous beam geometry and intensity map optimization in intensity-modulated radiation therapy. Int J Radiat Oncol Biol Phys. 2006;64(1):301–20. Epub 2005 Nov 14.

23. Ulmer W, Pyyry J, Kaissl W. A 3D photon superposition/convolution algorithm and its foundation on results of Monte Carlo calculations. Phys Med Biol. 2005;50(8):1767–90. Epub 2005 Apr 6.

24. Van Esch A, Tillikainen L, Pyykkonen J, Tenhunen M, Helminen H, Siljamäki S, et al. Testing of the analytical anisotropic algorithm for photon dose calculation. Med Phys. 2006;33 (11):4130–48.

25. Rogers DW, Bielajew AF. Monte Carlo technique of electron and photon transport for radiation therapy. In: Kase KR, Bjarngard BE, Attix FH, editors. The dosimetry of ionizing radiation, vol. III. New York: Academic; 1990. p. 427–539.

26. Mackie TR. Application of the Monte Carlo method in radiotherapy. In: Kase KR, Bjarngard BE, Attix FH, editors. The dosimetry of ionizing radiation, vol. III. New York: Academic; 1990. p. 541–620.

27. Berger MJ, Seltzer SM. ETRAN, Monte Carlo code system for electron and photon transport through extended media. Radiation Shielding Information Center Report CCC-107. Oak Ridge: Oak Ridge National Laboratory; 1973.

28. Nelson WR, Hirayama H, Rogers DWO. The EGS4 Code System. Stanford Linear Accelerator Center, Repot SLAC-265, Stanford; 1985.

29. Rogers DW, Faddegon BA, Ding GX, Ma CM, We J, Mackie TR. BEAM: a Monte Carlo code to simulate radiotherapy treatment units. Med Phys. 1995;22(5):503–24.

30. Lewis EE, Miller WF. Computational methods of neutron transport. New York: Wiley; 1984.

31. Vassiliev ON, Wareing TA, Davis IM, McGhee J, Barnett D, Horton JL, et al. Feasibility of a multigroup deterministic solution method for three-dimensional radiotherapy dose calculations. Int J Radiat Oncol Biol Phys. 2008;72(1):220–7. doi:10.1016/j.ijrobp.2008.04.057.

32. Vassiliev ON, Wareing TA, McGhee J, Failla G, Salehpour MR, Mourtada F. Validation of a new grid-based Boltzmann equation solver for dose calculation in radiotherapy with photon beams. Phys Med Biol. 2010;55(3):581–98. doi:10.1088/0031-9155/55/3/002. Epub 2010 Jan 7.

33. Han T, Mikell JK, Salehpour M, Mourtada F. Dosimetric comparison of Acuros XB deterministic radiation transport method with Monte Carlo and model-based convolution methods in heterogeneous media. Med Phys. 2011;38 Suppl 5:2651–64.

34. Fogliata A, Nicolini G, Clivio A, Vanetti E, Cozzi L. Dosimetric evaluation of Acuros XB advanced dose calculation algorithm in heterogeneous media. Radiat Oncol. 2011;6:82.

35. Bush K, Gagne IM, Zavgorodni S, Ansbacher W, Beckham W. Dosimetric validation of Acuros XB with Monte Carlo methods for photon dose calculations. Med Phys. 2011;38 Suppl 4:2208–21.
36. Papanikolaou N, Battista J, Boyer A, Kappas C, Klein E, Mackie T, Sharpe M, Van Dyk J. AAPM Report No. 85: tissue inhomogeneity corrections for megavoltage photon beams. In: AAPM Report No. 85 Medical Physics, Madison; 2004. pp. 1–135.
37. Benedict SH, Yenice KM, Followill D, Galvin JM, Hinson W, Kavanagh B, et al. Stereotactic body radiation therapy: the report of AAPM Task Group 101. Med Phys. 2010;37:4078–101.
38. Dempsey JF, Romeijn HE, Li JG, Low DA, Palta JR. A Fourier analysis of the dose grid resolution required for accurate IMRT fluence map optimization. Med Phys. 2005;32:380–8.
39. Chung H, Jin H, Palta J, Suh TS, Kim S. Dose variations with varying calculation grid size in head and neck IMRT. Phys Med Biol. 2006;51:4841–56.

Chapter 9
Treatment Planning

Mitsuhiro Nakamura

9.1 Respiratory Motion

The American Association of Physicists in Medicine (AAPM) has reported that the extent to which thoracic and abdominal tumors move during breathing varies widely [1]. Seppenwoolde et al. found that tumor motion caused by breathing was greatest in the cranial-caudal (CC) direction in patients with lower-lobe unfixed tumors, and highly elliptical if tumors were located anterior to the thorax [2]. Barnes et al. found that the average extent of motion of tumors in the lower lobe of the lung was significantly greater than that of tumors in the middle or upper lobe, or mediastinal tumors [3]. Mori et al. used volumetric cine-computed tomography (CT) to show that pancreatic tumors moved distances of over 10 mm in the inferior direction during respiration, and that geometrical variation was greater around the tail of the pancreas than around the body and head regions [4]. In addition, it is well-known that breathing patterns vary in both magnitude and period during treatment sessions, and that expiration baseline drift of respiratory signals also occurs [5, 6]. If treatment planning does not consider respiratory motion, the probability of missing a tumor may increase. Also, large target volumes, derived by overestimating respiratory motion, increase irradiation of surrounding normal tissues, trigger more local failure, and cause side-effects. Several investigators have described relationships between the irradiated volume and the extent of toxicity to normal tissue [7–9]. Thus, respiratory motion is a key consideration when planning treatment of thoracic and abdominal tumors using SBRT.

M. Nakamura (✉)

Department of Radiotherapy, Kyoto University Hospital, 54 Shogoin-Kawaharacho, Sakyo-ku, Kyoto 606-8507, Japan
e-mail: m_nkmr@kuhp.kyoto-u.ac.jp

9.2   Patient Fixation

SBRT commonly features extremely high fractional doses and high-dose gradients near the target boundary. Nagata et al. [10] found that most SBRT treatments were <30 min in duration. Hoogeman et al. noted that patients drifted away from their initial setup positions if treatment times were 15 min or longer, despite being immobilized [11]. Such movement may cause a tumor to receive an underdose or normal tissue an overdose. Therefore, secure immobilization is recommended to minimize intrafractional patient movement. The technical details of patient fixation have been described in Chap. 7. In the absence of fixation, the extent of positional verification should increase during treatment. Chapter 11 deals with this topic.

9.3   CT Imaging and Determination of Internal Target Volume

One major challenge to target delineation in moving tumors has been respiration-induced target motion, or interfraction motion, which can add considerable geometrical uncertainty to radiation treatment. This section describes the relationship between CT imaging and determination of internal target volume (ITV).

9.3.1   CT Slice Thickness

Current treatment planning is based primarily on CT. In most clinical situations, a CT slice thickness of 1–3 mm is recommended to improve longitudinal resolution and to enhance tumor detectability in the CC direction [12, 13]. High-level longitudinal resolution can decrease the partial volume effect and afford accurate delineation in the CC direction.

9.3.2   Respiratory Motion Management

As described in Sect. 9.1, thoracic and abdominal tumors move with and become deformed upon respiration. Various methods have been used to deal with tumor motion during SBRT, including inhibition of respiratory movement via abdominal compression, breath-holding, respiratory gating, and real-time tumor tracking. Appropriate CT imaging is required during delivery of each form of beam. Examples of specific types of CT imaging are described below.

9.3.2.1   Inhibition of Respiratory Movement via Abdominal Compression

CT visualization of the entire range of respiratory tumor motion is needed when respiratory movement is inhibited. However, it has been recognized that severe motion artifacts, including shuffling of axial slices out-of-order and imaging of individual organs as distinct parts, can sometimes be introduced if organ motion is present during standard CT scanning under free-breathing conditions [14–16]. Such motion artifacts may yield inaccurate representations of the shapes, volumes, and positions of normal organs, and target volumes, and cause crucial delineation errors in treatment planning. Three CT acquisition methods are commonly used; these are the inhale-and-exhale breath-hold CT scan, the slow CT scan, and the four-dimensional (4D) CT scan.

The Inhale-and-Exhale Breath-Hold CT Scan

One way to delineate a tumor-encompassing volume is to acquire breath-hold CT scans after both inhalation and exhalation. Two scans are thus obtained; and image fusion and extra contouring are subsequently required to obtain a plan. However, patients tend to breathe consciously under breath-hold conditions accompanied by audio instructions [17], which may increase the ITV size compared to that under forced-shallow or free-breathing conditions. Use of a visual feedback system can avoid amplification of lung tumor motion [18].

Slow CT Scan

In slow CT scanning, the CT gantry rotates very slowly during acquisition of each slice; the rotation time is typically 4–6 s. This yields a tumor-encompassing volume within a single rotation, but can fail to identify fine structures surrounding solid regions of a tumor [19]. Lagerwaard et al. found that a single slow CT scan captured only a mean of 80 % of the volume derived using three slow CT scans [20]. In addition, Nakamura et al. reported that a slow CT scan with a rotation time of 4 s did not totally capture the motion of a lung tumor if the breathing period was less than 4 s [21]. To overcome this drawback, repeat slow CT scanning, or a single slow scan combined with x-ray fluoroscopic examination, is required. At our institution, x-ray fluoroscopy is used to determine whether the ITV visualized on slow CT images is sufficiently large to encompass tumor motion. When the ITV is found to be insufficient, we manually correct the ITV using X-ray fluoroscopic data.

Four-Dimensional CT Scanning

Current approaches toward 4D CT acquisition use both oversampled CT data acquisition and retrospective sorting of respiratory signals recorded during CT scanning. Respiratory signaling is based on either the respiratory phase or abdominal displacement. Two principal approaches toward 4D CT acquisition have been developed; these are the helical approach [22–24] and cine approach [25–27]. In the helical approach, overlapping projection data are acquired using a very low helical pitch. The pitch is sufficiently low to permit projection data for a full respiratory cycle to be acquired for the location of each slice. Respiratory states of interest are selected prior to image reconstruction. Projection data corresponding to such selected respiratory states are sorted to reconstruct images, and three-dimensional (3D) datasets for these respiratory states are finally generated. Use of the cine approach allows repeated image acquisition in each couch position using the axial scan mode. The cine duration is set to longer than the maximum observed respiratory period, to allow acquisition of image data throughout the entire respiratory cycle. Multiple images are reconstructed in each couch position, and sorted in terms of respiratory signaling. Finally, 4D CT datasets are generated by assembling the CT images that are closest (in terms of respiratory phase or abdominal displacement) to the target for each position.

A common approach is to define an ITV that encompasses the range of tumor excursion in all 4D CT images. For lung tumors, some systems feature a maximum-intensity projection (MIP) tool that produces an image in which each voxel is set to the maximum CT number for that voxel in the 4D CT image set [27, 28]. The MIP image yields an ITV when a tumor is surrounded by low-density lung tissue, but can underestimate the ITV if the tumor is attached to the mediastinum, chest wall, or diaphragm [28]. In addition, the extent of volume underestimation using MIP tools has been found to increase with the extent of variability in patient respiration [29]. Modification of a delineated MIP image via visual verification of tumor coverage in each of the 4D CT images has been found to minimize underestimation of the ITV.

9.3.2.2 Breath-Holding

The advantage of a breath-hold technique is exploitation of physiological immobilization to minimize motion and to spare nearby normal tissues. However, this technique requires patient co-operation and staff effort in training all patients in a consistent manner. The several breath-hold techniques include active breath control, voluntary deep breath-holding, and breath-holding with or without respiratory monitoring. As shown in Table 9.1, intrafraction variations of up to 2.5 mm (one SD) have been observed [30–37]. After assessment of repeatability via acquisition of multiple breath-hold CT scans, any intrafraction variation should be included in the ITV.

Table 9.1 Intrafraction variations using breath-hold techniques

Study	Site	Technique	# of patients	Measurement	Repeatability (1SD, CC)
Hanley et al. (1999) [30]	Lung	DIBH	9	Diaphragm	0.9 mm
Remouchamps et al. (2003) [31]	Breast	mDIBH	14	Lung surface	1.1 mm
Dawson et al. (2001) [32]	Liver	ABC	8	Diaphragm	2.5 mm
Eccles et al. (2006) [33]	Liver	ABC	21	Diaphragm	1.5 mm
Koshani et al. (2006) [34]	Lung	ABC	10	GTV	1.4 mm
Hurst et al. (2010) [35]	Lung	ABC	9	GTV	Mean < 2.0 mm
Nakamura et al. (2010) [36]	Pancreas	Visual feedback	10	GTV	1.0 mm
Peng et al. (2011) [37]	Lung	Visual feedback	13	GTV	1.3 mm

Abbreviations: *DIBH* deep inspiration breath-hold, *mDIBH* moderately deep inspiration breath-hold, *ABC* active breathing control, *GTV* gross tumor volume

9.3.2.3 Respiratory-Gating and Real-Time Tumor Tracking

Breath-hold CT scans can also potentially be used during respiratory-gated and real-time tumor tracking irradiation; however, it should be noted that a 4D CT scan is preferred over a breath-hold CT scan taken at the same respiratory position, because the respiratory muscles used during breath-holding and free breathing may differ, and any tumor lag occurring during free breathing will be absent during breath-hold. It is also known that the positions of implanted markers do not always represent the tumor position because the tumor and the markers move at different rates during respiration [38]. The ITV should consider such intrafraction variations and potential changes in internal-external correlation factors [39, 40], both within the gating window and the entire cycle of respiration.

9.4 Targeting

The literature shows clearly shows that the single largest systemic source of error in radiation therapy is target delineation. Such errors can be minimized only by using site-specific delineation protocols and consensus delineation atlases. Inconsistencies in target delineation are considered to be significant sources of uncertainty in treatment planning [41]. In defining the gross tumor volume (GTV), clinical target volume (CTV), ITV, and planning target volume (PTV) when performing SBRT, the data in the International Commission on Radiation Units and Measurements (ICRU) Reports 50 [42] and 62 [43] must be taken into account.

9.4.1   GTV and CTV

The GTV (the primary tumor) may be identified using any of several imaging modalities, and should include any grossly involved lymph nodes. A CTV is an anatomically defined area (perhaps including the hilar or mediastinal lymph nodes, or a margin around a grossly visible tumor) believed to harbor micrometastases. One radiographic/histopathological study of lung parenchymal disease [44] found that GTV-to-CTV expansions of 6 mm (squamous cancers) and 8 mm (adenocarcinomas) were required to cover both the gross tumors and microscopic disease with 95 % accuracy. Grill et al. concluded that the CTV expansion required to cover microscopic extensions in 90 % of cases could be as high as 9 mm [45]. When SBRT is used, however, the GTV and CTV are often considered to be identical [46–48]. The typically very high local control rates reported after SBRT suggest that peripheral tumor components, if present, seem not to be a major cause of recurrence.

9.4.2   ITV

To address the issue of tumor motion, ICRU Report No. 62 [43] proposed use of an ITV, defined as an expansion of the CTV to explicitly reflect target motion. Several approaches have been taken to address the issue of intra- and interfraction motion, which in turn determines the ITV. Details of ITV determination for each type of beam are described in Sect. 9.3.

9.4.3   PTV

The PTV seeks to manage inaccuracies caused by daily setup of fractionated therapy, mechanical uncertainties of the equipment, and dosimetric uncertainties. When using internal surrogates, amount of marker migration and fixation rate were dependent on the procedure of implantation [38, 49, 50]. Since these may vary from center to center and, within a given center, from machine to machine, these uncertainties should also be included in a PTV.

9.5   Beam Arrangement

The goal of SBRT treatment is to ablate tissues within the PTV; destruction of such tissues is not considered to cause complications. Dose inhomogeneity inside a PTV is usually considered to be acceptable and need not be addressed as a priority during
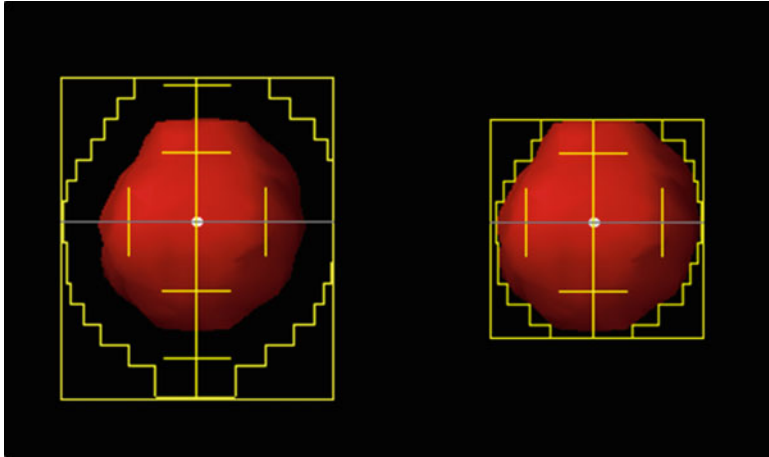
Fig. 9.1 Beam's eye view for (*Left*) isocenter prescription and (*Right*) marginal dose prescription. For isocenter prescription, the beam's eye view MLC aperture was often larger than the PTV. Meanwhile, the beam's eye view MLC aperture was typically fit to or smaller than the PTV edge for marginal dose prescription
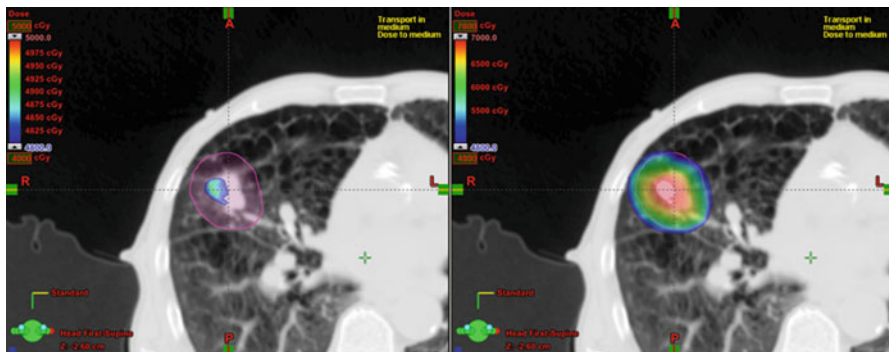

Fig. 9.2 Comparison of dose distributions. PTV is indicated by a *pink sphere*. Dose of greater than 48 Gy is shown. (*Left*) Isocenter prescription. The prescribed dose is 48 Gy at isocenter. PTV is not covered by prescribed dose of 48 Gy. (*Right*) Marginal dose prescription. The prescription dose of 48 Gy is given to the isodose line encompassing 100 % of the PTV

planning. Thus, a maximum point dose of up to around 160 % of the prescription dose is common in SBRT plans (Figs. 9.1, 9.2, and 9.3). Recently, treatment planning has been accomplished using standard beams, static conformal arcs, dynamic conformal arcs, IMRT, VMAT, or hybrid plans. Three-to-six non-coplanar arcs and five-to-nine (or more) non-coplanar static fields are commonly used. Such an approach optimally requires that radiation should converge on the target in as concentric a manner as possible, from many directions. Adjustment of the MLC margin is a key in terms of the dose distribution [51] (Fig. 9.1). If the
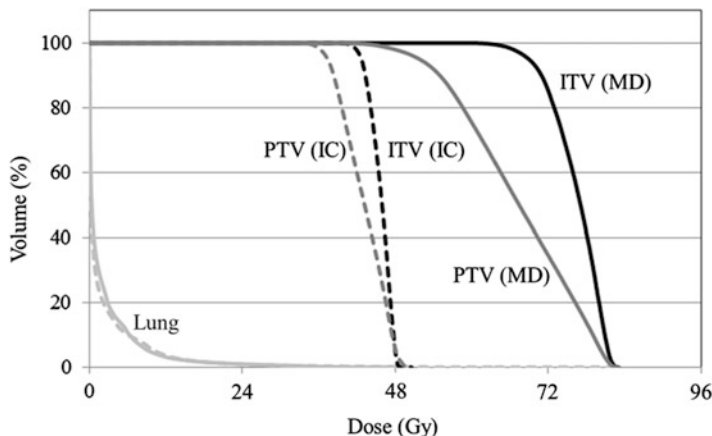
Fig. 9.3 Comparison of dose volume histograms. Marginal dose prescription (MD) vs. isocenter prescription (IC). Note that lung doses with marginal dose prescription were almost identical to those with isocenter prescription

MLC margin is close to the beam penumbra [Fig. 9.1 (Left)], a homogeneous PTV dose, the maximum of which is ~110 % of the prescription dose, can be achieved (Figs. 9.2 and 9.3); however, dose fall-off outside the PTV is slow. If the MLC margin is fit to or much less than the beam penumbra [Fig. 9.1 (Right)], dose fall-off outside the PTV is rapid, but the PTV dose can be inhomogeneous in that a maximum dose of ~125 % or more of the prescription dose can be attained (Figs. 9.2 and 9.3).

9.6 Beam Energy

For small beams, such as those commonly used in SBRT, the higher the beam energy, the larger the beam penumbra, due to lateral transport of electrons in the medium. In a low-density medium, such as lung tissue, this effect becomes more significant. Use of a lower photon beam, such as 6-MV, available on most modern treatment platforms, affords a reasonable compromise between beam penetration and the required penumbral characteristics for SBRT lung applications.

9.7 Dose Calculation

It is preferable that CT images used for dose calculation reflect respiratory status during beam delivery. As shown in Table 9.2, dose calculation should be performed using the CT dataset that is most appropriate for each patient.

Table 9.2 Ideal CT images used for dose calculation prior to use of particular beam delivery techniques

Beam delivery	Respiratory status during beam delivery	CT images
Inhibiting respiratory movement with abdominal compression	Forced shallow breathing	AIP or slow CT images with abdominal compression
Breath-holding	Breath-holding	Breath-holding
Respiratory gating	Free breathing (w/o abdominal compression)	Phase-specific images of 4D CT
Real time tumor tracking	Free breathing (w/o abdominal compression)	Phase-specific images of 4D CT

Abbreviation: *AIP* averaged intensity projection calculated after phase-binning of 4D CT images

The dose calculation algorithm (including a heterogeneity correction), and the grid size for calculation, used in any treatment planning system, affect the accuracy of the calculated dose distribution. Inaccurate dose calculation causes large discrepancies between planned and actually delivered doses; therefore, it is recommended that high-precision dose calculation algorithms with fine grid sizes be employed. The technical details of dose calculation have been discussed in this chapter.

9.8 Normal Tissue Dose Tolerance

Normal tissue dose limits for SBRT differ considerably from those of conventional radiotherapy because the dose/fractionation schemes are extreme. Thus, normal tissue dose limits for SBRT should not be directly extrapolated from conventional radiotherapy data. Particular attention should be paid to fraction size, total dose, time elapsing between fraction deliveries, and overall treatment time; these are important radiobiological factors that need to be maintained within clinically established parameters (often described in the SBRT literature). This issue assumes particular importance when planning new hypofractionated schedules and trials for which no reliable mechanism has yet been established to estimate the radiobiological effects. Therefore, in a clinical trial situation, not only fraction size, but also treatment frequency and overall treatment time, should be maintained for all patients throughout the entire trial, to obtain reliable outcome data. Critical organ tolerance doses based on SBRT experiences appearing in the evolving peer-reviewed literature must be respected [52, 53].

9.9 Treatment Plan Reporting

SBRT treatment plans often use a large numbers of beams, unconventional dose fractionations, and varying delivery frequencies. It is critical to accurately communicate the details of the treatment plan and the execution thereof to the treatment

team. The quality of planned SBRT dose distributions can be evaluated using parameters characterizing target coverage, dose homogeneity, dose delivered outside of the defined target, and the volume of normal tissue exposed to lower doses. Simple methods of describing these parameters may use combinations of DVHs for different organs and tables showing dose allocations to different subvolumes of such organs. The following metrics are relevant: "respiratory motion range", "dose calculation algorithm", "prescription dose", "prescription ICRU reference point or dose/volume", "number of treatment fractions", "total treatment delivery period", "target coverage", "heterogeneity index", "conformity index", and "dose to organs at risk".

References

1. Keall PJ, Mageras GS, Balter JM, Emery RS, Forster KM, Jiang SB, et al. The management of respiratory motion in radiation oncology report of AAPM Task Group 76. Med Phys. 2006;33:3874–900. doi:10.1118/1.2349696.
2. Seppenwoolde Y, Shirato H, Kitamura K, Shimizu S, van Herk J, Lebesque JV, et al. Precise and real-time measurement of 3D tumor motion in lung due to breathing and heartbeat, measured during radiotherapy. Int J Radiat Oncol Biol Phys. 2002;53:822–34. doi:10.1016/S0360-3016(02)02803-1.
3. Barnes EA, Murray BR, Robinson DM, Underwood LJ, Hanson J, Roa WH. Dosimetric evaluation of lung tumor immobilization using breath hold at deep inspiration. Int J Radiat Oncol Biol Phys. 2001;50:1091–8. doi:10.1016/S0360-3015(01)01592-9.
4. Mori S, Hara R, Yanagi T, Sharp CG, Kumagai M, Asakura H, et al. Four-dimensional measurement of intrafractional respiratory motion of pancreatic tumors using a 256 multi-slice CT scanner. Radiother Oncol. 2009;92:231–7. doi:10.1016/j.radonc.2008.12.015.
5. Korreman SS, Juhler-Nottrup T, Boyer AL. Respiratory gated beam delivery cannot facilitate margin reduction, unless combined with respiratory correlated image guidance. Radiother Oncol. 2008;86:61–8. doi:10.1016/j.radonc.2007.10.038.
6. Redmond KJ, Song DY, Fox JL, Zhou J, Rosenzweig CN, Ford E. Respiratory motion changes of lung tumors over the course of radiation therapy based on respiration-correlated four-dimensional computed tomography scans. Int J Radiat Oncol Biol Phys. 2009;75:1605–12. doi:10.1016/j.ijrobp.2009.05.024.
7. Murphy JD, Adusumilli S, Griffith KA, Ray ME, Zalupski MM, Lawrence TS, et al. Full-dose gemcitabine and concurrent radiotherapy for **unresectable** pancreatic cancer. Int J Radiat Oncol Biol Phys. 2007;68:801–7. doi:10.1016/j.ijrobp.2006.12.053.
8. Matsuo Y, Shibuya K, Nakamura M, Narabayashi M, Sakanaka K, Ueki N, et al. Dose-volume metrics associated with radiation pneumonitis after stereotactic body radiation therapy for lung cancer. Int J Radiat Oncol Biol Phys. 2012;83:e545–9. doi:10.1016/j.ijrobp.2012.01.018.
9. Nakamura A, Shibuya K, Matsuo Y, Nakamura M, Shiinoki T, Mizowaki T, et al. Analysis of dosimetric parameters associated with acute gastrointestinal toxicity and upper gastrointestinal bleeding in locally advanced pancreatic cancer patients treated with gemcitabine-based concurrent chemoradiotherapy. Int J Radiat Oncol Biol Phys. 2012;84:369–75. doi:10.1016/j.ijrobp.2011.12.026.
10. Nagata Y, Hiraoka M, Mizowaki T, Narita Y, Matsuo Y, Norishisa Y, et al. Survey of stereotactic body radiation therapy in Japan by the Japan 3-D Conformal External Beam Radiotherapy Group. Int J Radiat Oncol Biol Phys. 2009;75:343–7. doi:10.1016/j.ijrobp.2009.02.087.

11. Hoogeman MS, Nuyttens JJ, Levendag PC, Heijmen BJM. Time dependence of intrafraction patient motion assessed by repeat stereoscopic imaging. Int J Radiat Oncol Biol Phys. 2008;70:609–18. doi:10.1016/j.ijrobp.2007.08.066.

12. Somigliana A, Zonca G, Loi G, Sichirollo AE. How thick should CT/MR slices be to plan conformal radiotherapy? A study on the accuracy of three-dimensional volume reconstruction. Radiother Oncol. 1996;40:S66. doi:10.1016/S0167-8140(96)80261-1.

13. Winer-Muram HT, Jennings SG, Meyer CA, Liang Y, Aisen AM, Tarver RD, et al. Effect of varying CT section width on volumetric measurement of lung tumors and application of compensatory equations. Radiology. 2003;229:184–94. doi:10.1148/radiol.2291020859.

14. Balter JM, Ten Haken RK, Lawrence TS, Lam KL, Robertson JM. Uncertainties in CT-based radiation therapy treatment planning associated with patient breathing. Int J Radiat Oncol Biol Phys. 1996;36:167–74. doi:10.1016/S0360-3016(96)00275-1.

15. Shimizu S, Shirato H, Kagei K, Nishioka T, Bo X, Dosaka-Akita H, et al. Impact of respiratory movement on the computed tomographic images of small lung tumors in three-dimensional (3D) radiotherapy. Int J Radiat Oncol Biol Phys. 2000;46:1127–33. doi:10.1016/S0360-3016(99)00352-1.

16. Chen GT, Kung JH, Beaudette KP. Artifacts in computed tomography scanning of moving objects. Semin Radiat Oncol. 2004;14:19–26. doi:10.1053/j.semradonc.2003.10.004.

17. Nakamura M, Narita Y, Matsuo Y, Narabayashi M, Nakata M, Sawada A, et al. Effect of audio coaching on correlation of abdominal displacement with lung tumor motion. Int J Radiat Oncol Biol Phys. 2008;75:558–63. doi:10.1016/j.ijrobp.2008.11.070.

18. George R, Chung TD, Vedam SS, Ramakrishnan V, Mohan R, Weiss E, et al. Audio-visual biofeedback for respiratory-gated radiotherapy: impact of audio instruction and audio-visual biofeedback on respiratory-gated radiotherapy. Int J Radiat Oncol Biol Phys. 2006;65:924–33. doi:10.1016/j.ijrobp.2006.02.035.

19. Takeda A, Kunieda E, Shigematsu N, Hossain DM, Kawase T, Ohashi T, et al. Small lung tumors: long-scan-time CT for planning of hypofractionated stereotactic radiation therapy–initial findings. Radiology. 2005;237:295–300. doi:10.1148/radiol.2371032102.

20. Lagerwaard FJ, Van Sornsen de Koste JR, Nijssen-Visser MR, Schuchhard-Schipper RH, Oei SS, Munne A, et al. Multiple "slow" CT scans for incorporating lung tumor mobility in radiotherapy planning. Int J Radiat Oncol Biol Phys. 2001;51:932–7. doi:10.1016/S0360-3016(01)01716-3.

21. Nakamura M, Narita Y, Matsuo Y, Narabayashi M, Nakata M, Yano S, et al. Geometrical differences in target volumes between slow CT and 4D CT imaging in stereotactic body radiotherapy for lung tumors in the upper and middle lobe. Med Phys. 2008;35:4142–8. doi:10.1118/1.2968096.

22. Ford EC, Mageras GS, Yorke E, Ling CC. Respiration-correlated spiral CT: a method of measuring respiratory-induced anatomic motion for radiation treatment planning. Med Phys. 2003;30:88–97. doi:10.1118/1.1531177.

23. Vedam SS, Keall PJ, Kini H, Mostafavi H, Shukla HP, Mohan R. Acquiring a four-dimensional computed tomography dataset using an external respiratory signal. Phys Med Biol. 2003;48:45–62. doi:10.1088/0031-9155/48/1/304.

24. Keall PJ, Stargschall G, Shukla H, Foster KM, Ortiz V, Stecens CW, et al. Acquiring 4D thoracic CT scans using a multislice helical method. Phys Med Biol. 2004;49:2053–67. doi:10.1088/0031-9155/49/10/015.

25. Pan T, Lee TY, Rietzel E, Chen GTY. 4D-CT imaging of a volume influenced by respiratory motion on multi-slice CT. Med Phys. 2004;31:333–40. doi:10.1118/1.1639993.

26. Rietzel E, Pan T, Chen GTY. Four-dimensional computed tomography: image formation and clinical protocol. Med Phys. 2005;32:874–89. doi:10.1118/1.1869852.

27. Rietzel E, Liu AK, Doppke KP, Wolfgang JA, Chen AB, Chen GT, et al. Design of 4D treatment planning target volumes. Int J Radiat Oncol Biol Phys. 2006;66:287–95. doi:10.1016/j.ijrobp.2006.05.024.

28. Underberg RW, Lagerwaard FJ, Cuijpers JP, Slotman BJ, van Sörnsen de Koste JR, Senan S. Four-dimensional CT scans for treatment planning in stereotactic radiotherapy for stage I lung cancer. Int J Radiat Oncol Biol Phys. 2004;60:1283–90. doi:10.1016/j.ijrobp.2004.07.665.

29. Cai J, Read PW, Baisden JM, Larner JM, Benedict SH, Sheng K. Estimation of error in maximal intensity projection-based internal target volume of lung tumors: a simulation and comparison study using dynamic magnetic resonance imaging. Int J Radiat Oncol Biol Phys. 2007;62:895–902. doi:10.1016/j.ijrobp.2007.07.2322.

30. Hanley J, Debois MM, Mah D, Mageras GS, Raben A, Rosenzweig K, et al. Deep inspiration breath-hold technique for lung tumors: the potential value of target immobilization and reduced lung density in dose escalation. Int J Radiat Oncol Biol Phys. 1999;45:603–11. doi:10.1016/s0360-3016(99)00154-6.

31. Remouchamps VM, Vicini FA, Sharpe MB, Kestin LL, Martinez AA, Wong JW. Significant reductions in heart and lung doses using deep inspiration breath hold with active breathing control and intensity-modulated radiation therapy for patients treated with locoregional breast irradiation. Int J Radiat Oncol Biol Phys. 2003;55:392–406. doi:10.1016/S0360-3016(02)04143-3.

32. Dawson LA, Brock KK, Kazanjian S, Fitch D, McGinn CJ, Lawrence TS, et al. The reproducibility of organ position using active breathing control (ABC) during liver radiotherapy. Int J Radiat Oncol Biol Phys. 2001;51:1410–21. doi:10.1016/S0360-3016(00)80124-8.

33. Eccles CL, Dawson LA, Moseley JL, Brock KK. Interfraction liver shape variability and impact on GTV position during liver stereotactic radiotherapy using abdominal compression. Int J Radiat Oncol Biol Phys. 2006;80:938–46. doi:10.1016/j.ijrobp.2010.08.003.

34. Koshani R, Balter JM, Hayman JA, Henning GT, van Herk M. Short-term and long-term reproducibility of lung tumor position using active breathing control (ABC). Int J Radiat Oncol Biol Phys. 2006;65:1553–9. doi:10.1016/j.ijrobp.2006.04.027.

35. Glide-Hurst CK, Gopan E, Hugo GD. Anatomic and pathologic variability during radiotherapy for a hybrid active breath-hold gating technique. Int J Radiat Oncol Biol Phys. 2010;77:910–7. doi:10.1016/j.ijrobp.2009.09.080.

36. Nakamura M, Shibuya K, Shiinoki T, Matsuo Y, Nakamura A, Nakata M, et al. Positional reproducibility of pancreatic tumors under end-exhalation breath-hold conditions using a visual feedback technique. Int J Radiat Oncol Biol Phys. 2011;79:1565–71. doi:10.1016/j.ijrobp.2010.05.046.

37. Peng Y, Vedam S, Chang JY, Gao S, Sadagopan R, Bues M, et al. Implementation of feedback-guided voluntary breath-hold gating for cone beam CT-based stereotactic body radiotherapy. Int J Radiat Oncol Biol Phys. 2011;80:909–17. doi:10.1016/j.ijrobp.2010.08.011.

38. Ueki N, Matsuo Y, Nakamura M, Mukumoto N, Iizuka Y, Miyabe Y, et al. Intra- and interfractional variations in geometric arrangement between lung tumours and implanted markers. Radiother Oncol. 2014;110:523–8. doi:10.1016/j.radonc.2014.01.014.

39. Hoogeman M, Prevost JB, Nuyttens J, Poll J, Levendag P, Heijmen B. Clinical accuracy of the respiratory tumor tracking system of the CyberKnife by analysis of log files. Int J Radiat Oncol Biol Phys. 2009;74:297–303. doi:10.1016/j.ijrobp.2008.12.041.

40. Akimoto M, Nakamura M, Mukumoto N, Tanabe H, Yamada M, Matsuo Y, et al. Predictive uncertainty in infrared marker-based dynamic tumor tracking with Vero4DRT. Med Phys. 2013;40:091705-1-8. doi:10.1118/1.4817236.

41. Louie AV, Rodrigues G, Olsthoom J, Palma D, Yu E, Yaremko B, et al. Inter-observer and intra-observer reliability for lung cancer target volume delineation in the 4D-CT era. Radiother Oncol. 2010;95:166–71. doi:10.1016/j.radonc.2009.12.028.

42. ICRU. Prescribing, recording, and reporting photon beam therapy. ICRU Report No. 50. Bethesda: ICRU Publications; 1993.

43. ICRU. Prescribing, recording and reporting photon beam therapy (supplement to ICRU Report No. 50). ICRU Report No. 62. Bethesda: ICRU Publications; 1999.

44. Giraud PM, Antoin A, Larrouy B, Milleron P, Callard Y, De Rycke MF, et al. Evaluation of microscopic tumor extension in non-small-cell lung cancer for three-dimensional conformal radiotherapy planning. Int J Radiat Oncol Biol Phys. 2000;48:1015–24. doi:10.1016/S0360-3016(00)00750-1.

45. Grills IS, Fitch DL, Goldstein NS, Yan D, Chmielewski GW, Welsh RJ, et al. Clinicopathologic analysis of microscopic extension in lung adenocarcinoma: defining clinical target volume for radiotherapy. Int J Radiat Oncol Biol Phys. 2007;69:334–41. doi:10.1016/j.ijrobp.2007.03.023.

46. Wulf J, Hädinger U, Oppitz U, Thiele W, Ness-Dourdoumas R, Flentje M. Stereotactic radiotherapy of targets in the lung and liver. Strahlenther Onkol. 2001;177:645–55. doi:10.1007/pl00002379.

47. Timmerman R, Papiez L, McGarry R, Likes L, DesRosiers C, Frost S, et al. Extracranial stereotactic radioablation: results of a phase I study in medically inoperable stage I non-small cell lung cancer. Chest. 2003;124:1946–55. doi:10.1378/chest.124.5.1946.

48. Takayama K, Nagata Y, Negoro Y, Mizowaki T, Sakamoto T, Sakamoto M, et al. Treatment planning of stereotactic radiotherapy for solitary lung tumor. Int J Radiat Oncol Biol Phys. 2005;61:1565–71. doi:10.1016/j.ijrobp.2004.12.066.

49. Kirkpatrick JP, van der Kogel AJ, Schultheiss TE. Radiation dose-volume effects in the spinal cord. Int J Radiat Oncol Biol Phys. 2010;76:S42–9. doi:10.1016/j.ijrobp.2009.04.095.

50. Roman NO, Shepherd W, Mukhopadhyay N, Hugo GD, Weiss E. Interfractional positional variability of fiducial markers and primary tumors in locally advanced non-small-cell lung cancer during audiovisual biofeedback radiotherapy. Int J Radiat Oncol Biol Phys. 2012;83:1566–72. doi:10.1016/j.ijrobp.2011.10.051.

51. Oku Y, Takeda A, Sanuki N, Sudo Y, Oooka Y, Aolo Y, et al. Stereotactic ablative body radiation therapy with dynamic conformal multiple arc therapy for liver tumors: optimal isodose line fitting to the planning target volume. Pract Radiat Oncol. 2014;4:e7–13. doi:10.1016/j.prro.2013.04.001.

52. Persson GF, Josiprovic M, von der Recke P, Aznar MC, Juhler-Nøttrup T, Munck af Rosenschhöld, et al. Stability of percutaneously implanted markers for lung stereotactic radiotherapy. J Appl Clin Med Phys. 2013;14:187–95. doi:10.1120/jacmp.v14i5.4337.

53. Marks LB, Bentzen SM, Deasy JO, Kong F, Bradley JD, Vogelisu IS, et al. Radiation dose-volume effects in the lung. Int J Radiat Oncol Biol Phys. 2010;76:S70–6. doi:10.1016/j.ijrobp.2009.06.091.

Chapter 10
Verification of Target Localization

Shuichi Ozawa

10.1 Imaging for Radiation Therapy

Recent development of irradiation technique, such as VMAT or IMRT, enables us to give more conformal dose to the planning target volume (PTV). On the other hand stereotactic body radiation therapy (SBRT) is becoming standards, for example, for operable Stage I NSCLC as a radical treatment because SBRT is potentially comparable to that for surgery [1]. The SBRT involves large doses per fraction delivered in a few fractions and high dose conformation to PTV with steep dose gradient to minimize the damage to normal tissue. These state-of-the-art techniques required the stringent accuracy for target localization through the procedures of target delineation, treatment simulation, respiratory motion management, and verification of target localization based on the image-guidance techniques, called image-guided radiation therapy (IGRT). During IGRT procedure, it is necessary to match the on-board image of the patient with the images reconstructed by the treatment planning image as a reference to verify the accuracy of target localization.

10.2 Respiratory Motion Management

Guidelines on respiratory motion management (RMM) systems in radiotherapy have been published so far [2, 3]. In Japan, based on extensive discussions among the four radiotherapy-related societies (the Japan Conformal External Beam Radiotherapy Group, the Japanese Society for Therapeutic Radiology and Oncology, the

S. Ozawa (✉)

Department of Radiation Oncology, Hiroshima University, Institute of Biomedical & Health Science, 1-2-3 Kasumi, Minami-ku, Hiroshima 734-8551, Japan
e-mail: ozawa@hiroshima-u.ac.jp

Japan Society of Medical Physics, and the Japanese Society of Radiological Technology), the guidelines have been developed to enable medical staff (radiation oncologists, medical physicists, radiological technologists, and radiation oncology nurses, and others) involved in the RMM to radiation therapy for tumors subject to respiratory motion, safely and appropriately [2]. In this guideline, it is mentioned that the RMM may only be applied when the length of respiratory tumor motion exceeds 10 mm without RMM being implemented. Examples of methods to establish and verify the respiratory-induced tumor motion by X-ray fluoroscopy, 4D computed tomography (CT), ultrasonography, or cine magnetic resonance imaging (MRI). Moreover, RMM must be ascertained and recorded that the expansion of area of irradiation required to compensate for respiratory motion can be reduced to ≤5 mm in any three-dimensional direction. To verify that a tumor is included in the irradiated area by IGRT prior to the irradiation, such as cone-beam CT, MVCT, in-room CT, or Fluoroscopy that verifies at least two directions. Alternatively, it is also verified by the cine electronic portal imaging device (EPID), X-ray fluoroscopy, or respiratory movement modeling which predicts the 3D position of a tumor from external breathing signals and others during the irradiation.

10.3 Regions of Interests Settings for Treatment Plan

According to the International Commission on Radiation Units and Measurements (ICRU) reports 62 [4], have been described concept of planning target volume for the purpose of collateral of spatial position accuracy (PTV), PTV is the CTV internal margin (IM) and it is assumed that by adding the set-up margin (SM). IM is a margin corresponding to the physiological motion such as peristaltic or respiratory evaluated during X-ray fluoroscopy, or 4D-CT imaging under the free breathing. A combination of IM and CTV represents the internal target volume (ITV), is set as a range of target movement relative to the body structure, such as bone structure near the tumor. Furthermore, SM is a margin corresponding to the uncertainty of positioning the immobilization and patient equipment, are generally taken into account the position reproducibility of the bony structure when the external mark as a reference such as the skin mark setting. Therefore, SM to increase related to technical factors such as mechanical accuracy and uncertainty of image matching device. For margin setting to the PTV from CTV, it has been described for the simple addition and quadratic approach of IM and SM in ICRU report 62.

Because the following components contribute to the overall geometric error and should be considered when designing CTV-PTV margins [3]

- Inter- and intraobserver variations in GTV and CTV delineation;
- motion artifacts in the CT scan, which cause target de-lineation errors;

- respiratory motion and heartbeat during delivery, which are periodic functions of time;
- daily variations of respiratory motion;
- variations caused by changing organ volumes;
- tumor growth and shrinkage;
- treatment-related anatomic changes, such as reductions in bronchiole obstructions and changes in atelectasis collapsed lung regions;
- patient setup error: Typical 3–5 mm (1 standard deviation).

10.4 Geometric Uncertainty

Van Herk et al have proposed that to separate the uncertainty of geometry to systematic component and random component [5]. Systematic component means a displacement with a certain trend throughout the treatment course with respect to the image obtained for treatment planning, and it makes translational shifts of the dose distribution and causes of deterioration in the target dose. As a factor of systematic component, representation of the target delineation on CT image set by treatment planning system and relates to device geometry of linac including geometry change caused by the patient, unusual breathing and muscle tension, changes such as the bladder or rectum capacity, or tumor shrinkage can be mentioned as a cause of systematic error. For the geometry of the device, it is necessary to perform quality control of suitable apparatus based on TG-142 and other guidelines [6, 7]. Factors of random component due to the uncertainty of daily patient conditions and setup cause blurring of the dose distribution integrated throughout the treatment course. Random component is can be controlled by the use of appropriate immobilization devices.

In the time scale of radiation therapy, the uncertainty of the position of the bone structure and target long-term ones and minutes of daily, are classified as short-term ones in seconds. Change in the position of the simulation at each irradiation relative to the (in days) is called the inter-fractional variation, one of the irradiation (seconds, minutes) changes in bone structure and a target position of intra-fractional variation. We have to keep remembering that the patient motion increases as treatment time gets longer as shown in Fig. 10.1 [8].

So far, prescribe dose to the point such as isocenter or the reference point based on ICRU guideline was frequently used for SBRT treatment planning. On the other hand, prescribe dose to the isodose line covers target, which is common prescription for stereotactic irradiation for intracranial case, is also applied to SBRT cases. Figures 10.2 and 10.3 shows the comparison between two different prescription method (48 Gy/4 fractions) for HCC case. For the maginal prescription, 80 % isodoseline was adjusted to fit the PTV and isodose line is normalized to the dose to isocenter. As shown in Fig. 10.3, the marginal prescription gives rapid dose fall-off around PTV than iso center prescription, so that the required accuracy of target localization is more strict for marginal prescriptions.

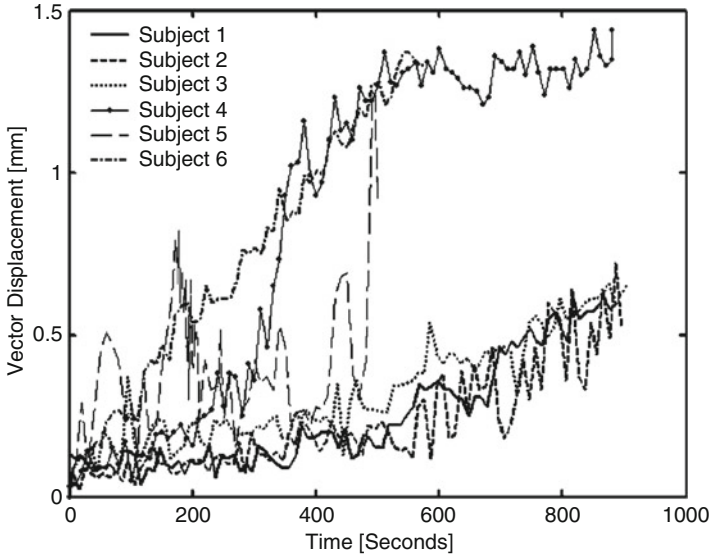**Fig. 10.1** Absolute overall displacement for six nonpatient subjects immobilized with the thermoplastic mask system. No repositioning was made for the whole test period (From Ref. [8])
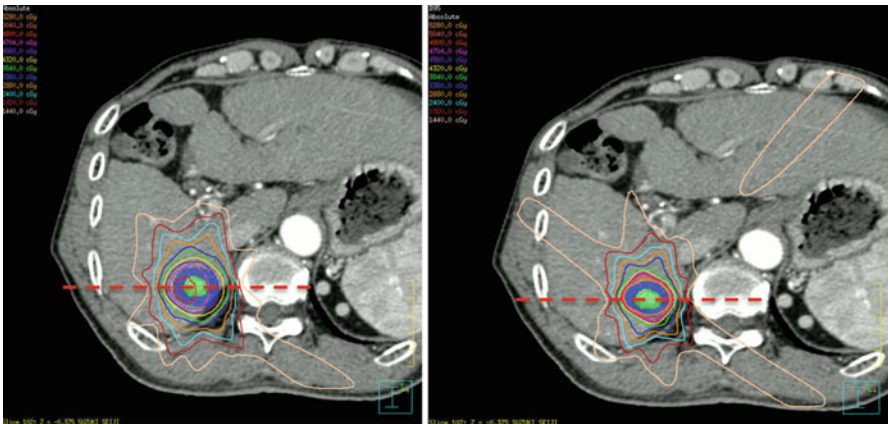

Fig. 10.2 Comparison of 2D dose distribution between two types of treatment of planning for liver SBRT, prescription at isocenter (*left*) and marginal prescription (*right*). 1D dose profiles of dashed line are shown in Fig. 10.3
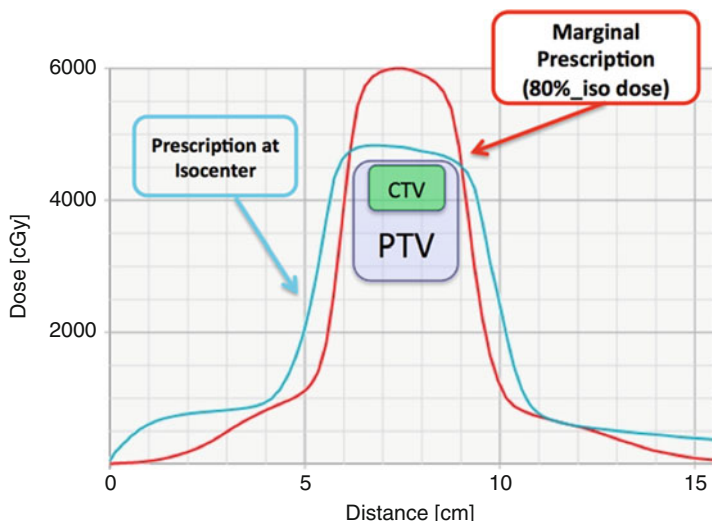
Fig. 10.3 1D dose comparison on the *dashed line* in Fig. 10.2

10.5 Evidence of Effectiveness About IGRT and Treatment Quality

Zelefsky et al. reported the retrospective comparison of the outcomes of a cohort of patients treated with definitive IGRT using implanted fiducial markers to the outcomes in a cohort treated with the same dose and margins with IMRT without daily target position correction (non-IGRT) [9]. In this report they compare the toxicity and tumor control outcomes of these two patient cohorts. Their findings showed the lower incidence of late urinary toxicity and improved early biochemical tumor control for high-risk patients in the IGRT-treated patients compared with the non-IGRT cohort (Fig. 10.4). Note that IGRT and respiration-motion management techniques not only for the accuracy of target localization, but also the normal tissue sparing.

In clinical trials group of Australia, tirapazamine for advanced head and neck cancer patients of 861 people in 2010: I have reported the results of a phase III trial on adding to cisplatin · radiation therapy (TPZ hypoxic cytotoxins) [10]. Results identify hypoxia, in advanced head and neck cancer patients that have not been selected, added to chemoradiotherapy TPZ not improve overall survival, clinical utility of TPZ, the hypoxia Although is that there is likely to be limited to cases to be confirmed, I would like addressed, "has been posted on the next page of this phase III trial of paper Critical Impact of Radiotherapy Protocol Compliance and Quality in the Treatment of Advanced Head and Neck Cancer: a paper titled Results From TROG 02.02" [11]. In this paper, we secondary analysis on the results of the phase III trial described above, is quantitatively evaluated the effect of radiotherapy quality has on the results of clinical trials, very interesting. Radiation therapy is interrupted cases and was not performed cases removed from the statistics, it is
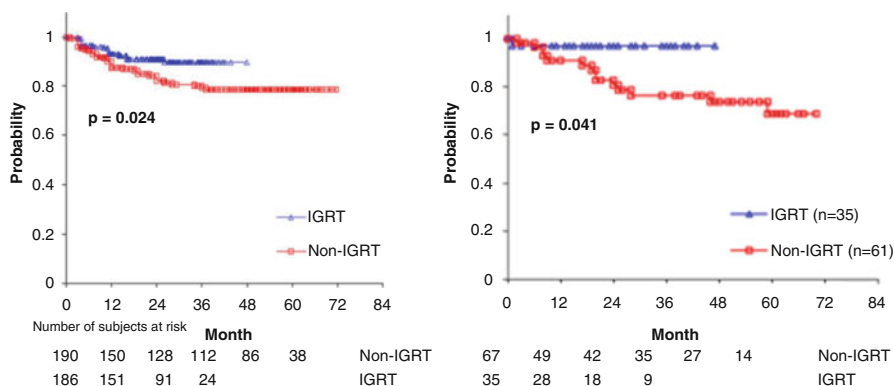
Fig. 10.4 *Left*: Comparison of actuarial likelihood of grade 2 or higher late urinary toxicity for patients treated with image-guided radio- therapy (IGRT) to 86.4 Gy vs. intensity-modulated radiotherapy. *Right*: Comparison of prostate specific antigen relapse-free survival outcomes between patients treated with image-guided radiotherapy (IGRT) to 86.4 Gy and those treated with intensity-modulated radiotherapy to the same dose level (Captured from Ref. [9])

classified 780 cases irradiated least 60 Gy over the four categories. Among them, deviations are expected to affect tumor control rate 87 cases of 11 % was found. While this itself is not in fact be arbitrarily uncommon in clinical trials, and surprised the 2-year survival rate obtained by extracting only the errant case group is 20 % compared to the group without deviating (70 % → 50 %) he that was worse! In other words, radiation therapy QA/QC is, it is suggested that than combined chemoradiotherapy using new drugs is a major factor in ensuring the local control, drug radiotherapy if properly administered it is possible to enhance the effect, the tumor dose insufficient by radiation therapy which means that it can not be compensated with a drug. And, this paper is the last to be summarized in the following sentence. "It is sobering to note that the value of good radiotherapy is substantially greater than the incremental gains that have been achieved with new drugs and/or biologicals."

10.6 Imaging Dose to the Patients

There is furthermore an interplay between increased imaging and improved thera-peutic dose conformity that suggests the possibility of optimizing rather than simply minimizing the imaging dose. For this reason, the management of imaging dose during radiotherapy is a different problem than its management during routine diagnostic or image-guided surgical procedures. It is necessary for medical phys-icists to pay attention to the imaging does to the patients during the procedure of IGRT. AAPM TG-75 was organized to addressing the issue of radiation dose delivered via image guidance techniques during radiotherapy, and the TG-75 report enables the design of image guidance regimens that are as effective and efficient [12].

10.7   MRI-Guided Technique

Speaking of image modalities that are used for image-guided radiation therapy (IGRT), but by CBCT or fluoroscopic or ultrasound was the main, [13]. However, IGRT device using an MRI image from the last appeared. ViewRay, Inc. is an MRI cobalt equipment MRIdian™ system was developed (Figs. 10.5 and 10.6) [13]. I for 2 years from 2006, had been studying in the University of Florida in the United States, venture companies that Dr. Jim Dempsey was assistant professor of the University of Florida was launched in 2004 at that time is ViewRay. In February 2014, the world's first radiation treatment of MRI image guidance (lung SBRT) has been carried out in the hospital of Washington University in St. Louis, MO, USA. The greatest advantage of the MRI image guided, while monitoring the body in real time MRI cine images is that which can be synchronized irradiation or tracking irradiation. MRI cine image can be obtained in real time, without any marker such, it is possible to beam on/off control while confirming the tumor position. In some cases, it is possible to synchronize the irradiated with based on the position of the organs at risk. In the apparatus of this ViewRay is using MRI of the weak magnetic field strength of 0.35 T to suppress the distortion of MRI images. On the other hand, in the Elekta is developing a treatment device that combines MRI and linac 1.5 T (Fig. 10.7) [14]. At the end of 2015 it is planned to install is performed in Canada of radiation therapy facility. The near future, IGRT by MRI is building a new era of radiation therapy, it is going to be able to change our values. Not only a clinical point of view, but also in the physical and technical quality control, MRI-based IGRT machine may bring us a major paradigm shift.

Fig. 10.5   Overview of MRI-based cobalt machine (Courtesy of Ref. 13)
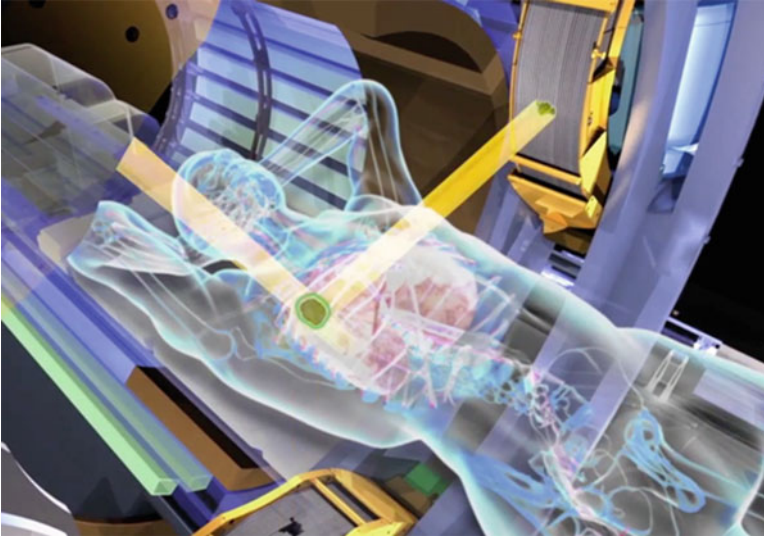
Fig. 10.6 Treatment by the MRI-based cobalt machine (Courtesy of Ref. 13)

Fig. 10.7 MRI-linac by Elekta (From elekta R&D website [14])

References

1. Onishi H, Shirato H, Nagata Y, Hiraoka M, Fujino M, Gomi K, Karasawa K, Hayakawa K, Niibe Y, Takai Y, Kimura T, Takeda A, Ouchi A, Hareyama M, Kokubo M, Kozuka T, Arimoto T, Hara R, Itami J, Araki T. Stereotactic body radiotherapy (SBRT) for operable stage I non-small-cell lung cancer: can SBRT be comparable to surgery? Int J Radiat Oncol Biol Phys. 2011;81:1352–8.

2. Matsuo Y, Onishi H, Nakagawa K, Nakamura M, Ariji T, Kumazaki Y, Shimbo M, Tohyama N, Nishio T, Okumura M, Shirato H, Hiraoka M. Guidelines for respiratory motion management in radiation therapy. J Radiat Res. 2013;54:561–8.
3. Keall PJ, Mageras GS, Balter JM, Emery RS, Forster KM, Jiang SB, Carpets JM, Low DA, Murphy MJ, Murray BR, Ramsey CR, van Herk MB, Vedam SS, Wong JW, Yorke E. The management of respiratory motion in radiation oncology: report of AAPM Radiation Therapy Committee Task Group No. 76. Med Phys. 2006;33:3874–900.
4. ICRU. Report 62. Prescribing, recording and reporting photon beam therapy (Supplement to ICRU report 50); 1999.
5. van Herk M, Remeijer P, Rasch C, et al. The probability of correct target dosage: dose-population histograms for deriving treatment margins in radiotherapy. Int J Radiat Oncol Biol Phys. 2000;47:1121–35.
6. Klein EE, Hanley J, Bayouth J, et al. Task Group 142 report: quality assurance of medical accelerators. Med Phys. 2009;36:4197–212.
7. Kutcher GJ, Coia L, Gillin M, et al. Comprehensive QA for radiation oncology: report of AAPM Radiation Therapy Committee Task Group 40. Med Phys. 1994;21:581–618.
8. Kim S, Akpati HC, Kielbasa JE, Li JG, Liu C, Amdur RJ, Palta JR. Evaluation of intrafraction patient movement for CNS and head & neck IMRT. Med Phys. 2004;31:500–6.
9. Zelefsky MJ, Kollmeier M, Cox B, Fidaleo A, Sperling D, Pei X, Carver B, Coleman J, Lovelock M, Hunt M. Improved clinical outcomes with high-dose image guided radiotherapy compared with non-IGRT for the treatment of clinically localized prostate cancer. Int J Radiat Oncol Biol Phys. 2012;84:125–9.
10. Rischin D. Tirapazamine, cisplatin, and radiation versus cisplatin and radiation for advanced squamous cell carcinoma of the head and neck (TROG 02.02, HeadSTART): a phase III trial of the Trans-Tasman Radiation Oncology Group. J Clin Oncol. 2010;28:2989–95.
11. Peters LJ. Critical impact of radiotherapy protocol compliance and quality in the treatment of advanced head and neck cancer: results from TROG 02.02. J Clin Oncol. 2010;28:2996–3001.
12. Murphy MJ, Balter J, Balter S, et al. The management of imaging dose during image-guided radiotherapy: report of the AAPM Task Group 75. Med Phys. 2007;34:4041–63.
13. ViewRay inc. http://www.viewray.com
14. Elekta R&D website. http://elekta-rd.creo.se

Part IV
Lung Cancer

Chapter 11
Japanese Experiences

Masaki Kokubo, Yasushi Nagata, Rikiya Onimaru, and Masahiro Hiraoka

11.1 Retrospective Outcome Reports of SBRT in Japan

Dr. Uematsu of National Defense Medical College in Japan, who is the pioneer of the Stereotactic Body Radiation Therapy (SBRT) for lung cancer, realized for the first time the accelerator combined with CT system (named with FOCAL unit) in the treatment room where the couch of the accelerator links that of the CT. By using this system, 50 patients with pathologically proven T1 or T2 N0 lung cancer, who were either medically inoperable or refused surgery, were treated between October 1994 and June 1999. In most patients the dose was 50–60 Gy in five to ten fractions for 1–2 weeks only to the primary lesion. Beam arrangements consisted of 6–15 noncoplanar arcs. With a median follow-up period of 36 months, the 3-year overall survival rate and the 3-year local control rate was 66 % and 94 %, respectively [1].

Onimari et al. reported the results of phase I/II SBRT consisted of 48–60 Gy in eight fractions over 2 weeks. They treated 57 lung tumors. The 3-year local control rate was 80 % with a median follow-up period of 17 months for survivors. The 3-year local control rate was 70 % for patients who received 48 Gy and 100 % for

M. Kokubo (✉)
Department of Radiation Oncology, Kobe City Medical Center General Hospital,
2-1-1, Minatojima-Minamimachi, Chuo, Kobe 650-0047, Japan
e-mail: mkokubo@kcho.jp

Y. Nagata
Department of Radiation Oncology, Hiroshima University Hospital, Hiroshima, Japan

R. Onimaru
Department of Radiation Medicine, Hokkaido University Graduate School of Medicine,
Sapporo, Japan

M. Hiraoka
Department of Radiation Oncology and Image-Applied Therapy, Graduate School of
Medicine, Kyoto University, Kyoto, Japan

patients who received 60 Gy. One patient with a central lesion died of a radiation-induced ulcer in the esophagus after receiving 48 Gy in eight fractions at isocenter. Although the contour of esophagus received 80 % or less of the prescribed dose in the planning, recontouring of esophagus in retrospective review revealed that one cc of esophagus might have received 42.5 Gy, with the maximum dose of 50.5 Gy [2].

Dr. Nagata of Kyoto University Graduate School in Medicine increased a single dose up to 12 Gy at the isocenter and reduced fraction to four times. Nagata and his colleague treated 45 patients between September 1998 and February 2004. Thirty-two patients had T1 lung cancer, and the other 13 had T2 lung cancer. Nagata et al. reported 16 % tumors completely disappeared after treatment. During a median follow-up of 30 months, no pulmonary complications greater than grade 3 of National Cancer Institute-Common Toxicity Criteria were noted. The 3-year local control rate was 98 %. The 3-year overall survival rate for T1 lung tumor was 83 % and that for T2 tumor was 72 % [3].

Koto et al. treated 19 patients with T1 lung tumor and 12 patients with T2 with 45 Gy at isocenter in three fractions. The median duration of observation for all patients was 32 months. The 3-year local control rates of T1 and T2 tumors were 77.9 % and 40.0 %, respectively. They stated that a more intensive treatment regimen should be considered for T2 tumors [4].

The largest series of SBRT for early-stage non-small lung cancer was reported by Dr. Onishi of Yamanashi University who went to the national questionnaire. One hundred and sixty-four patients with T1 lung cancer and 93 patients with T2 were treated with SBRT using a variety of techniques, all noncoplanar arcs or multiple static beams and mechanisms to reduce respiratory movement. Total dose of 18–75 Gy in one to 22 fractions were delivered. The median calculated biologic effective dose (BED) was 111 Gy (range, 57–180 Gy) based on alpha/beta = 10. The median age was 76 years old. During a median follow-up of 38 months, pulmonary complications greater than grade 2 of National Cancer Institute-Common Toxicity Criteria were noted in only 5.4 % of patients. In SBRT, local progression occurred in 36 patients (14.0 %), and the local recurrence rate was 8.4 % for a BED of 100 Gy or more compared with 42.9 % for less than 100 Gy (p < 0.001). The 5-year overall survival rate of medically operable patients was 70.8 % among those treated with a BED of 100 Gy or more compared with 30.2 % among those treated with less than 100 Gy (p < 0.05), and that of inoperable cases was 39 % with a BED of 100 Gy or more [5].

Nagata et al. reported the survey for the status of SBRT in Japan using the nationwide questionnaire. At the end of November 2005, 94 institutions responded to the questionnaire. A total of 1,111 patients with histologically confirmed lung cancer were treated, including 637 had T1N0M0 and 272 had T2N0M0 lung cancer. The most frequent schedule used for primary lung cancer was 48 Gy in four fractions, followed by 50 Gy in five fractions. There were 14 (0.6 % of all cases) reported grade 5 complications: 11 cases of radiation pneumonitis, 2 cases of hemoptysis, and 1 case of radiation esophagitis [6].

11.2 Prospective Clinical Trials of SBRT Conducted by Japan Clinical Oncology Group

11.2.1 JCOG 0403

In 2003, Radiation Therapy Study Group has been newly installed in Japan Clinical Oncology Group; JCOG. Principal investigator was Professor Hiraoka of Department of Radiation Oncology and Image-applied Medicine, Kyoto University Graduate School of Medicine. For the first clinical examination of this study group, the phase II study regarding SBRT for Stage IA non-small cell lung cancer, JCOG0403, was initiated.

The purpose of JCOG0403 was to evaluate the safety and efficacy of SBRT, consist of 48 Gy at isocenter in four fractions over 4–8 days, in both patients with operable and inoperable Stage IA non-small cell lung cancer. Answers to the following two clinical questions were sought by this trial: First; Can SBRT be an alternative standard treatment modality for inoperable patients? Second; Is SBRT promising as an alternative to lobectomy for operable patients received lobectomy for standard care? This study is different from Western study. Not only inoperable cases but operable cases were included in this study. The primary endpoint is the 3-year overall survival rate. The patients with histologically or cytologically proven stage IA non-small cell lung cancer, PS 0–2, $PaO2 \geq 60$ torr, $FEV1.0 \geq 700$ mL were included, Between July 2004 and November 2008, 169 patients from 15 institutions participated in the clinical trials were enrolled in this JCOG0403. One hundred inoperable and 64 operable in total 164 patients were eligible.

First, for the inoperable cases assessed by thoracic surgeons, it was assumed that the 3-year survival rate of treatment up to now could be 35 %, and that expected the 3-year survival rate of the study was 50 %. The sample size of inoperable population was determined as 100 to test the threshold value of 35 % in terms of overall survival rate of 3 years with the expected value of 50 %, one-sided alpha of 0.05, and power of 90 %. If the lower limit of 90 % confidence interval of the 3-year overall survival rate exceeds the threshold value of 35 %, SBRT is considered to be effective.

One hundred and four patients were included. Seventy-seven were male and 27 were female. The median age was 78 years old, and the median tumor size was 21 mm. The median follow-up period for inoperable patients was 47 months. Regarding the main endpoint, the 3-year overall survival rate was 59.9 % (95 % credible interval (CI): 49.6–68.8 %) of the 100 eligible patients in 104 inoperable patients. The 3-year local control rate, which does not include death as an event, was 87.3 %. Fifty-five patients died, 17 (31 %) of which died of lung cancer and 38 (69 %) of other causes. There were no lethal adverse events. Grade 4 toxicity was observed in the following two cases: one dyspnea and one hypoxia. Grade 3 toxicity was observed in the following nine cases: dyspnea, nine; hypoxia, eight; pneumonia, seven; chest pain, two; and cough, one (It was counted in duplicate) [7].

From these results, for the medically inoperable patients with T1 lung cancer, SBRT should be a new standard treatment method replacing conventional radiation therapy. Also the 3-year local control rate was almost similar as the results from Europe and the United States of America.

On the other hand, for operable cases, the 3-year overall survival rate of patients with T1 non-small lung cancer by the Japanese Lung Cancer Registry was 81.3 %. Since SBRT is considered to be a less toxic procedure than lobectomy, SBRT is promising enough to be an alternative treatment to surgery for operable patients when the upper limit of the 95 % CI of the 3-year overall survival rate obtained from this study exceeds 80 %. The sample size of operable population was determined as 62 by precision basis so that the 95 % CI for the estimated overall survival rate of 3 years would be +/−10 % around the expected value of 80 %.

Sixty-five patients were registered in this study. Forty-five were male and 20 were female. The median age was 79 and median tumor size was 21 mm. The median follow-up period for operable population was 45 months. Of the eligible 64 operable patients, the overall survival rate of 3 years was 76.0 % (95 % CI: 63.3–84.8 %). The 3-year local control rate, which does not include death as an event, was 85.4 %. During the follow-up, 37 patients died, 18 (49 %) of which died of disease and 19 (51 %) of other causes. In operable population, grade 4 and 5 toxicities were not observed. Grade 3 toxicity was observed in the following four cases: chest pain, one; dyspnea, two; hypoxia, one; and pneumonitis, two (It was counted in duplicate.) [8].

This is the first report in the world regarding SBRT efficacy and safety for medically operable patients with T1 lung tumor. This treatment is promising as an alternative to surgery for operable stage I non-small cell lung cancer.

11.2.2   JCOG 0702

JCOG Radiation Therapy Study Group have conducted the second clinical trial, JCOG0702. Although SBRT shows good clinical results, the efficacy and safety of SBRT for T2 lung tumors seem to be less certain than that for T1 lung tumors. The local control rates of 3 years for T2 tumor was not satisfactory. Onimaru et al. and Koto et al. reported that local control rate for T2 tumors was poorer than that for T1 tumors [4, 9]. Onishi et al. reported that local disease recurrence was 9.7 % for T1, and 20.0 % for T2, respectively. They also reported that there was no remarkable difference in overall survival between T1 tumors and T2 tumors in the group with biologically effective dose equal to or larger than 100 Gy [5]. These results suggest that dose escalation is one of the methods in order to improve clinical outcome of SBRT for T2 cancer.

JCOG0702 is the phase I study in order to investigate the maximum tolerated dose and to determine the recommended dose of SBRT for peripheral T2 non-small cell carcinoma. Dose limiting toxicity was grade 3 radiation pneumonitis within 180 days after the start of SBRT but grade 2 radiation pneumonitis was used as

surrogate dose limiting toxicity because the incidence of grade 3 radiation pneumonitis was expected very low. Recommended dose was defined as equal to the maximum tolerated dose. Dose was prescribed at D95 of PTV. Starting dose was 40 Gy in four fractions, and dose was escalated by 5-Gy step with calculation using the superposition algorithm or equivalent method. This starting dose was decided based on estimation that 40 Gy in four fractions at D95 of the PTV corresponds to 48 Gy in four fractions calculated by the Clarkson algorithm at the isocenter in JCOG0403. The isocenter dose of 40 Gy in four fractions at D95 ranged from 45.3 to 51.9 Gy in four fractions. The maximum dose level was determined as 65 Gy in four fractions at D95 of PTV before starting JCOG0702. Because the range of the volume of PTV is broad in T2 tumors, the enrolled patients in this study have been stratified by PTV volumes (PTV < 100 cc or PTV ≥ 100 cc) to assess toxicities accurately.

In JCOG0702, continual reassessment method (CRM) was used to determine the dose level that patients should be assigned to and the maximum tolerated dose, although traditional 3 + 3 design is popular in phase I study especially for cytotoxic chemotherapy. CRM is a Bayesian approach and has some important advantages compared to traditional 3 + 3 design. First, since CRM uses all the data of registered patients in order to determine next dose level, CRM can estimate the maximum tolerated dose more precisely than traditional 3 + 3 design. In JCOG0702 Onimaru et al. tried to determine the recommended dose based on the data with statistical evaluation. They estimated the lower limit of 95 % CI of the predicted maximum tolerated dose. Second, rapid dose escalation is possible. The dose limiting toxicity of radiotherapy sometimes needs to be observed long time, because some of the dose limiting toxicities like radiation pneumonitis are observed 3–6 months after the completion of radiotherapy. The need for long observation may result in the long period of phase I study in radiation oncology. In spite of required long observation, CRM can shorten the study period compared to traditional design, because smaller number of patients are assigned to some dose levels and the total number of patients can be smaller. In JCOG0702 the prior distribution of the dose–response curve and the maximum tolerated dose was calculated based on the expected frequency of grade 2 radiation pneumonitis. The maximum tolerated dose was the dose level that the expectation of posterior distribution for grade 2 radiation pneumonitis was around 25 % in the pre-planned decision rule. The dose level and the numbers of patients assigned to was calculated and updated once a month using CRM.

Eligibility criteria in JCOG0702 included pathologically or cytologically proven NSCLC, peripheral T2N0M0 over 3 cm in diameter, PS 0–2, PaO2 ≥ 60 torr, FEV1.0 ≥ 700 mL, either "age ≥20 years and unfit for lobectomy" or "age ≥ 70 years and refusing surgery.". By now, the results of the group with PTV < 100 cc were reported [10]. Fifteen patients were accrued from October 2008 to September 2012 in PTV < 100 cc group. Five patients were treated at 40 Gy, one at 45 Gy, three at 50 Gy, one at 55 Gy, and five at 60 Gy. Tumor size ranged from 31 to 39 mm with a median of 32 mm. Only one patient experienced grade 2 radiation pneumonitis at 60 Gy in four fractions. Other 14 patients had

grade 1 or 0 radiation pneumonitis. Mean lung dose ranged from 3.0 to 7.0 Gy for all patients. More patients should have been assigned to the level of 60 Gy according to CRM, but enrolling more than five patients to that level was not practical because of the difficulty of fulfilling the dose constrains. Considering the generalizability of this study result, the maximum assigned dose level was reduced from 60 to 55 Gy. Median overall survival was 2.6 years. The 3-year overall survival was 39 % (95 % CI 11.4–67.1 %). The recommended dose was determined as 55 Gy in four fractions because the lower limit of CI of the predicted recommended dose exceeded the adjacent dose level of 50 Gy. The mean lung dose and the isocenter dose with 55 Gy in four fractions at D95 were 4.6 Gy and 66.8 Gy, respectively.

11.3 Other Prospective Clinical Trial

Japan Radiation Oncology Study Group; JROSG conducts the ongoing phase I SBRT study for medically inoperable Stage IA non –small cell lung cancer which is present in the mediastinal-hilar side, in order to determine the recommend dose. The dose reference point is isocenter and the calculation algorithm is the superposition method equivalent. Initial dose is 60 Gy in eight fractions, here single dose be increased or decreased by 0.5 Gy depending on the toxicities. The primary endpoint is the proportion of non-hematological toxicity within 1 year after treatment. Patients treated with initial dose were already registered. The results will be reported shortly.

References

1. Uematsu M, Shioda A, Suda A, Fukui T, Ozeki Y, Hama Y, et al. Computed tomography-guided frameless stereotactic radiotherapy for stage I non-small cell lung cancer: a 5-year experience. Int J Radiat Oncol Biol Phys. 2001;51:666–70.
2. Onimaru R, Shirato H, Shimizu S, Kitamura K, Xu B, Fukumoto S, et al. Tolerance of organs at risk in small-volume, hypofractionated, image-guided radiotherapy for primary and metastatic lung cancers. Int J Radiat Oncol Biol Phys. 2003;56:126–35.
3. Nagata Y, Takayama K, Matsuo Y, Norihisa Y, Mizowaki T, Sakamoto T, et al. Clinical outcomes of a phase I/II study of 48 Gy of stereotactic body radiotherapy in 4 fractions for primary lung cancer using a stereotactic body frame. Int J Radiat Oncol Biol Phys. 2005;63:1427–31.
4. Koto M, Takai Y, Ogawa Y, Matsushita H, Takeda K, Takahashi C, et al. A phase II study on stereotactic body radiotherapy for stage I non-small cell lung cancer. Radiother Oncol. 2007;85:429–34.
5. Onishi H, Shirato H, Nagata Y, Hiraoka M, Fujino M, Gomi K, et al. Hypofractionated stereotactic radiotherapy (HypoFXSRT) for stage I non-small cell lung cancer: updated results of 257 patients in a Japanese multi-institutional study. J Thorac Oncol. 2007;2(7 Suppl 3): S94–100.

6. Nagata Y, Hiraoka M, Mizowaki T, Narita Y, Matsuo Y, Norihisa Y, et al. Survey of stereotactic body radiation therapy in Japan by the Japan 3-D Conformal External Beam Radiotherapy Group. Int J Radiat Oncol Biol Phys. 2009;75:343–7.

7. Nagata Y, Hiraoka M, Shibata T, Onishi H, Kokubo M, Karasawa K, et al. Stereotactic body radiation therapy for T1N0M0 non-small cell lung cancer: first report for inoperable population of a phase II trial by Japan Clinical Oncology Group (JCOG 0403). Int J Radiat Oncol Biol Phys. 2012;84:S46.

8. Nagata Y, Hiraoka M, Shibata T, Onishi H, Kokubo M, Karasawa K, et al. A phase II trial of stereotactic body radiation therapy for operable T1N0M0 non-small cell lung cancer: Japan Clinical Oncology Group (JCOG0403). Int J Radiat Oncol Biol Phys. 2010;78:S27–8.

9. Onimaru R, Fujino M, Yamazaki K, Onodera Y, Taguchi H, Katoh N, et al. Steep dose-response relationship for stage I non-small-cell lung cancer using hypofractionated high-dose irradiation by real-time tumor-tracking radiotherapy. Int J Radiat Oncol Biol Phys. 2008;70:374–81.

10. Onimaru R, Shirato H, Shibata T, Hiraoka M, Ishikura S, Onishi H, et al. A phase 1 study of stereotactic body radiation therapy (SBRT) for peripheral T2N0M0 non-small cell lung cancer (NSCLC): Japan Clinical Oncology Group Study (JCOG0702). Int J Radiat Oncol Biol Phys. 2013;87:S10.

Chapter 12
International Experience

Kazushige Hayakawa

12.1 Introduction

Multi-institutional trials from the United States, Japan, Germany and other countries are now underway to corroborate the results of single- or multi-institutional Phase I and II experiences in stereotactic body radiation therapy (SBRT) for early-stage lung cancer. Well-designed prospective studies with mature data have shown promising clinical outcomes overcoming those seen in the previous studies for conventionally fractionated radiotherapy. This chapter will provide an overview of the international clinical experiences with SBRT for lung cancer.

In the many countries, respiratory gating is commonly used for motion control that requires knowledge of tumor position within a respiratory cycle based on four-dimensional CT (4DCT). Generally, gating occurs at the end of expiration, which is a longer phase and relatively stable. The accuracy and reproducibility of patient positioning is commonly controlled by a stereotactic body frame, the commercially available vacuum pillow, and abdominal compression devices suppressing the diaphragmatic motion and so on. On the other hand, a frameless robotic radiosurgery system (the Cyberknife) is widely used for SBRT of lung tumors. The synchrony system with a combination of internal fiducials and light emitting optical markers mounted on the patient skin is available for chasing a tumor with respiratory motion.

K. Hayakawa (✉)
Department of Radiology and Radiation Oncology, Kitasato University School of Medicine, 1-15-1 Kitasato, Minami-Ku, Sagamihara, Kanagawa 252-0374, Japan
e-mail: hayakazu@med.kitasato-u.ac.jp

12.2 Clinical Study

12.2.1 Phase I Study

12.2.1.1 The North American Experiences (Table 12.1)

The Indiana University Dose Escalation Trial

At Indiana University a formal phase I dose escalation toxicity study was performed with 47 patients with medically inoperable non-small cell lung cancer (NSCLC) [1]. Three to five patients were treated within each dose cohort starting at 24 Gy in three fractions followed by successive dose escalations of 2 Gy per fraction (total increase per cohort, 6 Gy). Independent dose escalation trials were carried out in three separate patient groups: patients with T1 tumor, patients with T2 tumor less than 5 cm, and patients with T2 tumor 5–7 cm. In all cases, 95 % of the planning target volume (PTV) was covered by the 80 % prescription isodose volume. The PTV with setup uncertainty was designed from the gross tumor volume (GTV) by enlarging the volume 0.5 cm in the axial plane and 1.0 cm in the cranial-caudal plane in all directions. There was no limitation regarding the location of the tumor in the lung as both central and peripheral tumors were treated. Waiting periods occurred between dose cohorts to observe toxicity such as any grade 3 pulmonary, esophageal, cardiac or pericardial toxicity, or any grade 4 toxicity that was ascribed to the protocol treatment even after the acute period. A total of seven dose levels were tested. The maximal tolerated dose (MTD) was never reached for T1 tumors and T2 tumors less than 5 cm despite reaching 60–66 Gy in three fractions. For the largest tumors, dose was escalated all the way to 72 Gy in three fractions, which proved to be too toxic. Dose-limiting toxicity in that subset included pneumonia and pericardial effusion. Therefore, the MTD for tumors 5–7 cm in diameter was 66 Gy in three fractions, whereas the MTD for smaller tumors lies at an undetermined level beyond this dose.

For all patients on the study, 9 local failures occurred at doses ≤16 Gy per fraction, whereas only 1 patient recurred at higher doses. A dose-response curve for local control using SBRT in lung cancer from these data is shown in Fig. 12.1. As the dose was increased more than 48 Gy, the local control rate at 17 months reached over 80 % [2]. From this study, a dose of 60–66 Gy in three fractions was determined to be reasonably safe for enrolled patients with medically inoperable NSCLC.

Other Phase I Studies

Whyte et al. reported the preliminary results of a phase I study using a robotic frameless stereotactic radiosurgery system for early-stage lung cancer (n = 15) and metastatic lung tumors (n = 8) [3]. The enrolled patient were treated with a single

Table 12.1 Phase I trials of SBRT for early-stage NSCLC

Authors (year)	Target	Patients (Pts)	Staging	Equipment	PTV margin	Dose escalation	Outcomes			
							MTD	RD	LF	Failure Pattern
Whyte RI, et al. (Stanford Univ. & Cleveland clinic) (2003) [3]	1–5 cm in diameter, unresectable	15 pts; 8 pts (meta); Mean age 63	CT	Frameless stereotactic radiosurgery system (CyberKnife) Breath-holding technique (9 pts), Respiratory-tracking, robotic technique (14 pts)	N/A; Spinal cord <8 Gy, brachial plexus <10 Gy, 2/3 of total lung <5 Gy, 50 % of heart <10 Gy, 50 % of esophagus <10 Gy, 50 % of liver <7.5 Gy	15 Gy/single fraction	No grade 3–5 of RTOG complications	N/A	Response Complete, 2; Partial, 15; Stable, 4; Progressive, 2	N/A; Follow-up 1–26 mo (mean 7 mo)
Le QT, et al. (Stanford Univ.) (2006) [4]	Stage IA & IB NSCLC or metastatic tumor, ≤5 cm in diameter	32 pts; T1, 6; T2, 14; Meta/rec, 12; Med age 72	CT & PET (29)	Linac-based, vacuum–set immobilization cushion, Breath-holding technique or Synchrony respiratory tracking system	2–5 mm	D95; 15 Gy (n = 9); 20 Gy (n = 1); 25 Gy (n = 20); 30 Gy (n = 2)	Med f/u 18 mo; 25 Gy ≤; Grade 2, 4 pts; Grade 3. 1 pt; Grade 5, 3 pts (central type)	20 Gy ≤ <25 Gy/single fraction	≤20 Gy; T2: 4/7, met/rec: 1/3; 25 Gy; T1: 0/5, T2: 0/6; met/rec: 4/9; 30 Gy; T1: 0/1, T2: 1/1	1-year FFR; NSCLC: 67 %, met/rec: 25 %

Table 12.1 (continued)

Authors (year)	Target	Patients (Pts)	Staging	Equipment	PTV margin	Dose escalation	Outcomes			
							MTD	RD	LF	Failure Pattern
McGarry et al. (Indiana Univ. group) [1]	Stage IA & IB, Tumors ≤7 cm, any location, medically inoperable	47 pts, IA, 19; IIB, 28, med age 71 (IA), 74 (IIB)	CT & PET staging	Linac-based, body frame immobilization, abdominal compression for motion compensation	5 mm axial, 10 mm craniocaudal	D95: 3 × 8 Gy Cohorts of 3 patients received an additional 2.0 Gy /fr (total 6 Gy per increment at each dose escalation)	MTD 3 × 22 Gy (T2) Not achieved (T1)	3 × 20 Gy (T1) 3 × 22 Gy (T2)	LF 4/19(T1), 6/28 (T2) 9 LF at doses 16 Gy /fr, med time 3–31 mo (mean, 15.7 mo).	T1 1, regional alone 4, distant 3, both T2 2, regional alone 4, both

Abbreviation: *pt* patient, *med* median, *meta* metastatic, *rec* recurrent, *MTD* maximum tolerated dose, *RD* recommended dose, *LF* local failure, *mo* months, *FFR* freedom from relapse

Fig. 12.1 Dose-response
curve for local control after
stereotactic body radiation
therapy using three
fractions in a prospective
trial (Ref. [2])
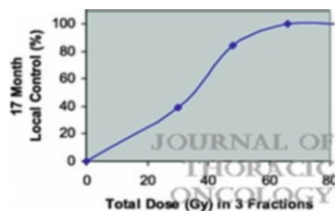
dose of SBRT prescribing 15 Gy to the margin of the tumor at two institutions. With
a mean follow-up of 7 months, toxicity was considered acceptable. Radiographic
response was scored as complete in 2 patients, partial in 15, stable in 4, and
progressive in 2.

In a Phase I dose-escalation study from Stanford University [4], 32 patients with
inoperable T1–2 N0 NSCLC (n = 21) or solitary metastatic tumors (n = 11)
received single fraction SBRT. Nine to 20 patients were treated per dose cohort
starting at 15 Gy/fraction followed by dose escalation of 5–10 Gy to a maximal dose
of 30 Gy/fraction. A minimal 3-month period was required between each dose level
to monitor toxicity. At a median follow-up of 18 months, RT-related complications
were noted for doses greater than 25 Gy and included four cases of grade 2–3
pneumonitis, one pleural effusion, and three possible treatment-related deaths.
Especially, central tumor location and tumor volume were associated with a greater
risk of severe to fatal toxicity.

Song et al. reported an experience in which they used a normal tissue compli-
cation probability (NTCP) formulation to guide dose escalation from 24 to 45 Gy in
three fractions [5]. SBRT prescribed within the confines of NTCP-restricted dosing
on this protocol resulted in no grade 3 or 4 radiation pneumonitis. However, late
toxicity developed in two patients who received treatment to peri-hilar tumors,
including one patient in whom bronchial stenosis developed with complete occlu-
sion and lobar atelectasis 6 months after treatment.

12.2.1.2   European and Other Countries' Experiences

European studies of SBRT [6–9] are shown in Table 12.2. In a retrospective study
from Technical University in Germany [7], 68 patients with Stage I NSCLC
received SBRT. Within the clinical protocol, SBRT was given starting at a total
dose of 24 Gy in 4 fractions. It was planned to escalate total dose to 30 Gy in
3 fractions. Thereafter, the fractionation schedule and the single doses depended on
lung function parameters, size and location of the target volume. For peripheral
tumors 30–37.5 Gy in 10–12.5 Gy fractions was applied, and for central tumors
35 Gy in 7 Gy fractions was the standard schedule. Dose was prescribed to the 60 %
isodose encompassing the PTV. Acute radiation pneumonitis occurred in 36 % of
patients, while only one patient developed late grade 3 radiation pneumonitis
(at 4 months) which progressed to fibrosis. One patient developed a grade 2 soft
tissue fibrosis. With a mean follow-up of 17 months, no other grade >2 toxicity was

Table 12.2 European studies of SBRT for early-stage NSCLC

Authors	Target	Patients (Pts)	Staging	Equipment	PTV margin	Dose	Toxicity		Outcomes	
							Acute	Late	LC, DFS	OS
Nyman et al., Sahlgrenka Univ Hosp (Sweden) 2006 [6]	Stage IA & IB, tumors < 5 cm, noncentral; 20 % without histology	45 pts (40 % IA), med age 74, med KPS 80 %	CT only	Linac-based, body frame, abdominal compression for motion compensation	5 mm axial, 10 mm craniocaudal	45 Gy in 3 Fx (BED 112.5), Dmax approx 140 %, 100 % PTV coverage	40 % Grade 1, 9 % Grade 2 (skin, cough, LRI)	11 % (rib fx, Atx/fibrosis)	Med F/U 43 mo, LC 80 %, FFDM 80 %	1/2/3/ 5 years = 80/71/55/30 %, Med OS 39 mo
Zimmermann et al., Technical Univ. (Munich) 2006 [7]	Stage IA & IB	68 pts,	CT & PET staging	Linac-based, vacuum couch, ExacTrak for motion compensation	ITV + safety margin	Starting (60 %-isodose): 24 Gy/4Fx–30 Gy/3Fx (BED 43.2–60), then	2.6 % Grade 3, 35.8 % Grade 2, 12.8 % Grade 1 RP	6.4 % Grade 3, 22.4 % Grade 2, 10.3 % Grade 1 (symptomatic /radiological RP)	Mean F/U 17 mo (3–50 mo),	OS 1/2/ 3 years = 83/71/51 %,
		Med age 76, sq (30), adeno (19), NSCLC (19)			Dose prescribed to 60 % isodose encompassing PTV	3 × 12.5 Gy (84.4) for peripheral tumors, or 5 × 7 Gy (59.5) for central tumors	15 % fatigue, 5.1 % shivering; 3.4 % nausea, 1.1 % dysphagia, 3.4 % dermatitis	5.1 % rib fx; 3.4 % subcutaneous fibrosis	LC 1/2/ 3 years = 96/88/88 %; DFS 1/2/3 years = 96/82/73 %	

Study	Patient characteristics	Staging	Technique	Margin	Dose	Toxicity		Outcomes	OS
Lagerwaard et al., VU Univ Med Ctr (Amsterdam) 2008 [8]	Stage IA & IB, tumors < 6 cm; 206 pts, 59 % IA, med age 73, 69 % without histology	PET staging	Linac-based, 4DCT for motion compensation	ITV + 3 mm	Risk-adapted: 3 × 20 Gy (BED 180), 5 × 12 Gy (132) or 8 × 7.5 Gy (105) based on potential for toxicity	49 %, most Grade 1 (fatigue, nausea, SOB, cough, CW pain)	7 % (symptomatic RP, rib fx, thoracic pain)	Med F/U 12 mo, LC 97 %, FFDM 85 % DFS 1/2 years = 83/68 % (signif correl with T stage)	OS 1/2 years = 81/64 %, Med OS 34 mo
Van Zyp et al., Erasmus Med Ctr (Rotterdam) 2009 [9]	Stage IA & IB, noncentral tumors, any PFTs; 70 pts, 56 % IA, med age 76, 49 % without histology	PET staging	CyberKnife (real-time tracking for motion comp.)	5 mm	Most 3 × 20 Gy (BED 180); Early pts 3 × 15 Gy (112.5)	46 % Grade 1–2 (fatigue, SOB, cough)	10 % Grade 3 (symptomatic RP, CW pain)	Med F/U 15 mo, crude FFDM 90 % 2 years LC 96 % (60 Gy) vs. 78 % (45 Gy)	OS 1/2 years = 83/62 %, DSS 94/86 %

Abbreviation: *med* median, *RP* radiation pneumonitis, *LC* local control, *DFS* disease-free survival, *FFDM* freedom from distant metastasis, *signif correl* significantly correlated, *mo* months, *OS* overall survival, *DSS* disease-specific survival, *CW* chest wall

observed. An actuarial local tumor control rate was 96 %, 88 % and 88 % after 1, 2 and 3 year follow-up, and an overall survival rate was 83 %, 71 %, and 51 % at 1, 2, and 3 years, respectively.

In a study from Hong Kong [10], 20 patients received SBRT with dose escalation of 45–54 Gy prescribed at 85 or 90 % isodose level in 3–4 fractions for peripheral Stage I NSCLC. No grade ≥ 2 acute or late toxicity was observed. Four patients received fractional doses >6 Gy to the esophagus. The maximum dose to the trachea and mainstem bronchus was 42.6 Gy in 14.2 Gy fractions (with ≤ 0.5 ml over 12 Gy) in one patient; 2 others received >10 Gy per fraction and 4 others received >8 Gy per fraction. The maximum dose to the aorta was 59.1 Gy in 19.7 Gy fractions (with ≤ 3.3 ml over 15 Gy) in one patient; 2 others received >10 Gy per fraction and 3 others received >8 Gy per fraction. The maximum dose to the heart was 40.4 Gy in 10 Gy fractions in one patient; other one received >10 Gy per fraction and 2 others received >8 Gy per fraction. The above range of the maximum point doses to the critical organs were considered to be safe because both acute and chronic toxicities were minimal.

12.2.2 Phase II Study

The phase II studies of SBRT for stage I NSCLC are shown in Table 12.3 [11–14]. The main results in these prospective studies demonstrated the high rate of primary tumor control (85–95 % at 3 years) and overall survival (40–60 % at 3 years).

12.2.2.1 The Indiana University Phase II Study

The Indiana group performed a phase II study enrolling 70 patients in the same population as a phase I [11]. The phase II study was aimed at validating toxicity in a larger patient population and determining efficacy (local control or survival) using a total dose of 60 Gy in three fractions for the small tumors and 66 Gy in three fractions for the large tumors (35 patients in each group). The tumor control rate for the statistical power calculation was 80 %, which is dramatically higher than those rates ranging from 30 to 45 % seen with conventionally fractionated radiotherapy. As such, it was required to have extensive processes in place for ensuring patient safety and monitoring the quality of data collected. An independent data safety–monitoring panel reviewed all high-grade adverse events (AEs) and was responsible for determining treatment-related toxicity and final scoring of efficacy such as determining local recurrence.

All 70 patients enrolled completed therapy as planned and median follow-up was 17.5 months. The 3-month major response rate was 60 %. The actuarial 2-year local control for this potent dose regimen is 95 %. Isolated hilar or mediastinal nodal relapse is extremely rare despite clinical staging. Altogether, 28 patients have died

Table 12.3 Phase II trials of SBRT for stage-I NSCLC

	No. of pts	Dose	3yLC	3yOS	Toxicity ≥ G3
Fakiris et al. [11] (Indiana, 2009)	T1: 34	T1: 60 Gy/3 fx	88 %	43 %	10 %
	T2 (≤7 cm): 36	T2: 66 Gy/3 fx (80 % isodose)			
Baumann et al. [12] (Sweden, 2009)	T1: 40	45 Gy/3 fx (67 % isodose)	92 %	60 %	28 %
	T2: 17				
Ricaridi et al. [13] (Italy, 2009)	T1: 43	45 Gy/3 fx (80 % isodose)	88 %	57 %	10 %
	T2: 19				
Timmerman et al. [14] (RTOG0236, 2010)	T1: 44	54 Gy/3 fx (D99)	98 %	56 %	16 ~ 27 %
	T2: 11	60 Gy/3fx (D95)			
Timmerman et al. [15] (RTOG0618, 2013)	T1: 23	54 Gy/3 fx (D99)	92 % (2y)	84 % (2y)	16 % G3 0 % G4–5
	T2a: 3 (operable)	60 Gy/3fx (D95)			

pts patients, *fx* fraction, *LC* local control, *OS* overall survival, *G* grade

as a result of cancer (n = 5), treatment (n = 6), or comorbid illnesses (n = 17). Median overall survival was 32.6 months and 2-year overall survival was 54.7 %. Grade 3–5 toxicity occurred in a total of 14 patients, confirming the phase I model. Among patients experiencing toxicity, the median time to observation was 10.5 months. Patients treated for tumors in the peripheral lung had 2-year freedom from severe toxicity of 83 % compared with only 54 % for patients with central tumors. In fact, the risk of severe toxicity is 11 times greater when treating central tumors compared with peripheral tumors.

The conclusions reached from this phase II trial is that local control is very high with the potent dose employed. However, this regimen should not be used for patients with tumors near the central airways due to excessive toxicity. Toxicity after SBRT occurs late, similar to local recurrence.

12.2.2.2   RTOG 0236 and 0618

Based on the Indiana University experience, the Radiation Therapy Oncology Group (RTOG) conducted a phase II trial (RTOG 0236) which was the first North American multicenter, cooperative group study to test SBRT in treating medically inoperable patients with early stage NSCLC [14]. A total of 59 patients accrued into this trial, of which 55 were evaluable (44 patients with T1 tumors and 11 patients with T2 tumors measuring <5 cm in diameter) with a median follow-up of 34.4 months (range, 4.8–49.9 months). The prescription dose was 18 Gy per fraction × 3 fractions (54 Gy total) with entire treatment lasting between $1\frac{1}{2}$ and 2 weeks. Only one patient had a primary tumor failure and the estimated 3-year primary tumor control rate was 97.6 %. Three patients had recurrence within the involved lobe and the 3-year primary tumor and involved lobe (local) control rate was 90.6 %. The local-regional control rate was 87.2 % which was more than

double those resulted from conventional radiotherapy in the previous reports. The rates for disease-free survival and overall survival at 3 years were 48.3 % and 55.8 % (median overall survival, 48.1 months), respectively which are more higher than the 2-year to 3-year overall survival rates ranging from 20 to 35 % in retrospective clinical studies concerning conventional radiotherapy for similar patient groups. Protocol-specified treatment-related grade 3 (AEs) were reported in 7 patients; grade 4 (AEs) were reported in 2 patients. No SBRT-related patient deaths were reported in RTOG 0236, perhaps because patients with centrally located tumors were not eligible for RTOG 0236.

The major problem in this trial was the distant-failure rates of 22.1 % at 3 years although all rates of the primary tumor, involved lobe, and regional failure were low. The distant metastases appearing fairly soon after SBRT suggested that many of these patients harbored undetectable occult tumors at initial staging diagnosis with CT and PET. These results would imply that effective adjuvant therapies after SBRT are necessary to improve the outcomes.

The RTOG protocol 0618 was a phase II trial utilizing SBRT to treat early stage (peripheral T1-T3 $\leq$ 5 cm, chest wall invasion only) NSCLC in operable patients [15]. All patients were deemed operable by a thoracic surgeon utilizing specific criteria. The prescription dose was 18 Gy $\times$ 3 fractions delivered in 1½–2 weeks. The primary endpoint was 2-year primary tumor control with overall and progression free survival, AEs, local, regional and distant failure as secondary endpoints. Early surgical salvage was directed as part of protocol design in the event of local failure after SBRT. A total of 33 patients were enrolled. Of 26 evaluable patients, 23 had T1, and 3 had T2 tumors. Median age was 72 years. Median FEV_1 and DLCO at enrollment were 72 % and 68 % predicted, respectively. Four patients (16 %) had SBRT-related grade 3 (AEs) while no patients had grade 4–5 AEs. Median follow-up was 25 months. An estimated 2-year primary tumor failure rate was 7.7 %, and 2-year rates of local failure (primary tumor plus involved lobe failure), regional node failure and distant failure were 19.2 %, 11.7 % and 15.4 %, respectively. The 2-year progression-free and overall survivals were 65.4 % and 84.4 %, respectively.

These results might support phase III trials comparing SBRT to surgery for operable early stage NSCLC.

12.2.2.3   RTOG 0915 and 0813

Currently, there are some questions on how best to administer SBRT. With respect to optimal dose-fractionation schedules, the RTOG 0915 trial comparing a single dose of 34–48 Gy in 4 fractions in medically inoperable patients with peripheral tumors was recently completed. In this trial two less toxic regimen will then be compared to the intensive 54 Gy in 3 fractions regimen standardized by RTOG 0236.

For centrally located tumors, the RTOG 0813 phase I trial was designed to determine the maximum tolerated dose in 5 fractions to refine the development of

risk-adapted dosing strategies. It will be some time before the data are mature enough to define the safety and efficacy of SBRT for tumors locating within the central zone of the lung. At the Mallinckrodt Institute of Radiology, either 9 Gy × 5 fractions or 10 Gy × 5 fractions was delivered to tumors that were central or near critical structures. The results had shown that treatment regimens of 10 Gy × 5 seemed to be efficacious almost as same as 18 Gy × 3 for peripheral lung cancer SBRT and provided superior local control and overall survival compared with 9 Gy × 5 [16].

12.2.3 Phase III Study: SBRT vs Surgery

Most studies for SBRT to date have focused on the medically inoperable population and the given outcomes were promising. But the patients analyzed in those series might include potentially operable patients, and SBRT for operable patients is obviously of interest.

Two phase III trials were conducted for comparing SBRT with surgery for patients with stage I NSCLC: the randomized clinical trial of either surgery or SBRT for stage IA NSCLC (ROSEL) trial in the Netherlands [17] and an international randomized trial of lobectomy vs. SBRT using the CyberKnife platform (the Lung Cancer STARS trial) [18]. However both trials were terminated due to poor enrollment of eligible patients. The ACOSOG Z4099-RTOG 1021 trial comparing SBRT to sublobar resection in surgery high-risk patients with operable stage I NSCLC are still ongoing. A propensity-matched comparison showed no difference between stereotactic body radiotherapy (RTOG0236) and surgery (ACOSOG Z4032) for 30-day grade 3+ AEs [19]. Furthermore the retrospective nonrandomized comparison of SBRT with wedge resection surgery for stage I NSCLC showed that the overall survival was higher in surgical patients. SBRT and surgery, however, had identical cause-specific survival [20].

References

1. McGarry RC, Papiez L, Williams M, Whitford T, Timmerman RD. Stereotactic body radiation therapy of early-stage non-small-cell lung carcinoma: phase I study. Int J Radiat Oncol Biol Phys. 2005;63:1010–5.
2. Timmerman RD, Park C, Kavanagh BD. The North American experience with stereotactic body radiation therapy in non-small cell lung cancer. J Thorac Oncol. 2007;2(7 Suppl 3): S101–12. doi:10.1097/JTO.0b013e318074e4fa.
3. Whyte RI, Crownover R, Murphy MJ, Martin DP, Rice TW, DeCamp Jr MM, et al. Stereotactic radiosurgery for lung tumors: preliminary report of a phase I trial. Ann Thorac Surg. 2003;75:1097–101.
4. Le QT, Loo BW, Ho A, Cotrutz C, Koong AC, Wakelee H, et al. Results of a phase I dose-escalation study using single-fraction stereotactic radiotherapy for lung tumors. J Thorac Oncol. 2006;1:802–9.

5. Song DY, Benedict SH, Cardinale RM, Chung TD, Chang MG, Schmidt-Ullrich RK. Stereotactic body radiation therapy of lung tumors: preliminary experience using normal tissue complication probability-based dose limits. Am J Clin Oncol. 2005;28:591–6.

6. Nyman J, Johansson KA, Hultén U. Stereotactic hypofractionated radiotherapy for stage I non-small cell lung cancer–mature results for medically inoperable patients. Lung Cancer. 2006;51:97–103.

7. Zimmermann FB, Geinitz H, Schill S, Thamm R, Nieder C, Schratzenstaller U, et al. Stereotactic hypofractionated radiotherapy in stage I (T1-2 N0 M0) non-small-cell lung cancer (NSCLC). Acta Oncol. 2006;45:796–801.

8. Lagerwaard FJ, Verstegen NE, Haasbeek CJ, Slotman BJ, Paul MA, Smit EF, et al. Outcomes of stereotactic ablative radiotherapy in patients with potentially operable stage I non-small cell lung cancer. Int J Radiat Oncol Biol Phys. 2012;83:348–53. doi:10.1016/j.ijrobp.2011.06.2003.

9. van der Voort van Zyp NC, Prévost JB, Hoogeman MS, Praag J, van der Holt B, Levendag PC, et al. Stereotactic radiotherapy with real-time tumor tracking for non-small cell lung cancer: clinical outcome. Radiother Oncol. 2009;91:296–300. doi:10.1016/j.radonc.2009.02.011.

10. Ng AWY, Tung SY, Wong VY. Hypofractionated stereotactic radiotherapy for medically inoperable stage I non-small cell lung cancer – report on clinical outcome and dose to critical organs. Radiother Oncol. 2008;87:24–8. doi:10.1016/j.radonc.2008.02.015.

11. Fakiris AJ, McGarry RC, Yiannoutsos CT, Papiez L, Williams M, Henderson MA, et al. Stereotactic body radiation therapy for early-stage non-small-cell lung carcinoma: four-year results of a prospective phase II study. Int J Radiat Oncol Biol Phys. 2009;75:677–82. doi:10.1016/j.ijrobp.2008.11.042.

12. Baumann P, Nyman J, Hoyer M, Wennberg B, Gagliardi G, Lax I, et al. Outcome in a prospective phase II trial of medically inoperable stage I non-small-cell lung cancer patients treated with stereotactic body radiotherapy. J Clin Oncol. 2009;27:3290–6. doi:10.1200/JCO.2008.21.5681.

13. Ricardi U1, Filippi AR, Guarneri A, Giglioli FR, Ciammella P, Franco P, et al. Stereotactic body radiation therapy for early stage non-small cell lung cancer: results of a prospective trial. Lung Cancer. 2010;68:72–7. doi:10.1016/j.lungcan.2009.05.007.

14. Timmerman R, Paulus R, Galvin J, Michalski J, Straube W, Bradley J, et al. Stereotactic body radiation therapy for inoperable early stage lung cancer. JAMA. 2010;303:1070–6. doi:10.1001/jama.2010.261.

15. Timmerman RD, Paulus R, Pass HI, Gore E, Edelman MJ, Galvin JM, et al. RTOG 0618: stereotactic body radiation therapy (SBRT) to treat operable earlystage lung cancer patients. J Clin Oncol. 2013;31(15 suppl):Abst. 7523.

16. Olsen JR, Robinson CG, El Naqa I, Creach KM, Drzymala RE, Bloch C, et al. Dose-response for stereotactic body radiotherapy in early-stage non-small-cell lung cancer. Int J Radiat Oncol Biol Phys. 2011;81:e299–303. doi:10.1016/j.ijrobp.2011.01.038.

17. Hurkmans CW, Cuijpers JP, Lagerwaard FJ, Widder J, van der Heide UA, Schuring D, et al. Recommendations for implementing stereotactic radiotherapy in peripheral stage IA non-small cell lung cancer: report from the Quality Assurance Working Party of the randomised phase III ROSEL study. Radiat Oncol. 2009;4:1. doi:10.1186/1748-717X-4-1.

18. International randomized study to compare CyberKnife stereotactic radiotherapy with surgical resection in stage I non-small cell lung cancer (STARS). http://www.clinicaltrials.gov/ct2/show/NCT00840749. Accessed 30 May 2011.

19. Crabtree T, Puri V, Timmerman R, Fernando H, Bradley J, Decker PA, et al. Treatment of stage I lung cancer in high-risk and inoperable patients: comparison of prospective clinical trials using stereotactic body radiotherapy (RTOG 0236), sublobar resection (ACOSOG Z4032), and radiofrequency ablation (ACOSOG Z4033). J Thorac Cardiovasc Surg. 2013;145:692–9. doi:10.1016/j.jtcvs.2012.10.038.

20. Grills IS, Mangona VS, Welsh R, Chmielewski G, McInerney E, Martin S, et al. Outcomes after stereotactic lung radiotherapy or wedge resection for stage I non-small-cell lung cancer. J Clin Oncol. 2010;28:928–35. doi:10.1200/JCO.2009.25.0928.

Chapter 13
Toxicity and Treatment Evaluation

Yoshiyuki Shioyama, Katsumasa Nakamura, and Hiroshi Honda

13.1 Toxicity

Acute toxicity after SBRT includes radiation pneumonitis and mild dermatitis. Most of radiation pneumonitis is asymptomatic. Systemic symptoms such as malaise and fatigue occur rarely, but if occur, it is generally mild. Late toxicity after SBRT is also generally well tolerable. However, various toxicities including pneumonitis, chronic cough, pulmonary bleeding, pulmonary function decline, hypoxia, pleural effusion, bronchial stricture and obstruction, bronchial fistula, tracheal necrosis, chest wall pain, rib fracture, brachial plexopathy, and esophageal ulceration have been reported so far [1]. The total dose, fractional doses, dose-volume metrics of normal tissue, and location of the tumor are critical variables in predicting late toxicity. However, the normal tissue dose constraints have not yet fully understood in SBRT because of limited clinical data based on long-term follow-up. Preferable approach is to refer to dose constraints adopted in well-conducted prospective clinical trials. Table 13.1 shows the dose constraints used in several clinical trials.

13.1.1 Radiation Pneumonitis

Radiation pneumonitis (acute and late) is most common toxicity after SBRT in the treatment for lung cancers. Most of radiation pneumonitis observed after SBRT is

Y. Shioyama (✉)
Department of Heavy Particle Therapy and Radiation Oncology, Graduate School of Medical Sciences, Kyushu University, 3-1-1 Maidashi, Higashi-ku, 812-8582 Fukuoka, Japan
e-mail: shioyama@radiol.med.kyushu-u.ac.jp

K. Nakamura • H. Honda
Department of Clinical Radiology, Graduate School of Medical Sciences, Kyushu University, Fukuoka, Japan

Table 13.1 Dose constraints used selected clinical trials

Organ at risk	JCOG 0403 (4 fractions)	RTOG 0618 (3 fractions)	JROSG10-1 (8 fractions)	RTOG 0813 (5 fractions)
Spinal cord	≤25 Gy	≤18 Gy	≤35.5 Gy	≤30 Gy
				(22.5 Gy < 0.25 cc)
				(13.5 Gy < 0.5 cc)
Esophagus	40 Gy ≤ 1 cc	≤27 Gy	40 Gy < 5 cc	≤105 % of PTV prescription
	35 Gy ≤ 10 cc			(27.5 Gy < 5 cc)
Pulmonary artery	40 Gy ≤ 1 cc	–	54.5 Gy < 1 cc	<105 % of PTV prescription
	35 Gy ≤ 10 cc		47.5 Gy < 10 cc	(47 Gy < 10 cc)
Aorta	–	–	58 Gy < 10 cc	<105 % of PTV prescription
				(47 Gy < 10 cc)
SVC/Pulmonary vein	–	–	48 Gy < 1 cc	<105 % of PTV prescription
				(47 Gy < 10 cc)
Heart/Pericardium	–	≤30 Gy	40 Gy < 15 cc	<105 % of PTV prescription
				(32 Gy < 15 cc)
Trachea/Bronchus	40 Gy ≤ 10 cc	≤30 Gy	54.5 Gy < 10 cc	<105 % of PTV prescription
				(18 Gy < 4 cc)
Brachial plexus	–	≤24 Gy	≤40 Gy	≤32 Gy
				(30 Gy < 3 cc)
Skin	–	≤24 Gy	≤40 Gy	≤32 Gy
				(30 Gy < 10 cc)
Stomach/Intestine	36 Gy < 10 cc	–	–	–
	30 Gy < 100 cc			
Lung (right & left)	40 Gy < 100 cc	V20 ≤ 10 %	V20 < 20 %	V20 < 10 %
	V20 ≤ 20 %			(12.5 Gy < 1,500 cc)
	V15 ≤ 25 %			(13.5 Gy < 1,000 cc)
	MLD ≤ 18 Gy			
Other organs	48 Gy ≤ 1 cc	–	65.5 Gy < 1 cc	–
	40 Gy ≤ 10 cc		54.5 Gy < 10 cc	

Abbreviation: *MLD* mean lung dose, Other organs do not include skin, chest wall and liver in JCOG 0403, and chest wall, rib liver and spleen in JROSG10-1

grade 1–2, and grade 3 or greater radiation pneumonitis is reported less than 10 % [2, 3]. Grade 5 pulmonary complications including radiation pneumonitis has been reported 0.6 % in multi-institutional survey in Japan [4]. Most cases of Grade 5 pneumonitis is reported to be accompanied with interstitial lung disease [5–7].
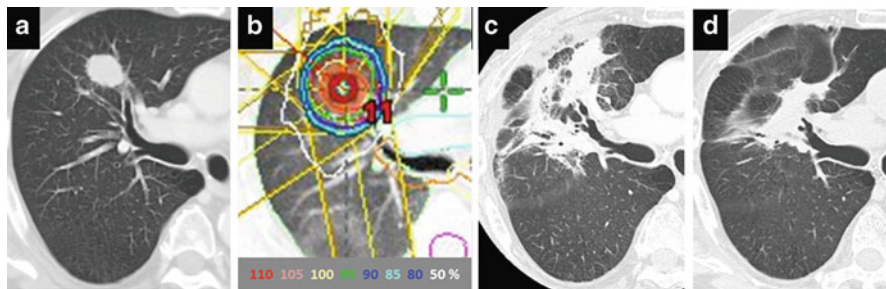
Fig. 13.1 Post-SBRT radiation fibrosis considered modified conventional pattern. (**a**) CT image before SBRT, (**b**) Isodose distribution prescribed with 48 Gy in 4 fractions at isocenter, (**c**) CT image at 5 months after SBRT, (**d**) CT image at 24 months after SBRT

Generally, radiation pneumonitis develops from 2 to 6 months after SBRT [8]. Symptomatic pneumonitis tends to appear earlier than asymptomatic pneumonitis [9]. Acute radiological changes are typically categorized to five patterns as follows; (1) diffuse consolidation, (2) patchy consolidation, (3) diffuse ground glass opacities, (4) patchy ground glass opacities, and (5) no evidence of increasing density [10.11]. Among them, diffuse consolidation is most common and the frequency is approximately 20–30 % [12]. These acute radiological changes typically correspond to the lung volume exposed to 20 Gy or over doses of radiation (V20). Radiation pneumonitis gradually proceeds to the process of fibrosis as late radiological changes. Radiation fibrosis is categorized into modified conventional pattern, mass-like pattern, and scar-like pattern, and no evidence of increasing density [10–12]. The most predominant pattern is modified conventional pattern [10–12]. Figures 13.1 and 13.2 show the cases the radiation fibrosis of modified conventional pattern and scar-like pattern, respectively. Among them, radiation fibrosis showing mass-like pattern, also called mass-like consolidation (fibrosis), sometimes is difficult to be distinguished from local recurrence. These radiological changes are usually fixed within 24 months after SBRT [10, 13], and tend to be mild in the patients with pulmonary emphysema [14].

Dosimetric factors including V5, V20, and MLD have been well documented in conventional radiotherapy [15, 16]. Also in SBRT, dose-volume metrics such as V20, V25 and MLD are considered to be correlates with symptomatic radiation pneumonitis after SBRT [17–20]. Barriger et al. documents that V20 and MLD are significant factors correlated with grade 2 or greater radiation pneumonitis after SBRT with 60 Gy in 3 fractions. In their results, grade 2–4 pneumonitis developed in 16.4 % and 17.6 % of patients with V20 > 4 % and those with MLD > 4 Gy, respectively. In contrast, the incidence of grade 2 or greater pneumonitis was reported 4 % in the patients with V20 < 4 % and MLD < 4 Gy [18]. Matsuo et al. report that PTV and V25 is significant dose-volume metric associated with grade 2 or greater pneumonitis in their series of SBRT with 48 Gy in 4 fractions [19]. Takeda et al. report that grade 2 pneumonitis is well correlated with dose-volume metrics including V5-V30 and MLD, but grade 3 or higher pneumonitis
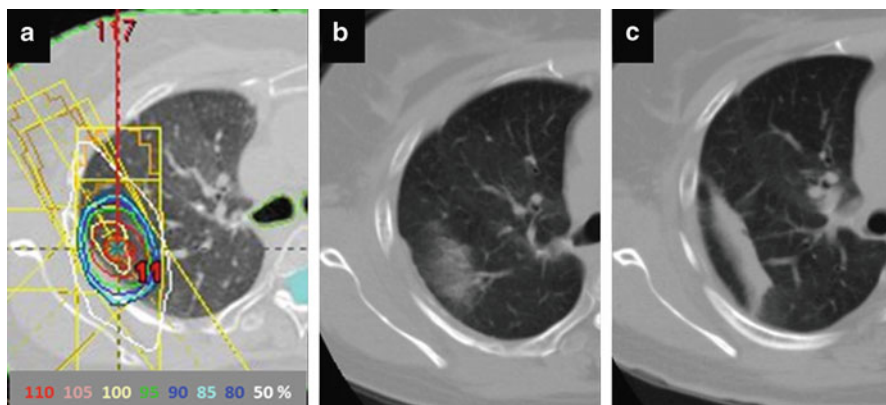
Fig. 13.2 Post-SBRT radiation fibrosis considered scar-like pattern. (**a**) Isodose distribution prescribed with 48 Gy in 4 fractions at isocenter, (**b**) CT image at 3 months after SBRT, (**c**) CT image at 24 months after SBRT

tend to be associated with variables of the host rather than those of dose-volume metrics [20]. In addition to these dose-volume metrics, patient factors including gender, age, pulmonary function (FEV1.0) and smoking history are suggested to be associated with the risk of radiation pneumonitis.

Bronchiolitis obliterans organizing pneumonia (BOOP) is well known as a particular from of pneumonitis developing beyond the radiation field, which is observed in 2–3 % of the breast cancer patients who received postoperative irradiation. Radiation pneumonitis similar to BOOP is reported to be found in 4.8 % of patients with stage I NSCLC and metastatic lung tumor [21]. Also, radiation recall pneumonitis induced by chemotherapy is reported [22]. The risk of recall pneumonitis may be considered in the setting of adjuvant chemotherapy after SBRT.

13.1.2 Pulmonary Function

In the treatment for small lung tumors, typically in stage I NSCLC, SBRT does not significantly affect pulmonary function. Although the clinical evidence regarding pulmonary function changes is still limited, most of previous retrospective studies have shown that impairment of pulmonary function is generally little and transient. Ohashi et al. report that there is no significant change in total lung capacity (TLC), vital capacity (VC) and forced expiratory volume in 1 s (FEV1.0) 1 year after SBRT. Conversely, diffusing capacity of lung for carbon monoxide (DLCO) is found to be improved in patients who had been heavy smokers before SBRT [23]. Stephans et al. also report that pulmonary function is not substantially altered by SBRT, although individual patients may exhibit increased or decreased FEV1.0 and DLCO values after treatment [24]. In contrast, there are several studies showing

significant decrease of FEV1.0 or DLCO. Henderson et al. show that DLCO decrease by 1.11 ml/min/mmHg while FEV1.0 does not change over time [25]. Mclnerney et al. show that FEV1.0 and DLCO were reduced 6–7 % and 16–17 %, respectively, and that DLCO decrease correlated with MLD and V10–20 [26]. However, it is generally difficult to show the correlation of dose-volume parameters and impairment of pulmonary function because many of patients treated with SBRT have pre-existing chronic obstructive disease which affects worsening of pulmonary function rather than radiation toxicity.

13.1.3 Skin and Chest Wall Toxicity

Toxicities of the skin and chest wall are common in the treatment for periphery located lung tumors. The risk factors predicting grade 2 or greater skin toxicity are shown a limited number of beams, distance from the tumor to the chest wall, and a maximum skin dose of exceed 50 % of the prescribed dose [27]. In Radiation Therapy Oncology Group (RTOG) 0618 trial using 3 fractions for stage I NSCLC, dose constraint ($\leq$24 Gy) is determined for the skin as one of the organ-at-risk. On the other hand, in the Japan Clinical Oncology Group (JCOG) 0403 trial using 4 fractions, the skin is not included as an organ-at-risk because the risk of severe skin toxicity is very low in total dose of 48 Gy.

Toxicities of the chest wall include chest wall pain, fibrosis of soft tissue, and rib fracture [28]. Rib fracture can be asymptomatic and is found incidentally on follow-up CT examination. Approximately 50 % of patients with rib fracture are reported asymptomatic [29]. Therefore, the incidence of rib fracture might be underestimated in early retrospective series. Including asymptomatic rib fracture, the incidence is reported 30–50 % in the patients after SBRT in recent literatures [29, 30]. Figure 13.3 shows a case with asymptomatic rib fracture after SBRT. The chest wall toxicity is more likely to be observed in patients with periphery located lung tumors close to the chest wall ($\leq$1.8 or 2.0 cm) [29, 31]. Dunlap et al. report that the chest wall volume receiving more than 30 Gy predicts risk of severe pain and/or rib fracture [30]. In studies focusing on the rib dose, high dose volume including maximum dose and D2cc is well correlated with the risk of rib fracture [29, 32].

Regarding chest wall pain, Welsh et al. report that 25 % of patients treated with SBRT experienced chest wall pain, and many of them had no rib fractures. They also found that body mass index (BMI) and diabetes were strong predictors for the development of chest pain [33]. By contrast, the incidence of grade 2 or higher chest wall pain is reported very low in Japanese SBRT series [29, 34]. Difference in BMI or diabetes rate between nationalities might be a cause of the difference of symptomatic presentation.
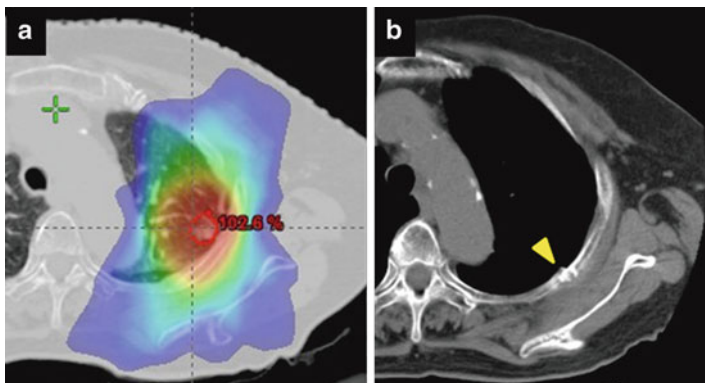
Fig. 13.3 Asymptomatic rib fracture developed at 24 months after SBRT. (**a**) Isodose distribution prescribed with 48 Gy in 4 fractions at isocenter, (**b**) CT image 18 months after SBRT. A *yellow arrow* shows the SBRT-induced rib fracture with a linear sclerotic change and discontinuity of the cortex

13.1.4   Brachial Plexus Toxicity

Brachial plexus is an organ-at –risk in patients with lung tumors at apical locations. Tolerance dose of the brachial plexus in SBRT using high fractional doses is not well known. Recent investigation from Indiana University reported that 7 of 36 patients (19 %) with apical lung tumors who were treated with SBRT using median dose of 57 Gy in 3–4 fractions experienced Grade 2–4 brachial plexopathy after the treatment (range 6–23 months). The 2-year rate of brachial plexopathy is documented 46 % for maximum dose > 26 Gy versus 8 % for ≤ 26 Gy [35]. In the RTOG trial (0618), dose constraint for brachial plexus is defined ≤ 24 Gy (8 Gy/fraction).

13.1.5   Esophagus/Bronchus/Pulmonary Artery/Heart

In the treatment with hypofractionated SBRT for centrally located lung cancers, special attention should be paid to the risk for severe toxicities of mediastinal organs such as esophagus, central bronchus, pulmonary artery or heart in addition to pulmonary toxicity. In the previous and pioneering studies of SBRT, various severe toxicities including fatal pulmonary bleeding, esophageal ulceration, bronchial fistula, bronchial stricture/obstruction, tracheal necrosis are documented [1, 36]. In SBRT with 60–66 Gy in 3 fractions, 2-year incidence of grade 3 or higher toxicity is recorded 46 % for the patients with centrally located tumors, and 6 patients suffered from grade 5 toxicities [36]. However, Senthi et al. suggest in their systematic review, that SBRT achieves favorable local control with limited toxicity for centrally located tumors when appropriate fractionation schedules

(e.g. 60 Gy in 8 fractions, 50 Gy in 5 fractions) are used [37]. For centrally located stage I NSCLC, two dose escalation studies (JROSG10-1 in Japan starting from 7.5 Gy administered 8 times and RTOG 0813 in USA starting from 10 Gy administered 5 times) are on-going.

13.1.6   *Pleural Effusion/Pneumothorax*

Pleural effusion is a relatively common toxicity after SBRT for periphery located lung tumors. However, in most of cases, the amount of effusion is minimal and transient. Symptomatic effusion is generally rare. In a prospective phase II study of medically inoperable patients with stage I NSCLC, the pleural effusion was observed in 13 of 54 patients (23 %) within 18 months after SBRT. They also reported that only two patients (<4 %) experienced grade 3 pleural effusion [38]. Pneumothorax is one of the rare late toxicities after SBRT. In the review of over 500 patients treated with SBRT for lung tumors, pneumothorax is found in 1.5 %, and most of which is grade 1–2 and self-limiting. Emphysema and overlapping of PTV and pleura could be the risk factor of pneumothorax after SBRT [39].

13.2   Treatment Evaluation

Response Evaluation Criteria in Solid Tumors (RECIST) measurements is the standard method used for response assessment in clinical studies of oncology. Also in SBRT for lung cancers, treatment response is evaluated using RECIST. CT scanning is the standard measure of imaging in the response evaluation and follow-up for SBRT patients. However, accurate measurement of the tumor size is sometimes difficult on CT images after radiotherapy for lung cancers due to radiation-induced injury (radiation pneumonitis and fibrosis). In SBRT, early changes (radiation pneumonitis) and late changes (radiation fibrosis) have been reported to be found in 54–79 % and 80–100 % of patients, respectively [12].

Major issue is how diagnose tumor progression early as possible. It is important clinically in terms of early identification of patients who are candidates for salvage treatment. Unfortunately however, radiographic findings of post-SBRT lung injury dynamically change from acute phase to late phase at least from up to 12 months after the treatment. Therefore, it is not easy to determine just on CT images whether the tumors are controlled or not in this periods. In particular, mass-like radiation fibrosis after SBRT can mimic to tumor recurrence, so that it is difficult to distinguish mass-like radiation fibrosis from tumor progression only on CT findings at single point. Matsuo et al. document that the size of mass-like radiation fibrosis did not increase after 12 months or later after SBRT, but the opacity including tumor recurrence can increase thereafter [40]. High-risk features of tumor

progression on CT images are reported as follows: (1) sequential enlargement on repeat CT, opacity enlargement after 12 months, bulging margin, disappearance of air bronchograms, linear margin disappearance, ipsilateral pleural effusion, or lymph node enlargement [41]. However, it is difficult in practice to diagnose tumor progression only with CT findings.

The role of FDG-PET is well understood in staging and also response evaluation of the tumor after radiotherapy and/or chemotherapy. Recently, several investigators report the usefulness of FDG-PET in response evaluation and in detection of tumor recurrence after SBRT [42–45]. In the tumor with low pre-SBRT SUV, FDG uptake can be transiently increased and the avidity can also be observed relatively long time after SBRT because of normal radiation reaction of lung tumor and parenchyma. However, a SUVmax is rarely elevated over 5.0 in the acute radiation reaction of the tumor and normal tissue. Huang et al. conclude, in their systematic review, that tumor recurrence should be suspected if high-risk features on CT images and SUV elevation over than five or pretreatment level on FDG-PET are seen after SBRT [12].

13.3   Conclusion

Recent clinical data has demonstrated the efficacy and safety of SBRT in the treatment for early stage lung cancer. However, normal tissue dose-volume constraints have not been fully understood. Moreover, the optimal method of post-SBRT evaluation including early detection of tumor recurrence is still under investigation. Further clinical evidences based on longer follow-up should be accumulated both in the toxicities and response evaluation after SBRT.

References

1. Milano MT, Constine LS, Okunieff P. Normal tissue toxicity after small field hypofractionated stereotactic body radiation. Radiat Oncol. 2008;3:36.
2. Nagata Y, Wulf J, Lax I, Timmerman R, Zimmermann F, Stojkovski I, et al. Stereotactic radiotherapy of primary lung cancer and other targets: results of consultant meeting of the international atomic energy agency. Int J Radiat Oncol Biol Phys. 2011;79:660–9.
3. Onishi H, Araki T. Stereotactic body radiation therapy for stage I non-small-cell lung cancer: a historical overview of clinical studies. Jpn J Clin Oncol. 2013;43:345–50.
4. Nagata Y, Hiraoka M, Mizowaki T, Narita Y, Matsuo Y, Norihisa Y, et al. Survey of stereotactic body radiation therapy in Japan by the Japan 3-D conformal external radiotherapy group. Int J Radiat Oncol Biol Phys. 2009;75:343–7.
5. Yamashita H, Kobayashi-Shibata S, Terahara A, Okuma K, Haga A, Wakui R, et al. Prescreening based on the presence of CT-scan abnormalities and biomarkers (KL-6 and SP-D) may reduce severe radiation pneumonitis after stereotactic radiotherapy. Radiat Oncol. 2010;5:32.

6. Yamaguchi S, Ohguri T, Ide S, Aoki T, Imada H, Yahara K, et al. Stereotactic body radiotherapy for lung tumors in patients with subclinical interstitial lung disease: the potential risk of extensive radiation pneumonitis. Lung Cancer. 2013;82:260–5.
7. Aibe N, Yamazaki H, Nakamura S, Tsubokura T, Kobayashi K, Kodani N, et al. Outcome and toxicity of stereotactic body radiotherapy with helical tomotherapy for inoperable lung tumor: analysis of Grade 5 radiation pneumonitis. J Radiat Res. 2014;55:575–82.
8. Aoki T, Nagata Y, Negoro Y, Takayama K, Mizowaki T, Kokubo M, et al. Evaluation of lung injury after three-dimensional conformal stereotactic radiation therapy for solitary lung tumors: CT appearance. Radiology. 2004;230:101–8.
9. Takeda A, Ohashi T, Kunieda E, Enomoto T, Sanuki N, Takeda T, et al. Early graphical appearance of radiation pneumonitis correlates with the severity of radiation pneumonitis after stereotactic body radiotherapy (SBRT) in patients with lung tumors. Int J Radiat Oncol Biol Phys. 2010;77:685–90.
10. Linda A, Trovo M, Bradley JD. Radiation injury of the lung after stereotactic body radiation therapy (SBRT) for lung cancer: a timeline and pattern of CT changes. Eur J Radiol. 2011;79:137–54.
11. Trovo M, Linda A, El Naqa I, Javidan-Nejad C, Bradley J. Early and late lung radiographic injury following stereotactic body radiation therapy (SBRT). Lung Cancer. 2010;69:77–85.
12. Huang K, Dahele M, Senan S, Guckenberger M, Rodrigues GB, Ward A, et al. Radiographic changes after lung stereotactic ablative radiotherapy (SABR) – can we distinguish recurrence from fibrosis? A systematic review of the literature. Radiother Oncol. 2012;102:335–42.
13. Takeda T, Takeda A, Kunieda E, Ishizaka A, Takemasa K, Shimada K, et al. Radiation injury after hypofractionated stereotactic radiotherapy for peripheral small lung tumors: serial changes on CT. Am J Roentgenol. 2004;182:1123–8.
14. Kimura T, Matsuura K, Murakami Y, Hashimoto Y, Kenjo M, Kaneyasu Y, et al. CT appearance of radiation injury of the lung and clinical symptoms after stereotactic body radiation therapy (SBRT) for lung cancers: are patients with pulmonary emphysema also candidates for SBRT for lung cancers? Int J Radiat Oncol Biol Phys. 2006;66:483–91.
15. Marks LB, Bentzen SM, Deasy JO, Kong FM, Bradley JD, Vogelius IS, et al. Radiation dose-volume effects in the lung. Int J Radiat Oncol Biol Phys. 2010;76:S70–6.
16. Wang S, Liao Z, Wei X, Liu HH, Tucker SL, Hu CS, et al. Analysis of clinical and dosimetric factors associated with treatment-related pneumonitis (TRP) in patients with non- small-cell lung cancer (NSCLC) treated with concurrent chemotherapy and three-dimensional conformal radio- therapy (3D-CRT). Int J Radiat Oncol Biol Phys. 2006;66:1399–407.
17. Ricardi U, Filippi AR, Guarneri A, Giglioli FR, Mantovani C, Fiandra C, et al. Dosimetric predictors of radiation- induced lung injury in stereotactic body radiation therapy. Acta Oncol. 2009;48:571–7.
18. Barriger RB, Forquer JA, Brabham JG, Andolino DL, Shapiro RH, Henderson MA, et al. A dose-volume analysis of radiation pneumonitis in non-small cell lung cancer patients treated with stereotactic body radiation therapy. Int J Radiat Oncol Biol Phys. 2012;82:457–62.
19. Matsuo Y, Shibuya K, Nakamura M, Narabayashi M, Sakanaka K, Ueki N, et al. Dose–volume metrics associated with radiation pneumonitis after stereotactic body radiation therapy for lung cancer. Int J Radiat Oncol Biol Phys. 2012;83:e545–9.
20. Takeda A, Ohashi T, Kunieda E, Sanuki N, Enomoto T, Takeda T, et al. Comparison of clinical, tumour-related and dosimetric factors in grade 0–1, grade 2 and grade 3 radiation pneumonitis after stereotactic body radiotherapy for lung tumours. Br J Radiol. 2012;85:636–42.
21. Murai T, Shibamoto Y, Nishiyama T, Baba F, Miyakawa A, Ayakawa S, et al. Organizing pneumonia after stereotactic ablative radiotherapy of the lung. Radiat Oncol. 2012;7:123.
22. Ding X, Ji W, Li J, Zhang X, Wang L. Radiation recall pneumonitis induced by chemotherapy after thoracic radiotherapy for lung cancer. Radiat Oncol. 2011;6:24.

23. Ohashi T, Takeda A, Shigematsu N, Kunieda E, Ishizaka A, Fukada J, et al. Differences in pulmonary function before vs. 1 year after hypofractionated stereotactic radiotherapy for small peripheral lung tumors. Int J Radiat Oncol Biol Phys. 2005;62:1003–8.
24. Stephans KL, Djemil T, Reddy CA, Gajdos SM, Kolar M, Machuzak M, et al. Comprehensive analysis of pulmonary function test (PFT) changes after stereotactic body radiotherapy (SBRT) for stage I lung cancer in medically inoperable patients. J Thorac Oncol. 2009;4:838–44.
25. Henderson M, McGarry R, Yiannoutsos C, Fakiris A, Hoopes D, Williams M, et al. Baseline pulmonary function as a predictor for survival and decline in pulmonary function over time in patients undergoing stereotactic body radiotherapy for the treatment of stage I non-small-cell lung cancer. Int J Radiat Oncol Biol Phys. 2008;72:404–9.
26. McInerney E, Grills I, Galerani A, Martinez A, Wallace M, Robertson B, et al. Changes in pulmonary function and toxicity after image guided lung stereotactic body radiotherapy (SBRT). Int J Radiat Oncol Biol Phys. 2008;72:S445.
27. Hoppe BS, Laser B, Kowalski AV, Fontenla SC, Pena-Greenberg E, Yorke ED, et al. Acute skin toxicity following stereotactic body radiation therapy for stage I non-small-cell lung cancer: who's at risk? Int J Radiat Oncol Biol Phys. 2008;72:1283–6.
28. Zimmermann F, Geinitz H, Schill S, Thamm R, Nieder C, Schratzenstaller U, et al. Stereotactic hypofractionated radiotherapy in stage I (T1-2N0M0) non-small cell lung cancer (NSCLC). Acta Oncol. 2006;45:796–801.
29. Asai K, Shioyama Y, Nakamura K, Sasaki T, Ohga S, Nonoshita T, et al. Radiation-induced rib fractures after hypofractionated stereotactic body radiation therapy: risk factors and dose-volume relationship. Int J Radiat Oncol Biol Phys. 2012;84:768–73.
30. Dunlap NE, Cai J, Bidermann GB, Yang W, Benedict SH, Sheng K, et al. Chest wall volume receiving >30 Gy predicts risk of severe pain and/or rib fracture after lung stereotactic body radiotherapy. Int J Radiat Oncol Biol Phys. 2010;76:796–801.
31. Voroney JP, Hope A, Dahele MR, Purdie TG, Franks KN, Pearson S, et al. Chest wall pain and rib fracture after stereotactic radiotherapy for peripheral non small cell lung cancer. J Thorac Oncol. 2009;4:1035–7.
32. Pettersson N, Nyman J, Johansson KA. Radiation-induced rib fracture after hypofractionated stereotactic body radiation therapy of non-small cell lung cancer: a dose- and volume-response analysis. Radiother Oncol. 2009;91:360–8.
33. Welsh J, Thomas J, Shah D, Allen PK, Wei X, Mitchell K, et al. Obesity increases the risk of chest wall pain from thoracic stereotactic body radiation therapy. Int J Radiat Oncol Biol Phys. 2011;81:91–6.
34. Onimaru R, Shirato H, Shimizu S, Kitamura K, Xu B, Fukumoto S, et al. Tolerance of organs at risk in small-volume, hypofractionated, image-guided radiotherapy for primary and meta-static lung cancers. Int J Radiat Oncol Biol Phys. 2003;56:126–35.
35. Forquer JA, Fakiris AJ, Timmerman RD, Lo SS, Perkins SM, McGarry RC, et al. Brachial plexopathy from stereotactic body radiotherapy in early-stage NSCLC: dose-limiting toxicity in apical tumor sites. Radiother Oncol. 2009;93:408–13.
36. Timmerman R, McGarry R, Yiannoutsos C, Papiez L, Tudor K, DeLuca J, et al. Excessive toxicity when treating central tumors in a phase II study of stereotactic body radiation therapy for medically inoperable early-stage lung cancer. J Clin Oncol. 2006;24:4833–9.
37. Senthi S, Haasbeek CJA, Slotman BJ, Senan S. Outcomes of stereotactic ablative radiotherapy for central lung tumours: a systematic review. Radiother Oncol. 2013;106:276–82.
38. Baumann P, Nyman J, Hoyer M, Wennberg B, Gagliardi G, Lax I, et al. Outcome in a prospective phase II trial of medically inoperable stage I non-small-cell lung cancer patients treated with stereotactic body radiotherapy. J Clin Oncol. 2009;27:3290–6.
39. Asai K, Shioyama Y, Nakamura K, Sasaki T, Ohga S, Yoshitake T, et al. Spontaneous pneumothorax after stereotactic body radiation therapy for lung tumor. Int J Radiat Oncol Biol Phys. 2013;87:S505.

40. Matsuo Y, Nagata Y, Mizowaki T, Takayama K, Sakamoto T, Sakamoto M, et al. Evaluation of mass-like consolidation after stereotactic body radiation therapy for lung tumors. Int J Clin Oncol. 2007;12:356–62.
41. Kato S, Nambu A, Onishi H, Saito A, Kuriyama K, Komiyama T, et al. Computed tomography appearances of local recurrence after stereotactic body radiation therapy for stage I non-small-cell lung carcinoma. Jpn J Radiol. 2010;28:259–65.
42. Hoopes DJ, Tann M, Fletcher JW, Forquer JA, Lin PF, Lo SS, et al. FDG-PET and stereotactic body radiotherapy (SBRT) for stage I non-small-cell lung cancer. Lung Cancer. 2007;56:229–34.
43. Henderson MA, Hoopes DJ, Fletcher JW, Lin PF, Tann M, Yiannoutsos CT, et al. A pilot trial of serial 18 F- fluorodeoxyglucose positron emission tomography in patients with medically inoperable stage I non-small-cell lung cancer treated with hypofractionated stereotactic body radiotherapy. Int J Radiat Oncol Biol Phys. 2010;76:789–95.
44. Matsuo Y, Nakamoto Y, Nagata Y, Shibuya K, Takayama K, Norihisa Y, et al. Characterization of FDG-PET images after stereotactic body radiation therapy for lung cancer. Radiother Oncol. 2010;97:200–4.
45. Nakajima N, Sugawara Y, Kataoka M, Hamamoto Y, Ochi T, Sakai S, et al. Differentiation of tumor recurrence from radiation-induced pulmonary fibrosis after stereotactic ablative radio-therapy for lung cancer: characterization of 18 F-FDG PET/CT findings. Ann Nucl Med. 2013;27:261–70.

Part V
Liver Cancer

Chapter 14
Liver Cancer (Hepatocellular Carcinoma; HCC)

Tomoki Kimura

14.1 Treatment Strategy for Early-Stage HCC

Hepatocellular carcinoma (HCC) is the world's third most common cancer causing death [1], and is closely associated with hepatitis B (HBV) or hepatitis C (HCV) viral infections and alcohol intake. Recently, the incidence of other causes, such as nonalcoholic fatty liver disease, has been increasing. These causes lead to cirrhosis and the development of HCC. Antiviral treatment for chronic viral hepatitis can eradicate infection, increase patient survival, and reduce the need for liver transplantation [2].

Curative therapy for early-stage HCC involves resection or transplantation surgery [3–5]. According to Japanese nation-wide survey, the 5-year overall survival rates of early-stage HCC is 60–73 % [6]. Liver transplantation can cure both liver cancer and underlying liver disease. The 4-year overall survival rates for HCC within the Milan criteria (single nodule <5 cm or ≤3 HCC nodules <3 cm) is 70–85 % after transplantation [7]. However, because of liver dysfunction, underlying cirrhosis, or the presence of multifocal tumors arising from viral infection, only 10–30 % of patients who initially present with HCC are eligible for surgery [8]. For such patients, locoregional therapies, such as ablative therapies or transarterial chemoembolization (TACE), are recommended [9–11]. Ablative therapies, such as radiofrequency ablation (RFA) and percutaneous ethanol injection, are considered safe, effective, and reliable treatment for small HCC [4–6]. However, they are limited by HCC undetectable by ultrasonography or a tumor located near large vessels and in deep liver layers. TACE is also a widely used and is reportedly effective in patients with any type of HCC, regardless of tumor size, location, or number [12, 13]. However, TACE is also limited by incomplete necrosis due to

T. Kimura (✉)
Department of Radiation Oncology, Hiroshima University, 1-2-3 Kasumi,
Minami-ku, Hiroshima 734-8551, Japan
e-mail: tkkimura@hiroshima-u.ac.jp

hypovascularity, dual blood supply around the HCC capsule and multiple collateral feeding circulation, and therapy resistance, which often occurs after several courses. Therefore, TACE is not an option for first-line treatment of small HCC [14]. Radiotherapy, a locoregional therapy, can be considered as an alternative to ablation and TACE when these therapies have failed. stereotactic body radiotherapy (SBRT), which delivers high radiation doses to focal HCC, is particularly helpful to avoid radiation-induced liver damage. However, according to the Barcelona Clinic Liver Cancer (BCLC) classification, which is provided by the European Association for the Study of the Liver/European Organization for Research and Treatment of Cancer Clinical Practice Guidelines, detailed radiotherapy data, including SBRT for HCC, are insufficient to determine efficacy and safety [3].

14.2   Treatment Results of SBRT for HCC

Several studies have reported good treatment outcomes with SBRT for HCC with or without TACE using several dose/fractionations [15–19]. The use of radiotherapy for HCC has increased rapidly over the past decade [20]. Table 14.1 summarizes treatment results of several reports of SBRT for HCC. The dose/fractionations ranged from 24 to 60 Gy per 3–6 fractions. In addition, most patients received previous treatment, including resection, ablative therapies, and TACE. Bujold et al. conducted a phase I/II trial of SBRT for 102 patients with locally advanced BCLC stage A-C HCC [15]. The median dose of SBRT was 36 Gy in 6 fractions based on irradiated liver volume. Although 65.7 % had BCLC stage C, the 1-year local control rate was 87 % (95 % CI, 78–93 %). In other studies of small HCC with a tumor size of 20–30 mm, the local control rate was approximately 90–100 % at 2 years and 60–90 % at 3 years. This was also excellent. These results indicate the possibility of achieving local control for HCC, including advanced cases.

In these studies, some patients underwent TACE before SBRT. Kang et al. reported an excellent 2-year local control rate 94.6 % with SBRT for inoperable HCC as a local salvage treatment after incomplete TACE and concluded that SBRT plus TACE is promising [18]. They suggested several theoretical advantages of combined SBRT and TACE, such as tumor shrinkage, the remaining lipiodol as a target for image guided radiotherapy, and enhance sensitivity to irradiation. We retrospectively compared the treatment results of SBRT plus TACE with TACE alone in patients with small, solitary HCC [21]. No significant difference was observed in overall survival and toxicity between the groups. However, local tumor control was significantly superior in the SBRT plus TACE group than in the TACE alone group ($p < 0.001$), and disease-free survival of 12 patients without previous HCC treatment in the SBRT group was significantly superior to that of the TACE alone group (15.7 months versus 4.2 months; $p = 0.029$). In these studies of combined SBRT and TACE, local control is promising; however whether this combination can improve overall survival is unclear because of the lack of a phase III study.

Table 14.1 Reports of Stereotactic Body Radiotherapy for Hepatocellular Carcinoma

Author/year	n	Median tumor size (mm)	BCLC[a] stage C (%)	Previous treatment (%)	Dose/fraction (Gy/fr)	Prescription	Local control rate	Overall survival rate	Toxicity ≧Grade 3 (%)
Bujold, 2013, Canada [15]	102	72	65.7	52	24–54 Gy/6 fr	N.A.	87.0 % (1y)	34.0 % (2y)	30[c]
Andolino, 2011, USA [16]	60	31	N.A.[b]	N.A.	24–48 Gy/3–5 fr	80 % isodose	90 % (2y)	67 % (2y)	35[c]
Kwon, 2010, Korea [17]	42	N.A.	0	81	30–39 Gy/3 fr	70–85 % isodose	67.5% (3y)	58.6% (3y)	2.4[d]
Kang, 2012, Korea [18]	47	29	17	100	42–60 Gy/3 fr	70–80 % isodose	94.6 % (2y)	68.7 % (2y)	10.7[e]
Sanuki, 2013, Japan [19]	185	26	N.A.	68.1	40 or 35 Gy/5 fr	70–80 % isodose	91.0 % (3y)	70.0 % (3y)	13[c]
Kimura, unpublished, Japan	65	16	0	92.3	48 Gy/4 fr	Isocenter	100 % (2y)	76.0 % (2y)	23.1[c]

Abbreviations
[a]*BCLC* Barcelona clinic liver cancer
[b]*N.A.* not available
[c]Toxicity was assessed by Common Terminology Criteria for Adverse Events (CTCAE) ver. 4.0
[d]Toxicity was assessed by Radiation Therapy Oncology Group (RTOG) guidelines
[e]Toxicity was assessed by Common Terminology Criteria for Adverse Events (CTCAE) ver. 3.0

14.3   Adverse Effects of SBRT and Dose Constraints
       for Liver

Radiation-induced liver disease (RILD) is an adverse effect that is pathologically characterized as a veno-occlusive disease (VOD) [22], and is categorized into "classic" and "nonclassic" RILD [23]. "Classic" RILD involves anicteric hepatomegaly and ascites, typically occurring within 4 months, and often exhibits severe or fatal complications following conventional radiotherapy for large hepatic volumes [23, 24]. In contrast, "nonclassic" RILD, typically occurring between 1 week and 3 months after therapy, involves liver transaminases elevated more than 5 times the normal upper limit or Common Terminology Criteria for Adverse Events (CTCAE) grade 4 levels in patients with baseline values more than 5 times the normal upper limit within 3 months after completion of radiotherapy, or a decline in liver function [measured by a worsening of Child-Pugh (CP) score by 2 or more], in the absence of classic RILD [23]. Recent advances in imaging and radiation techniques provide high radiation doses to conform to focal HCC, such as SBRT, and several studies listed in Table 14.1 have described good treatment results for SBRT without severe clinical signs of "classic" RILD. However, toxicities of more than grade 3 CTCAE criteria (so called "nonclassic" RILD) is frequently observed, shown in Table 14.1. Particularly, patients with worse baseline liver function are at higher risk for developing "nonclassic" RILD even in SBRT. Lee et al. reported that in their experience of 131 patients with HCC who received 3-dimensional conformal radiotherapy, the incidence of liver complications was significantly increased in patients with CP class B ($p = 0.044$). They concluded that indicators of liver function status such as CP class may be important and useful parameters for predicting radiation-related liver disease [25]. In addition, in our unpublished data of 65 patients (56 patients with CP class A and 9 patients with CP class B) who underwent SBRT (median 48 Gy/4 fr), 15 patients (23.1 %) developed grade 3 toxicity including 5 patients with decreased platelet counts before SBRT. CP class B was the only significant factor associated with more than grade 3 (CTCAE ver 4.0.) hepatic toxicity. Irradiated liver dose is also risk factor for severe hepatic toxicity. Bujold et al. reported a significantly higher median liver mean dose was observed in patients who developed grade 5 toxicity (CTCAE ver 4.0.) compared with those who did not (18.1 Gy versus 15.4 Gy; $p = 0.02$) in their phase I/II study [15]. Son et al. reported in their experience of 47 patients with HCC who received SBRT using CyberKnife, 4 (11 %) showed progression of CP class, and multivariate analysis showed that the only significant parameter associated with the progression of CP class was liver volume after receiving a dose of less than 18 Gy [26]. To avoid hepatic toxicity, the dose- volume limits guidelines recommended by the Quantitative Analyses of Normal Tissue Effects in the Clinic (QUANTEC) for normal liver dose constraints of 3–6 fractions of SBRT, have been offered. For example, the MLD (liver minus GTV) should receive <13–18 Gy, or that an MLD of ≥700 mL of the normal liver should receive ≤15 Gy [23].

Gastrointestinal toxicity is another severe problem associated with SBRT for HCC. Kang et al. reported that 5 (10.5 %) of 47 patients experienced more than grade 3 gastrointestinal toxicity including grade 4 gastric ulcer perforation in 2 patients (4.3 %) [18]. In patients with liver cirrhosis, portal hypertension probably affects the gastrointestinal mucosal defensive and healing mechanisms, whereas liver cirrhosis increases gastrointestinal toxicity [27]. It is recommended that target proximity to luminal gastrointestinal tract should be far from tumor more than, i. e., 2 cm [20].

14.4 Assessment of HCC Response and Normal Liver Reaction After SBRT

14.4.1 Assessment of HCC Response

The modified Response Evaluation Criteria in Solid Tumors (mRECIST) was proposed to assess HCC response [28]. HCC is usually diagnosed by its character-istic appearance of early arterial-phase enhancement and portal venous phase hypodensity, which is revealed in most patients with either dynamic computed tomography (CT) or combined angiography CT. These guidelines consider any necrotizing effects or tumor blood flow, and complete response was defined as the disappearance of any intratumoral arterial enhancement in all target lesions. Thus observation of residual early arterial enhancement is important. In our previous report, we mentioned the dynamic CT appearance of tumor responses after SBRT for HCC [29], whereas residual early arterial enhancement was observed >3 months after SBRT in 28.4 % lesions (19/67 lesions; Fig. 14.1). We concluded that early assessments within 3 months could result in misleading response evaluations. In this study, we also observed shrinkage or disappearance of residual early arterial enhancement for more than 6 months after SBRT in 2 patients at 10 and 11 months. Therefore a follow-up of at least 12 months would be required for accurate
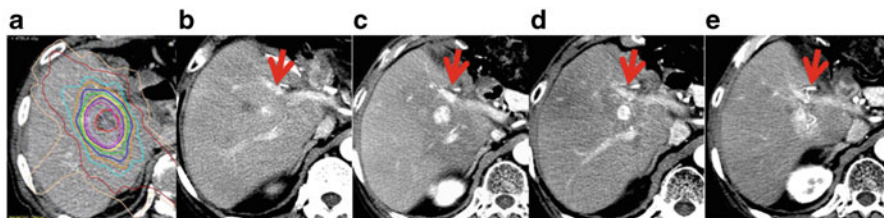

Fig. 14.1 The dynamic computed tomographic appearance of tumor responses (arterial phase). (**a**) Dose distribution (48 Gy/4 fractions). (**b**) Before stereotactic body radiotherapy (SBRT), early arterial enhancement is visible (*red arrow*). (**c**) After 2 and (**d**) 6 months, early arterial enhance-ment is more evident than before SBRT (*red arrow*). (**e**) After 11 months, enhancement remains, although the tumor is shrinking (*red arrow*)

assessments. Other modalities should also be considered in these cases, such as gadoxetate disodium enhanced-magnetic resonance imaging (EOB-MRI) or enhanced ultrasound (US).

14.4.2 Imaging of Normal Liver Reaction After SBRT for HCC

Focal radiation injury to normal or cirrhotic liver tissue around the tumor has been observed on follow-up dynamic CT or MRI. The appearance of focal radiation injury reflects the irradiated area of the normal liver; therefore, it is important to correctly investigate the imaging finding following SBRT because patients with HCC may require additional multiple therapies in the future. The typical CT appearance of radiation injury following SBRT, which was isodense/hyperdense in the portal-venous phase and hyperdense in the late contrast phase, is shown in Fig. 14.2 [30, 31]. This appearance can be explained by decreased vascular perfusion and reduced hepatic venous drainage due to VOD with subsequent stasis of the contrast medium [32].

Liver enhancement on EOB-MRI has been correlated with liver dysfunction, including radiotherapy [33]. Nakamura et al. reported that the liver-spleen contrast of the liver irradiated with more than 30 Gy in 4 fractions was significantly smaller than that of the nonirradiated liver and concluded that EOB-MRI, hepatobiliary phase, was useful to evaluate the irradiated liver treated with doses exceeding 30 Gy in 4 fractions (Fig. 14.3) [34]. Sanuki et al. reported that the threshold dose was significantly correlated with baseline liver function, and they proposed 30 Gy for CP class A disease and 25 Gy for CP class B disease in 5 fractions [35].
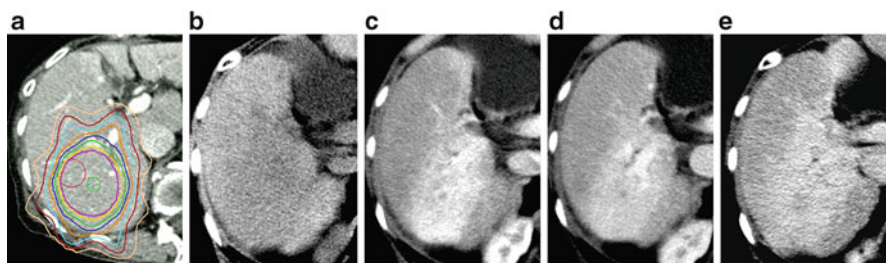

Fig. 14.2 The dynamic CT appearance of focal liver injury 10 months after SBRT. (**a**) Dose distribution (**b**) Plain (**c**) Arterial phase (**d**) Portal phase (**e**) Venous phase Hypodensity in plain CT and hyperdensity in all enhanced phases

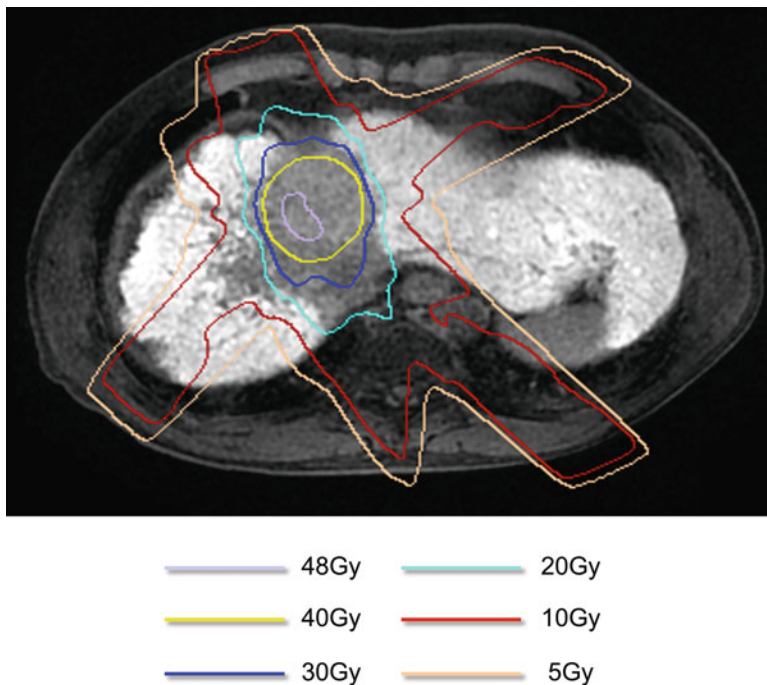|			
———	48Gy	———	20Gy
———	40Gy	———	10Gy
———	30Gy	———	5Gy

Fig. 14.3 The EOB-MRI at hepatobiliary phase 6 months after SBRT. The signal intensity of the irradiated liver parenchyma exceed 30 Gy is low

14.5   Summary -Eligibility of SBRT for HCC

SBRT for HCC appears to achieve excellent local control; however, because of poor evidence and the lack of prospective studies, this is still under investigation as a therapeutic option for the management of liver malignancies. We should consider the eligibility of SBRT for patients who are presently ineligible for resection or ablation therapies. We summarized the good eligibility for SBRT as follows:

1. CP class A or B
2. <3 HCC nodules, each up to 50 mm in diameter, with or without vascular invasion
3. Inoperability because of poor general condition or surgery refusal
4. Unsuitability for RFA because of tumor location (on the liver surface and near the porta hepatis), tumor invisibility on ultrasonography, or bleeding tendencies.
5. The exclusion criteria were uncontrolled ascites and gastrointestinal tract-adjacent tumors.

References

1. Jemal A, Bray F, Center MM, et al. Global cancer statistics. Cancer J Clin. 2011;61:69–90.
2. Buti M, San Miguel R, Brosa M, et al. Estimating the impact of hepatitis C virus therapy on future liver-related morbidity, mortality and costs related to chronic hepatitis C. J Hepatol. 2005;42:639–45.
3. European Association for the Study of the Liver and European Organisation for Research and Treatment of Cancer. EASL–EORTC clinical practice guidelines: management of hepatocellular carcinoma. J Hepatol. 2012;56:908–43.
4. Klein J, Dawson LA. Hepatocellular carcinoma radiation therapy: review of evidence and future opportunities. Int J Radiat Oncol Biol Phys. 2013;87:22–32.
5. Thomas MB, Jaffe D, Choti MM, et al. Hepatocellular carcinoma: consensus recommendations of the National Cancer Institute Clinical Trials Planning Meeting. J Clin Oncol. 2010;28:3994–4005.
6. Kudo M, Arii S, Ikai I, et al. Report of the 18th follow-up survey of primary liver cancer in Japan. Osaka-Sayama: Liver Cancer Study Group of Japan; 2009.
7. Mazzaferro V, Regalia E, Doci R, et al. Liver transplantation for the treatment of small hepatocellular carcinomas in patients with cirrhosis. N Engl J Med. 1996;334:693–9.
8. Choi E, Rogers E, Ahmad S, et al. Hepatobiliary cancers. In: Feig BW, Berger DH, Fuhrman GM, editors. The M. D. Anderson surgical oncology handbook. Philadelphia: Lippincott Williams &Wilkins; 2006.
9. Shiina S, Teratani T, Obi S, et al. A randomized controlled trial of radiofrequency ablation with ethanol injection for small hepatocellular carcinoma. Gastroenterology. 2005;129:122–30.
10. Goldberg SN, Grassi CJ, Cardella JF, et al. Image-guided tumor ablation: standardization of terminology and reporting criteria. Radiology. 2005;235:728–39.
11. Liu JG, Wang YJ, Du Z. RFA in the treatment of small HCC: a meta-analysis. World J Gastroenterol. 2010;16:3450–6.
12. Miyayama S, Matsui O, Yamashiro M, et al. Ultraselective transcatheter arterial chemoembolization with a 2-f tip microcatheter for small hepatocellular carcinomas: relationship between local tumor recurrence and visualization of portal vein with iodized oil. J Vasc Interv Radiol. 2007;18:365–76.
13. Takayasu K, Arii S, Kudo M, et al. Superselective transarterial chemoembolization for hepatocellular carcinoma: validation of treatment algorithm proposed by Japanese guidelines. J Hepatol. 2012;56:886–92.
14. Arii S, Yamaoka Y, Futagawa S, et al. Results of surgical and nonsurgical treatment for small sized hepatocellular carcinomas: a retrospective and nationwide survey in Japan: The Liver Cancer Study Group of Japan. Hepatology. 2000;32:1224–9.
15. Bujold A, Massey CA, Kim JJ, et al. Sequential Phase I and II trials of stereotactic body radiotherapy for locally advanced hepatocellular carcinoma. J Clin Oncol. Published ahead of print.
16. Andolino DL, Johnson CS, Maluccio M, et al. Stereotactic body radiotherapy for primary hepatocellular carcinoma. Int J Radiat Oncol Biol Phys. 2011;81:e447–53.
17. Kwon JH, Bae SH, Kim JY, et al. Long-term effect of stereotactic body radiation therapy for primary hepatocellular carcinoma ineligible for local ablation therapy or surgical resection: stereotactic radiotherapy for liver cancer. BMC Cancer. 2010;10:475.
18. Kang JK, Kim MS, Cho CK, et al. Stereotactic body radiation therapy for inoperable hepatocellular carcinoma as a local salvage treatment after incomplete transarterial chemoembolization. Cancer. 2012;118:5424–31.
19. Sanuki N, Takeda A, Oku Y, et al. Stereotactic body radiotherapy for small hepatocellular carcinoma: a retrospective outcome analysis in 185 patients. Acta Oncol. Published ahead of print.

20. Dawson LA. Overview: where does radiation therapy fit in the spectrum of liver cancer local – regional therapies? Semin Radiat Oncol. 2011;21:241–6.
21. Honda Y, Kimura T, Aikata H, et al. Stereotactic body radiation therapy combined with transcatheter arterial chemoembolization for small hepatocellular carcinoma. J Gastroenterol Hepatol. 2013;28:530–6.
22. Sempoux C, Horsmans Y, Geubel A, et al. Severe radiation-induced liver disease following localized radiation therapy for biliopancreatic carcinoma: activation of hepatic stellate cells as an early event. Hepatology. 1997;26:128–34.
23. Pan CC, Kavanagh BD, Dawson LA, et al. Radiation-associated liver injury. Int J Radiat Oncol Biol Phys. 2010;76:S94–100.
24. Guha C, Kavanagh BD. Hepatic radiation toxicity: avoidance and amelioration. Semin Radiat Oncol. 2011;21:256–63.
25. Lee IJ, Seong J, Shin SJ, et al. Radiotherapeutic parameters predictive of liver complications induced by liver tumor radiotherapy. Int J Radiat Oncol Biol Phys. 2009;73:154–8.
26. Son SH, Choi BO, Ryu MR, et al. Stereotactic body radiotherapy for patients with unresectable primary hepatocellular carcinoma: dose-volumetric parameters predicting the hepatic complication. Int J Radiat Oncol Biol Phys. 2010;78:1073–80.
27. Bae SH, Kim MS, Cho CK, et al. Predictor of severe gastroduodenal toxicity after stereotactic body radiotherapy for abdominopelvic malignancies. Int J Radiat Oncol Biol Phys. 2012;84: e469–74.
28. Lencioni R, Llovet JM. Modified RECIST (mRECIST) assessment for hepatocellular carcinoma. Semin Liver Dis. 2010;30:52–60.
29. Kimura T, Takahashi S, Kenjo M, et al. Dynamic computed tomography appearance of tumor response after stereotactic radiation therapy for hepatocellular carcinoma: how should we evaluate treatment effects? Hepatol Res. 2013;43:717–27.
30. Herfarth KK, Hof H, Bahner ML, et al. Assessment of focal liver reaction by multiphasic CR after stereotactic single-dose radiotherapy of liver tumors. Int J Radiat Oncol Biol Phys. 2003;57:444–51.
31. Sanuki-Fujimoto N, Takeda A, Ohashi T, et al. CT evaluations of focal liver reactions following stereotactic body radiotherapy for small hepatocellular carcinoma with cirrhosis: relationship between imaging appearance and baseline liver function. Br J Radiol. 2010;83:1063–71.
32. Willemart S, Nicaise N, Struyven J, et al. Acute radiation-induced hepatic injury: evaluation by triphasic contrast enhanced helical CT. Br J Radiol. 2000;73:544–6.
33. Motosugi U, Ichikawa T, Sou H, et al. Liver parenchymal enhancement of hepatocyte-phase images in Gd-EOB-DTPA-enhanced MR imaging: which biological markers of the liver function affect the enhancement? J Magn Reson Imaging. 2009;30:1042–637.
34. Nakamura Y, Kimura T, Higaki T, et al. Imaging findings of liver parenchyma after stereotactic body radiation therapy for hepatocellular carcinoma: evaluation by gadoxetate disodium-enhanced hepatic MRI. Radiology. Abstract.
35. Sanuki N, Takeda A, Oku Y, et al. Threshold doses for focal liver reaction after stereotactic ablative body radiation therapy for small hepatocellular carcinoma depend on liver function: evaluation on magnetic resonance imaging with Gd-EOB-DTPA. Int J Radiat Oncol Biol Phys. 2014;88:306–11.

Part VI
Other Indications

Chapter 15
Other Indications

Keiji Nihei, Hiroshi Tanaka, and Katsuyuki Karasawa

15.1 SBRT for Prostate Cancer

15.1.1 Background and Rationale of Hypofractionation for Prostate Cancer

From the biological perspective, α/β ratio in the linear-quadratic model for prostate cancer is estimated to range from 1.5 to 1.85 Gy according to clinical data from hypofractionation research [1, 2]. This low α/β ratio suggests that prostate cancer has high sensitivity to dose per fraction, and a hypofractionation strategy may be advantageous for prostate cancer compared with other types of cancer. On the other hand, the α/β ratio of the rectum has been calculated as 5.4 +/− 1.5 Gy from an analysis of clinical data for late rectal bleeding after hypofractionated radiation therapy [3]. If the α/β ratio of the rectum is actually higher than that of prostate cancer, a hypofractionation approach could be beneficial, leading to maximum clinical gain between its efficacy and toxicity, although the linear-quadratic model may not be simply applicable to SBRT using larger fraction sizes.

In the 3-dimensional era, some institutions have suggested that PSA control is improving as the total dose to the prostate increased to more than 70 Gy with conventional fractionation [4, 5]. After the IMRT technique emerged and was introduced to clinical practice, high-dose radiation therapy was proven to be the standard for prostate cancer according to results of several randomized clinical trials. From the biological background described above, some mild hypofractionation schedules using >2–3 Gy per fraction are now being investigated in clinical trials in order to reduce the total treatment duration.

K. Nihei • H. Tanaka • K. Karasawa (✉)
Radiation Oncology Division, Department of Radiology, Tokyo Metropolitan
Cancer and Infectious Diseases Center, Komagome Hospital, 3-18-22 Honkomagome,
Bunkyo-ku, Tokyo 113-8677, Japan
e-mail: karasawa@cick.jp

The ideal dose distribution to the target can be achieved using the IMRT technique. Furthermore, from a physics perspective, image-guided radiation therapy can achieve more aggressive dose delivery through precise positioning of the target. Stereotactic radiation therapy, established first for brain tumors, has been applied to the prostate, and super-hypofractionation with larger fraction sizes (>3 Gy) has been introduced in clinical trials for prostate cancer.

15.1.2   Clinical Trials of SBRT for Prostate Cancer

The early investigation of hypofractionation for prostate cancer was initiated in the 1960s, long before the PSA era. The long-term outcomes of hypofractionation with conventional radiation therapy at 36 Gy/6 fr twice a week were reported in 1990 [6].

The first publication on SBRT for prostate cancer was the SHARP trial by Madsen et al., in which 33.5 Gy in 5 daily fractions was prescribed to the prostate using conventional linac with a stereotactic technique. At the median follow-up of 5 years, the biochemical relapse-free survival rate was 93 % with acceptable late toxicities [7, 8]. Since then, SBRT for prostate cancer in various schedules as 35–50 Gy in 4–6 fractions has been attempted (Table 15.1).

From Stanford University, King et al. reported the results of a single institutional phase II trial in which 41 patients with low-risk prostate cancer were treated by SBRT with a total dose of 36.25 Gy/5 fr. The PSA relapse-free survival rate was 100 % after a median follow-up period of 33 months [9]. The updated results showed that, in 67 patients with a median follow-up period of 2.7 years, the PSA relapse-free survival rate was 94 % at 4 years and the frequencies of long-term genitourinary (GU) and gastrointestinal (GI) toxicities were 3 % and 0 %, respectively [10]. Freidland et al. from Florida University also reported promising results for SBRT using 35 Gy/5fr [11]. Katz et al. treated more than 300 patients using schedules of both 35 Gy and 36.25 Gy, and reported long-term results with a median follow-up of 60 months. Comparison between the two schedules showed that the frequencies of late GU and GI toxicities tended to be higher in the 36.25-Gy group than in the 35-Gy group, although there was no significant difference [12, 13].

Meier et al. reported the results of a multi-institutional phase II trial using a schedule of 40 Gy/5 fr [14]. Boik et al. also reported on a multi-institutional phase I dose-escalation trial, which increased the total dose from 40 Gy, to 45 Gy, up to 50 Gy in 5 fractions [15]. In both trials, the conclusion was that high-dose SBRT over 40 Gy was safely implemented with good efficacy, but toxicity rates tended to be higher compared with moderate-dose SBRT with 35 Gy or 36.25 Gy in 5 fractions.

From the Stanford trial, King et al. compared toxicity rates between every-other-day (QOD) treatments and daily treatments (QD). QOD resulted in substantially less frequent Grade 1–2 GU toxicity (17 % vs. 56 %, p = 0.007) and less frequent Grade 1–2 GI toxicity (5 % vs. 44 %, p = 0.001) [9].

Table 15.1 Published data on SBRT for prostate cancer

Institute/trial [reference no.]	No. of patients (risk group)	Schedule	Free from PSA failure	Toxicities	Median follow-up
SHARP trial [6, 7]	40 (Low)	33.5 Gy/5 fr	93 % at 5 years	1 acute Gr 3 toxicity; Late GU/GI Gr2: 12.5 %/7.5 %, Gr3:2.5 %/0 %	5 years
Stanford University [8, 9]	41 (Low)	36.25 Gy/5 fr	100 %	GU Gr 2/3: 24 %/5 % GI Gr 2/3: 15 %/0 %	33 months
	67 (Low)		94 % at 4 years	GU Gr 1/2/3: 23 %/5 %/3 % GI Gr 1/2/3: 12.5 %/2 %/0 %	2.7 years
Florida University [10]	102/10 (Low/Int.-High)	35 Gy/5 fr	98 %	GU Gr 3: 0 Rectal bleeding: 1 patient	2 years
Katz et al. [11, 12]	50 (Low/Int./High: 45/5/0)	35 Gy/5 fr	Low/Int./High: 97 %/ 90.7 %/74.1 % at 5 years	Acute GU/GI Gr2: < 5 % Late GU Gr2/3: 4 %/0 % 9 % Late GI Gr2: 2 %	72 months
	254 (Low/Int./High: 166/76/12)	36.25 Gy/5 fr		Acute GU/GI Gr2: < 5 % Late GU Gr2/3: 9 %/2 % Late GI Gr2: 5 %	60 months
Multi-institutional phase II [13]	211	40 Gy/5 fr	PSA failure: 1 pt	Acute GU/GI Gr 2: 20 %/8.5 % Late GU/GI Gr2: 1 %/6 % bladder necrosis (Gr3): 1 patient	18 months
Dose Escalation Study [14]	45 (15 for each dose group)	45 Gy/5 fr	100 %	GU/GI Gr2≤: 31 %/18 %, Gr3≤: 4 %/2 %	30 months
		47.5 Gy/5 fr		(Group of 50 Gy Acute GU/GI Gr2: 33 %/7 %, Gr3: 7 %/0 % Late GU Gr4: 7 %)	18 months
		50 Gy/5 fr			12 months

Low low risk, *Int.* intermediate risk, *High* high risk, *GU* genitourinary, *GI* gastrointestinal, *Gr* grade

RTOG is now conducting a randomized phase II trial of SBRT (RTOG 0938), in which patients with favorable-risk prostate cancer are being randomized to receive either 36.25 Gy/5 fr (QOD) or 51.6 Gy/12 fr (QD), delivered by conventional linacs, CyberKnife, or protons [16].

15.1.3 Future Directions of SBRT for Prostate Cancer

A retrospective comparative analysis regarding toxicities between SBRT and IMRT for prostate cancer was recently published. Yu et al. analyzed more than 4,000 patients with prostate cancer treated by SBRT or IMRT, and reported that there appeared to be a greater rate of GU toxicity for patients undergoing SBRT compared with IMRT (15.6 % vs. 12.6 % at 6 months, p = 0.009; 43.9 % vs. 36.3 % at 2 years, p = 0.001) [17].

SBRT is a potentially beneficial treatment strategy for localized prostate cancer, but its clinical significance remains under investigation. Further prospective research including randomized trials is needed to determine the optimal schedule and to confirm efficacy and toxicity.

15.2 Spine SBRT

15.2.1 Introduction

Spine stereotactic body radiotherapy (SBRT) is an emerging treatment for patients with spinal metastases that is rapidly being adopted without level 1 evidence, particularly in North America [18]. The aim of this review is to update information concerning spine SBRT in relation to its efficacy and associated complications.

15.2.2 Efficacy

To date, results have been reported from two phase 2 trials and several prospective and retrospective studies.

Xin et al. reported the first clinical trial (phase 1–2 trial) of 149 patients with 166 lesions [19]. In that trial, significant reductions were observed in the severity of patient-reported pain between baseline and both 4 weeks post-treatment (mean, 3.4 [Standard Deviation (SD) 2.9] at baseline, 2.1 [2.4] at 4 weeks on the BPI pain at its worst item [0–10 scale]; effect size 0.47, p = 0.00076) and 6 months post-treatment (mean of 3.4 [SD 2.9] at baseline, 1.7 [2.4] at 6 months; effect size 0.64, p < 0.0001). The proportion of patients reporting no spine pain on the BPI increased
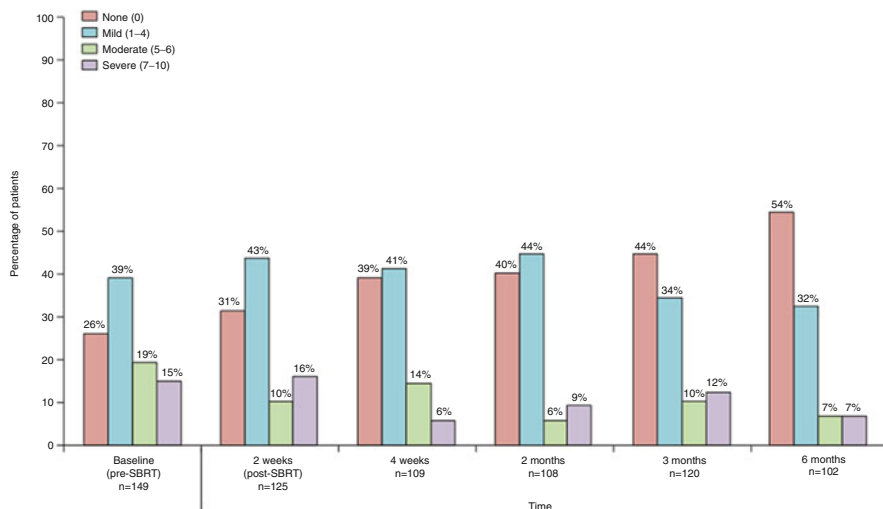
Fig. 15.1 SBRT plan for prostate cancer by CyberKnife (35 Gy/5 fr)

significantly between baseline and 4 weeks post-treatment, from 49 of 149 (26 %) to 43 of 109 (39 %) (p = 0.038). This improvement continued throughout the study, with 53 of 120 patients (44 %) reporting no pain at 3 months (p = 0.004), and 55 of 102 patients (54 %) reporting no pain at 6 months (p < 0.0001) (Fig. 15.1).

Peter et al. reported one of the biggest prospective evaluations, of 500 cases [20]. In that report, long-term pain control was achieved in 290 of the 336 cases (86 %), and long-term radiographic control was observed in 88 % cases. Pain and radiographic outcomes for the common histopathologies are shown in the Table 15.2.

15.2.3 Complications

One of the most critical and dose-limiting organs at risk in safe SBRT practice is the spinal cord. Sahgal et al. reported a series of 9 cases of radiation-induced myelopathy (RM) that were compared with a cohort of 66 spine SBRT patients without RM [21]. In that report, dose-volume histograms (DVH) of the thecal sac were compared between the RM and no-RM cohorts.

Median doses to small volumes (smaller than 1 cc) differed significantly. These findings suggest that the small volume of the high-dose area in the thecal sac causes RM. They recommended limiting the maximum dose to the thecal sac to 12.4 Gy in 1 fraction, 17.0 Gy in 2 fractions, 20.3 Gy in 3 fractions, 23.0 Gy in 4 fractions or 25.3 Gy in 5 fractions to reduce the risk of RM to less than 5 %. (see Table 15.3).

Spine SBRT may increase the risk of vertebral compression fracture. Sahgal reported a series of 252 patients in 3 institutes with 410 vertebral metastases treated

Table 15.2 Summary of pain and radiographic outcome for the four most common histopathologies (n = 294)

Long-term pain improvement	
All patients	86 %
Renal cell	94 %
Breast	96 %
Lung	93 %
Melanoma	96 %
Long-term radiographic control	
All patients	88 %
Renal cell	87 %
Breast	100 %
Lung	100 %
Melanoma	75 %

Table 15.3 Comparison of median and mean nBED between the radiation myelopathy (RM) and no-RM cohorts

	No-RM cohort (n = 66) (Gy$_{2/2}$)	RM cohort (n = 9) (Gy$_{2/2}$)	Mann–Whitney/t test (P value)
Median/mean Pmax volume nBED	35.69/38.82	73.69/70.60	.0003/.0006
Median/mean 0.1 cc nBED	28.32/29.28	56.20/56.63	.001/.006
Median/mean 0.2 cc nBED	27.65/26.89	54.08/52.53	.003/.008
Median/mean 0.3 cc nBED	26.34/25.10	52.46/49.32	.005/.01
Median/mean 0.4 cc nBED	24.36/23.87	49.85/46.69	.006/.01
Median/mean 0.5 cc nBED	20.35/22.64	47.45/44.30	.01/.02
Median/mean 0.6 cc nBED	21.20/22.08	41.86/41.75	.01/.02
Median/mean 0.7 cc nBED	20.54/21.32	39.75/39.44	.02/.03
Median/mean 0.8 cc nBED	19.91/20.69	38.30/37.24	.03/.04
Median/mean 0.9 cc nBED	19.13/20.12	36.55/35.12	.04/.05
Median/mean 1 cc nBED	17.63/19.51	35.05/33.68	.08/.05
Median/mean 2 cc nBED	13.48/16.07	22.15/23.44	.35/.14

using SBRT. In that series, 57 fractures (57 of 410, 13.9 %) were observed, 27 of which (27 of 57, 47 %) were de novo and 30 of which (30 of 57, 53 %) represented progression of existing fractures. The median time to fracture was 2.46 (range,

0.03–43.01) months. In multivariate analysis, a dose of 20 Gy or greater per fraction, baseline fracture, lytic-type tumor and bone alignment were all associated with higher risk of fracture [1].

Esophageal toxicity has also been reported with high-dose single-fraction SBRT. Brett et al. reported a series of 182 patients with 204 vertebral metastases abutting the esophagus [22]. In that series, 31 acute esophageal toxicities (15 %) and 24 late esophageal toxicities (12 %) were observed, and grade 3 or greater acute or late toxicity was seen in 14 patients (6.8 %). To minimize the risk, that report recommended that 2.5 cc or less of esophagus should receive 14 Gy, and that the maximum dose to the esophagus should be <22 Gy.

15.2.4 Summary

Results of several phase 2 trials and several prospective and retrospective studies have been published, but findings have yet to be obtained from randomized control trials. Promising results have been seen in the reports, but whether SBRT is superior to conventional RT in terms of pain or local control has not been confirmed by randomized control trials.

15.3 Pancreatic Cancer

15.3.1 Introduction

The standard treatment for resectable pancreatic cancer is surgical resection, and one of the standard treatments for unresectable locally advanced pancreatic cancer is definitive radiotherapy combined with chemotherapy. The recommended dose fractionation is usually 50–50.4 Gy/58–28 fr/5–5.6 w plus a boost dose of 9–10 Gy/ 5 fr/1 w [23]. Results with this approach have been gradually improving.

Stereotactic body radiation therapy (SBRT) has been utilized because of its high local control rates, low systemic adverse effects, and short overall treatment time. It is well known that the majority of patients with pancreatic cancer will die of systemic rather than local progression, but a certain percentage of patients still die of local tumor progression. SBRT thus has a considerable role to play in the treatment of pancreatic cancer. With the optimal integration of chemotherapy, survival results would be improved.

15.3.2 Patient Selection

No established criteria currently exist for selecting patients eligible for SBRT. However, pancreatic tumor without lymph node metastasis is preferred. In addition, the maximum diameter of the tumor is preferably less than 5 cm, and the distance from critical organs such as the stomach, duodenum, and small intestines has to be as high as possible.

15.3.3 Fiducial Marker Placement

The position of the pancreas is usually influenced by respiratory motions. Gold fiducial markers should therefore be placed inside or near the pancreatic tumor using an endoscopic, transcutaneous, laparoscopic or laparotomic approach. Treatment should then be performed under a tumor-tracking or respiratory-gated method.

15.3.4 Treatment Planning and Dose Prescription

Treatment is planned and then performed with the patient in a supine position with their arms placed above their head. They are immobilized using a custom-made Alfa Cradle. Planning CT scans are taken with intravenous contrast agents using a pancreas protocol. Results are obtained as 4D-CT, and PET-CT scans should preferably be fused. The GTV is usually best seen as a hypodense lesion in the early arterial-phase CT. Proper ITV margins should be added to GTV, and very strict margins such as 2~3 mm should be added as set-up errors. Regional lymph nodes are not included in the target volume.

Dose prescriptions have not yet been established for pancreatic SBRT. However, the most experienced institution, Stanford University, is currently using 33 Gy in 5 fractions. Their normal tissue constraints for stomach, duodenum, and other bowel are V15Gy < 9 ml, V25Gy < 3 ml, and V33Gy < 1 ml.

15.3.5 Clinical Results

Koong et al. from Stanford University reported in a Phase I clinical trial that at the dose of 25 Gy/1 fr, 100 % local control was achieved with an MST of 11 months before reaching maximum tolerable dose [24]. By changing chemotherapy from 5-FU to gemcitabine, Schellenberg et al. reported an MST of 11.4 months in a Phase II study [25]. These results were about the same as those with conventional chemoradiotherapy. Mahadevan et al. from Harvard Medical School reported in a

Phase II study using gemcitabine and SBRT of 24~36 Gy/3 fr depending on the site of the tumor that the local control rate for 39 cases was 85 % with an MST of 20 months [26]. Further studies seeking the optimal combination of SBRT and chemotherapy should be performed.

15.4   Cancer of the Kidney

15.4.1   Introduction

Renal cell cancer (RCC) has been known to be radioresistant and is only treated palliatively with conventional fractionation. However, as the fraction dose increases, renal cell cancers become relatively radiosensitive, and radiosurgical treatment has been playing a role in the treatment of solitary brain metastasis from renal cell cancer. Mori et al. reported in their series of RCC patients with brain metastases that, among 52 lesions in 35 patients, the local control rate was 90 % with a 17-Gy Gamma Knife and whole-brain irradiation (average, 29.3 Gy) [27]. As for primary tumors, Svedman reported 7 cases of RCCs treated with an SBRT of 30–40 Gy/3–4 fr [28]. Among these, 6 cases achieved local control (86 %), and concerning toxicity, and only 1 case developed mild renal dysfunction. SBRT with a higher dose per fraction might thus hold promise in the treatment of primary kidney cancers.

15.4.2   Indications

Kidney cancers that are inoperable for reasons such as poor renal function or history of contralateral nephrectomy can be a good indication. Similarly, patients who decline to undergo resection of the tumor might be a good indication.

15.4.3   Treatment Planning and Dose Constraints

An individual cast is made for fixation. Four-dimensional treatment-planning CT should be performed if available. CTV is the same as GTV, and in every phase of 4D-CT, the CTV is drawn and summed-up and the ITV is determined. PTV is made by adding certain set-up margins, preferably of 2–3 mm, around the ITV. Usually, certain leaf margins will be added. Beam arrangement should consist of non-coplanar static or rotational beams. The most frequently used fractionation is 30~40 Gy/3~5 fr. When dose constraints are not met, fraction doses will be decreased, while total doses are increased.

In terms of dose constraints, bowel doses should be under 7 Gy/fr in a 5-fraction regimen. Dose constraints for normal kidneys have not been established. However, the remnant functional kidney on the affected side should not be irradiated with more than 30 Gy when an intact contralateral kidney exists, and not with more than 26 Gy if the contralateral kidney is not functional.

15.4.4 Clinical Studies

Few studies concerning SBRT for primary renal cell cancers have been reported. As already mentioned, Svedman reported a very good local control rate (6/7) for primary tumors. Kaplan reported a Phase I study of SBRT for primary RCC, using dose levels of 21 Gy, 28 Gy, 32 Gy, and 39 Gy in 3 fractions [29]. Only 1 case in the 21-Gy group developed local recurrence, and all other cases (3 cases in each dose group) achieved local control. These results were very encouraging. A Japanese study group is now conducting a multi-center Phase I/II trial of SBRT for RCC [30]. The results are eagerly awaited.

15.5 Other Indications

15.5.1 Head & Neck Cancer: Recurrence

The standard treatment for locally advanced squamous cell carcinoma of the head and neck is chemoradiotherapy; however, some cases show loco-regional recurrence. In such cases, if the lesion is unresectable, SBRT is indicated for salvage treatment. The PTV margins should not be abundant and serious toxicities should be avoided. Carotid blow-out is the most serious complication, with the potential to result in fatality. Cases with tumors surrounding the carotid artery and/or tumors invading to the skin are more likely to develop carotid blow-out.

15.5.2 Adrenal Metastasis

Adrenal gland metastasis often develops from lung cancers, typically as an oligometastasis. In such cases, surgical resection is considered to be the standard treatment. However, if there is high risk of surgical complications, such as anesthesia risk, infection, prolonged hospital stay, etc., SBRT might become a reasonable alternative. Dose fractionations, which are typically used, are 30 Gy in 3 fractions, are 30–40 Gy in 5 fractions. Organs at risk are the small intestine,

stomach, duodenum, spinal cord, and kidneys. Like kidney cancer, doses to the gastrointestinal tract should be under 7 Gy/fraction in 5 fraction regimen.

15.5.3 Gynecological Tumors

The standard treatment for locally advanced cancer of the uterine cervix is chemoradiotherapy, which consists of external beam RT and brachytherapy. In some cases, brachytherapy is very difficult to provide, and SBRT has been recognized as a useful alternative in such cases.

15.5.4 Colorectal Cancer: Recurrence

Standard treatment for rectal cancer has been considered to be preoperative chemoradiotherapy followed by surgery (typically total mesorectal excision [TME]). Control is achieved in most cases, but local recurrence is sometimes encountered. In such cases, SBRT to the recurrent site with doses of 25 Gy in 5 fractions has been safely applied, achieving fairly good local control.

15.5.5 Lymph Node Oligometastases

In various cancers of the chest, abdomen, and pelvis, recurrence appears as solitary lymph node involvement alone. This is called oligometastasis, and the prognosis of this pathology is relatively good compared with systemic disease. In such occasions, SBRT might be indicated.

15.5.6 Benign Diseases

For the treatment of heart rhythm disorders such as atrial fibrillation, SBRT has been attempted in animal experiments to ablate the electrical pathway around the pulmonary vein. This approach appears effective [31]. If this technique enters clinical use in the future, the number of patients treated by SBRT will become enormous, as atrial fibrillation is the most common heart disease.

References

1. Brenner DJ, Hall EJ. Fractionation and protraction for radiotherapy of prostate carcinoma. Int J Radiat Oncol Biol Phys. 1999;43:1095–101.
2. Daşu A. Is the alpha/beta value for prostate tumours low enough to be safely used in clinical trials? Clin Oncol (R Coll Radiol). 2007;19:289–301.
3. Brenner DJ. Fractionation and late rectal toxicity. Int J Radiat Oncol Biol Phys. 2004;60:1013–5.
4. Hanks GE, Hanlon AL, Pinover WH, et al. Dose selection for prostate cancer patients based on dose comparison and dose response studies. Int J Radiat Oncol Biol Phys. 2000;46:823–32.
5. Pollack A, Smith LG, Von Eschenbach AC. External beam radiotherapy dose response characteristics of 1127 men with prostate cancer treated in the PSA era. Int J Radiat Oncol Biol Phys. 2000;48:507–12.
6. Lloyd-Davies RW, Collins CD, Swan AV. Carcinoma of prostate treated by radical external beam radiotherapy using hypofractionation. Twenty-two years' experience (1962–1984). Urology. 1990;36:107–11.
7. Madsen BL, His RA, Pham HT, et al. Stereotactic hypofractionated accurate radiotherapy of the prostate (SHARP), 33.5 Gy in five fractions for localized disease: first clinical trial results. Int J Radiat Oncol Biol Phys. 2007;67:1099–105.
8. Pham HT, Song G, Badiozamani K, et al. Five-year outcome of stereotactic hypofractionated accurate radiotherapy of the prostate (SHARP) for patients with low-risk prostate cancer. Int J Radiat Oncol Biol Phys. 2010;78:S58.
9. King CR, Brooks JD, Gill H, et al. Stereotactic body radiotherapy for localized prostate cancer: interim results of a prospective phase II clinical trial. Int J Radiat Oncol Biol Phys. 2009;73:1043–8.
10. King CR, Brooks JD, Gill H, et al. Long-term outcomes from a prospective trial of stereotactic body radiotherapy for low-risk prostate cancer. Int J Radiat Oncol Biol Phys. 2012;82:877–82.
11. Friedland JL, Freeman DE, Masterson-McGary ME, et al. Stereotactic body radiotherapy: an emerging treatment approach for localized prostate cancer. Technol Cancer Res Treat. 2009;8:387–92.
12. Katz AJ, Santoro M, Ashley R, et al. Stereotactic body radiation therapy for low- and low-intermediate-risk prostate cancer: is there a dose effect? Front Oncol. 2011;1:49.
13. Katz AJ, Santoro M, Diblasio F, et al. Stereotactic body radiotherapy for localized prostate cancer: disease control and quality of life at 6 years. Radiat Oncol. 2013;8:118.
14. Meier R, Beckman A, Kaplan I, et al. Stereotactic radiotherapy for organ-confined prostate cancer: early toxicity and quality of life outcomes from a multi-institutional trial. Int J Radiat Oncol Biol Phys. 2010;78:S57.
15. Boike TP, Lotan Y, Cho LC, et al. Phase I dose-escalation study of stereotactic body radiation therapy for low- and intermediate-risk prostate cancer. J Clin Oncol. 2011;29:2020–6.
16. RTOG 0938 (Radiation Therapy Oncology Group). http://www.rtog.org/. Last accessed 08 July 2014
17. Yu JB, Cramer LD, Herrin J, et al. Stereotactic body radiation therapy versus intensity-modulated radiation therapy for prostate cancer: comparison of toxicity. J Clin Oncol. 2014;3212:1195–201.
18. Sahgal A, et al. Vertebral compression fracture after spine stereotactic body radiotherapy: a multi-institutional analysis with a focus on radiation dose and the spinal instability neoplastic score. J Clin Oncol. 2013;31:1–6.
19. Shelley X, et al. Stereotactic body radiation therapy for management of spinal metastases in patients without spinal cord compression: a phase 1–2 trial. Lancet Oncol. 2012;13:395–402.
20. Gerszten PC, et al. Clinical experience in 500 cases from a single institution. Spine. 2007;32:193–9.
21. Sahgal A, et al. Probabilities of radiation myelopathy specific to stereotactic body radiation therapy to guide safe practice. Int J Radiat Oncol Biol Phys. 2012;85:341–7.

22. Cox BW, et al. Esophageal toxicity from high-dose, single-fraction paraspinal stereotactic radiosurgery. Int J Radiat Oncol Biol Phys. 2012;83:e661–7.
23. http://www.nccn.org/professionals/physician_gls/pdf/pancreatic.pdf
24. Koong AC, Le QT, Ho A, et al. Phase I study of stereotactic radiosurgery in patients with locally advanced pancreatic cancer. Int J Radiat Oncol Biol Phys. 2004;58(4):1017–21.
25. Schellenberg D, Goodman KA, Lee F, et al. Gemcitabine chemotherapy and single-fraction stereotactic body radiotherapy for locally advanced pancreatic cancer. Int J Radiat Oncol Biol Phys. 2008;72(3):678–86.
26. Mahadevan A, Miksad R, Goldstein M, et al. Induction gemcitabine and stereotactic body radiotherapy for locally advanced nonmetastatic pancreas cancer. Int J Radiat Oncol Biol Phys. 2011;81(4):e615–22.
27. Mori Y, Kondziolka D, Flickinger JC, et al. Stereotactic radiosurgery for brain metastasis from renal cell carcinoma. Cancer. 1998;83(2):344–53.
28. Svedman C, Karlsson K, Rutkowska E, et al. Stereotactic body radiotherapy of primary and metastatic renal lesions for patients with only one functioning kidney. Acta Oncol. 2008;47(8):1578–83.
29. Kaplan ID, Redrosa I, Martin C, et al. Results of a phase I dose escalation study of stereotactic radiosurgery for primary renal tumors. Int J Radiat Oncol Biol Phys. 2010;78:S191.
30. Onishi H. Personal communication
31. Sharma A, Wong D, Weidlich G, et al. Noninvasive stereotactic radiosurgery (CyberHeart) for creation of ablation lesions in the atrium. Heart Rhythm. 2010;7(6):802–10.

Part VII
Development of Machines

Chapter 16
Development and Clinical Application of Vero4DRT System

Yukinori Matsuo, Masaki Kokubo, and Masahiro Hiraoka

16.1 Introduction

Stereotactic body radiotherapy (SBRT) was developed as a new treatment modality for early stage lung cancer in the late 1990s. Many retrospective studies and several multi-institutional prospective trials [1–3] have demonstrated excellent local control with acceptable toxicity after SBRT. Thus, SBRT is now an important treatment option for patients with early stage non-small-cell lung cancer who are medically inoperable [4].

Current three-dimensional radiotherapy techniques can ensure high accuracies in treatment delivery in a few millimeter levels for a static target. However, for a moving target, additional techniques for motion management are required [5, 6]. When the whole trajectory of tumor movement is covered by an irradiation field, adjacent normal tissues are also widely included into the field. That might lead to toxicities and to limit the indication of SBRT to a smaller tumor or to a less-moving tumor. A new four-dimensional (4D) irradiation technique that can deliver a high dose to the tumor and limit a dose to normal tissues will have the potential to improve the outcomes and to expand the indications of SBRT.

The Vero4DRT (formerly called the MHI-TM2000; Mitsubishi Heavy Industries [MHI] Ltd., Tokyo, Japan, and BrainLab AG, Feldkirchen, Germany; Fig. 16.1) is a novel and innovative radiotherapy system. Two major advantages of this system are high-precision image-guided radiotherapy (IGRT) and 4D

Y. Matsuo (✉) • M. Hiraoka
Department of Radiation Oncology and Image-Applied Therapy, Graduate School of Medicine, Kyoto University, 54, Shogoin-Kawaharacho, Sakyo, Kyoto 606-8507, Japan
e-mail: ymatsuo@kuhp.kyoto-u.ac.jp

M. Kokubo
Department of Radiation Oncology, Kobe City Medical Center General Hospital, Kobe, Japan

Division of Radiation Oncology, Institute of Biomedical Research and Innovation, Kobe, Japan

Fig. 16.1 Vero4DRT system

irradiation of dynamic tumor tracking (DTT). This paper introduces development, physics evaluations and clinical applications of the Vero4DRT system.

16.2 Specification of Vero4DRT

A system overview of Vero4DRT is shown in Fig. 16.2. The characteristic components of the system are an O-ring gantry, a beam delivery system, an imaging system and a precise robotic couch system. The rigid O-ring gantry supports both the subsystems of beam delivery and imaging, that allows accurate beam delivery and image guidance. The O-ring can skew around the vertical axis, which realizes non-coplanar irradiation without couch movement that may cause an intrafractional setup error.

The beam delivery subsystem consists of an ultra-small C-band linear accelerator (LINAC), multi-leaf collimators (MLC) and a gimbals mechanism. The LINAC produces 6-megavolt (MV) photon beam with a maximal dose rate of 500 cGy/min. The MLC has 30 pairs of leaves of 5-mm thickness at the isocenter and allows a maximal field size of 15×15 cm^2. The gimbals can swing the treatment beam along the two orthogonal gimbals (pan and tilt rotations) up to ± 2.4 degrees, which corresponds to ± 4.2 cm in each direction on the isocenter plane perpendicular to the beam. The gimbals mechanism realizes high accuracy in positioning of static treatment beam and DTT irradiation for a moving target.
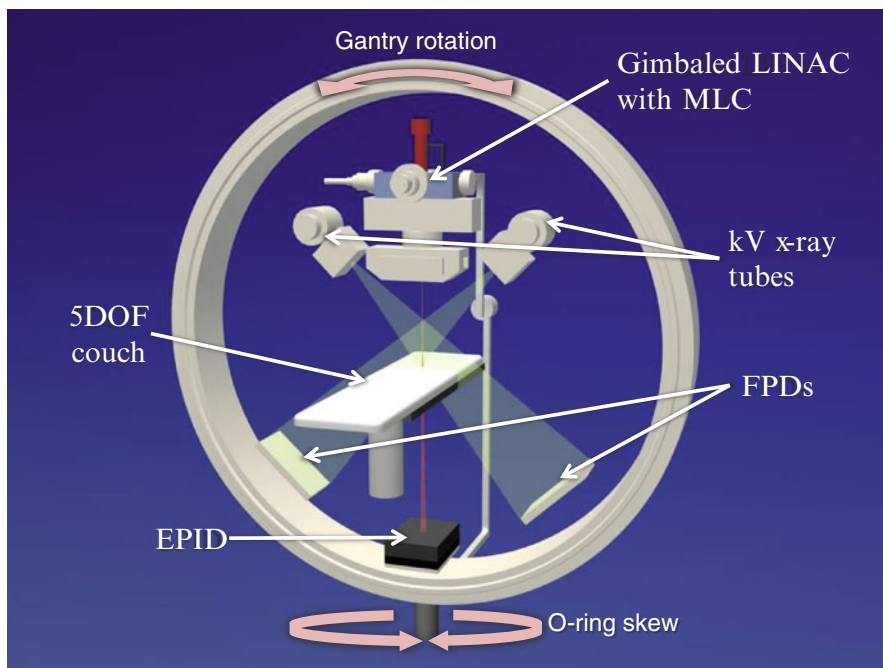
Fig. 16.2 Internal configuration of the Vero4DRT. Abbreviations: *LINAC* linear accelerator, *MLC* multi-leaf collimator, *DOF* degree of freedom, *FPD* flat panel detector, *EPID* electric portal imaging device

The imaging subsystem includes two sets of kV x-ray on-board imaging (OBI) and an electric portal imaging device (EPID). The OBI provides orthogonal radiographs or cone-beam computed tomography (CBCT) for image-guided setup. The ExacTrac system (BrainLab AG) is integrated with the OBI system. The EPID visualizes a treatment field with a treatment beam through the patient body. Both of the imaging systems are used for real-time monitoring of treated position in DTT.

The robotic couch system can compensate setup errors with 5 degrees of freedom (translations along vertical, coronal and sagittal axes; and rotations of roll and pitch). The remaining yaw rotation is compensated with the O-ring skew. An infrared (IR) camera system helps precise localization of the couch. The IR camera also works for monitoring of respiratory phases via markers on the abdomen during DTT radiotherapy.

16.3 History of Development

The project for the development of Vero4DRT had started in 2000 in MHI. MHI, already having succeeded to introduce an ultrasmall C-band LINAC at the time [7], tried to develop a new radiotherapy machine with this LINAC on to gimbals

mechanism, thus possessing the ability to track and irradiate a moving target. To realize this objective, MHI have started the collaboration with Kyoto University (Kyoto, Japan), Institute of Biomedical Research and Innovation (IBRI; Kobe, Japan) as medical partners. Machine design and concepts were discussed and decided in the collaboration team including functional enhancement of image guidance, high precision setup, and DTT. Some prototype machines were made and tested between 2002 and 2005.

The clinical version of the IGRT system was developed in 2006. The system was firstly approved by the US Food and Drug Administration in August 2007, and then by the Japanese Ministry of Health, Labor, and Welfare in January 2008 as "MHI-TM2000". The CE Mark certification in Europe was acquired in 2010. Outside Japan, the unit is marketed as the "Vero" through BrainLAB AG as an original equipment manufacturer (OEM) supply partner.

The first application of the MHI-TM2000 to clinical treatment had been done in May 2008 at IBRI [8]. The clinical treatment initially applied to palliation of symptoms with metastasis to the bone or the lymph node. Then, the application was extended to high-precision radiotherapy with curative intent including SBRT for the lung using static beams and intensity modulated radiotherapy (IMRT) for the prostate. Kyoto University started treatment with the system in October 2010.

Based on the initial clinical experiences and physics evaluations, DTT with real-time monitoring was started with SBRT for lung tumor in September 2011 at Kyoto University [9] and in December 2011 at IBRI. DTT-SBRT for the liver was initiated in 2012 at UZ Brussel, followed by Kyoto University in March 2013. After success of DTT-SBRT, MHI changed the market name for the system in Japan from "MHI-TM2000" to "Vero4DRT". DTT was also combined with IMRT. Kyoto University performed DTT-IMRT for pancreatic cancer in June 2013 [10, 11]. This is the world's first case treated with tumor tracking IMRT.

16.4 Physics Evaluation and Clinical Application

16.4.1 *Physics Evaluation*

For introduction of the new treatment technique to the clinics, extensive basic evaluation has been done. Table 16.1 summarizes results of the physics evaluations for the Vero4DRT system. The evaluated items include accuracy in static beam delivery [12, 13], specification of MLC [14], accuracy in image guidance [15], errors in dynamic tracking irradiation [12, 16–21] and commissioning process [22].

Table 16.1 Summary of physics evaluations for the Vero4DRT system

Evaluation		Results	Author (year)
Static beam	Positioning accuracy (RMS)	0.08 mm (pan axis), 0.10 mm (tilt axis)	Kamino (2006) [12]
	IC radius in starshot	0.12–0.43 mm (gantry), 0.01–0.08 mm (O-ring)	Depuydt (2012) [13]
MLC	Field size	<0.5 mm	Nakamura (2010) [14]
	Leaf position	0.0 ± 0.1 mm	
	Leakage	<0.21 % (interleaf), <0.12 % (intraleaf)	
Image guidance	Error at 50-mm offcenter	0.2 mm (kV x-ray), 1.0 mm (CBCT)	Miyabe (2011) [15]
Tracking	Beam positioning error	<0.6 mm	Kamino (2006) [12]
(Direct tracking)	Motion blurring effects	significantly reduced	Takayama (2009) [16]
	System lag	47.7 ms (pan), 47.6 ms (tilt)	Depuydt (2011) [17]
	Tracking error (90-percentile)	0.54 mm	
	Tracking error (RMS)	1.2 mm (prediction), 0.1 mm (mechanical), 1.2 mm (total)	Mukumoto (2012) [18]
Tracking	Tracking error (SD)	0.55 mm (pan direction), 0.95 mm (tilt direction)	Depuydt (2013) [19]
(Model based tracking)	4D modeling error (SD)	0.1–1.0 mm (LR), 0.1–1.6 mm (AP), 0.2–1.3 mm (SI)	Akimoto (2013) [20]
	Tracking error (95-percentile)	<1 mm	Mukumoto (2013) [21]
Other	Commissioning process		Solberg (2014) [22]

Abbreviations: *RMS* root mean square, *IC* isocenter, *MLC* multi-leaf collimator, *CBCT* cone-beam computed tomography, *SD* standard deviation, *LR* left-right, *AP* anteroposterior, *SI* superoposterior

16.4.2 Initial Clinical Application

In the first phase of the clinical application, ten palliative treatments were performed to the patients with bone metastases and/or lymph node metastases at IBRI [8]. The purpose of the phase was to check the usability and the limitation of the system functions. The typical IGRT session for palliation took less than 10 min including patient setup, image-guidance, verification, and beam delivery. Through the first phase, an IGRT flow suitable for the system was established. In the next phase, high-precision radiation treatments including IMRT for the prostate and SBRT for the lung were performed. Image-guided setup verification after couch correction demonstrated that the setup error was mostly within 1 mm. Accuracies in image guidance, couch movement and beam delivery were confirmed in the clinical situations.

16.4.3 Dynamic Tracking Treatment

Based on the physics and clinical evaluations as described above, DTT with the Vero4DRT was considered to be feasible. We conducted a prospective feasibility study on DTT-SBRT for the lung after approval from the institutional review board and a revision of the software in the Vero.

Details on our procedures for DTT were available in the previous paper [23]. Figure 16.3 summarizes the treatment steps. Spherical gold markers with a diameter of 1.5 mm (FMR-201CR; Olympus Medical Systems, Tokyo, Japan) were placed around the tumor under bronchoscope guidance prior to treatment planning. A simulation with 4D CT was performed 1 week after the marker placement. An internal target volume (ITV) for tracking was delineated on a breath-hold CT at end-exhale followed by modification to compensate intrafractional variations between the fiducials and the tumor using the 4D CT [24]. The 4D modeling, which correlates abdominal motion with tumor position during respiration, was performed in the planning procedure and in each treatment fraction. Planning target volume (PTV) for tracking was defined as the ITV plus additional internal margins and setup error. The additional internal margins were defined individually for each patient, considering the 4D modeling errors and baseline drift of the abdominal position. Prescription dose was 48 or 56 Gy in 4 fractions at the isocenter. Treatment beam irradiation was performed with the gimbaled x-ray head toward predicted position based on the 4D model and the abdominal wall. During the irradiation, the tumor and the fiducials were monitored with OBI and EPID.

Five patients were enrolled into this study during the initial 3 months (Table 16.2). Tumor tracking irradiation was successfully done for 4 of the 5 patients. The remaining one patient had highly irregular respiration which did not allow the tumor position to be predicted with the abdominal wall.

Fig. 16.3 A summary of procedures for dynamic tumor tracking radiotherapy

Pre-simulation
• Fiducial marker placement

Simulation
• 4D CT scan
• 4D modeling
• Target volume definition (ITV and PTV)
• Beam arrangement and dose prescription

Treatment
• 4D modeling
• Irradiation with real-time monitoring
• Rebuild of 4D model, if needed
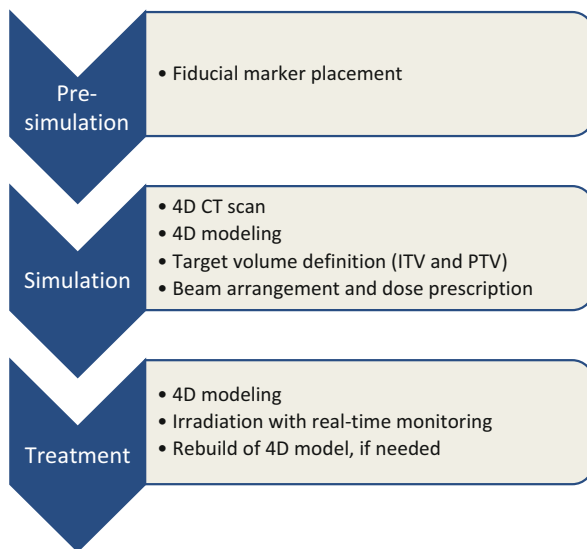
Table 16.2 Patient characteristics

Patient	Age	Gender	PS	Tumor diameter (mm)	Histology	Prescribed dose (Gy)
1	85	F	1	32	Metastasis from colon cancer	56
2	82	M	2	15	Unconfirmed	48
3	86	F	1	21	Adenocarcinoma	48
4	84	M	0	24	Squamous cell carcinoma	48
5	84	M	1	12	Adenocarcinoma	–

Abbreviations: *PS* performance status

Dose-volume metrics were compared in the 4 patients between the tracking irradiation and conventional SBRT using an in-house developed software. The tracking irradiation could reduce lung doses by about 20 %, while tumor doses were not spoiled (Table 16.3 and Fig. 16.4). A mean treatment time per fraction was 36 min. The log files revealed the 99-percentile intervals of the errors which were defined as difference between the delivered position and detected tumor position were 1.6 mm, 3.4 mm and 1.3 mm in mediolateral, craniocaudal and anteroposterior directions, respectively.

The success in dynamic tracking in lung SBRT drove us to apply the technique to liver SBRT. The procedures for the liver were almost the same as in the lung except that a linear fiducial marker (Visicoil; IBA Dosimetry GmbH, Schwarzenbruck, Germany) was used. For the first patient, DTT reduced PTV volume from 133.3 to 85.6 cc and mean liver dose from 14.3 to 11.5 Gy.

Table 16.3 Dose-volume parameter comparison between tracking and static irradiation methods

	PTV volume (cc)		GTV D95 (Gy)		Mean lung dose (Gy)		Lung V20 (%)	
Patient	Tracking	Static	Tracking	Static	Tracking	Static	Tracking	Static
1	87.0	113.6	54.2	53.9	8.0	9.3	13.7	17.2
2	34.6	55.8	46.4	46.6	2.5	2.7	3.5	4.1
3	38.0	63.3	47.0	47.7	3.1	4.3	4.2	6.2
4	50.1	72.4	44.2	44.7	4.3	5.1	5.5	7.0
Average	52.4	76.3	47.9	48.2	4.5	5.4	6.7	8.6

Abbreviations: *PTV* planning target volume, *GTV* gross tumor volume, *D95* dose covering 95 % volume, *V20* volume irradiated with 20 Gy or more
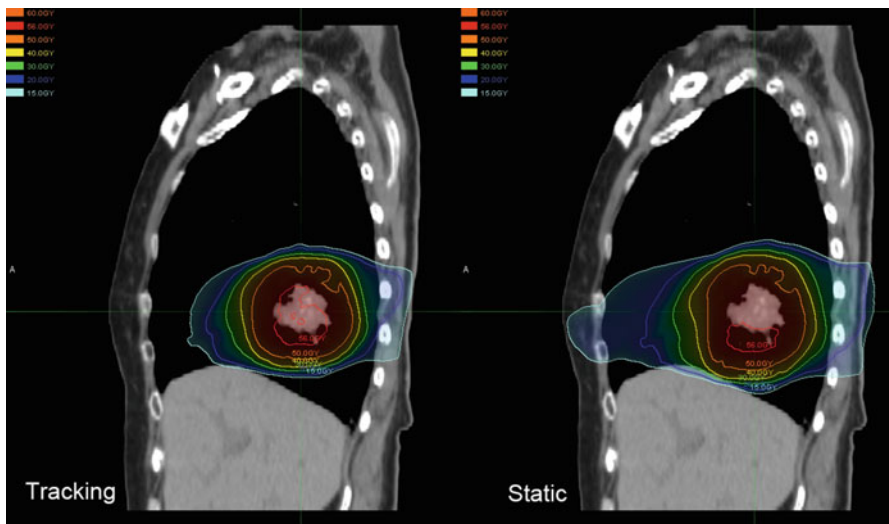
Fig. 16.4 Comparison of dose distributions in Patient 1 between dynamic tumor tracking (*left*) and conventional static irradiation (*right*)

To our best knowledge, the Vero4DRT is the first system capable of simultaneous dynamic tracking irradiation and real-time monitoring of the tumor in patients with lung cancer. Two major advantages were gained from this novel technique. The first is that tumor position can be monitored in real time using kV imagers and an EPID. Several errors should be considered in the 4D irradiation, including prediction error and beam delivery errors. OBI can ensure that the positions of the tumor and fiducial markers, and EPID can visualize the tumor in the center of the irradiation field. Furthermore, log files allow retrospective confirmation of the accuracy in the delivery of tumor tracking after treatment. The second is that no extra treatment time over conventional technique and no special training for breath control are needed for the 4D treatment, which is clinically beneficial both for patient comfort and the throughput of the treatment system.

16.5 Future Directions

The Vero4DRT system has much potential for novel irradiation techniques because it has high degrees of freedom in irradiation angles with the gantry rotation, the O-ring skew and the pan-tilt movements of the gimbaled x-ray head. One is the dynamic wave arc technique [25]. This technique can deliver multiple non-coplanar beams during a rotation of the gantry, which leads to reduction in monitor unit number and treatment time. The dynamic wave arc could achieve comparable dose distribution to that with static beam IMRT. The other potential technique is dynamic tracking with conformal arc irradiation [26]. The phantom-based study confirmed that the gimbal positional accuracy was not degraded by gantry motion and that the dose distribution in a moving phantom with tracking arc irradiation agreed well with that in static conditions.

The superb imaging system may also contribute to expand the application of IGRT technique. The current imaging system is used to monitor tumor position in real time during a treatment fraction, although no modification of treatment beam is performed. If we could acquire information on tumor deformation or shrinkage through the imagers, the real-time adaptive treatment might be possible.

In summary, the history of development and clinical applications of the Vero4DRT have been described. The system has high accuracies both in image guidance and in treatment delivery. It is also capable of dynamic tumor tracking irradiation with real-time monitoring. Further development is anticipated towards a new paradigm in radiotherapy.

References

1. Baumann P, Nyman J, Hoyer M, Wennberg B, Gagliardi G, Lax I, et al. Outcome in a prospective phase II trial of medically inoperable stage I non-small-cell lung cancer patients treated with stereotactic body radiotherapy. J Clin Oncol. 2009;27:3290–6.
2. Timmerman R, Paulus R, Galvin J, Michalski J, Straube W, Bradley J, et al. Stereotactic body radiation therapy for inoperable early stage lung cancer. JAMA. 2010;303:1070–6.
3. Nagata Y, Hiraoka M, Shibata T, Onishi H, Kokubo M, Karasawa K, et al. Stereotactic body radiation therapy for T1N0M0 non-small cell lung cancer: first report for inoperable population of a Phase II Trial by Japan Clinical Oncology Group (JCOG 0403). Int J Radiat Oncol Biol Phys. 2012;84:S46.
4. National Comprehensive Cancer Network. Non-small cell lung cancer version 3.2014. Available from: http://www.nccn.org/professionals/physician_gls/pdf/nscl.pdf. Accessed 16 Feb 2014.
5. Matsuo Y, Onishi H, Nakagawa K, Nakamura M, Ariji T, Kumazaki Y, et al. Guidelines for respiratory motion management in radiation therapy. J Radiat Res. 2013;54:561–8.
6. Keall PJ, Mageras GS, Balter JM, Emery RS, Forster KM, Jiang SB, et al. The management of respiratory motion in radiation oncology report of AAPM Task Group 76. Med Phys. 2006;33:3874–900.

7. Kamino Y, Miura S, Kokubo M, Yamashita I, Hirai E, Hiraoka M, et al. Development of an ultrasmall C-band linear accelerator guide for a four-dimensional image-guided radiotherapy system with a gimbaled x-ray head. Med Phys. 2007;34:1797–808.

8. Takayama K, Kokubo M, Mizowaki T, Nagano K, Narita Y, Yamashita M, et al. Initial clinical experiences of a newly developed Image-guided Radiotherapy (IGRT) system "MHI-TM2000". Int J Radiat Oncol Biol Phys. 2009;75:S120.

9. Matsuo Y, Sawada A, Ueki N, Miyabe Y, Nakamura M, Yano S, et al. An initial experience of dynamic tumor tracking irradiation with real-time monitoring using Vero4DRT (MHI-TM2000). Radiother Oncol. 2012;103:S69.

10. Mitsubishi Heavy Industries. Press Information: Pancreatic Cancer Therapy by MHI's "vero4DRT" Radiation Therapy System – World's First Application of Dynamic Tracking with IMRT Monitored in Real Time. Available from: http://www.mhi.co.jp/en/news/story/1307301694.html. Accessed 12 Mar 2004.

11. Nakamura A, Mizowaki T, Itasaka S, Nakamura M, Ishihara Y, Mukumoto N, et al. First implementation of intensity-modulated dynamic tumor-tracking RT in pancreatic cancer using a gimbaled linac. Radiother Oncol. 2014;111:S500.

12. Kamino Y, Takayama K, Kokubo M, Narita Y, Hirai E, Kawawda N, et al. Development of a four-dimensional image-guided radiotherapy system with a gimbaled X-ray head. Int J Radiat Oncol Biol Phys. 2006;66:271–8.

13. Depuydt T, Penne R, Verellen D, Hrbacek J, Lang S, Leysen K, et al. Computer-aided analysis of star shot films for high-accuracy radiation therapy treatment units. Phys Med Biol. 2012;57:2997–3011.

14. Nakamura M, Sawada A, Ishihara Y, Takayama K, Mizowaki T, Kaneko S, et al. Dosimetric characterization of a multileaf collimator for a new four-dimensional image-guided radiotherapy system with a gimbaled x-ray head, MHI-TM2000. Med Phys. 2010;37:4684–91.

15. Miyabe Y, Sawada A, Takayama K, Kaneko S, Mizowaki T, Kokubo M, et al. Positioning accuracy of a new image-guided radiotherapy system. Med Phys. 2011;38:2535–41.

16. Takayama K, Mizowaki T, Kokubo M, Kawada N, Nakayama H, Narita Y, et al. Initial validations for pursuing irradiation using a gimbals tracking system. Radiother Oncol. Elsevier Ireland Ltd. 2009;93:45–9.

17. Depuydt T, Verellen D, Haas O, Gevaert T, Linthout N, Duchateau M, et al. Geometric accuracy of a novel gimbals based radiation therapy tumor tracking system. Radiother Oncol. 2011;98:365–72.

18. Mukumoto N, Nakamura M, Sawada A, Takahashi K, Miyabe Y, Takayama K, et al. Positional accuracy of novel x-ray-image-based dynamic tumor-tracking irradiation using a gimbaled MV x-ray head of a Vero4DRT (MHI-TM2000). Med Phys. 2012;39:6287–96.

19. Depuydt T, Poels K, Verellen D, Engels B, Collen C, Haverbeke C, et al. Initial assessment of tumor tracking with a gimbaled linac system in clinical circumstances: a patient simulation study. Radiother Oncol. 2013;106:236–40.

20. Akimoto M, Nakamura M, Mukumoto N, Tanabe H, Yamada M, Matsuo Y, et al. Predictive uncertainty in infrared marker-based dynamic tumor tracking with Vero4DRT. Med Phys. 2013;40:091705.

21. Mukumoto N, Nakamura M, Sawada A, Suzuki Y, Takahashi K, Miyabe Y, et al. Accuracy verification of infrared marker-based dynamic tumor-tracking irradiation using the gimbaled x-ray head of the Vero4DRT (MHI-TM2000). Med Phys. 2013;40:041706.

22. Solberg TD, Medin PM, Ramirez E, Ding C, Foster RD, Yordy J. Commissioning and initial stereotactic ablative radiotherapy experience with Vero. J Appl Clin Med Phys. 2014;15:205–25.

23. Matsuo Y, Ueki N, Takayama K, Nakamura M, Miyabe Y, Ishihara Y, et al. Evaluation of dynamic tumour tracking radiotherapy with real-time monitoring for lung tumours using a gimbal mounted linac. Radiother Oncol. 2014;112:360–4.

24. Ueki N, Matsuo Y, Nakamura M, Mukumoto N, Iizuka Y, Miyabe Y, et al. Intra- and interfractional variations in geometric arrangement between lung tumours and implanted markers. Radiother Oncol. 2014;110:523–8.
25. Mizowaki T, Takayama K, Nagano K, Miyabe Y, Matsuo Y, Kaneko S, et al. Feasibility evaluation of a new irradiation technique: three-dimensional unicursal irradiation with the Vero4DRT (MHI-TM2000). J Radiat Res. 2013;54:330–6.
26. Ono T, Miyabe Y, Yamada M, Shiinoki T, Sawada A, Kaneko S, et al. Geometric and dosimetric accuracy of dynamic tumor-tracking conformal arc irradiation with a gimbaled x-ray head. Med Phys. 2014;41:031705.

Chapter 17
Real Time Tracking Radiotherapy (RTRT) System

Rikiya Onimaru, Shinichi Shimizu, Hiroki Shirato, and Masayori Ishikawa

17.1 Introduction

Real time tracking radiotherapy system (RTRT system) was developed in 1998 with support of the Education Ministry Grant-in-Aid for Scientific Research [1]. The 1st system was launched at Hokkaido University Hospital. The 1st RTRT system was able to recognize a 2.0 mm gold marker location in patient with an accuracy of 1 mm every 0.03 s during delivery of irradiation from synchronized linac [2]. The system made "Wait and Shoot" radiation method more precise than ever before. The 1st system was composed of four sets of image intensifier on the ceiling and x-ray tube under the floor [2] and this system calculated the marker location in 3D coordinate [3]. When a gold marker inserted in patient was out of the range of gating window, linac stopped irradiation. When a gold marker was inside the range of gating window from the planned position, irradiation was delivered. Dose distribution on X-ray films on moving phantom with RTRT system was comparable to dose distribution on static phantom [2]. Marker recognition was precisely done in clinical setting with appropriate gating window (permitted dislocation) [4].

We now have 2nd generation RTRT system. The 2nd generation RTRT system is composed of two set of fluoroscope with image intensifier (I.I.) on ceiling and X-ray tube under the floor. The position of fluoroscope is able to change by rotating on the ceiling and under the floor (Fig. 17.1).

R. Onimaru (✉) • S. Shimizu • H. Shirato
Department of Radiation Medicine, Hokkaido University Graduate School of Medicine, Kita 15 Nishi 7, Kita-ku, Sapporo, Hokkaido, Japan
e-mail: onimaru-rad@umin.ac.jp

M. Ishikawa
Department of Medical Physics and Engineering, Graduate School of Medicine, Hokkaido University, Sapporo, Japan

Fig. 17.1 RTRT system in Hokkaido University. *Black arrow* shows the image intensifier (I.I.)

We have reported the clinical results of stereotactic body radiation therapy (SBRT) for non-small cell lung cancer (NSCLC), hepatocellular carcinoma (HCC), adrenal tumor, and spinal schwannoma [5–8]. Analysis of marker motion was also done and several interesting findings were reported [9–12].

In this article, we describe experiences about gold marker insertion, clinical results of SBRT using RTRT system, analysis of marker movements, and the future direction of RTRT system.

17.2 The Method of Gold Marker Insertion

17.2.1 Non-small Cell Lung Cancer

The method of implantation of gold marker into lung is described by Harada et al. [13] and Imura et al. [14]. They used bronchoscope and catheter to insert gold markers. Gold marker was inserted into catheter and pushed by hard plastic wire. The gold marker was inserted and wedged into the bronchial trees near the tumor. The location of bronchoscope, catheter, and markers were visualized by fluoroscopy [13].

Imura et al. reported that 94 % of markers that were seen in CT for radiotherapy planning were detected throughout the radiotherapy delivery [14]. They also reported that the 95 % of distance variation between implanted markers was within 2 mm. The location of tumor and marker fixation rate was correlated. The fixation rate in the left upper lobe was lower than in the other lobes. They suggested that learning curve existed. Pneumothorax was found in only 1 of 57 patients [14].

Imura et al. reported the histological change after marker insertion. They found that fibrotic change was seen after 5–7 days after marker insertion [15]. They suggested that radiotherapy should be started above 5 days after gold marker insertion because marker dislocation tended not to occur due to fibrotic change around the marker.

17.2.2   Hepatocellular Carcinoma

Gold marker was also able to insert into liver and prostate [16, 17]. Implantation of the marker into liver through skin was done under ultrasound and/or CT guidance. The implantation kit for spinal lesions and prostate and liver tumors was manufactured by Medikit Co. Ltd. (Tokyo, Japan). There was only 1 migration of 21 implanted markers in liver. Shirato et al. reported that no serious complication due to marker implantation was observed [16]. However, we experienced transient bile ductal bleeding in 1 patient in SBRT for HCC after the report of Taguchi et al. [6].

17.3   CT Acquisition and Treatment Planning

CT for treatment planning was performed 3 days after insertion of gold marker in general. Patients were asked to hold breath at exhale phase during CT acquisition. Slice thickness was 2.5 mm in principle.

Gross tumor volume and clinical target volume (CTV) was made as other SBRT methods without RTRT system. Markers were also contoured. Gating window was usually 2 mm, but this was changed to 3 mm by respiratory irregularity in actual treatment. PTV was made by adding margin of gating window and other uncertainty to CTV, the margin was usually 5 mm. Six beams, 4 coplanar and 2 - non-coplanar beams, were typically selected for treatment in Hokkaido University Hospital. Figure 17.2 shows the flow chart from the assessment of indication to the treatment.

Fig. 17.2 Flow chart of treatment with RTRT system
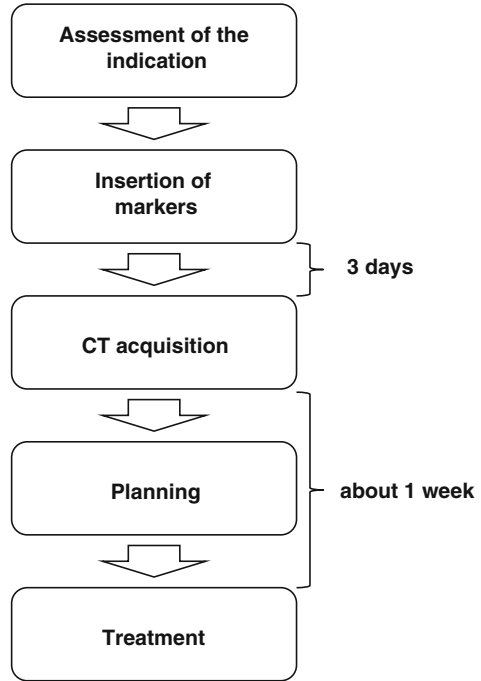
17.4 Clinical Results

17.4.1 *Non-small Cell Lung Cancer*

Inoue et al. reported the results of stereotactic body radiation therapy (SBRT) using RTRT system for non-small cell lung cancer (NSCLC) [5]. They used superposition algorithm for inhomogeneity correction and 48 Gy in 4 fractions at isocenter or 40 Gy in 4 fractions at D_{95} of PTV. The 5-year local control rate (LC) was 78 % (95 % confidence interval (CI), 68–90 %) and the 5-year overall survival rate (OS) was 64 % (95 % CI, 53–78 %), respectively. The 5 year overall survival (OS) in patients with T1a was 75 %. The 5 year OS in patients with T1b or T2 ($p = 0.01$) was 56 %, which was statistically worse than that of patients with T1a ($P = 0.01$). They also reported that the maximum amplitude of marker movement in lower lobe was significantly larger than that in upper lobe; however, there was no significant difference in LC between the lower lobe and the other lobe. The fact that no difference existed in LC between the lower and the other lobes shows that we treat properly the moving tumor using RTRT system.

17.4.2 Hepatocellular Carcinoma

Taguchi et al. reported the results of SBRT using RTRT system for 18 lesions of HCC [6]. Various dose fractionation schedule was used, and 48 Gy in 8 fractions at isocenter was mostly used (n = 7). A symptomatic complication due to the insertion of the fiducial marker occurred in 1 patient, who experienced transient bile ductal bleeding and inflammation. The 2 year OS was 44 % after SBRT and the LC within the CTV was 83 % at 30 months after SBRT. The intrahepatic control rate was 17 % at 2 years after SBRT. An adverse reaction due to radiation was seen in 2 patients. A transient gastric ulcer was occurred in 1 patient and radiation pneumonitis was occurred in 1 patient, respectively.

This result is difficult to interpret. Patients were highly selected, HCC shows multicentric nature, and dose was varied. Adding to that, several local treatments are effective for HCC. Surgery, RFA, and TACE is major therapy in Japan. Radiotherapy is not recognized as standard first treatment option for HCC. However, radiotherapy like SBRT or proton beam therapy is reported effective in retrospective studies; SBRT may be regarded as one of the effective local treatment based on future clinical trials.

17.4.3 Other Tumors

Katoh et al. reported the results of the treatment for metastatic adrenal tumor using RTRT system [7]. They treated 10 lesions with 48 Gy in 8 fractions and 1 lesion with 30 Gy in 8 fractions. They reported that no symptomatic adverse effects were observed and the actuarial freedom-from local progression rate was 100 % at 12 months. The concept of oligometastases changed the treatment policy for patients with small number of metastatic lesions [18]. Curative dose for metastatic adrenal tumor may be beneficial for the selected patients with metastatic adrenal tumor.

Onimaru et al. reported that the experience the radiotherapy treatment for spinal schwannoma using RTRT system [8]. They calculated the rotation using 3 markers. It seems to be important to consider the rotation and the deformation of target, however, the strategy to the rotation and the deformation is still to be investigated.

17.5 Marker Movement Analysis

RTRT system records log file about marker motion. The log file is very valuable because it is the exact data during irradiation delivery. Several investigators reported the results of analyzing log files of RTRT system and showed interesting results [9–12].

Seppenwoolde et al. developed analyzing system and reported the marker motion in the lung [9]. This report showed that respiratory movement of marker shows a hysteresis. It was the first report about baseline shift during the radiation delivery and intra-fractional error based on data during irradiation delivery [9].

Onimaru et al. reported the relationship between the marker location and the amplitude of marker movement in NSCLC [10]. They showed that marker movement for the craniocaudal direction was smaller in the anterior part and the cranial part of lung.

Onodera et al. evaluated the relationship between lung parenchymal findings on CT and the amplitude of marker movement [11]. They found that presence of fibrosis and pleural tumor contacts were weakly associated with marker motion. There was no correlation between lung fibrosis and marker motion in the lower lung. There was also no correlation between emphysematous finding and marker motion.

Log files of the patients with lung cancer were used to develop a dynamic-multileaf real-time tumor tracking [12]. Pepin et al. simulated the dynamic gating simulation based on log files of RTRT and showed that dynamic gating treatment had higher fluences with less tumor obstruction. Usefulness of new technique is able to be evaluated using log file analysis as Pepin et al. did.

Marker movement in liver was evaluated by Nishioka et al. [19]. The mean craniocaudal total movements were 15.98 ± 6.02 mm. They reported that the fluctuations from the baseline position in liver tumors were smaller than that in lung tumor. This result suggested that liver tumor motion was stable in amplitude compared with lung tumor. The reason of this phenomenon is unclear.

As shown here, the finding from log files of RTRT system contribute to the understanding of tumor or organ movement. The precise understandings of tumor and organ movement result in precise internal margin. It is critical to reduce margins in SBRT in order to avoid radiation morbidities. Analysis of log files of RTRT system is also contributing the developing the new technology like dynamic MLC and so on. Analysis of log files of RTRT system is important basic research in SBRT.

17.6 Future

RTRT system is developing. Miyamoto et al. developed the pattern recognition score prediction method using template pattern matching in order to minimize the fluoroscopic dose [20]. This method can reduce manual adjustment of x-ray tube voltage and so on. RTRT system is going to be combined with proton beam therapy system at Hokkaido University Hospital. It is concerned that gold markers had influence on dose distribution of proton beam. Matsuura et al. evaluate the effect of fiducial gold marker in proton beam therapy [21]. They evaluate the effect using Monte Carlo simulation and reported that 1.5 mm markers should be used to avoid the decrease in TCP and 2 mm markers should be used with more than 2 fields and

location of 2 mm markers should be determined carefully. Although there needs caution, RTRT system contribute to precise proton beam therapy.

17.7   Conclusion

RTRT system provides precise irradiation delivery. This system provides the precise SBRT and valuable information about organ motion during irradiation delivery. Analysis of log files of RTRT system shows interesting results and is beneficial to develop new technique to deal with respiratory motion. RTRT system is going to be combined with proton beam therapy system. It is expected that RTRT system contribute to precise radiotherapy including proton beam therapy.

References

1. Shirato H, Shimizu S, Shimizu T, Nishioka T, Miyasaka K. Real-time tumour-tracking radiotherapy. Lancet. 1999;353(9161):1331–2. doi:10.1016/S0140-6736(99)00700-X.
2. Shirato H, Shimizu S, Kitamura K, Nishioka T, Kagei K, Hashimoto S, et al. Four-dimensional treatment planning and fluoroscopic real-time tumor tracking radiotherapy for moving tumor. Int J Radiat Oncol Biol Phys. 2000;48(2):435–42.
3. Shirato H, Shimizu S, Kunieda T, Kitamura K, van Herk M, Kagei K, et al. Physical aspects of a real-time tumor-tracking system for gated radiotherapy. Int J Radiat Oncol Biol Phys. 2000;48(4):1187–95.
4. Shimizu S, Shirato H, Ogura S, Akita-Dosaka H, Kitamura K, Nishioka T, et al. Detection of lung tumor movement in real-time tumor-tracking radiotherapy. Int J Radiat Oncol Biol Phys. 2001;51(2):304–10.
5. Inoue T, Katoh N, Onimaru R, Shimizu S, Tsuchiya K, Suzuki R, et al. Stereotactic body radiotherapy using gated radiotherapy with real-time tumor-tracking for stage I non-small cell lung cancer. Radiat Oncol. 2013;8:69. doi:10.1186/1748-717X-8-69.
6. Taguchi H, Sakuhara Y, Hige S, Kitamura K, Osaka Y, Abo D, et al. Intercepting radiotherapy using a real-time tumor-tracking radiotherapy system for highly selected patients with hepatocellular carcinoma unresectable with other modalities. Int J Radiat Oncol Biol Phys. 2007;69 (2):376–80. doi:10.1016/j.ijrobp.2007.03.042.
7. Katoh N, Onimaru R, Sakuhara Y, Abo D, Shimizu S, Taguchi H, et al. Real-time tumor-tracking radiotherapy for adrenal tumors. Radiother Oncol. 2008;87(3):418–24. doi:10.1016/j.radonc.2008.03.013.
8. Onimaru R, Shirato H, Aoyama H, Kitakura K, Seki T, Hida K, et al. Calculation of rotational setup error using the real-time tracking radiation therapy (RTRT) system and its application to the treatment of spinal schwannoma. Int J Radiat Oncol Biol Phys. 2002;54(3):939–47.
9. Seppenwoolde Y, Shirato H, Kitamura K, Shimizu S, van Herk M, Lebesque JV, et al. Precise and real-time measurement of 3D tumor motion in lung due to breathing and heartbeat, measured during radiotherapy. Int J Radiat Oncol Biol Phys. 2002;53(4):822–34.
10. Onimaru R, Shirato H, Fujino M, Suzuki K, Yamazaki K, Nishimura M, et al. The effect of tumor location and respiratory function on tumor movement estimated by real-time tracking radiotherapy (RTRT) system. Int J Radiat Oncol Biol Phys. 2005;63(1):164–9. doi:10.1016/j.ijrobp.2005.01.025.

11. Onodera Y, Nishioka N, Yasuda K, Fujima N, Torres M, Kamishima T, et al. Relationship between diseased lung tissues on computed tomography and motion of fiducial marker near lung cancer. Int J Radiat Oncol Biol Phys. 2011;79(5):1408–13. doi:10.1016/j.ijrobp.2010.01.008.

12. Pepin EW, Wu H, Shirato H. Use of dMLC for implementation of dynamic respiratory-gated radiation therapy. Med Phys. 2013;40(10):101708. doi:10.1118/1.4820534.

13. Harada T, Shirato H, Ogura S, Oizumi S, Yamazaki K, Shimizu S, et al. Real-time tumor-tracking radiation therapy for lung carcinoma by the aid of insertion of a gold marker using bronchofiberscopy. Cancer. 2002;95(8):1720–7. doi:10.1002/cncr.10856.

14. Imura M, Yamazaki K, Shirato H, Onimaru R, Fujino M, Shimizu S, et al. Insertion and fixation of fiducial markers for setup and tracking of lung tumors in radiotherapy. Int J Radiat Oncol Biol Phys. 2005;63(5):1442–7. doi:10.1016/j.ijrobp.2005.04.024.

15. Imura M, Yamazaki K, Kubota KC, Itoh T, Onimaru R, Cho Y, et al. Histopathologic consideration of fiducial gold markers inserted for real-time tumor-tracking radiotherapy against lung cancer. Int J Radiat Oncol Biol Phys. 2008;70(2):382–4. doi:10.1016/j.ijrobp.2007.06.064.

16. Shirato H, Harada T, Harabayashi T, Hida K, Endo H, Kitamura K, et al. Feasibility of insertion/implantation of 2.0-mm-diameter gold internal fiducial markers for precise setup and real-time tumor tracking in radiotherapy. Int J Radiat Oncol Biol Phys. 2003;56(1):240–7.

17. Kitamura K, Shirato H, Shimizu S, Shinohara N, Harabayashi T, Shimizu T, et al. Registration accuracy and possible migration of internal fiducial gold marker implanted in prostate and liver treated with real-time tumor-tracking radiation therapy (RTRT). Radiother Oncol. 2002;62(3):275–81.

18. Niibe Y, Hayakawa K. Oligometastases and oligo-recurrence: the new era of cancer therapy. Jpn J Clin Oncol. 2010;40(2):107–11. doi:10.1093/jjco/hyp167.

19. Nishioka T, Nishioka S, Kawahara M, Tanaka S, Shirato H, Nishi K, et al. Synchronous monitoring of external/internal respiratory motion: validity of respiration-gated radiotherapy for liver tumors. Jpn J Radiol. 2009;27(7):285–9. doi:10.1007/s11604-009-0332-5.

20. Miyamoto N, Ishikawa M, Bengua G, Sutherland K, Suzuki R, Kimura S, et al. Optimization of fluoroscopy parameters using pattern matching prediction in the real-time tumor-tracking radiotherapy system. Phys Med Biol. 2011;56(15):4803–13. doi:10.1088/0031-9155/56/15/011.

21. Matsuura T, Maeda K, Sutherland K, Takayanagi T, Shimizu S, Takao S, et al. Biological effect of dose distortion by fiducial markers in spot-scanning proton therapy with a limited number of fields: a simulation study. Med Phys. 2012;39(9):5584–91. doi:10.1118/1.4745558.

Chapter 18
Others: Four-dimensional Cone-Beam CT During SBRT

Akihiro Haga, Satoshi Kida, Naoya Saotome, Wataru Takahashi, Hideomi Yamashita, Yoshitaka Masutani, and Keiichi Nakagawa

18.1 Principle of 4D CBCT Reconstruction

In this section, we introduce the typical strategy to reconstruct 4D-CBCT images with the image guidance system mounted on LINAC.

18.1.1 Respiratory Signal

4D-CBCT images are reconstructed by classifying acquired projection images to respiratory phases divided by several bins. In this process, the knowledge of a respiratory phases during projection imaging plays a key role. The measuring of a respiratory signal synchronized with projection images is categorized by two methods; the use of an external respiratory monitoring system and the image-based respiratory phase recognition. The former includes AZ-733 V (Anzai Medical Co.) and real-time position management (Varian Medical System) [1–3], both of which give an external information about respiratory phase. The latter derives the respiratory phase directly from image processing algorithms of the projection images [4–6]. For the prediction of the respiratory signal, the latter is more powerful than the former because there is no need to investigate the correlation between the inner movement and the signal of the external system. On the other hand, this is not true in the situation that the respiratory signal concerned with the respiration was partly observed during acquisition of the projection image (this is likely in case that the diaphragm is *not* visible in the image sets for all projection

A. Haga (✉) • S. Kida • N. Saotome • W. Takahashi • H. Yamashita • Y. Masutani
K. Nakagawa
Department of Radiology, The University of Tokyo Hospital,
7-3-1 Hongo, Bunkyo, Tokyo 113-8655, Japan
e-mail: haga-haga@umin.ac.jp
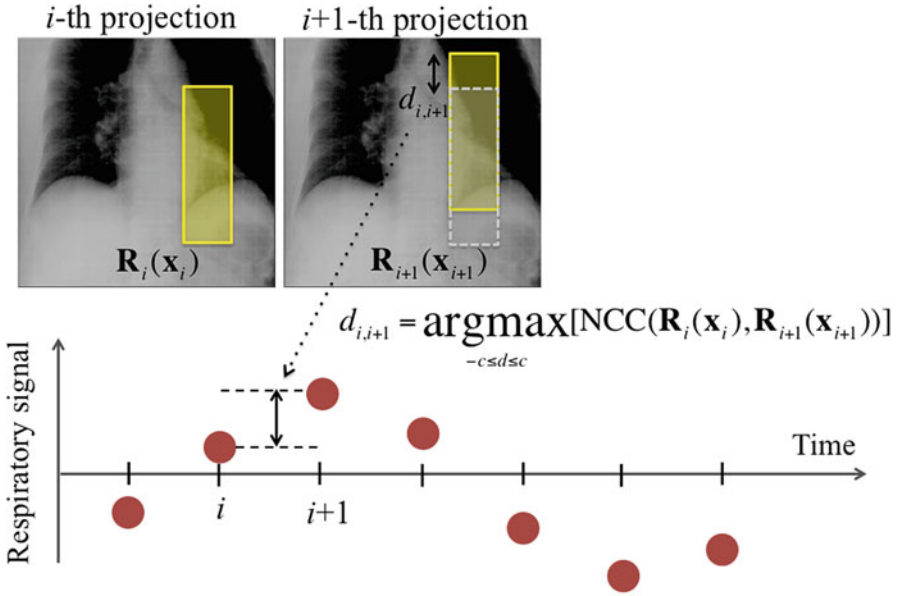
Fig. 18.1 Illustrative explanation of the image based phase recognition using NCC between adjacent projections in a limited area (*yellow box*), which is shifted along with the cranio-caudal axis on the next projection image (*i + 1*-th projection) in the search for the maximum value of NCC with the segments on previous projection images (*i*-th projection)

angles). Such the case might be complemented with an external monitoring system to reproduce the all respiratory phases.

Figure 18.1 shows the outline of the image processing method in the image based phase recognition developed at The University of Tokyo Hospital [6]. This method implements normal cross correlation (NCC) between adjacent projections in a limited area, which is shifted along with the cranio-caudal axis on the next projection image in the search for the maximum value of NCC with the segments on previous projection images. In general, a signal produced by an image-based phase recognition method includes a low periodic noise caused by the gantry rotation. This low periodic component can be removed by employing a high-pass (*or* band pass) filter.

18.1.2 Phase Selecting Reconstruction

For modern helical CT scanners, the rotation cycle of the gantry is sufficiently faster than the breathing cycle, such that a single slice of a three-dimensional (3D) CT scan is regarded as belonging to a certain respiratory phase, whereas different slices represent different respiratory phases. Therefore, a 4D-CT image set can be
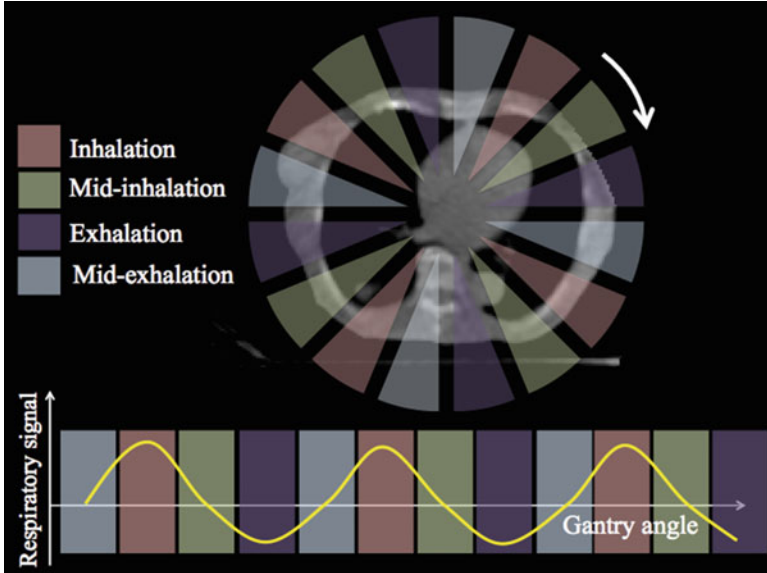
Fig. 18.2 Principle of 4D CBCT reconstruction using image-guided system mounted on LINAC. The projection images are classified into the phase bins defined with the respiratory signal. Thus, 4D CBCT set is generated by reconstructing with each subset of projections

obtained from a single CT scan by subsequently selecting the slices corresponding to a certain respiratory phase [7, 8].

For a CBCT mounted on LINAC, the rotation speed of the gantry is very slow; more than 1 min for one rotation cycle, which is considerably longer than the breathing cycle, and thus, the conventional technique developed in helical CT scans cannot be used any more. In this case, the reconstructed volumes at multiple respiratory phases can be obtained by retrospective sorting in projection space. Figure 18.2 demonstrates the method of the respiratory signal sorting with four phase bins. The projection images are classified by means of the respiratory signal. A 4D-CBCT image set is thus generated by reconstructing with each subset of projections [1, 4].

Obviously, the image quality of 4D CBCT images is degraded due to the larger gap of the gantry-angle increment per projection than that in 3D CBCT. In order to suppress this degradation, the slower gantry speed (typically 4 min per rotation) is used in 4D CBCT imaging. The CBCT images for a moving phantom reconstructed with 3D (2 min per rotation), 4D (4 min per rotation), 4D (2 min per rotation), 4D (1 min per rotation) are shown in Fig. 18.3, where the images for the expiration phase are selected in 4D CBCT. The 4D CBCT with 1 and 2 min per rotation has a severe streak artifact, whereas the 4D CBCT with 4 min per rotation reduces this artifact.

The space-time information of a tumor location from the clear images of 4D CBCT would play an important role in the delivery of precise radiation therapy.
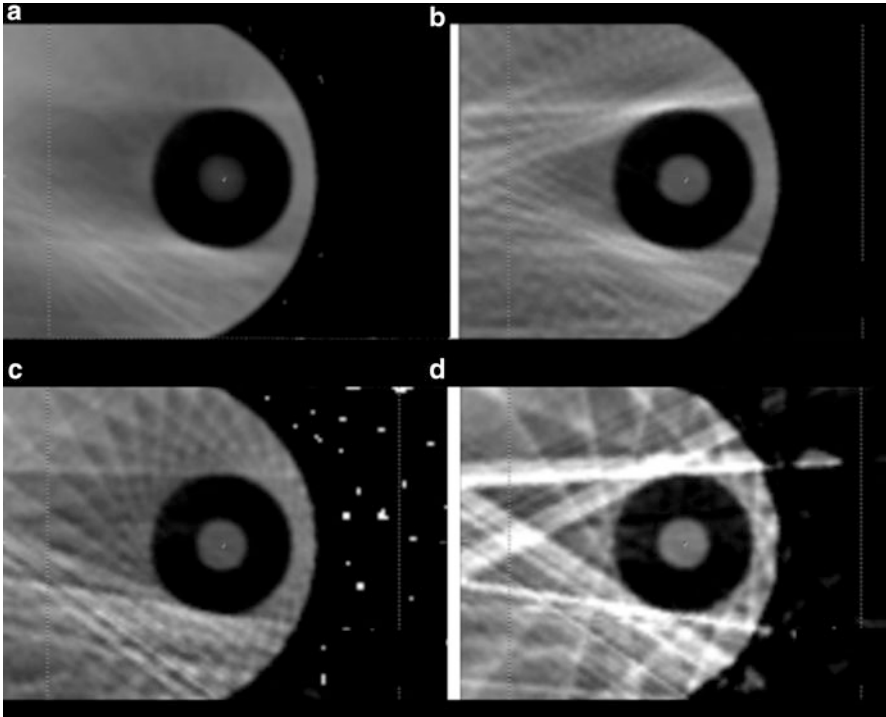
Fig. 18.3 CBCT images (*Axial view*) for a moving phantom (QUASAR; Modus Medical Devices Inc.); (**a**) 3D (2 min per rotation), (**b**) 4D (4 min per rotation), (**c**) 4D (2 min per rotation), and (**d**) 4D (1 min per rotation) images

However, it should be noted that the slower gantry speed in 4D-CBCT imaging could add a significant radiation dose to the patient. Therefore, it would be desirable to optimize radiation parameters to reduce the imaging dose as low as reasonably achievable. In Fig. 18.3, the mA per frame and ms per frame are 20 mA/frame and 40 ms/frame, which are clinically used in The University of Tokyo Hospital. With those parameters, the CT dose index (CTDI) volume is approximately 12 mGy for 4D CBCT imaging with 4 min per rotation, measured with a 15-cm length CTDI phantom.

18.2 Volumetric Modulated Arc Therapy for Lung SBRT

Intensity-modulated radiation therapy (IMRT) extensively includes a rotational therapy, namely intensity-modulated arc therapy (IMAT). IMAT was first proposed in 1995 as a conventional MLC with the various leaf pattern changing continuously as the gantry rotates [9]. To deliver IMRT fields in a gantry angle, several rotational arcs with different MLC patterns were considered to be required for IMAT delivery.

At that time, several rotations were not realistic because it was time consuming. In addition, the fixed-dose rate delivery prohibited progress of IMAT. Nevertheless, in 2008, a variation of the gantry speed and the dose rate, and a rapid MLC control, compensated the weak points of IMAT [10]. This new delivery technique is called VMAT. VMAT achieved comparable intensity modulation level compared with IMRT [11–13]. In addition, VMAT drastically reduced the amount of the monitor unit (MU). Thus, VMAT was found to be able to deliver the desired dose distribution in a shorter time than IMRT. This feature is valuable, in particular, for SBRT [14, 15]. In fact, the delivery time is about 4 min in a conventional LINAC. Using flattening-filter-free techniques, delivery time for lung VMAT is under 2 min [16, 17].

Nowadays, VMAT plays an important role in high-precision radiation therapy treatment. On the other hand, there are some challenges in use of VMAT with regard to a moving target such the lung tumor. Clearly, if a movement occurs between delivery of any of the IMRT fields, the dose may not add up to the desired total dose as planned [18]. This is known as the "interplay effect". In the following subsections, the influence of the interplay effect to the patient dose in VMAT for lung SBRT, and its reduction strategy are discussed.

18.2.1   Interplay Effect in Lung SBRT

The interplay effect on IMRT delivery has been investigated by many authors. Bortfeld et al. [19] predicted that the interplay effect would, for the most part, average out with a large number of fractions. However, this is not the case with a hypo-fractionated radiosurgery-type course of treatment (a few fractions for a course of treatment). In addition, there are substantially fewer studies of the interplay effect in VMAT [20, 21], particularly for hypo-fractionated dose regimens.

The interplay effect is occurred due to the lack of the link between the respiratory signal and the IMRT field. One of the simple solutions is to use the conformal field in the VMAT delivery, where the changes of the dose rate and of the gantry speed have a role of the intensity modulation. Figure 18.4 shows the variation of the measurement dose as a function of the tumor amplitude of a respiratory motion phantom (QUASAR; Modus Medical Devices Inc.) using the Agility accelerator (Elekta), which has rapid 160 interdigitating leaves with 5 mm width at isocenter and continuous dose rate delivery system. The dose measurement was conducted four times for two different plans; (1) VMAT with conformal field and (2) VMAT without field constraint. Both plans were created with SmartArc in Pinnacle v9.2 (Philips). Without target motion, the reproducibility of the dose at the center of target (corresponding to the isocenter) was less than 0.3 % for four sequential measurements. As the amplitude is large, the dose difference from the mean dose without target motion is large. The variation of the dose for each amplitude is characteristic; VMAT without field constraint has a larger variation than VMAT
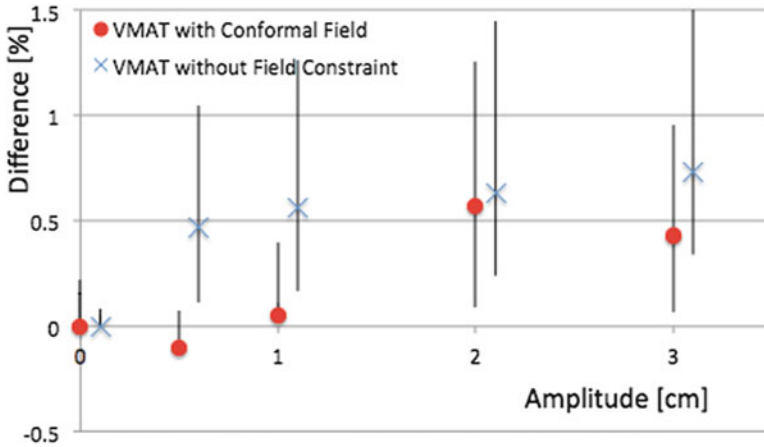
Fig. 18.4 Dose difference [%] between the calculation and the measurement as a function of the motion amplitude of the moving phantom. The measurement was conducted four times for two different plans; (1) VMAT with conformal field (*red circles*) and (2) VMAT without field constraint (*blue crosses*)

with conformal field, as expected. This result implies that it is effective to impose a constraint on the field shape, or MLC motion for the reduction of the interplay effect.

The constraint on the MLC motion, however, may significantly affect the quality of a treatment plan. In the next subsection, the plans with the MLC constraint are compared to those without the MLC constraint.

18.2.2   Constraint on MLC Motion

To reduce the interplay effect, the conformal field shape was effective, as described in the previous subsection. In inverse planning of the VMAT, the conformal-like field shape can be created by imposing a constraint on MLC motion speed; the MLC moves smoothly during VMAT delivery, so that the constraint intents to form field shapes that do not hide the target. With the MLC constraint, degrees of freedom in inverse planning are decreased. Therefore, it is informative to compare between the treatment plans with and without MLC constraint.

In the comparison between lung SBRT plans with MLC constraint and without MLC constraint, the prescribed dose was set as a D_{95} prescription of 55 Gy in four fractions for planning target volume (PTV) of the lung tumour, which was created with a 5-mm isotropic margin of internal target volume (ITV) generated from 10 4D-CT sets by using a volumetric CT scanner. The single-arc VMAT using the Agility system with 6 MV was selected in the treatment plan for SmartArc in the Pinnacle v9.2 treatment planning system. The constraint on MLC motion of
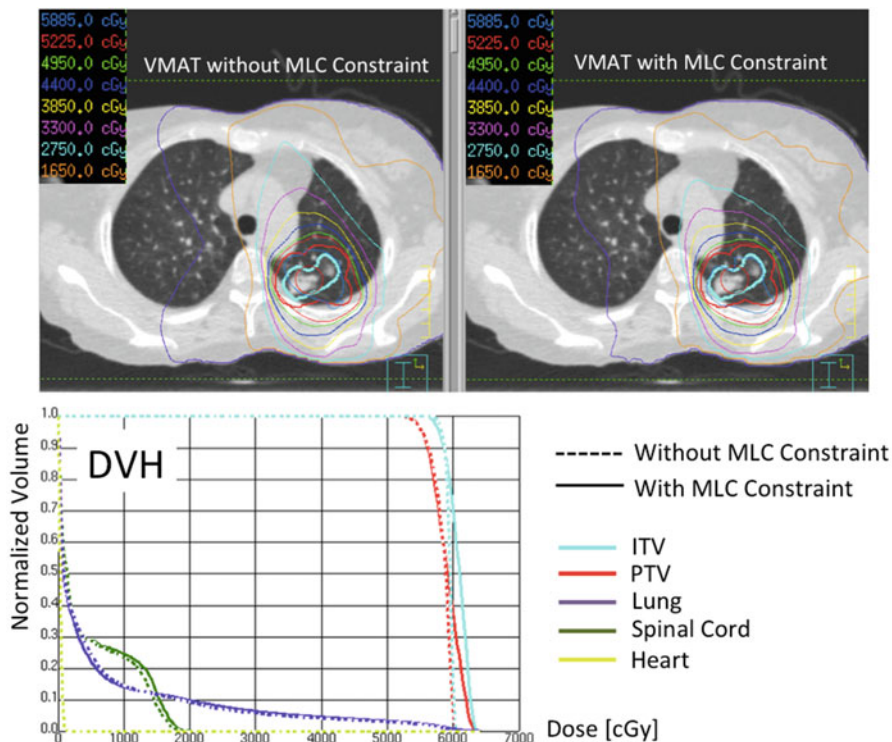
Fig. 18.5 Example of the dose distribution and DVH imposing the MLC constraint of 0.1 cm/degree

0.1 cm/degree was applied in the VMAT inverse plan so that MLC had little chance to hide the PTV in beam's eye view.

One example of the dose-volume histogram (DVH) and the corresponding dose distribution are shown in Fig. 18.5, where the solid curves denote the DVHs with an MLC constraint of 0.1 cm/degree, whereas the dashed curves denote DVHs without MLC constraint. The dose homogeneity of the plan without MLC constraint was better than the plan with MLC constraint. The dose for spinal cord was also decreased by removing the MLC constraint. On the other hand, dose conformity for PTV and the lung dose were comparable.

The result shown here is almost same as that using Synergy accelerator, which has relatively slow MLC with 1 cm width [22]. We may conclude that there is little difference between the plans with and without MLC constraints for lung SBRT. Of course, we note that there is a trade-off between the plan quality and the dose uncertainty due to the target motion. As far as the plans with MLC constraints were acceptable for clinical use, however, imposing the MLC constraint can be justified to manage the target motion.

18.3 Clinical Verification by Use of *In-Treatment* 4D CBCT During VMAT

VMAT for lung SBRT achieves a dose distribution with high-dose gradients to spare the normal tissue close to the tumor. This dose distribution may not be reproduced in the actual treatment, when the patient and his/her anatomies change from the situation at treatment planning. The uncertainties arising from patient positioning and anatomical changes are, in general, considered as the "margin" in the target and the OARs. One of the important things in the high-precise radiation therapy is to verify that the tumor is really located at the irradiated area within the applied margin as the OARs are spared.

The ideal is to obtain the image-volume sets in the state of delivered beams. With CBCT system mounted on the LINAC, this has been achieved by "*in-treatment CBCT*" imaging, which was preformed with the projection images acquired simultaneously during rotational treatment [23–26]. Using the respiratory sorting technique described in 18.1, the tumor dynamics during treatment can be also obtained by, so-called, "*in-treatment 4D CBCT*" [6]. Figure 18.6 shows the example of the in-treatment 4D CBCT with 10-phase bins. Clearly, the tumor trajectory is found to be inside the PTV with these image sets.

In the next two subsections, the retrospective analysis of the tumor location during treatment will be shown with in-treatment 4D CBCT images acquired at The University of Tokyo Hospital. The workflow of the verification is shown in Fig. 18.7. There, the patient setup for 15 patients was performed by 3D CBCT registration (Sep. 2009 – Jan. 2012), while that for 15 patients was performed by 4D CBCT registration (Feb. 2012 – Nov. 2012). All patients were treated with an abdominal compressor.

18.3.1 *Image Registration with* 3D *CBCT Verified by In-Treatment 4D CBCT* [27]

The PTV margin was isotropically taken as 5 mm. Registration was automatically performed using "pre"-3D CBCT. Then, the discrepancy between the actual tumor location and the ITV was evaluated in the lateral, vertical, and longitudinal directions by comparing with in-treatment four-phase 4D CBCT images acquired in each fraction; the actual displacement of tumor from ITV was measured by in-treatment four-phase 4D CBCT in each fraction and the required PTV margins were evaluated in each fraction.

Overall, 55 4D CBCT sets during VMAT-SBRT were successfully obtained. The average displacements between the ITV and the actual tumor location during treatment were 0.41 ± 0.93, 0.15 ± 0.58, and 0.60 ± 0.99 mm for the CC, LR, and AP directions, respectively. The discrepancy in each phase did not exceed 5 mm in any direction.
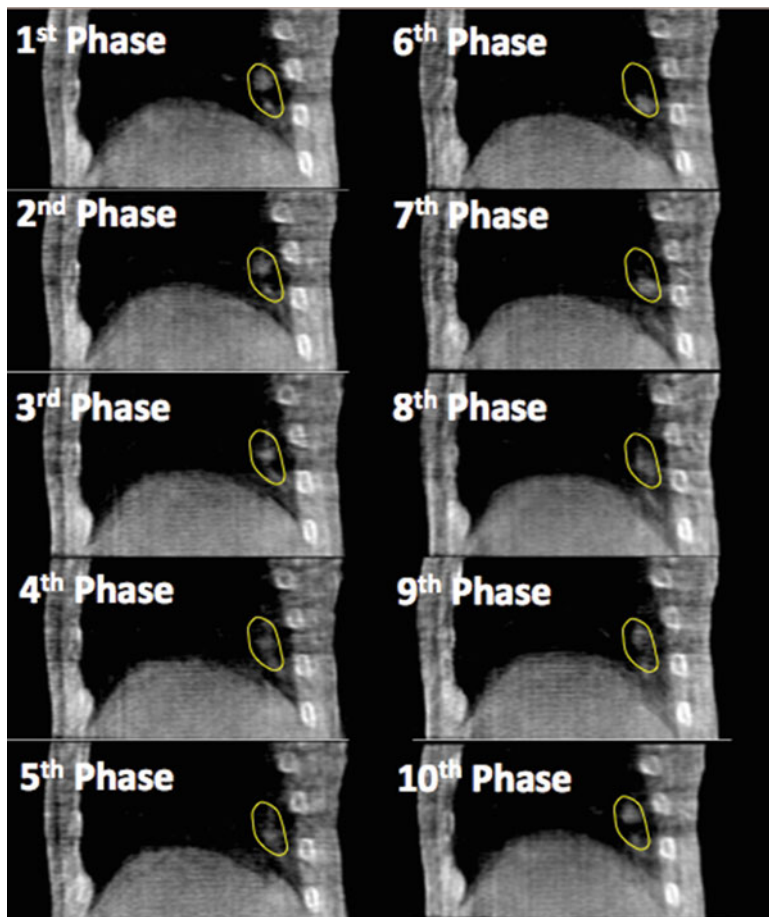
Fig. 18.6 Example of the in-treatment 4D CBCT with 10-phase bins. The *yellow* means the PTV

18.3.2   Image Registration with 4D CBCT Verified by In-Treatment 4D CBCT

The latest x-ray volume imaging feature provided by Elekta enabled us to perform the patient registration with "pre"-4D CBCT with 10 phases. During VMAT delivery, kV projection images were acquired, and in-treatment four-phase 4D CBCT was subsequently reconstructed in each of four fractions thereby providing moving tumor locations along with ITV contours. The average over-travel distances during treatment (58 4D CBCT sets for the 15 patients) were 0.24 ± 0.45, 0.19 ± 0.46, and 0.42 ± 0.43 mm for the CC, LR, and AP directions, respectively. The discrepancy in each phase did not exceed 3 mm in any directions. Figure 18.8
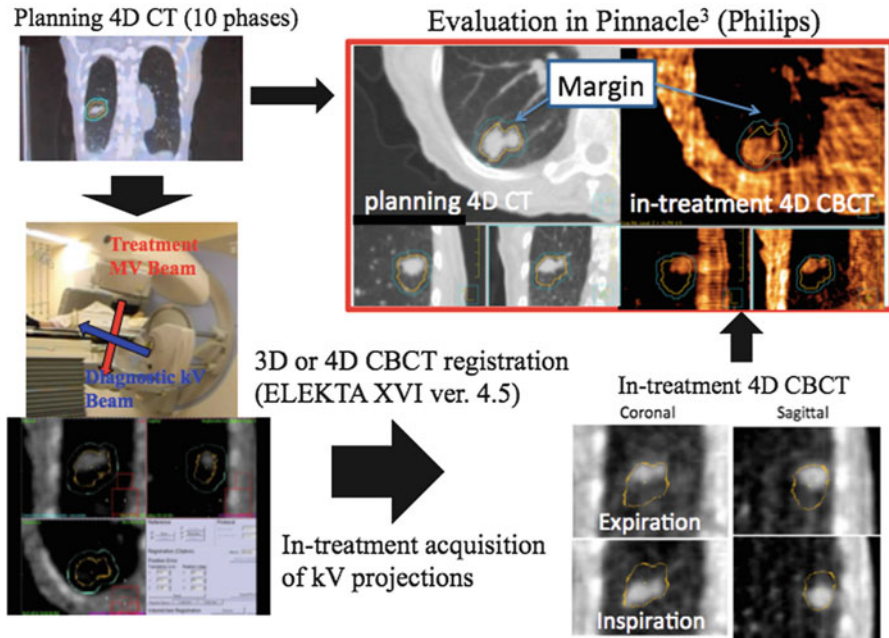
Fig. 18.7 Workflow of the clinical verification using in-treatment 4D CBCT: Patient setup was done either 3D CBCT registration or 4D CBCT registration. Sequentially, the simultaneous acquisition of the kV projections was performed during VMAT treatment. The in-treatment 4D CBCT images were reconstructed, and were compared with the PTV defined by planning 4D CT
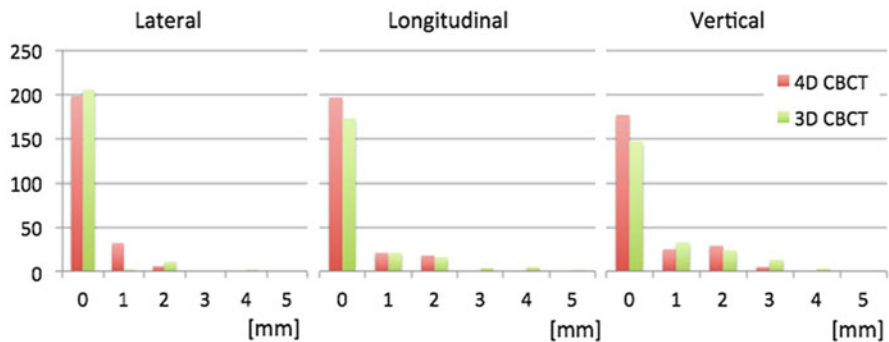
Fig. 18.8 Histograms of the displacement between ITV and actual tumor location for each direction

shows histograms of the displacement between ITV and actual tumor location during treatment for each direction both with 3D and 4D CBCT registrations.

The standard deviation of the margin required in each fraction by 4D CBCT registration was smaller than that by 3D CBCT one. We observed a 2-mm protruding

in only 3 out of 15 patients for 4D CBCT registration (All for AP direction). Actually, 4D CBCT has a sharp edge in peripheral region to compare with 3D CBCT. So, it is likely to improve the registration accuracy by 4D CBCT registration.

On the other hand, no relation between a tumor motion and a required margin was observed. Relatively, the large discrepancy was observed in the AP direction, where the tumor motion amplitude is not so large.

18.4   Conclusions

Having established the reliable technique to derive the respiratory signal, it has become feasible to detect tumors from the reconstructed 4D data for lung cancer during SBRT. The image quality of in-treatment 4D-CBCT images in each phase bin was enough to preclude identifying the tumor location.

The development of a rotational delivery technique such as VMAT was essential for clinical implementation of in-treatment CBCT. In the optimization for the lung SBRT planning, the MLC constraint produced the conformal-like field shape, so that the interplay effect was negligibly small. In-treatment 4D CBCT is a direct method for quantitatively assessing the intrafractional location of a moving target. With in-treatment 4D CBCT, the required PTV margins were estimated when the registration for moving target was performed using pre-3D or -4D CBCT. The 4D CBCT registration can potentially improve the registration accuracy. It is also important to establish the robust registration protocol to reproduce the tumor position in the treatment planning CT. The next phase would include the commercialization of packages in record and verification system with in-treatment 4D CBCT.

References

1. Dietrich L, Jetter S, Tucking T, Nill S, Oelfke U. Linac-integrated 4D cone beam CT: first experimental results. Phys Med Biol. 2006;51:2939–52.
2. Lu J, Guerrero TM, Munro P, Jeung A, Chi PC, Balter P, et al. Four-dimensional cone beam CT with adaptive gantry rotation and adaptive data sampling. Med Phys. 2007;34:3520–9.
3. Leng S, Zambelli J, Tolakanahalli R, Nett B, Munro P, Star-Lack J, et al. Streaking artifacts reduction in four-dimensional cone- beam computed tomography. Med Phys. 2008;35:4649–59.
4. Sonke JJ, Zijp L, Remeijer P, van Herk M. Respiratory correlated cone beam CT. Med Phys. 2005;32:1176–86.
5. Kavanagh A, Evans MP, Hansen NV, Webb S. Obtaining breathing patterns from any sequential thoracic X-ray image set. Phys Med Biol. 2009;54:4879–88.
6. Kida S, Masutani Y, Yamashita H, Imae T, Matsuura T, Saotome N, et al. In-treatment 4D cone-beam CT with image-based respiratory phase recognition. Radiol Phys Technol. 2012;5:138–47.
7. Mori S, Endo M, Tsunoo T, Kandatsu S, Tanada S, Aradate H, et al. Physical performance evaluation of a 256-slice CT-scanner for four-dimensional imaging. Med Phys. 2004;31:1348–56.

8. Rietzel E, Pan T, Chen GT. Four-dimensional computed tomography: image formation and clinical protocol. Med Phys. 2005;32:874–89.

9. Yu CX. Intensity-modulated arc therapy with dynamic multileaf collimation: an alternative to tomotherapy. Phys Med Biol. 1995;40:1435–49.

10. Otto K. Volumetric modulated arc therapy: IMRT in a single gantry arc. Med Phys. 2008;35:310–7.

11. Bedford L, Alan W. Commissioning of volumetric modulated arc therapy (VMAT). Int J Radiat Oncol Biol Phys. 2009;73:537–45.

12. Korreman S, Medin J, Kjaer-Kristoffersen F. Dosimetric verification of RapidArc treatment delivery. Acta Oncol. 2009;48:185–91.

13. Schreibmann E, Dhabaan A, Elder E, Fox T. Patient-specific quality assurance method for VMAT treatment delivery. Med Phys. 2009;36:4530–5.

14. Ong CL, Verbakel WF, Cuijpers JP, Slotman BJ, Lagerwaard FJ, Senan S. Stereotactic radiotherapy for peripheral lung tumors: a comparison of volumetric modulated arc therapy with 3 other delivery techniques. Radiother Oncol. 2010;97:437–42.

15. Matuszak MM, Yan D, Grills I, Martinez A. Clinical applications of volumetric modulated arc therapy. Int J Radiat Oncol Biol Phys. 2010;7:608–16.

16. Convery DJ, Rosenbloom ME. Treatment delivery accuracy in intensity-modulated conformal radiotherapy. Phys Med Biol. 1995;40:979–99.

17. Scorsetti M, Alongi F, Castiglioni S, Clivio A, Fogliata A, Lobefalo F, et al. Feasibility and early clinical assessment of flattening filter free (FFF) based stereotactic body radiotherapy (SBRT) treatments. Radiat Oncol. 2011;6:113.

18. Nakagawa K, Haga A, Sakumi A, Yamashita H, Igaki H, Shiraki T, et al. Impact of flattening-filter-free techniques on delivery time for lung stereotactic volumetric modulated arc therapy and image quality of concurrent kilovoltage cone-beam computed tomography: a preliminary phantom study. J Radiat Res. 2013;54:1–3.

19. Bortfeld T, Jokivarsi K, Goitein M, Kung J, Jiang SB. Effects of intra-fraction motion on IMRT dose delivery: statistical analysis and simulation. Phys Med Biol. 2002;4:2203–20.

20. Court LE, Seco J, Lu XQ, Ebe K, Mayo C, Ionascu D, et al. Use of a realistic breathing lung phantom to evaluate dose delivery errors. Med Phys. 2010;37:5850–7.

21. Rao M, Wu J, Cao D, Wong T, Mehta V, Shepard D, Ye J. Dosimetric impact of breathing motion in lung stereotactic body radiotherapy treatment using intensity modulated radiotherapy and volumetric modulated arc therapy [corrected]. Int J Radiat Oncol Biol Phys. 2012; e251–6. Erratum in Int J Radiat Oncol Biol Phys. 2013;87:859 and Int J Radiat Oncol Biol Phys. 2014;88:462.

22. Kida S, Saotome N, Masutani Y, Yamashita H, Ohtomo K, Nakagawa K, et al. 4D-CBCT reconstruction using MV portal imaging during volumetric modulated arc therapy. Radiother Oncol. 2011;100:380–5.

23. Nakagawa K, Yamashita H, Shiraishi K, Igaki H, Terahara A, Nakamura N, et al. Verification of in-treatment tumor position using kilovoltage cone-beam computed tomography: a preliminary study. Int J Radiat Oncol Biol Phys. 2007;69:970–3.

24. Nakagawa K, Haga A, Shiraishi K, Yamashita H, Igaki H, Terahara A, et al. First clinical cone-beam CT imaging during volumetric modulated arc therapy. Radiother Oncol. 2009;90:422–3.

25. Ling C, Zhang P, Etmektzoglou T, Star-Lack J, Sun M, Shapiro E, et al. Acquisition of MV-scatter-free kilovoltage CBCT images 5 during RapidArc or VMAT. Radiother Oncol. 2011;100:145–9.

26. Boylan CJ, Marchant TE, Stratford J, Malik J, Choudhury A, Shrimali R, et al. A megavoltage scatter correction technique for cone-beam CT images acquired during VMAT delivery. Phys Med Biol. 2012;57:3727–39.

27. Takahashi W, Yamashita H, Kida S, Masutani Y, Sakumi A, Ohtomo K, et al. Verification of planning target volume settings in volumetric modulated arc therapy for stereotactic body radiation therapy by using in-treatment 4-dimensional cone beam computed tomography. Int J Radiat Oncol Biol Phys. 2013;86:426–31.

Part VIII
Future Perspectives

Chapter 19
Future of Stereotactic Irradiation – Dose Composition Radiotherapy (DCRT)

Hiroki Shirato, Rikiya Onimaru, Shinichi Shimizu, Naoki Miyamoto, Ruijiang Li, Albert C. Koong, and Masahiro Mizuta

19.1 Dose Composition Radiotherapy (DCRT)

What advances will the future hold for stereotactic body radiotherapy (SBRT), also known as stereotactic ablative body radiotherapy (SABR)? A basic principle of SBRT/SABR is to spatially confine the absorbed dose to the tumor-bearing region while temporally administering the dose in order to maximize tumor cell killing while minimizing damage to adjacent normal cells. The biological property of

H. Shirato (✉)
Department of Radiation Medicine, Hokkaido University Graduate School of Medicine,
Kita 15 Nishi 7, Kita-ku, Sapporo 060-8638, Japan

Division of Quantum Medical Science and Engineering, Hokkaido University, Sapporo, Japan
e-mail: shirato@med.hokudai.ac.jp

R. Onimaru
Department of Radiation Medicine, Hokkaido University Graduate School of Medicine,
Kita 15 Nishi 7, Kita-ku, Sapporo 060-8638, Japan

S. Shimizu
Department of Radiation Oncology, Hokkaido University Graduate School of Medicine,
Kita 15 Nishi 7, Kita-ku, Sapporo 060-8638, Japan

Division of Quantum Medical Science and Engineering, Hokkaido University, Sapporo, Japan

N. Miyamoto
Department of Medical Physics, Hokkaido University Hospital, Sapporo, Japan

R. Li • A.C. Koong
Division of Quantum Medical Science and Engineering, Hokkaido University, Sapporo, Japan

Department of Radiation Oncology, Hokkaido University Graduate School of Medicine,
Kita 15 Nishi 7, Kita-ku, Sapporo 060-8638, Japan

M. Mizuta
Department of Advanced Data Science, Information Initiative Center,
Hokkaido University, Sapporo, Japan

tumors and normal structures should be understood as precisely as possible while accounting for the spatial distribution and the temporal fractionation of the absorbed dose. Thus, the future of radiation therapy will require cooperation between specialists in imaging, physics, biology, and oncology. These experts with complementary skills will all work together within the field of radiation oncology.

SBRT has paved the way for using narrow beams to treat the gross tumor volume (GTV) with a minimal margin expansion. As SBRT techniques have evolved, photon beams with a much narrower diameter than the diameter of the GTV have been used in intensity modulated radiotherapy (IMRT) and volumetric modulated arc therapy (VMAT). Similarly, proton beams with a diameter of <1 cm and a correspondingly smaller Bragg-peak have been utilized in spot scanning particle beam therapy (SSPT) and intensity modulated particle beam therapy (IMPT) [1, 2]. It is logical to expect that the future radiotherapy of SBRT will utilize these technologies to compose optimal spatial dose distributions.

After more than three decades of neglect, there has been renewed interest in hypofractionated radiotherapy. The clinical observations of hypofractionated SBRT have confirmed the importance of biological considerations regarding dose fractionation and treatment time as a function of normal tissues [3–5]. Understanding these factors is critical to further optimizing SBRT especially when balancing tumor cell kill with normal tissue damage.

Thus, the future of radiotherapy will be composed of absorbed dose in the four-dimensional coordinates of time and space with an emphasis on optimizing spatial dose distribution and temporal dose distribution. We refer to this concept as "dose composition radiotherapy (DCRT)" and anticipate that future generations of radiation therapy will incorporate these principles routinely into clinical practice.

What are the technical challenges that need to be overcome before DCRT can be widely implemented? We will discuss these issues in the following sections.

19.2   Real-Time Four-Dimensional Radiotherapy (R4RT) Technology

Interfractional as well as intrafractional variation effects between each beam pass, set-up error, organ motion, and deformation of the tumor are significant issues for DCRT. Recently, concerns have been raised in IMRT regarding the potential for worse treatment outcomes because of dosimetric inaccuracies related to tumor motion in patients with locally advanced non-small cell lung cancer (NSCLC) [6]. Harris et al. showed that IMRT did not compromise the outcome for stage III NSCLC in a population-based analysis. However, simulation studies have repeatedly shown inevitable deterioration in physical dose distribution by the interplay effect in DCRT [7–9]. As the achievable dose distribution will be more conformal

in DCRT than conventional radiotherapy, it is logical to reduce the uncertainty due to tumor motion in DCRT to improve the treatment outcome.

Four-dimensional radiotherapy technology is expected to reduce the uncertainty of tumor motion in DCRT for tumor. The concept of four-dimensional radiotherapy (4DRT), where the temporal changes in anatomy are explicitly considered during the imaging, planning, and delivery of radiotherapy, was first introduced in 2000 [10]. Since then, 4DCT has been shown to be useful for radiotherapy treatment planning of tumors in moving organs. Studies describing the relationship between surface surrogate markers and internal tumor motion have indicated a good correlation between these parameters [11]. However, conflicting reports suggest that 4DCT and surface markers on the abdominal wall may not always be reliable as a surrogate for the internal tumor motion [12]. The major drawback for fiducials implanted in the lung is the potential for migration especially for those inserted vis bronchoscopy and pneumothorax for those implanted percutaneously. In contrast, endoscopic placement of fiducials for pancreatic tumors as well as percuatenous implantation for prostate and liver has been shown to be safe and reliable [13–15]. Development of techniques to reduce the incidence of fiducial migration is an active area of investigation [16, 17].

Real-time four-dimensional radiotherapy (R4RT), in which internal tumor position is detected during the delivery of irradiation and the tumor is irradiated only when its position matches with the treatment planning, is the optimal method to minimize tumor motion uncertainty [18]. Real-time tumor-tracking technology using internal radiopaque fiducial markers has been shown to increase the accuracy of radiotherapy with respect to time and space [19]. The amplitude and speed varied considerably between patients and between treatment days for the same patient. The standard deviation of the absolute amplitude was greater than 5 mm in 23 % of lung cancer [19]. Tumor position during expiration phase longer and more stable than during inspiration phase. These data indicate that expiration phase is the most appropriate phase for respiratory-gated radiotherapy. However, the tumor position during expiration may vary by more than 2 mm, suggesting that the largest source of error in respiratory-gated radiotherapy without real-time detection of internal tumor position. In average, 4 shifts for intrafractional baseline motion were necessary during each treatment session to maintain an accuracy of 2 mm. Furthermore, the trajectory of the marker during inspiration is often different from that in expiration (hysteresis) which can further complicate targeting of moving tumors [20]. Therefore, in DCRT in which narrow therapeutic beam is moved or scanned along the predicted trajectory of the tumor, there can be serious discrepancy between the planning and the motion of the beam. Further studies regarding R4RT technology in DCRT is strongly warranted [21].

The latency between the recognition of the tumor position and the irradiating the beam is another uncertainty that is inherent to R4RT. Although the fiducial marker can be detected in 30 ms, a latency of 30 ms or more is required before the actual irradiation occurs in R4RT. Since the maximum speed of lung tumors can be more than 33 mm/s in 29 % of patients, the latency can lead to significant variation in

delivered dose to the tumor. The latency period can be less than 100 ms in electronic gating but be longer in mechanical tracking system such as robotics and multi-leaf collimators [22]. Many investigators have attempted to model the respiratory pattern and to predict the internal motion of the lung tumors. The respiratory patterns are not simple sine waves and may be categorized into several types using a finite state model taking into account regular breathing, frequency changes, baseline shifts, amplitude changes, cardiac motion, or a combination of these patterns [23]. Approximately 85 % patients have a breathing cycle consisting of 3 states (exhale, end-of-exhale, inhale). However 10 % have exhale and inhale states without end-of-exhale state, 5 % have an additional relaxation state after inhale, and some patients have combinations of all breathing states. Prediction models should also be able to handle daily change of the respiratory patterns in the same patients.

The position of the internal marker and the center of GTV also changes during respiration. A limitation of R4RT is that there is no direct confirmation of the relationship between the tumor and the isocenter of the treatment machine during the irradiation. Li et al. developed and clinically evaluated a volumetric imaging technique for assessing intrafraction geometric and dosimetric accuracy of VMAT in 20 patients who received SBRT for lung tumors. At the beginning of each fraction, a pretreatment cone beam computed tomography (CBCT) was used to align the tumor with the position of the tumor on the planning CT. Simultaneous with dose delivery, fluoroscopic radiograph projections were obtained during VMAT using the on-board imaging system. Those kilovolt projections acquired during treatment delivery were automatically extracted, and intrafraction CBCT images were reconstructed using a filtered back projection technique. The average target shift during VMAT was determined by calculating the center of mass of the tumor target in the intrafraction CBCT relative to the planning CT. The 95th percentile shift was 5.2, 3.1, 3.6 mm along the anterior-posterior, left-right, and superior-inferior directions, respectively. These data help to define appropriate margin expansion for these tumors. Thus, intrafraction CBCT during VMAT can provide geometric and dosimetric verification of SBRT valuable for quality assurance and potentially for treatment adaptation [24].

19.3 Overcoming Volume Effect

In general, smaller volume of irradiation results in lower rate of late complications. This clinical observation is referred to as the "volume effect" [25]. The volume effect can be defined as the dependency of radiation damage to normal tissue on the overall volume of tissue irradiated. The current dogma holds that with regards to late complications, parallel structures such as liver are more sensitive to larger irradiated volumes whereas series structures such as spinal cord are more sensitive to absolute dose. The accuracy and preciseness of stereotactic irradiation allows

reduction in margin expansion which reduces unnecessary irradiation of normal tissues and certain clinical scenarios, should reduce long-term complications of radiotherapy [18].

Organs with parallel structures consist of organs in which a unit of volume can be completely destroyed without any clinical symptoms but the sum of partially destroyed volumes will result in clinical symptoms when a threshold is exceeded. For example, peripheral lung and liver tissues can be surgically removed without symptoms but viral or bacterial infection of a large volume can be fatal. Efficient usage of this principle for organs with parallel structures has been a fundamental strategy of SBRT. Although the risk of complications can be minimized by staying within normal tissue tolerances, there remains a risk of fatal radiation pneumonitis or hepatitis for treating lung and liver tumors with large volume or large amplitude of organ motion [26]. Because IMRT and VMAT spreads low dose to a larger normal tissue volume compared to conventional 3D conformal radiotherapy, there is an increased concern for induction of radiation induced malignancies [27].

Spot scanning proton beam therapy and IMPT have the potential to improve the therapeutic ratio even for large tumors in organs with parallel structures because of the improved dose distribution results in a smaller volume receiving lower dose irradiation [28]. Toramatsu et al. have shown that peripheral liver tumors with the diameter of 6 cm or more will be better treated with SSPT compared to IMRT [29].

Serial organs are organs in which complete destruction of one segment will result in clinical symptoms but the sum of partially destroyed volumes will not result in clinical symptoms. Trachea, main bronchus, aorta, and main pulmonary arteries are examples of serial organs and excess dose even to a small volume will result in organ dysfunction. Precise irradiation with accurate tumor localization can safely treat tumors to a higher radiobiologically equivalent dose (RBE) than with conventional techniques, particularly when the tumor is close to a serial organ. If the tumor is located within a serial organ, recent studies have suggested that improvement of accuracy by even a few millimeters may enhance the tolerance of a portion of the serial organ [30]. The surface of serial organs was suggested to be tolerable with the higher dose of irradiation than CFRT. With SBPT for pediatric patients, dose constraints to the surface of organs at risk (OARs) were determined as follows; maximum dose (D2) of 54.0 and 63.0 Gy(RBE) to the center and surface of the brainstem or spinal cord, 60.0 Gy(RBE) to the optic chiasm and optic nerves, maximum dose (D2) of 64.0 Gy(RBE) to the center of cauda equina and sacral nerve roots, bowel 60.0 Gy(RBE); kidney tolerance levels were determined as entire organs receiving <20 Gy, two-thirds of the organ >30 Gy(RBE), or one-third of the organ receiving >40 Gy(RBE). These are higher than usual dose constraints with uniform dose delivery [30]. This finding is consistent with the low incidence of rectal bleeding in patients with prostate cancers who are treated with high dose, intensity modulated radiotherapy (IMRT) since high dose IMRT can reduce the dose to the posterior part of rectum but increase the dose to the anterior surface of the rectum. Having said that, there is no scientific evidence in precise animal studies to expect increase in tolerance dose by using inhomogeneous dose

distribution [31]. Therefore, careful clinical trials are still required for the investigation to overcome volume effect in DCRT.

19.4 Optimal Dose Fractionation Determined by Physical Dose Distribution

In the era of three-dimensional treatment planning, dose distribution is optimized independent of dose fractionation by using computed tomography. However, can the dose fractionation be independent of physical dose distribution? A simple but potentially powerful model to optimize dose fractionation based on physical dose distribution has been developed recently [32].

A novel mathematical method was proposed for selecting hypofractionated or multi-fractionated irradiation regime based on physical dose distribution in addition to biological considerations. The linear-quadratic (LQ) model was employed to describe the radiation effects on tumor and normal tissues. Based on the assumption that the organ at risk (OAR) receives a fraction of the dose intended for the tumor, the minimization problem for the damage effect on the OAR was treated under the constraint that the radiation effect on tumor is fixed. For an N-time fractionated irradiation regimen, the constraint of tumor lethality was described by an N-dimensional hypersphere. The total dose for fractionated irradiation was considered for minimizing the damage effect on the OAR under the hypersphere condition. The advantage of hypofractionated or multi-fractionated irradiation depends on the magnitude of the ratio of α/β parameters for the OAR and the tumor in the LQ model and the ratio of the dose for the OAR and the tumor. The mathematical method shows that the multi-fractionated irradiation with a constant dose is better if the ratio of α/β for the OAR and the tumor is less than the ratio of the dose for the OAR and the tumor, while hypofractionated irradiation is better otherwise. Application of this model may lead to better treatment outcomes through the selection of optimal dose fractionation for each patient.

For a multi-fraction radiation therapy with N-fraction doses $(d_1, d_2, \ldots, d_N)$, the radiation effect for the tumor is represented by $\sum_{i=1}^{N} \left(\alpha_1 d_i + \beta_1 d_i^2 \right)$ and is fixed as E_1, that is

$$E_1 = \sum_{i=1}^{N} \left(\alpha_1 d_i + \beta_1 d_i^2 \right) \tag{19.1}$$

Since the doses for the OAR are denoted as $\delta d_1, \delta d_2, \ldots, \delta d_N$, the damage effect on the OAR (E_0) by N times exposure is given by

$$E_0 = \sum_{i=1}^{N} \left[\alpha_0(\delta d_i) + \beta_0(\delta d_i)^2 \right] \tag{19.2}$$

Thus, the problem for the fractionation regimen can be handled mathematically as an optimization problem,

$$\sum_{i=1}^{N} \left[\alpha_0(\delta d_i) + \beta_0(\delta d_i)^2 \right] \rightarrow \text{Min}$$

under the constraint of Eq. (19.1). If the damage effect on the OAR in formula (19.2) is smaller with an increase in the number of fractions, then multi-fractionated irradiation is better. If the damage effect on the OAR in formula (19.2) is larger with an increase in the number of fractions, then hypofractionated irradiation is better. The formula (19.2) can be transformed as follows.

$$\begin{aligned}
E_0 &= \sum_{i=1}^{N} \left(\alpha_0 \delta d_i + \beta_0 \delta^2 d_i^2 \right) = \alpha_0 \delta \sum_{i=1}^{N} d_i + \beta_0 \delta^2 \sum_{i=1}^{N} d_i^2 \\
&= \alpha_0 \delta \sum_{i=1}^{N} d_i + \beta_0 \delta^2 \frac{1}{\beta_1} \left(E_1 - \alpha_1 \sum_{i=1}^{N} d_i \right) \\
&= \frac{\alpha_1 \beta_0 \delta}{\beta_1} \left(\frac{\alpha_0/\beta_0}{\alpha_1/\beta_1} - \delta \right) \sum_{i=1}^{N} d_i + \frac{\beta_0 \delta^2}{\beta_1} E_1
\end{aligned}$$

Ultimately, the adjudication can be described as follows:

(i) if $\frac{\alpha_0}{\beta_0}/\frac{\alpha_1}{\beta_1} \geq \delta$, hypofractionated irradiation is better than multi-fractionated irradiation.

(ii) if $\frac{\alpha_0}{\beta_0}/\frac{\alpha_1}{\beta_1} < \delta$, multi-fractionated irradiation with a constant dose is better.

The result does not depend on the value E_1, nor the parameters, $\alpha_0, \beta_0, \alpha_1, \beta_1$, but the ratio $\frac{\alpha_0}{\beta_0}/\frac{\alpha_1}{\beta_1}$ and δ.

The clinical feasibility of this model can be examined assuming two lung tumors with the same volume of 2.0 cm^3 but situated in different locations: for example peripheral lung vs. central lung. The organs at risk are normal lung tissue, spinal cord, brachial plexus, pulmonary artery, heart, esophagus, and the proximal bronchial tree [33, 34]. Using SBRT technology, one can assume that the major complication probabilities are related to the central mediastinal structures such as pulmonary artery, heart, esophagus, and the proximal bronchial. α_0/β_0 for the central mediastinal structures is very likely to be smaller than α_1/β_1 for the tumor so that we can assume $\frac{\alpha_0}{\beta_0}/\frac{\alpha_1}{\beta_1}$ is smaller than 1.0. In the treatment of peripheral lung tumors, the central mediastinal structures do not receive any significant dose ($\delta = 0.0$). However, in the treatment of central lung tumors, the central mediastinal structures receive nearly the same dose as the target volume ($\delta = 1.0$). Consequently, the model predicts that hypofractionated radiotherapy is preferable for

the peripheral tumor and multi-fractionated irradiation is preferable for the central tumor. These preferences are consistent with clinical findings for SBRT of stage I squamous cell carcinoma of the lung. Further refinement of this model must incorporate our understanding of radiobiology as many investigators have demonstrated the importance of parameters such as DNA repair, cell cycle, hypoxia, and reoxygenation.

19.5   Functional Imaging for DCRT

Functional imaging may well be useful in DCRT in order to optimize the dose delivery based upon metabolic activity of the tumor as it relates to the functional capacity of nearby normal tissues. Positron emission tomography (PET) can be used for the determination of these function of normal tissue and abnormal function of cancer cells only if the signal to noise ratio of imaging is sufficient for quantitative analysis [35]. The reproducibility of functional imaging is strongly dependent on the interval between the injection of the probe and the detection of images. Radiation oncologists should work closely with diagnostic radiologist to define a common imaging protocol so that quantitative analysis is comparable between scans. For example, in the detection of tumor hypoxia by functional imaging, accumulation of FMISO following requires 4 h to reach steady state levels. Imaging prior to early after injection of the tracer will result in inaccurate estimation of the degree of tumor hypoxia [36]. When images are acquired 4 h after the injection of FMISO, the detection and reproducibility of the hypoxic areas of tumors are excellent [37]. Since the signal to noise ratio (SNR) of FMISO imaging is much lower than FDG imaging, the efficiency of positron emission tomography (PET) is critical for the quantitative accuracy [38].

19.6   Molecular Technologies Expected to Be Useful
         for DCRT

Although the incidence of grade III radiation pneumonitis (RP) in SBRT has been quite low after SBRT, the consequences of severe RP are so clinically significant that reliable biologic markers to predict RP before treatment are warranted [26]. Yuan et al. investigated the association between single nucleotide polymorphisms (SNPs) in the transforming growth factor 1 (TGFbeta1) gene and risk of RP. These investigators reported that CT/CC genotypes of TGFbeta1 rs1982073: T869C to be associated with a lower risk of RP compared with the TT genotype [39]. Further study of this SNP as well as the development of other associated SNPS will enhance our predictive models of RP after high dose radiation.

Selection of patients who are most likely to benefit from DCRT alone and those who should receive additional systemic therapy are important clinical decisions that factor into the appropriateness of DCRT. The effectiveness of a local therapy is maximized when the risk of systemic disease is lowest. Measurement of circulating tumor DNA (ctDNA) has been proposed as a method to improve the selection of the patients for DCRT and for systemic therapy [40]. Newman et al. introduced cancer personalized profiling by deep sequencing (CAPP-Seq), an economical and ultrasensitive method for quantifying ctDNA. They implemented CAPP-Seq for NSCLC with a design covering multiple classes of somatic alterations that identified mutations in >95 % of tumors. These investigators detected ctDNA in 100 % of patients with stage II-IV NSCLC and in 50 % of patients with stage I, with 96 % specificity for mutant allele fractions down to approximately 0.02 %. Levels of ctDNA were highly correlated with tumor volume and distinguished between residual disease and treatment-related imaging changes, and measurement of ctDNA levels allowed for earlier response assessment than radiographic approaches. The CAPP-Seq could be routinely applied clinically to detect and monitor diverse malignancies, thus facilitating personalized cancer therapy and improving the therapeutic outcomes.

19.7 Informatics to Use New Radiotherapy Technologies Properly

Scientific, economic, and ethical considerations to prevent inappropriate use of new radiotherapy technology is strongly desired. Process analysis of the physicians' decision making using advanced technologies in informatics may be useful for this purpose. Widespread adoption of electronic medical records will help to facilitate uniformity and transparency of clinical radiation oncologic decisions. For example, a common clinical scenario is to determine if re-irradiation is feasible in an area of tumor recurrence. Re-irradiation using small treatment volume with stereotactic technology may be clinically feasible for selected patients [41]. However, the long-term biological consequence for re-irradiation of serial organs is largely unknown. DCRT holds great promise to provide exact 4D dose distribution of both the tumor and normal tissues. This knowledge will improve the therapeutic ratio for this technology.

The future of radiotherapy will incorporate advancements in the fields of biology, physics, and imaging. Applying this knowledge to clinical radiotherapy will improve the outcomes for patients. However, rigorous standards must be utilized to select the patients that would be most appropriate for these advanced radiotherapy techniques. Clinicians must work closely with researchers to maximize the benefits of these techniques for our patients.

References

1. Gillin MT, Sahoo N, Bues M, et al. Commissioning of the discrete spot scanning proton beam delivery system at the University of Texas M.D. Anderson Cancer Center, Proton Therapy Center, Houston. Med Phys. 2010;37:154–63.
2. Baumert BG, Norton IA, Lomax AJ, et al. Dose conformation of intensity-modulated stereotactic photon beams, proton beams, and intensity-modulated proton beams for intracranial lesions. Int J Radiat Oncol Biol Phys. 2004;60:1314–24.
3. Onishi H, Araki T, Shirato H, et al. Stereotactic hypofractionated high-dose irradiation for stage I nonsmall cell lung carcinoma: clinical outcomes in 245 subjects in a Japanese multiinstitutional study. Cancer. 2004;101:1623–31.
4. Timmerman R, McGarry R, Yiannoutsos C, et al. Excessive toxicity when treating central tumors in a phase II study of stereotactic body radiation therapy for medically inoperable early-stage lung cancer. J Clin Oncol. 2006;24:4833–9.
5. Le QT, Loo BW, Ho A, et al. Results of a phase I dose-escalation study using single-fraction stereotactic radiotherapy for lung tumors. J Thorac Oncol. 2006;1:802–9.
6. Harris JP, Murphy JD, Hanlon AL, et al. A population-based comparative effectiveness study of radiation therapy techniques in stage III non-small cell lung cancer. Int J Radiat Oncol Biol Phys. 2014;88:872–84.
7. Court LE, Wagar M, Ionascu D, et al. Management of the interplay effect when using dynamic MLC sequences to treat moving targets. Med Phys. 2008;35:1926–31.
8. Riley C, Yang Y, Li T, et al. Dosimetric evaluation of the interplay effect in respiratory-gated RapidArc radiation therapy. Med Phys. 2014;41:011715.
9. Matsuura T, Maeda K, Sutherland K, et al. Biological effect of dose distortion by fiducial markers in spot-scanning proton therapy with a limited number of fields: a simulation study. Med Phys. 2012;39:5584–91.
10. Shirato H, Shimizu S, Kitamura K, et al. Four-dimensional treatment planning and fluoroscopic real-time tumor tracking radiotherapy for moving tumor. Int J Radiat Oncol Biol Phys. 2000;48:435–42.
11. Li R, Lewis JH, Berbeco RI, et al. Real-time tumor motion estimation using respiratory surrogate via memory-based learning. Phys Med Biol. 2012;57:4771–86.
12. Li R, Mok E, Chang DT, et al. Intrafraction verification of gated RapidArc by using beam-level kilovoltage X-ray images. Int J Radiat Oncol Biol Phys. 2012;83:e709–15.
13. Kitamura K, Shirato H, Shimizu S, et al. Registration accuracy and possible migration of internal fiducial gold marker implanted in prostate and liver treated with real-time tumor-tracking radiation therapy (RTRT). Radiother Oncol. 2002;62:275–81.
14. Park WG, Yan BM, Schellenberg D, et al. EUS-guided gold fiducial insertion for image-guided radiation therapy of pancreatic cancer: 50 successful cases without fluoroscopy. Gastrointest Endosc. 2010;71:513–8.
15. Shirato H, Harada T, Harabayashi T, et al. Feasibility of insertion/implantation of 2.0-mm-diameter gold internal fiducial markers for precise setup and real-time tumor tracking in radiotherapy. Int J Radiat Oncol Biol Phys. 2003;56:240–7.
16. Hong JC, Eclov NC, Yu Y, et al. Migration of implanted markers for image-guided lung tumor stereotactic ablative radiotherapy. J Appl Clin Med Phys. 2013;14:4046.
17. Hong JC, Yu Y, Rao AK, et al. High retention and safety of percutaneously implanted endovascular embolization coils as fiducial markers for image-guided stereotactic ablative radiotherapy of pulmonary tumors. Int J Radiat Oncol Biol Phys. 2011;81:85–90.
18. Shirato H, Onimaru R, Ishikawa M, et al. Real-time 4-D radiotherapy for lung cancer. Cancer Sci. 2012;103:1–6.
19. Shirato H, Suzuki K, Sharp GC, et al. Speed and amplitude of lung tumor motion precisely detected in four-dimensional setup and in real-time tumor-tracking radiotherapy. Int J Radiat Oncol Biol Phys. 2006;64:1229–36.

20. Seppenwoolde Y, Shirato H, Kitamura K, et al. Precise and real-time measurement of 3D tumor motion in lung due to breathing and heartbeat, measured during radiotherapy. Int J Radiat Oncol Biol Phys. 2002;53:822–34.
21. Matsuura T, Miyamoto N, Shimizu S, et al. Integration of a real-time tumor monitoring system into gated proton spot-scanning beam therapy: an initial phantom study using patient tumor trajectory data. Med Phys. 2013;40:071729.
22. Fledelius W, Keall PJ, Cho B, et al. Tracking latency in image-based dynamic MLC tracking with direct image access. Acta Oncol. 2011;50:952–9.
23. Wu H, Sharp GC, Salzberg B, et al. A finite state model for respiratory motion analysis in image guided radiation therapy. Phys Med Biol. 2004;49:5357–72.
24. Li R, Han B, Meng B, et al. Clinical implementation of intrafraction cone beam computed tomography imaging during lung tumor stereotactic ablative radiation therapy. Int J Radiat Oncol Biol Phys. 2013;87:917–23.
25. Withers HR, Taylor JM. Volume effect in spinal cord. Br J Radiol. 1988;61:973–5.
26. Nagata Y, Hiraoka M, Mizowaki T, et al. Survey of stereotactic body radiation therapy in Japan by the Japan 3-D Conformal External Beam Radiotherapy Group. Int J Radiat Oncol Biol Phys. 2009;75:343–7.
27. Arvold ND, Niemierko A, Broussard GP, et al. Projected second tumor risk and dose to neurocognitive structures after proton versus photon radiotherapy for benign meningioma. Int J Radiat Oncol Biol Phys. 2012;83:e495–500.
28. Mizumoto M, Okumura T, Hashimoto T, et al. Evaluation of liver function after proton beam therapy for hepatocellular carcinoma. Int J Radiat Oncol Biol Phys. 2012;82:e529–35.
29. Toramatsu C, Katoh N, Shimizu S, et al. What is the appropriate size criterion for proton radiotherapy for hepatocellular carcinoma? A dosimetric comparison of spot-scanning proton therapy versus intensity-modulated radiation therapy. Radiat Oncol. 2013;8:48.
30. Rombi B, Ares C, Hug EB, et al. Spot-scanning proton radiation therapy for pediatric chordoma and chondrosarcoma: clinical outcome of 26 patients treated at paul scherrer institute. Int J Radiat Oncol Biol Phys. 2013;86:578–84.
31. Medin PM, Foster RD, van der Kogel AJ, et al. Spinal cord tolerance to single-session uniform irradiation in pigs: implications for a dose-volume effect. Radiother Oncol. 2013;106:101–5.
32. Mizuta M, Takao S, Date H, et al. A mathematical study to select fractionation regimen based on physical dose distribution and the linear-quadratic model. Int J Radiat Oncol Biol Phys. 2012;84:829–33.
33. Onimaru R, Shirato H, Shimizu S, et al. Tolerance of organs at risk in small-volume, hypofractionated, image-guided radiotherapy for primary and metastatic lung cancers. Int J Radiat Oncol Biol Phys. 2003;56:126–35.
34. Kong FM, Ritter T, Quint DJ, et al. Consideration of dose limits for organs at risk of thoracic radiotherapy: atlas for lung, proximal bronchial tree, esophagus, spinal cord, ribs, and brachial plexus. Int J Radiat Oncol Biol Phys. 2011;81:1442–57.
35. Katoh N, Yasuda K, Shiga T, et al. A new brain positron emission tomography scanner with semiconductor detectors for target volume delineation and radiotherapy treatment planning in patients with nasopharyngeal carcinoma. Int J Radiat Oncol Biol Phys. 2012;82:e671–6.
36. Lin Z, Mechalakos J, Nehmeh S, et al. The influence of changes in tumor hypoxia on dose-painting treatment plans based on 18 F-FMISO positron emission tomography. Int J Radiat Oncol Biol Phys. 2008;70:1219–28.
37. Okamoto S, Shiga T, Yasuda K, et al. High reproducibility of tumor hypoxia evaluated by 18 F-fluoromisonidazole PET for head and neck cancer. J Nucl Med. 2013;54:201–7.
38. Yasuda K, Onimaru R, Okamoto S, et al. [18 F]fluoromisonidazole and a new PET system with semiconductor detectors and a depth of interaction system for intensity modulated radiation therapy for nasopharyngeal cancer. Int J Radiat Oncol Biol Phys. 2013;85:142–7.

39. Yuan X, Liao Z, Liu Z, et al. Single nucleotide polymorphism at rs1982073:T869C of the TGFbeta 1 gene is associated with the risk of radiation pneumonitis in patients with non-small-cell lung cancer treated with definitive radiotherapy. J Clin Oncol. 2009;27:3370–8.
40. Newman AM, Bratman SV, To J, et al. An ultrasensitive method for quantitating circulating tumor DNA with broad patient coverage. Nat Med. 2014;20:548–54.
41. Trakul N, Harris JP, Le QT, et al. Stereotactic ablative radiotherapy for reirradiation of locally recurrent lung tumors. J Thorac Oncol. 2012;7:1462–5.

Index

A
Abches, 96
Abdominal compression, 51
Absorption revision, 82–87
Acceptance testing, 61
Adrenal metastasis, 198–199
Air-bag system, 96
α/β ratio, 15
Annual Quality Assurance, 63
Atrial fibrillation, 199
Attenuation coefficient, 28
Attenuation rate, 83, 84
AZ-733V, 96

B
Barcelona clinic liver cancer (BCLC), 178
Beam arrangement, 49–50
Benign diseases, 199
Biologically effective dose/biologically
    equivalent dose (BED), 16, 104
Body fix, 78
Body frame, 76
BOOP. *See* Bronchiolitis obliterans organizing
    pneumonia (BOOP)
Brachial plexopathy, 168
Breath-hold technique, 51–52, 120
Breath-track, 96
Bremsstrahlung X-rays, 40
Bronchiolitis obliterans organizing pneumonia
    (BOOP), 166

C
Calypso, 96
Centrally located tumor, 160

Chest
Chest wall pain, 167
Child-pugh (CP), 180
Circulating tumor DNA (ctDNA), 247
Clinical target volume (CTV), 122
Colorectal cancer, 199
Commissioning, 61
Compton edge, 30
Compton scattering, 28
Convolution method, 107–108
Convolution/superposition method, 108
CyberKnife, 46
CyberKnife G4, 100–101

D
Daily Quality Assurance, 63
Differential cross section, 31
Dose composition radiotherapy (DCRT),
    239–240
Dose kernel, 39
Dose-volume histograms (DVHs), 126
Dose-volume metrics, 165
Dosimetric verification, 53
DTT. *See* Dynamic tumor tracking (DTT)
DTT-IMRT, 208
DTT-SBRT, 210
Dynamic tumor tracking (DTT), 206, 208, 213
    irradiation, 76, 78
    method, 75
Dynamic wave arc, 213

E
ELEKTA, 46
Energy selection, 49–50
Energy spectrum, 30